Title
Molecular Beam Studies of Oxygen Atom Reactions with Unsaturated Hydrocarbons

Author
Schmoltner, A.M.

Publication Date
1989-10-01

LBL-27916

Lawrence Berkeley Laboratory

UNIVERSITY OF CALIFORNIA

Materials & Chemical Sciences Division

Molecular Beam Studies of Oxygen Atom Reactions with Unsaturated Hydrocarbons

A.-M. Schmoltner
(Ph.D. Thesis)

October 1989

Prepared for the U.S. Department of Energy under Contract Number DE-AC03-76SF00098.

DISCLAIMER

LBL-27916

Molecular Beam Studies of Oxygen Atom Reactions with Unsaturated Hydrocarbons

A.-M. Schmoltner
(Ph.D. Thesis)

Department of Chemistry
University of California
and
Materials and Chemical Sciences Division
Lawrence Berkeley Laboratory
1 Cyclotron Road
Berkeley, California 94720
USA

October 1989

MOLECULAR BEAM STUDIES OF OXYGEN ATOM REACTIONS WITH UNSATURATED HYDROCARBONS

by

Anne-Marie Schmoltner

Abstract

The dynamics of several elementary reactions relevant to combustion was investigated. The reactive scattering of ground state oxygen atoms with small unsaturated hydrocarbons was studied using a crossed molecular beam apparatus with a rotatable mass spectrometer detector. The infrared and ultraviolet photodissociation of anisole was studied using a rotating beam source/fixed detector apparatus.

In the $O(^3P)$ + hydrocarbon experiments, major primary reactions were identified and approximate branching ratios determined. In all cases, oxygen atom addition leads to a long-lived triplet diradical intermediate which subsequently decomposes into products. In the case of the $O(^3P)$ + C_2H_2 and the $O(^3P)$ + C_2H_4 reactions, the two major decay channels are (a) 1,2-hydrogen migration followed by C-C bond rupture and (b) hydrogen atom elimination from the intermediate.

In the $O(^3P)$ + C_2H_4 case, channel (a) is possible only if the rate of triplet → singlet intersystem crossing in the intermediate is comparable to or faster than the rate of H

atom elimination. The crossed beam experiment proves that this occurs under collision free conditions prior to hydrogen migration.

In the $O(^3P)$ + allene reaction, channels analogous to the acetylene and ethylene systems were identified. In addition, oxygen atom attack on the central carbon atom leads to the formation of CO and C_2H_4 via a cyclopropanone intermediate. This channel also involves rapid triplet → singlet intersystem crossing under collision free conditions.

The infrared multiphoton dissociation of anisole resulted in only one major primary channel, the production of phenoxy and methyl radicals. Under high laser fluence conditions, the secondary dissociation of the phenoxy radicals into carbon monoxide and cyclopentadienyl radicals was observed.

In the ultraviolet photodissociation of anisole at 193 and 248 nm, several channels were observed, major ones being the formation of phenoxy and methyl radicals and the formation of methanol and benzyne. Our results indicate that most of the decomposition channels involve electronically excited states and that internal conversion to highly vibrationally excited ground state plays a minor role.

Für meine Mutter

ACKNOWLEDGEMENTS

It has been an honor and a privilege to work in the research group of Yuan T. Lee. It is to Yuan T. Lee that I owe my foremost thanks. His truly outstanding qualities as a scientist have been praised by many others, and I can only add that he deserves any conceivable recognition. We were proud to see him receive the highest honor in science, and despite the enormous demands on his time, Yuan has made a great effort to keep up with the research in his group and devoted his interest to science. In addition, he continuously shows his deep concern with non-scientific issues both here and far away.

Yuan's love of science, commitment, and hard work have greatly influenced all of us and have been an everlasting source of motivation. Yuan not only has great ideas and good advice, he also comes to the lab on many occasions and solves the problems right then and there. Yuan's guidance and encouragement, but also his tolerance for my moods, have enabled me to persevere in my own research.

I also owe a great deal to the members of the Lee group. Some taught me how to work with the awesome molecular beam machines, others participated in the work that now comprises my thesis, and many supported me in various ways throughout graduate school.

Peter Felder, my first teacher in the lab, showed remarkable insight into how much I didn't know when I first

entered the group. He did a great job showing me everything from filling the detector to how to convince a computer to start. Sheng Yu Huang and I managed to start up the oxygen source again. I learned a lot from him about science and China. Rick Brudzynski was a very tolerant, friendly and selfless co-worker, and he has been a model of an extremely careful and thorough scientist for me. Pam Chu's energy for and commitment to science has helped greatly in carrying out most of the work described in this thesis. Day and night, she spent countless hours taking data and helping to keep the machine going. Thanks to her efforts (later James Chesko helped, also) YTLEE1 and YTLEE2 have been extremely reliable and fun computers to work with. Rich Ferrieri helped a great deal with the move and with the O + butene experiment in its initial stage. At the end of the oxygen atom era, John Allman joined the team.

My venture into photochemistry would not have been possible without the help and advice from Eric Hintsa, Xin Sheng Zhao, and Pam Chu. Felicia Etzkorn helped "synthesize" phenol-OD - those were the days when Eric tried to convince me that one could do an experiment and get famous in one day. In the final (and somewhat lengthier) anisole experiments, Deon Anex was a very friendly, patient and thorough co-worker.

Many group members taught me something or helped me in the lab, and I can only mention a few. Rob Continetti has been very kind and helpful from our first year on and especially during the time of the move. Laurie Butler always took the time to

answer questions and her faith in my abilities encouraged me. Tim Minton introduced me to Tell-a-Graph and the complicated world of connectors. Lisa Yeh cheered me up during the time before my prelim. Barbara Balko was a kind and pleasant office mate. Post-docs Thomas Trickl, Gereon Niedner and Manfred Vodegel have helped improve my German, both scientific and otherwise. The interaction with the A-team (Hartmuth Schmidt, Paul Weiss, Jean-Michel Mestdagh, Mike Covinsky, Floyd Davis, and Arthur Suits) was always productive and pleasant.

Many people at LBL and on campus not only solved numerous experimental problems, but also,, as importantly, they taught me a lot about their field of expertise: Randy Michelson, Tony Moscorelli, Ed Arnold, Fred Vogelsberg, Yau Man Chen, and Don Wilkinson.

Ann Weightman has been an amazing help with all types of bureaucratic as well as all kinds of other problems. Her intimate knowledge of the inner workings of this place and her talent for making things happen NOW have saved all of us a lot of time and energy.

I would like to thank all the people who considerably helped improve this thesis by thoroughly reading and criticizing my manuscripts, in particular Gary Robinson, Pam Chu, Deon Anex, Rick Brudzynski, Dr. Gunnar Lyman, and of course Y. T. Lee.

Many group members have not only helped me in the lab. Eric Hintsa supplied Kimwipes and support in times of need. I admire his kindness, tolerance, and ability to talk to everyone,

but also his talents as a scientist. Ralph Page became a good friend, and I value his openness and qualities as a listener. As an office mate, Xin Sheng Zhao was curious about everything from computer cables to European culture; and later he also became a good friend. I thoroughly enjoyed the time spent with Marion Helfand and Rosy Georgiadis. Both are wonderful friends and I am grateful for their ongoing support. Gary Robinson shared some good times and many interests with me. I enjoyed many conversations with Laisheng and Liqiong Wang, Marc Vrakking, Di-Jia Liu and many other past and present group members.

Many friends from "outside" have made these years in graduate school pleasant and memorable; they also helped me through the difficult times. In particular I would like to mention Thomas D. Y. Chung, Susi Stadler, Shankar Sastry, Randy Michelson, Pat Sieber, and all the wonderful people at Canterbury House, especially Severino Toscano Melo, Basanta Chaudhuri, Xin Wu, Qiuyue Wu, Branka Pavlovic, Paul Wright and Deborah LaFond. I learned a great deal about issues beyond science from the women at Connexions magazine. I also appreciate my friends in Austria and elsewhere who have kept in touch with me.

Just when I was about to complete my thesis work and leave, Elihu Blotnick entered my life. His love has uplifted and inspired me, and I can't wait to learn about all the other interesting things that can be done with photons.

I would have never come to Berkeley if I had not received encouragement in Austria from Doz. Harald Kauffmann as well as from Frau Trude Wild at the American Embassy. My early science teachers Mag. Sieglinde Fürst, Dr. Rosa Hagenauer, Mag. Roderich Magyar, and Dr. Edith Jarisch were instrumental in fostering my enthusiasm for chemistry. Finally I want to thank my parents who have been supportive of me and my interest in science from early on.

This work was supported by the Director, Office of Energy Research, Office of Basic Energy Sciences, Materials Sciences Division of the U.S. Department of Energy under Contract No. DE-AC03-76SF00098.

TABLE OF CONTENTS

CHAPTER 1

INTRODUCTION

The goal of chemical dynamics research is to study chemical reactions on a fundamental level with all reactants prepared in well defined states and under well controlled reaction conditions. If all the properties of the products and their distribution functions are measured, the complete picture of a chemical reaction emerges. Many techniques have been developed in the past and much progress has been made, however most chemical systems remain unexplored.

The method used in our group is the crossed beam technique. For reactive scattering experiments, two supersonic molecular beams are crossed at a fixed angle of 90°, and the properties of the collision products can be measured as a function of laboratory angle. In the case of the universal crossed molecular beam apparatus[1], the detector consists of a rotatable mass spectrometer. Combined with electron impact ionization, this detection method is applicable to most species of interest.

Photodissociation in supersonic molecular beams is a variant of the crossed beams method. The supersonic molecular beam is crossed with a laser beam at a fixed angle. The work reported here was carried out in the rotating source apparatus[2], where the laser and the mass spectrometer detector are at 90°

with respect to each other and the molecular beam source is rotatable, allowing the angle between molecular beam and detector to be varied. In both types of experiments, detailed information on the identity of the products, the translational energy release and the reaction or dissociation mechanism is obtained by measuring angular and time-of-flight distributions.

This dissertation contains three chapters (2-4) on reactive scattering and two chapters (5 and 6) on photodissociation. The purpose of this introduction is to explain the connection between the different experiments performed and to discuss their relevance. The techniques employed will be introduced, but no attempt will be made here to present an extensive review of previous work.

In order to identify primary reaction steps unambiguously and investigate the dynamics of the reaction, single collision conditions are essential. The crossed molecular beam technique is the most straightforward and yet the most difficult way of accomplishing this.

In a typical experiment, there is a finite spread in the velocity of the molecules and the collision angle and therefore in the collision energy and geometry. This is less critical if the emphasis is on obtaining qualitative information about reaction channels and the approximate relative cross sections rather than about the details of the translational energy release, the excitation function, or the detailed features of

the angular distributions as in elastic scattering. In the reactions studied, our interest is mostly in identifying the primary reaction products and determining the branching ratios between the major channels. Since the cross sections of the reactions studied are comparatively small, often the first concern is in obtaining any signal at all, and significant improvements of the experimental resolution are not practicable.

It is of great interest to compare the results of chemical activation with those of photochemical activation. In the case of a random distribution of vibrational energy, these two excitation methods should be comparable and the products of the dissociation of the complexes should be the same, at least if the energy content is similar in both cases. A special situation is IR multiphoton dissociation (IRMPD), where the excitation energy is always randomly distributed and dissociation takes place from the vibrationally excited electronic ground state. This process can therefore "mimic" thermal dissociation - with one important difference: if IRMPD is induced in a molecular beam, the excitation and dissociation processes take place under collision free conditions. It is well established that IR multiphoton excitation with an intense IR source is indeed possible without the aid of collisions, and this technique has been applied for studying the primary dissociation processes of numerous molecules[3].

In the case of UV excitation - which has become a very popular research tool due to the availability of intense,

although not necessarily tunable, UV sources - a variety of processes can occur, such as fluorescence, predissociation or direct dissociation from an electronically excited state, or internal conversion followed by dissociation of vibrationally excited molecules in the ground electronic state. While collisions can be avoided by employing molecular beams, complications stemming from the intense radiation still have to be considered, in particular multiphoton absorption processes and secondary dissociation following further photon absorption by the primary products.

Chapters 5 and 6 respectively describe the IRMPD and UV photodissociation of anisole. A comparison of the data obtained in these two types of experiments immediately illustrates the fundamental differences between the two processes. In fact, the UV dissociation experiment was initially undertaken in order to study hot ground state dissociation, which was expected to resemble the IRMPD case, and it actually shed some light on the IR data which at the time were not understood. (Repeating the experiment with a much superior IR laser proved to be the better approach.) It quickly became clear how complicated the situation in the UV photodissociation was, and in fact not all of the questions could be resolved in the analysis.

A very important aspect of our research is the comparison of our experimental results with state of the art ab initio theory. This allows conclusions on how well systems of the size

we study can be understood theoretically and how reliable such qualitative and quantitative predictions about primary reaction (or dissociation) channels are. The possibilities and limitations of ab initio theory are illustrated in chapters 2-4. While the $O(^3P)$ + acetylene system appears to be understood thoroughly based on ab initio calculations combined with additional experimental information, the limitations become obvious in the $O(^3P)$ + ethylene case. Here rapid intersystem crossing (ISC) between triplet and singlet plays a crucial role, and as of yet no theoretical calculation has addressed this specific question. The interplay between theory and experiment will continue; in this case, the next step has to be taken by the theoreticians.

Apart from the conceptual elegance of the crossed molecular beam experiments, another important aspect of this research has to be mentioned: All experiments described in this dissertation are of direct or indirect relevance to combustion chemistry. In particular, the reactions of oxygen atoms with simple hydrocarbons (chapters 2-4) are of fundamental and practical importance for combustion research as model systems. The goal of the photodissociation experiments (chapters 5 and 6) has been to produce phenoxy radicals, which are important intermediates in the combustion of aromatic hydrocarbons, and to study the dynamics of their decay.

The focus of this dissertation is the chemistry of ground

state oxygen atoms with unsaturated and aromatic hydrocarbons, and all the experiments described in the following chapters are connected to this topic in some way. Several experiments which would make the connection clearer are not included in the following chapters - some because they were done by others, some because they were not done at all, and some were left out because of time constraints.

The starting point is the reaction of oxygen atoms with the simplest hydrocarbons. Ground state oxygen atoms do not react with alkanes at low collision energies, but $O(^1D)$ atoms do. $O(^3P)$ does react, however, with alkenes and alkynes.

Crossed beam experiments of the reactions $O(^3P) + C_2H_2$ and C_2H_4 are the subject of chapters 2 and 3. These are important model systems not only from a chemical dynamics standpoint, but also for combustion research. An enormous amount of information is necessary to model and predict a "real life" system, particularly one as complicated as for instance the atmosphere or a flame. If some model systems are understood in great detail, a clearer picture will evolve. Examples for such model systems are the reactions of atoms with the simplest alkene and alkyne, ethylene and acetylene, and the simplest aromatic molecule, benzene. Other reactions of great importance are those of OH and other radicals with hydrocarbons, but these yet have to be studied using the crossed molecular beam method. Important progress has been made in our group[4] and in others[5] towards the development of supersonic radical beams, however,

the universal applicability of these techniques is still an unreached goal.

The extension of the $O(^3P)$ + ethylene results to the next larger olefins has been attempted, and some of these experiments are described in R. Baseman's thesis[6]. We originally had planned to continue that work and study butenes, but soon realized the potential difficulties in the experiment associated with the relevant mass numbers in this special case. Hydrogen substitution in analogy to the O + ethylene reaction should be easily detectable because of the favorable kinematics. However, all the C_4H_7O radicals prefer to fragment extensively in the ionizer and can not be detected as $C_4H_xO^+$. The other channel considered, substitution of a methyl radical, presents serious problems because the reactant (C_4H_8) and the product (C_3H_5O) have almost the same masses, 56 and 57 amu, respectively. Because of the enormous interference from elastic scattering, this channel could not be observed, at least not in the angular distributions.

The idea that saved us at the time was to study allene, which has the useful property of containing very few hydrogen atoms. This promised simplified mass spectra, which indeed proved to be the case. Also, M. C. Lin had just published an interesting paper on this reaction[7]. Our initial intention was to prove wrong the earlier work which claimed that the major process was the formation of CO and ethylene via triplet→singlet ISC, however, many years and many experiments later, we

discovered that both the CO + C_2H_4 channel and the hydrogen substitution channel in analogy to $O(^3P)$ + C_2H_4 takes place under single collision conditions.

The allene experiment is a good example of how the lessons learned from simple molecules can indeed be applied to larger systems, and also how new features and special cases must be considered. One of the important questions arising from the O + ethylene system which is also central to O + allene is whether rapid collisionless ISC occurs in a small molecule or radical. Interestingly, this has been addressed theoretically only for the latter reaction.[8]

Moving on to much larger molecules, our attention turns to the reaction of oxygen atoms with aromatic systems. The simplest reaction of this kind, $O(^3P)$ + benzene, was studied carefully in our group[9]. In this system, one of the most important results there is the occurrence of ISC leading to ground state phenol which lives long enough to reach the detector. The other major channel involves elimination of a hydrogen atom from the collision complex forming the phenoxy radical. A third channel, considered of minor importance, is the formation of carbon monoxide and C_5H_6, probably cyclopentadiene, by way of dissociation of the hot singlet phenol. The direct dissociation of phenol yielding CO was suggested as a pathway by Cypres and Bettens[10] to interpret the results of a phenol pyrolysis experiment. A crossed molecular beam experiment by Sloan[11] also suggested the formation of CO

and C_5H_6 as primary products. In the O + benzene experiment performed in this laboratory[9], however, at least a large fraction of the phenol apparently survives for the several hundred microseconds which are required to reach the detector, indicating that the rate of phenol dissociation is small. This actually casts some doubt on the barrier suggested by Lin and Lin[12]. In view of the experiments on halogen-substituted benzenes[13], which will be discussed below, questions arise regarding the origin of the m/e=65 ($C_5H_5^+$) signal detected in the O + benzene reaction.

The other possible source of CO and a product of m/e=65 is the dissociation of phenoxy radical which was studied previously. The activation energy for this dissociation process was determined to be about 44 kcal/mole[12] and thus significantly higher than the available energy for phenoxy formed in the O + benzene reaction.

A very elegant idea to test these assumptions is to study the reactions of oxygen atoms with halogen-substituted benzenes. By substituting chlorine, bromine and iodine for a hydrogen atom, different amounts of vibrational energy can be deposited into the resultant phenoxy radical. This energy will be less than the barrier determined by Lin and Lin[12] for benzene and chlorobenzene, but higher for bromo- and iodobenzene. This allows one to "chemically tune" the available energy (See Fig. 1, chapter 3 of Ref. 13). All three halobenzenes mentioned were studied in our laboratory using the crossed molecular beam

method and the results are summarized in Ref. 13. The surprising result of this research was a fast feature in the m/e=65 spectra from all three halobenzenes studied. The origin of this fast signal remains somewhat unclear.

In order to resolve the questions in the O + halobenzene experiments, a better understanding of the O + benzene reaction would be helpful. According to Sibener et al.[9], after the initial formation of the triplet diradical, a competition takes place between hydrogen elimination on the triplet surface and ISC to singlet phenol. The ISC was found to be enhanced by higher collision energy and substitution of hydrogen by deuterium atoms. It can be expected that halogen atoms would further increase the rate of ISC. It is thus likely that the fast part of the signal at m/e=65 in the halobenzene experiments is due to the dissociation of the singlet state of a C_6H_5OX (X=Cl, Br, I) isomer into C_5H_5X + CO, and that extensive ionizer fragmentation of the products prevented us from detecting these products at their parent masses. In view of the results of the O + ethylene and O + allene experiments, it now appears even more likely that rapid ISC occurs in these oxygen-containing diradicals. Consequently, the other channels observed in the O + halobenzene experiment, such as hydrogen elimination, could actually be occurring on the singlet surface as well. The crossed molecular beam experiment generally does not allow a distinction between different electronic states.

To our disappointment, the "chemical tuning" idea for

studying the decomposition of phenoxy radical formed in a chemical reaction did not work as expected. Thus, our hope of being able to bracket the decomposition barrier was not realized. Different approaches were sought. Photodissociation of an appropriate precursor presents another possibility for producing the phenoxy radical. Two precursor molecules were considered: anisole and phenol. Anisole was chosen because the CH_3-OC_6H_5 bond dissociation energy is only about 64 kcal/mole. The IR multiphoton dissociation of anisole which is the subject of chapter 5, indeed proved to be a convenient and clean way of producing phenoxy radicals, and the comparison of the data taken with two different CO_2-lasers shows that by carefully choosing the conditions, secondary dissociation of the phenoxy radicals can either be avoided or induced.

The other precursor considered (and used) is phenol. The attempts toward IRMPD of phenol were initially unsuccessful, presumably because of the lower absorption cross section and the higher bond dissociation energy (87 kcal/mole), however, the higher power laser made that experiment possible as well. An additional problem in the phenol case lies in the kinematics: A heavy particle (phenoxy) recoiling from the very light hydrogen atom, is not expected to be scattered significantly away from the molecular beam and will therefore be hard to detect. Indeed, no indication for the phenoxy radical was found in the experiment, but there was evidence for secondary dissociation products. Surprisingly, two clearly separate channels were

found which differ in the mass spectrum of the products and in the translational energy release. One of these is very likely due to the secondary decomposition of phenoxy into the cyclopentadienyl radical and carbon monoxide, while the other one probably represents another phenol decomposition channel leading to CO and a C_5-species. The latter is possibly isomerization of phenol followed by CO-expulsion. These data and their detailed analysis are not included in this dissertation.

As mentioned above, in addition to the IRMPD studies, the UV photodissociation of anisole was also studied, and is the subject of chapter 6. UV photodissociation of phenol was not carried out, yet it promises to be a very interesting and important experiment.

The idea of approaching a system from two different angles, such as chemical vs. photochemical activation, was considered in the context of the O + olefin reactions as well. An example is briefly mentioned in chapter 3: the reaction of O + ethylene, among other channels, leads to the formation of the highly vibrationally excited electronic ground state of acetaldehyde. In order to study the decomposition pathways of this molecule and to corroborate the conclusions of the crossed molecular beam experiment, the UV photodissociation of acetaldehyde at 248 and 193 nm was attempted, but with no success.

Similarly, the photodissociation of C_3H_4O-isomers is of relevance to the O + allene experiment, as discussed in chapter

4. In particular, the dissociation of cyclopropanone to ethylene and carbon monoxide should be considered. Unfortunately, this experiment can not be performed with a molecular beam apparatus because of the instability of cyclopropanone. However, cyclopropanone is the smallest member of a whole family of cyclo-alkanones which typically decompose by either ring-opening forming an olefin or CO-expulsion forming the next smaller cycloalkane.[14] Instead of cyclopropanone, we studied the photodissociation of cyclobutanone at 308 nm, and the results are described at the end of chapter 4. Evidence for both channels mentioned was found, but the absorption cross section at this wavelength was found to be too low to achieve reasonable signal-to-noise.

The CO-expulsion process accompanied by a ring contraction is of considerable interest in organic chemistry, even for preparative purposes. It in turn relates to the channel involving CO expulsion from phenoxy radical and possibly phenol itself where the second product again is a cyclic molecule or radical.

In all the systems mentioned, many questions remain open, and there is much room for further exploration. In the following chapters some of the progress made is explained in detail. Hopefully most of the material will soon appear in scholarly journals. Additional information is included in most chapters particularly on experimental details which might be of use for future experiments.

References

1. Y. T. Lee, J. D. McDonald, P. R. LeBreton, and D. R. Herschbach, Rev. Sci. Instrum. 40, 1402 (1969).
2. A. M. Wodtke and Y. T. Lee, J. Phys. Chem. 89, 4744 (1985).
3. P. A. Schulz, Aa. S. Sudbo, D. J. Krajnovich, H. S. Kwok, Y. R. Shen, and Y. T. Lee, Ann. Rev. Phys. Chem. 30, 379 (1979).
4. G. N. Robinson, G. M. Nathanson, R. E. Continetti, and Y. T. Lee, J. Chem. Phys. 89, 6744 (1988); E. J. Hintsa, Ph. D. Thesis, University of California, Berkeley, 1989.
5. P. Andresen, D. Häusler, and H. W. Lülf, J. Chem. Phys. 81, 571 (1984); P. Andresen, N. Aristov, V. Beushausen, D. Häusler, H. W. Lülf, J. Chem. Phys., to be published; D. E. Powers, J. B. Hopkins, and R. E. Smalley, J. Phys. Chem 85, 2711, (1981).
6. R. J. Baseman, Ph. D. Thesis, University of California, Berkeley, 1982.
7. M. C. Lin, R. G. Shortridge, and M. E. Umstead, Chem. Phys. Lett. 37, 279 (1976).
8. Y.-N. Chiu and M. S. F. A. Abidi, J. Phys. Chem. 86, 3288 (1982).
9. S. J. Sibener, R. J. Buss, P. Casavecchia, T. Hirooka, and Y. T. Lee, J. Chem. Phys. 72, 4341 (1980).
10. R. Cypres and B. Bettens, Tetrahedron 30, 1253 (1974).
11. T. M. Sloane, J. Chem. Phys. 67, 2267 (1977).

12. C.-Y. Lin and M. C. Lin, J. Phys. Chem. 90, 425 (1986).

13. R. J. Brudzynski, Ph. D. Thesis, University of California, Berkeley, 1987.

14. S. W. Benson and G. B. Kistiakowski, J. Am. Chem. Soc. 64, 80 (1942).

CHAPTER 2

CROSSED MOLECULAR BEAM STUDY OF THE REACTION $O(^3P) + C_2H_2$

2.1. Introduction

Detailed information on elementary chemical reactions is essential for a thorough understanding of complex systems such as combustion and atmospheric chemistry. Combustion processes and flames have been studied very extensively, yet a great deal is still to be learned about the elementary reaction steps involved. For a complete description of a system, identification of the products of chemical reactions, branching ratios and rate constants, or, ideally, knowledge about detailed reaction dynamics, and subsequent energy transfer and diffusion processes are needed.

Acetylene flames have been studied extensively and much effort has been devoted to elucidating the mechanism of acetylene combustion[1]. Acetylene flames are noted for their intense chemiluminescence covering the whole frequency range from the VUV[2,3], through the near UV and visible[4], to the IR[5]. They are also known for the formation of large amounts of ions[6], of polyacetylenes and other higher hydrocarbons[7], and soot[8]. Furthermore, acetylene reactions are part of the oxidation

mechanism of the other hydrocarbon fuels, particularly under fuel-rich conditions[9].

The fuel consumption in an acetylene flame is largely due to the reaction of oxygen atoms with acetylene[10]. The overall rate constant for this reaction,

$$O(^3P) + C_2H_2 \rightarrow \text{products}, \qquad (1)$$

has been measured over a wide temperature range[11], and the identity of the primary products is well known. The following reaction channels are considered to be involved:

$$O(^3P) + C_2H_2 \rightarrow CH_2 + CO \qquad (1a)$$

$$O(^3P) + C_2H_2 \rightarrow HCCO + H \qquad (1b)$$

$$O(^3P) + C_2H_2 \rightarrow CH_2CO \qquad (1c)$$

$$O(^3P) + C_2H_2 \rightarrow OH + CCH \qquad (1d)$$

$$O(^3P) + C_2H_2 \rightarrow H_2 + C_2O \qquad (1e)$$

Ground state (^3P) oxygen atoms are electrophilic and can add to carbon-carbon double or triple bonds[12], forming a diradical intermediate $(HCCHO)^{\ddagger}$. This intermediate and the isomerized $(CH_2CO)^{\ddagger}$ can subsequently undergo unimolecular decomposition into CH_2 + CO (1a) or HCCO + H (1b). Both channels (1a) and (1b) were first suggested by Fenimore and Jones[13]. The formation of methylene and carbon monoxide was considered the main reaction path in most of the earlier work.

The ketenyl radical HCCO (often referred to as "ketyl") was first observed as a product of reaction (1) by Jones and Bayes[14] using photoionization mass spectroscopy. Recently, the microwave[15] and LIF[16] spectra of the ketenyl radical were reported.

Stabilization of the $(CH_2CO)^{\ddagger}$ intermediate yields ground state ketene (1c) and is possible only in an environment where the excess energy can be removed through collisions. The formation of ketene has been observed by Haller and Pimentel[17] in a 20 K argon matrix and by Gaedtke et al.[18] at very high pressures (up to 1000 atmospheres). In other experiments performed at high pressures, no ketene or only traces could be found.

The abstraction reaction (1d) forming the hydroxyl radical was suggested by Bradley and Kistiakowsky[19] and in earlier work was considered a major reaction path by many authors. However, this reaction is endothermic by approximately 32 kcal/mole[20] and is therefore expected to be only of minor importance even at the very high temperatures in the flame or shock tube studies.

The formation of hydrogen molecule and C_2O, reaction (1e), was suggested as a minor primary reaction step[3,21] in order to explain the $CO(A^1\Pi)$ chemiluminescence in acetylene and carbon suboxide flames. Indirect evidence for this channel was found by Williamson and Bayes[22] from experiments with C_2H_2 and C_2D_2, but it accounted for only 0.3% of the products.

Although agreement has been reached on the identity of the

primary reaction products, there is still considerable uncertainty concerning the relative importance of the various channels, in particular the branching ratio between the two major channels (1a) and (1b). Several authors derived values for the branching ratio from the interpretation of kinetic data. Vinckier and Debruyn[23] monitored the concentration of CH_2 in the oxidation of acetylene and found that about 50% of the initial reaction of O atoms with C_2H_2 proceeded according to (1a). Aleksandrov et al.[24] measured O-and H-concentrations and obtained a value of 5% for channel (1b) at room temperature from the kinetic analysis of the concentration vs. time profiles. Löhr and Roth[25] measured the time dependence of the O- and H-concentrations in shock tube oxidation experiments of acetylene and obtained values for k_{1a} and k_{1b} in the temperature range 1500-2570 K. 64% of the primary reaction was found to follow (1a) at 1500 K and 46% at 2500 K. In a very similar experiment Frank et al.[26] derived rate expressions resulting in 30-40% for channel (1a) with little temperature dependence of the branching ratio.

Williamson and Bayes[22], using gas chromatographic product analysis, concluded that channel (1a) accounted for at least 12% and probably 25% of the decay of the original diradical intermediate. Later, Williamson[27] studied the reaction of O with C_2D_2 in the presence of H_2 and determined the D atom yield (channel 1b) to be 42±10% from the measurement of HD formed. Mass spectrometric detection following either photoionization[28]

or low energy electron impact ionization[29,30] has given values of 15-50%[28], 95%[29], and 41%±20%[30] for the yield of channel (1a). In a recent investigation detecting $^3CH_2$ using laser magnetic resonance[31], channel (1a) was found to contribute about 38%.

It has to be emphasized that none of these experiments were performed under truly single collision conditions and that secondary reactions of the initially formed radicals had to be taken into account. Nevertheless, there is a consensus that reactions (1a) and (1b) are the major reaction channels.

Recent ab initio calculations[32,33] provide detailed information on the triplet potential energy surface for the O/C_2H_2 system. Harding and Wagner[32] also performed calculations of the rate constants and product branching ratios based on statistical theory. Channel (1b) was found to contribute at least 25% and most likely more than 50% of the total reaction.

This chapter describes the investigation of the reaction $O(^3P) + C_2H_2$ using the crossed molecular beam technique. This method is particularly well suited for studying elementary reactions since the experiments are performed under single collision conditions, and one can identify primary reaction products unambiguously, measure relative cross-sections, and elucidate details of the reaction dynamics.

Although the ketenyl radical has been observed previously in crossed molecular beam studies of the $O(^3P) + C_2H_2$ reaction[34,35], Clemo et al.[34] did not observe channel (1a) at all, and the data obtained earlier in our laboratory[35] were

unsatisfactory for deriving definitive conclusions due to the high CO background in the detector chamber. By using $^{18}O_2$ and with an improved experimental arrangement, we have been able to obtain detailed dynamical information on both channels (1a) and (1b).

2.2. Experimental

The universal crossed molecular beam apparatus used for the present study is an improved version of an apparatus described in detail previously[36]. Briefly, two continuous supersonic beams of reagent atoms and molecules, pass through one or two stages of differential pumping, and cross at 90° in a reaction chamber held at a pressure of about $1x10^{-7}$ Torr. The scattered species are monitored using a triply differentially pumped detector, consisting of a Brink's type[37] electron impact ionizer, quadrupole mass filter and Daly ion detector[38]. The nominal electron energy was 200 eV. The detector is rotatable in the plane of the beams, the center of rotation being the collision zone which has a size of typically 2x2x3mm. Under ordinary conditions, the whole collision zone is viewed by the detector. A schematic view of the setup is given in Fig. 1.

Two types of measurements were performed for this investigation: Angular distributions of the reaction products at a specific mass-to-charge-ratio (m/e) and time-of-flight (TOF)

measurements at several angles yielding information on the translational energy distribution for a given species.

Angular distributions were determined by modulating one of the beams at 150 Hz using a tuning fork chopper and accumulating pulse counts in a dual channel scaler which allowed for background subtraction. Typically, 6-8 angular scans were obtained for each m/e value, with a total counting time of 6-16 min per angle.

For the TOF measurements, the cross-correlation method[39] was used. The reaction product at a given laboratory angle was modulated using a slotted disk containing a total of 255 equally spaced open and closed segments in a pseudo-random sequence. The data were accumulated in a 255-channel scaler interfaced with an LSI-11 laboratory computer. The disk was spun in front of the detector chamber at 436 Hz resulting in a resolution of 9μs/channel. Total accumulation times for the TOF-measurements ranged from 10 minutes to several hours depending on the m/e value monitored.

In an attempt to obtain TOF spectra with an improved signal-to-noise ratio, a set of measurements was performed using an assembly consisting of two disks replacing the cross-correlation wheel. The disks of 17.8 cm diameter had eight open slots each and were mounted 0.5 cm apart. The width of the slots in the disk closer to the interaction region was 0.15 cm, the width of the slots in the other disk was 0.20 cm. The leading edges of the corresponding slots in the two wheels were

aligned. A short pulse of particles was allowed to pass by each set of slots, but only particles with a certain minimum velocity (which is a function of the width of the second slot, the distance between the two disks, and the frequency of rotation of the disk) could pass through to the detector. Thus interference from slow particles stemming from an earlier pulse was avoided. A detailed description of a similar setup was given in Ref. 40. Data were taken with a wheel speed of 200 Hz and a channel width of 5μs. The advantages of this configuration with narrower slots in the disk are better time resolution in the TOF spectra and the elimination of cross-correlation noise. In the case of cross-correlation, the absolute noise-level is the same for all channels, making small peaks harder to discern in the presence of very large peaks. The disadvantage of the double disk method is the reduced duty cycle, requiring counting times of up to 25 hours.

A supersonic beam of oxygen atoms was produced by dissociating molecular oxygen in a radio frequency plasma. The RF, typically 14.7 MHz at 200 to 300 W, was applied through a tank circuit in which the inductance consisted of a water cooled copper coil surrounding a water cooled quartz nozzle assembly. This high pressure supersonic oxygen source has been described in detail previously[41]. A mixture containing 5% oxygen in neon carrier gas was used at a stagnation pressure of 400 to 600 Torr for all experiments. After expansion through the quartz nozzle, the beam passed through a boron nitride skimmer and a set of

defining slits collimating the beam to an angular divergence of 2.5° vertically and 1.7° horizontally. The diameter of the nozzles used varied between 0.10 and 0.25 mm. Using the method described in Ref. 41, we estimate that about 90% of the O_2-molecules were dissociated. With neon as a carrier gas, only ground state (^3P) oxygen atoms are produced. The absence of appreciable amounts of $O(^1D)$ in the beam was repeatedly confirmed by crossing the oxygen beam with a supersonic beam of molecular hydrogen, which reacts with a large cross-section with $O(^1D)$ forming OH[42]. No OH was observed. However, formation of very small amounts of excited (^1D) oxygen atoms can not be completely ruled out. Ions formed in the discharge were deflected out of the beam by applying a field of about 2 kV/cm across the beam behind the skimmer.

A supersonic beam of acetylene was produced by expanding 200 Torr of neat acetylene, which had been passed through a dry ice/acetone trap, through a 0.15 mm nozzle at room temperature. For the angular distribution measurements, the beam passed through a skimmer and a set of defining slits collimating the beam to a divergence of about 2.3° horizontally and 3.5° vertically.

For most of the TOF data presented in this paper, the skimmer for the hydrocarbon beam was mounted directly on the wall of the collision chamber. Thus the beam passed through only one differential pumping region. The beam divergence was defined by the skimmer to 8.6°. Under these conditions, the

signal intensity was about fifty times higher than in the standard configuration, which was used for accurate measurements of product angular distributions.

The velocity distributions of the molecular beams were determined by replacing the cross-correlation wheel with a disk with four slots (0.8 mm wide) spun at 300 Hz allowing a time resolution of 1-2 μs/channel. The measured TOF distributions were fitted to the functional form[43]

$$N(v) = v^2 \exp[-(\frac{v}{\alpha} - S)^2]$$

where v denotes the velocity of the molecules, S the speed ratio, α a parameter, and N(v) the number density of molecules with velocity v. The peak velocity of the acetylene was 8.6×10^4 cm/s with a speed ratio S of 6.3, the peak velocity of the oxygen beams ranged from 1.8×10^5 to 2.1×10^5 cm/s, with speed ratios around 5. The resultant most probable collision energies were between 5.5 and 6.3 kcal/mole, with a FWHM of the energy distribution of about 50%.

The acetylene was obtained from Matheson with a stated purity of 99.6% min. and oxygen/neon mixtures were purchased from Matheson and Airco and had a stated minimum purity of 99.99% and 99.995%, respectively. $^{18}O_2$ with a stated isotopic purity of 95% minimum was obtained from Los Alamos National Laboratory and was mixed with neon of 99.995% stated minimum purity purchased from Airco. All gases were used without

further purification, except for acetylene, which was passed through a dry ice/acetone trap to remove acetone which was used as a stabilizer in the acetylene cylinder.

2.3. **Results and Analysis**

The major complication in experiments using electron impact ionization and mass spectrometric detection is extensive fragmentation of molecules and radicals upon ionization. This problem can be overcome in a crossed molecular beams experiment, however, since products can be identified by their characteristic angular or TOF distributions, governed by the kinematic relations. Therefore measurements at different mass-to-charge-ratios (m/e) clearly establish parent/daughter ion relationships.

Angular distributions were measured for m/e=12, 13, 14, 24, 26, 28, 29, 32, 40, and 41 (corresponding to the ions C^+, CH^+, CH_2^+, C_2^+, $C_2H_2^+$, CO^+, CHO^+, O_2^+, C_2O^+, and $HCCO^+$, respectively) for the reaction of $^{16}O + C_2H_2$, and for m/e=30 and 43 (corresponding to the ions $C^{18}O^+$ and $HCC^{18}O^+$) in the case of $^{18}O + C_2H_2$. The maximum count rates for the ketenyl radical product both at m/e=41 ($HCC^{16}O^+$) and 43 ($HCC^{18}O^+$) were approximately 120 counts/sec, and the shapes of the distributions were very similar. The laboratory angular distribution of m/e=43 is shown in Fig. 2. The error bars represent 95% confidence intervals.

For this set of data, time dependent drifts in the signal were accounted for by scaling all measured points to the value at the reference angle chosen at 30°. The signal at the reference angle was monitored frequently during the measurement of the angular distribution. The direction of the oxygen atom beam is defined as 0°.

From the analysis of the angular distributions it was possible to extract information on the ionizer cracking pattern of ketenyl radical (Fig. 3). Using ^{16}O, the ketenyl radical and its major fragments are expected at m/e=12, 13, 24, 25, 28, 29, 40 and 41. Cross-correlation TOF data were also obtained from the reaction of ^{16}O with acetylene at m/e=12, 13, 24, 26, 29, 40 and 41 at 35°, which was close to the angle of maximum signal intensity for ketenyl radical. As in the case of angular distributions, the spectra obtained could be interpreted as due to nonreactive scattering, reactive scattering, or a combination of both. The relative contributions of nonreactive and reactive scattering could be estimated since the angular distributions as well as the TOF distributions for reactive and nonreactive scattering are distinctly different. Two components stemming from the two different types of scattering can be distinguished easily in most cases. The m/e=26 signal represents nonreactive scattering only. The total reactive signal for each m/e was then used to determine the cracking pattern of the ketenyl radical.

In order to study the formation of methylene and carbon

monoxide, channel (1a), and compare the results with the ketenyl radical channel (1b), it was necessary to perform experiments using $^{18}O_2$, since in experiments using ^{16}O no meaningful data were obtained at m/e=28 (CO^+) because of a very large inherent detector background at this mass. $C^{18}O^+$ could be detected at m/e=30. However, no dynamic information could be obtained from the m/e=30 angular distribution, since a large fraction of the products is scattered outside the detector scanning range and the product signal obtained in the detector scanning range not only showed broad angular distributions with little dependence on laboratory angle, but also had large uncertainties.

This result is not surprising in view of the kinematics of the collision. Because of momentum conservation the velocities of two recoiling fragments in the center-of-mass coordinate frame are inversely proportional to their masses. In the case of ketenyl radical recoiling from the very light hydrogen atom (channel 1b), the center-of-mass velocity of the ketenyl radical is expected to be very small, and therefore in the laboratory frame the flux will be concentrated in a small angular range, leading to a sharply peaked angular distribution as shown in Fig. 2. In the case of carbon monoxide recoiling from methylene, even with only a few kcal/mole of recoil energy, the center-of-mass velocities of both particles are expected to be large and a large fraction of the products will appear outside of the detector scanning range, therefore the entire angular distribution cannot be measured. In all these cases, however,

detailed dynamical information can be extracted from TOF data.

The kinematic differences between the two channels are illustrated in Figs. 4 and 5. Fig. 4 shows the simulated angular distributions for channel (1a) at $HCCO^+$, solid curve, and (1b) measured at CO^+, dashed curve, as calculated from the results of our data analysis as described below, taking into account the actual branching ratio, ionization probabilities and fragmentation ratios. It can be seen that the signal at each angle for channel (1a) is small and that the distribution is relatively flat. In an experimental distribution, however, an additional contribution from the fragmentation of HCCO to CO would be expected. This contribution is not included in the dashed curve in Fig. 4. As can be seen in Fig. 3, the component arising from HCCO at the mass of CO, would be about 20% of that detected as HCCO. Fig. 5 shows contour diagrams of the product flux for channels (1a) and (1b).

Cross-correlation TOF spectra were measured at laboratory angles of 20°, 35°, 45°, and 55°, using both ^{16}O and ^{18}O. The m/e=41 ($HCC^{16}O^+$) data and the m/e=43 ($HCC^{18}O^+$) data both correspond to the parent ion of the ketenyl radical and contain equivalent information. Only the m/e=43 data will be discussed here. Fig. 6 shows the TOF spectra obtained at m/e=43 at the four different angles (open circles) as well as the best fit (solid line), as discussed below. TOF spectra of m/e=30 ($C^{18}O^+$) were measured under the same conditions as the m/e=43 data, allowing direct and quantitative comparison. Using ^{16}O, TOF-

spectra were measured at m/e=30 in order to detect impurities from various sources contributing the m/e=30 signal. These spectra represent a small correction and were subtracted from the m/e=30 data obtained with ^{18}O. The results are shown in Fig. 7. It is apparent that these spectra consist of two distinct components, one having similar features and peak positions as the corresponding m/e=43 spectra, the other being considerably faster. The slower feature can be attributed to ketenyl radical cracking in the ionizer, whereas the faster component stems from a distinctly different reaction channel, identified as the product CO of reaction (1a).

We also made an attempt to detect the second product of channel (1a), methylene, at m/e=14 using ^{16}O. TOF measurements were made at m/e=14, 16, 26, and 41 using the double-disk assembly. The m/e=26 signal comes from nonreactively scattered acetylene only, m/e=16 from nonreactively scattered oxygen atoms, and m/e=41 from the ketenyl radical. The m/e=14 signal is expected to have components from nonreactively scattered acetylene and a very small amount of leakage of the intense m/e=16 signal (oxygen atoms) to m/e=14 in the quadrupole mass filter, plus an additional, very fast component corresponding to methylene. Despite the very long counting times, the signal-to-noise ratio was very low. However, a fast component which is very likely to be due to methylene formed in reaction (1a) could be identified.

Several complications arose in our TOF measurements.

First, a very fast peak was observed in the TOF-spectra of certain masses, which corresponded to velocities on the order of 10^6 cm/s. This is much faster than any possible product of the primary reaction could be. It is therefore an artifact which does not directly interfere with our analysis, although it does increase the overall noise level in the cross-correlation TOF spectra. This artifact is possibly due to VUV photons created in the oxygen discharge[41] which get scattered into the detector and cause ionization of background atoms or molecules. Another possible source of the fast signal is charge exchange of energetic ions from the source with oxygen atoms.

Second, in some of our data a sinusoidally varying background was observed. Since this background variation was spread over all 255 channels, it appears likely that it arose from an interference of the spinning wheel with the detection process. This artifact was dependent on the dwell time used, suggesting mechanical resonances of the wheel at certain frequencies with other components of the apparatus, and often was completely absent. The data presented here are free of this effect.

Third, a complication arose from a time-correlated signal at several masses, particularly those having a high background count rate, which arose from slow molecules scattering off the walls of the reaction chamber or desorbing from surfaces opposite the detector and passing through the cross-correlation wheel. In order to reduce background scattering, a copper panel

was installed in the viewing zone of the detector behind the scattering region (see Fig. 1) and cooled to about 17 K. This effectively eliminated the time-correlated effusive background from the scattering chamber, but instead gave rise to small dips in the TOF spectra. This effect can be understood in the following way: If all the surfaces near the detector had the same temperature, the number of background molecules entering it would be the same regardless of whether the detector is facing an open or a closed segment of the chopper wheel. Therefore, the dips were created by the absence of molecules desorbing or backscattering from closed segments of the wheel (which is now significantly warmer than the cold panel) and detected at times when the detector faces an open segment of the chopper. The TOF data for m/e=30 shown in Fig. 7 were corrected for this effect.

Analysis of the data was performed using a forward-convolution method. The FORTRAN code was based on versions used previously[44]. The goal of the analysis was to find the product translational energy distribution ($P(E_T)$) and the angular distribution ($T(\theta)$) for the reaction in the center-of-mass frame. $P(E_T)$ and $T(\theta)$ were assumed to be independent of each other. Furthermore, the relative cross-sections within the range of collision energies in our experiment were assumed to be independent of the collision energy. From the $P(E_T)$ and $T(\theta)$ functions, angular distributions and TOF spectra were calculated and averaged over beam velocities and collision angles as well as the detector acceptance angle and the length of the ionizer

and then scaled to the experimental data. This was repeated until a best fit to the experimental data was found. For maximum flexibility, the $P(E_T)$ trial functions were not confined to a particular functional form. The $T(\theta)$ functions on the other hand were represented as linear combinations of Legendre polynomials. For channel (1a), unique angular distributions could not be determined based on the collected data. However, this reaction is expected to go through a long lived complex, as discussed below, and therefore forward-backward symmetry in the center-of-mass angular distribution was imposed in the analysis of the data. The $P(E_T)$ and $T(\theta)$ distributions obtained for channels (1a) and (1b) are shown in Figs. 8 and 9. The solid and dashed lines in Figs. 2, 6 and 7 represent the fits to the data. In Fig. 7 both components contributing to signal at m/e=30, $C^{18}O$ and $HCC^{18}O$, are shown. The agreement of the fits with the experimental data is excellent for the TOF-distributions, and satisfactory for the angular distributions. Deviations between angular distribution data and fit at angles close to either beam are likely to be due to interferences from impurities in the beams.

Since the absolute intensities of the molecular beams, the exact size of the collision volume, and the detection efficiency are not known but do not change in the course of an experiment, only relative reaction cross-sections can be determined for the two reaction channels. The fitting procedure yielded values for the relative total cross-sections σ_a^0 and σ_b^0 for channels (1a)

and (1b), respectively. Corrections for the ionization cross-sections and the fragmentation patterns of the product species have to be applied to obtain the true branching ratio R, defined as the ratio of the total reaction cross-sections σ_a and σ_b for channels (1a) and (1b):

$$R = \frac{\sigma_a}{\sigma_b} = \frac{\sigma_a^0}{\sigma_b^0} \times \frac{Q_{HCCO}}{Q_{CO}} \times \frac{f_{HCCO}^{43}}{f_{CO}^{30}} .$$

Here σ_a^0 and σ_b^0 are the apparent cross-sections derived from the signal at m/e=30 and 43, Q_{HCCO} and Q_{CO} are the ionization cross-sections approximated using the method of Fitch and Sauter[45], and f_{CO}^{30} and f_{HCCO}^{43} are the fractions of $C^{18}O$ and $HCC^{18}O$ which yield ions of m/e=30 and 43, respectively, upon ionization. The mass spectrum of CO from channel (1a) was assumed to be that of the cold molecule and taken from standard tables[46], and the mass spectrum for HCCO (Fig. 3) was constructed from angular distributions and TOF data for major fragments. The values for the minor fragments m/e=12, 16, 24 and 25 were estimated from the comparison with published mass spectra[46] of ketene. The transmission of the quadrupole mass spectrometer was checked by measuring mass spectra of stable molecules and was found to be independent of mass in the small range of masses measured in this experiment.

The TOF measurements at different angles were performed under slightly different beam conditions, but for comparison of

the data for the two different reaction channels at a given angle, great care was taken to maintain constant conditions by frequently alternating between the different masses monitored. Therefore a value for R was calculated from the data at 20°, 35° and 45° separately (the data at 55° were considered too noisy and unreliable). The results are R(20°)=1.4, R(35°)=1.0, and R(45°)=1.7, with an average value of R=1.4.

The error limits on our determination are sizable and due to three main sources. The experimentally derived quantity σ_a^0/σ_b^0 contains errors due to fluctuations in the detection efficiency and errors due to uncertainty in the $P(E_T)$ and $T(\theta)$ distributions, particularly for channel (1a). The correction factor Q_{HCCO}/Q_{CO} is estimated to be reliable to about 20% since an empirical method was used[45] whose applicability to polyatomic radicals has not been tested. The fragmentation pattern for HCCO was measured, but is associated with the same uncertainties all quantitative measurements in our systems carry. The fragmentation of CO was taken from the literature[46]. Fragmentation patterns are known to depend on internal energy[47], however, no large effect is expected for diatomic molecules with a multiple bond. We estimate the uncertainty of the factor $f_{HCCO}^{43}/f_{CO}^{30}$ to be about 20%.

2.4 Discussion

Fig. 10 shows a schematic energy diagram for the reaction $O(^3P) + C_2H_2$. The values in Fig. 10 represent the "best estimates" for the heats of formation at 0 K given by Harding and Wagner[32], which are based on standard tables[48], recent measurements for HCCO[49] and CH_2[50], and ab initio calculations[32,33]. Two triplet states of HCCHO are accessible in the reaction, the higher one ($^3A'$) via an estimated barrier of about 6 kcal/mole. The only reaction path open to this state is dissociation back to reactants. The $^3A''$ state is accessible via a barrier of 3.3 kcal/mole, a value obtained from measured overall rate constants for reaction (1)[32]. In a crossed molecular beams experiment, Clemo et al.[34] measured a threshold energy of about 2 kcal/mole for this process.

1,2-hydrogen migration from the $^3A''$ state of HCCHO leads to triplet ketene, which decomposes to CO and CH_2 via an exit channel barrier. Alternatively, HCCHO in its $^3A''$ state can eliminate a hydrogen atom and form ground state ketenyl radical. The barrier heights for hydrogen elimination and 1,2-hydrogen migration are practically identical[32] and lie well below the total available energy in our experiments. Thus both channels are expected to occur on this triplet surface.

The experimental results are in agreement with the theoretical predictions[32,33]. The maximum release of translational energy in both cases approximately corresponds to

the total available energy, the sum of exothermicity, collision energy, and the internal energy of C_2H_2 left after the supersonic expansion. The exothermicities of channel (1a) and (1b), 46.9 and 19.1 kcal/mole, respectively, were taken from the best estimates in Ref. 32. Both $P(E_T)$ distributions peak at a large fraction of this maximum energy (27% or 14 kcal/mole for channel (1a), 34% or 11 kcal/mole for channel (1b)), which is indicative of an exit channel barrier[51,52] in each case. It should be noted that the center-of-mass to laboratory frame transformation Jacobian caused the fits to be much more sensitive to the low energy part of the $P(E_T)$ and that a change of the maximum energy by several kcal/mole did not greatly affect the fits, particularly for channel (1a). Therefore, the exact exothermicities could not be determined in this experiment.

In the case of channel (1b), the fit was significantly improved by allowing translational energies of up to 32 kcal/mole, or about 7 kcal/mole more than the total available energy according to Fig. 10. It is possible that the true exothermicity for channel (1b) is somewhat larger than that shown in Fig. 10. On the other hand, there are two possible sources of reaction products with large translational energies. First, there could be products of the reaction of acetylene dimers with $O(^3P)$ detected at m/e=43 and m/e=41. However, no indication of the presence of dimers in the acetylene beam was found. Second, small amounts of $O(^1D)$ atoms could be present,

even though they could not be detected in the beam. The reaction cross section for $O(^1D)$ could be significantly higher than for $O(^3P)$, and since the energy available to the products would be considerably larger, larger product velocities would be expected.

The $T(\theta)$ or angular distribution in the center-of-mass frame for channel (1b) is symmetric about 90° indicating that the lifetime of the collision complex exceeds its rotational period[53] which is estimated to be about 10^{-12}s. The observation of an intermediate life time exceeding one rotational period is in agreement with early bulk phase results that estimated the lifetime of the adduct as 10^{-9} - 10^{-11} s[22,54].

The $T(\theta)$ for channel (1a) could not be obtained easily from our data since, in contrast to the other case, both the laboratory angular distributions and the TOF distributions for the CO product only probe a limited range of $T(\theta)$ due to the unfavorable kinematic relations. Although the coarse angular distribution obtained by integrating over the TOF distributions for the four angles available were better fit using the assumption of more forward than backward scattered product, the $T(\theta)$ for this channel was also chosen to be symmetric about 90°. This appears to be a reasonable assumption since both hydrogen migration and hydrogen elimination take place from the same precursor with similar barrier heights and they are the rate determining steps for channel (1a) and (1b). Using the forward peaking $T(\theta)$ would result in a calculated branching ratio of 0.9

instead of 1.4.

Comparing our results for channel (1b) with a previous crossed molecular beams experiment[34], we find that the $P(E_T)$ reported by these authors fits our TOF-data reasonably well, but results in larger deviations between the calculated and experimental laboratory angular distribution. This is due to the fact that the low-energy part and the peak of their $P(E_T)$ resembles ours, whereas they propose a sharp cutoff at a translational energy of about 20 kcal/mole. Thus the wings of our angular distribution, corresponding mostly to faster products, are not reproduced well.

Little is known about the internal energy distribution of the products from channels (1a) and (1b). Shaub et al.[55] have measured the vibrational energy distribution in the CO product using a CO-laser absorption technique and found about 6% of the total available energy in CO-vibration (excitation up to v=5). Their results were compatible with a statistical model[52]. Inoue and Suzuki[16] obtained laser induced fluorescence spectra for HCCO produced from the reaction of $O(^3P)$ + acetylene and determined the vibrational frequencies of the HCCO radical, but not the nascent energy distribution.

The possibility of intersystem crossing to the singlet surface in the long lived intermediate has to be considered. The products expected from the decomposition of singlet HCCHO are CO and $CH_2(^1A_1)$. Intersystem crossing was shown to take place under collisionless conditions in C_2H_4O, the radical

formed from $O(^3P)$ addition to ethylene[56]. For the reaction $O(^3P) + C_2H_2$, Harding and Wagner[32] estimate that inclusion of intersystem crossing in their calculations causes only a small increase in the branching ratio σ_a/σ_b at temperatures below 500K.

Although we are unable to distinguish between singlet and triplet CH_2 with our detection techniques, our data are consistent with product translational energy in channel (1a) extending out to the total available energy for the formation of $^3CH_2$. In the case of $^1CH_2$ formation about 9 kcal/mole less energy would be available[57]. Furthermore, the $P(E_T)$ distribution found for channel (1a) peaks at a relatively large value, indicating the existence of an exit channel barrier typical for dissociation on triplet surfaces, whereas such barriers are usually not found on singlet surfaces. Ab initio calculations by Bargon et al.[58] show that the singlet HCCHO lies about 17 kcal/mole higher than the corresponding triplet and that there is no barrier to 1,2-hydrogen migration forming ketene on the singlet surface. Hayden et al.[59] have studied the photodissociation of ketene in a molecular beam and found that at 308 nm ketene is excited only to its singlet state. The distribution of translational energy in the dissociation products peaked at 0 kcal/mole, whereas dissociation on the triplet surface after excitation at 351 nm resulted in a $P(E_T)$ peaking well away from zero. This indicates that in our crossed beams experiment at least a large fraction of the HCCHO formed

in the O + acetylene reaction decomposes on the triplet surface.

No attempts were made in our experiment to search for the hydrogen abstraction channel (1d) since it was not energetically accessible under our experimental conditions. It is also unlikely that channel (1e), the formation of C_2O, is major one, since the shapes of the TOF spectra and angular distributions of m/e=41 ($HCCO^+$) and m/e=40 (CCO^+) in our experiments were superimposable within error limits after appropriate scaling. This indicates that both ions derive from the same parent and no additional components are present.

Having established channels (1a) and (1b) as the only major channels in the O + C_2H_2 reaction, we obtained a value of 1.4 ± 0.5 for the branching ratio corresponding to 58% (46-65%) production of CH_2 + CO. Our result of approximately equal probability for both channels is in good agreement with the most recent values from other laboratories of 30-40%[26], 38%[31], 41%[30], 46-64%[25], and about 50%[23] reaction for channel (1a) and the calculations by Harding and Wagner[32].

Despite the large error margins our determination yields important information since we measured the branching ratio under truly single collision conditions. The uncertainties in the results of previous investigations are sizable as well: In their study of CH_2 kinetics, Vinckier and Debruyn[23] found a factor of two uncertainty in the absolute CH_2 concentration determinations causing a substantial uncertainty in the branching ratio of the O + C_2H_2 reaction. In the shock tube

experiments of Löhr and Roth[25], expressions for the rate coefficients for reactions (1a) and (1b) were obtained from fits to H- and O-atom concentration profiles. No error limits were reported. From a more recent shock tube experiment, Frank et al.[26] obtained rate coefficients whose error was estimated to be about 20-30% for both channels (1a) and (1b). Peeters et al.[30] measured the HCCO yield mass spectrometrically and reported error limits of ±20%. In all of these experimental investigations[23,25,26,30] secondary processes had to be included in the analysis of the system. The results of the calculations by Harding and Wagner[32] indicate a range of about 5-75% occurrence of channel (1a) at 300K.

We did not measure the dependence of the relative cross-sections on collision energy. However, both recent theoretical[32] and experimental results[26,30] indicate only a small temperature dependence of the branching ratio. This is most probably due to the fact that the barrier for either dissociation channel is substantially lower than the barrier to adduct formation. As a consequence, the adduct always has enough energy to decay to either product.[60]

2.5 **Conclusions**

Using the crossed molecular beams technique, we have confirmed the occurrence of two major channels in the reaction

of ground state oxygen atoms and acetylene under single collision conditions, namely formation of methylene and carbon monoxide (channel (1a)) and formation of hydrogen atom and ketenyl radical (channel (1b)). We have determined an approximate value for the branching ratio which is in agreement with recent bulk phase measurements. The center-of-mass frame angular distributions show that the reaction proceeds through a long-lived intermediate, which consequently dissociates along two different reaction paths, each characterized by an exit channel barrier, resulting in large releases of product translational energy. The dynamical features of this reaction were found to be in agreement with recent theoretical predictions.

2.6. References

1. P. R. Westmoreland, J. B. Howard, and J. P. Longwell, Twenty-First Symposium (International) on Combustion (Combustion Institute, Pittsburgh, 1988), p. 773.
2. A. Fontijn and S. E. Johnson, J. Chem. Phys. 59, 6193 (1973).
3. K. H. Becker and K. D. Bayes, J. Chem. Phys. 48, 653 (1968).
4. J. Grebe and K. H. Homann, Ber. Bunsenges. Phys. Chem. 86, 587 (82).
5. D. M. Creek, C. M. Melliar-Smith, and N. Jonathan, J. Chem. Soc. (A) 1970, 646; P. N. Clough, S. E. Schwartz, and B. A. Thrush, Proc. Royal Soc. Lond. A 317, 575 (1970).
6. A. N. Hayhurst and D. B. Kittelson, Combust. Flame 31, 37 (1978); C. Vinckier, M. P. Gardner, and K. D. Bayes, Sixteenth Symposium (International) on Combustion (Combustion Institute, Pittsburgh, 1977), p. 881.
7. K. H. Homann and Ch. Wellmann, Ber. Bunsenges. Phys. Chem. 87, 609 (1983); J. Warnatz, H. Bockhorn, A. Moser, and H. W. Wenz, Nineteenth Symposium (International) on Combustion (Combustion Institute, Pittsburgh, 1982), p. 197.
8. M. Frenklach, D. W. Clary, T. Yuan, W. C. Gardiner, Jr., and S. E. Stein, Comb. Sci. and Tech. 50, 79 (1986); H. Gg. Wagner, Seventeenth Symposium (International) on Combustion

(Combustion Institute, Pittsburgh, 1979), p. 3.

9. C. K. Westbrook and F. L. Dryer, Eighteenth Symposium (International) on Combustion (Combustion Institute, Pittsburgh, 1981), p. 749; J. Warnatz, Eighteenth Symposium (International) on Combustion (Combustion Institute, Pittsburgh, 1981), p. 369.

10. J. A. Miller, R. E. Mitchell, M. D. Smooke, and R. J. Kee, Nineteenth Symposium (International) on Combustion (Combustion Institute, Pittsburgh, 1982), p. 181; A. Garo, P. R. Westmoreland, J. B. Howard, and J. P. Longwell, Combust. Flame 72, 271 (1988).

11. K. Mahmud and A. Fontijn, J. Phys. Chem. 91, 1918 (1987), and references therein.

12. R. Cvetanovic, Adv. Photochem. 1, 115 (1963).

13. C. P. Fenimore and G. W. Jones, J. Chem. Phys. 39, 1514 (1963).

14. I. T. N. Jones and K. D. Bayes, J. Am. Chem. Soc. 94, 6869 (1972).

15. Y. Endo and E. Hirota, J. Chem. Phys. 86, 4319 (1987).

16. G. Inoue and M. Suzuki, J. Chem. Phys. 84, 3709 (1986).

17. I. Haller and G. C. Pimentel, J. Am. Chem. Soc. 84, 2855 (1962).

18. H. Gaedtke, K. Glänzer, H. Hippler, K. Luther, and J. Troe, Fourteenth Symposium (International) on Combustion (Combustion Institute, Pittsburgh, 1973), p. 295.

19. J. N. Bradley and G. B. Kistiakowsky, J. Chem. Phys. 35,

264 (1961).

20. A. M. Wodtke and Y. T. Lee, J. Phys. Chem. 89, 4744 (1985).

21. K. H. Becker and K. D. Bayes, J. Chem. Phys. 45, 396 (1966); K. H. Becker, D. Kley, and R. J. Norstrom, Twelfth Symposium (International) on Combustion (Combustion Institute, Pittsburgh, 1969), p. 405.

22. D. G. Williamson and K. D. Bayes, J. Phys. Chem. 73, 1232 (1969).

23. C. Vinckier and W. Debruyn, Seventeenth Symposium (International) on Combustion (Combustion Institute, Pittsburgh, 1979), p. 623.

24. E. N. Aleksandrov, V. S. Arutyunov, and S. N. Kozlov, Kinet. Katal. 22, 513 (1981).

25. R. Löhr and P. Roth, Ber. Bunsenges. Phys. Chem. 85, 153 (1981).

26. P. Frank, K. A. Bhaskaran, and Th. Just, Twenty-First Symposium (International) on Combustion (Combustion Institute, Pittsburgh, 1988), p. 885.

27. D. G. Williamson, J. Phys. Chem. 75, 4053 (1971).

28. I. T. N. Jones and K. D. Bayes, Fourteenth Symposium (International) on Combustion (Combustion Institute, Pittsburgh, 1973), p. 277.

29. B. Blumenberg, K. Hoyermann, and R. Sievert, Sixteenth Symposium (International) on Combustion (Combustion Institute, Pittsburgh, 1977), p. 841.

30. J. Peeters, M. Schaekers, and C. Vinckier, J. Phys. Chem.

90, 6552 (1986).

31. F. Temps, personal communication.

32. L. B. Harding and A. F. Wagner, J. Phys. Chem. 90, 2974 (1986).

33. C. F. Melius, unpublished results.

34. A. R. Clemo, G. L. Duncan, and R. Grice, Trans. Faraday Soc. 2, 78, 1231 (1982); 79, 637 (1983).

35. R. J. Baseman, Ph. D. Thesis, University of California, Berkeley, 1982.

36. Y. T. Lee, J. D. McDonald, P. R. LeBreton, and D. R. Herschbach, Rev. Sci. Instrum. 40, 1402 (1969).

37. G. O. Brink, Rev. Sci. Instrum. 37, 857 (1966).

38. N. R. Daly, Rev. Sci. Instrum. 31, 264 (1960).

39. K. Sköld, Nucl. Instrum. Methods 63, 114 (1968); V. L. Hirschy and J. P. Aldridge, Rev. Sci. Instrum. 42, 381 (1971); G. Comsa, R. David, and B. J. Schumacher, Rev. Sci. Instrum. 52, 789 (1981).

40. J. M. Parson, K. Shobatake, Y. T. Lee, and S. A. Rice, J. Chem. Phys. 59, 1402 (1973).

41. S. J. Sibener, R. J. Buss, C. Y. Ng, and Y. T. Lee, Rev. Sci. Instrum. 51, 167 (1980).

42. R. J. Buss, P. Casavecchia, T. Hirooka, S. J. Sibener, and Y. T. Lee, Chem. Phys. Lett. 82, 386 (1981).

43. D. J. Krajnovich, Ph. D. Thesis, University of California, Berkeley, 1983.

44. R. J. Buss, Ph. D. Thesis, University of California,

Berkeley, 1979.

45. W. L. Fitch and A. D. Sauter, Anal. Chem. 55, 832 (1983).

46. Atlas of Mass Spectral Data, E. Stenhagen, S. Abrahamsson, and F. W. McLafferty, editors, Vol. 1 (Wiley, New York, 1969).

47. H.-G. Rubahn, J. P. Toennies, and M. Wilde, Chem. Phys. Lett. 120, 11 (1985), and references therein.

48. M. W. Chase, Jr., J. L. Curnutt, J. R. Downey, Jr., R. A. McDonald, A. N. Syverus, and E. A. Valenzuela, J. Phys. Chem. Ref. Data 11, 695 (1982): JANAF Thermochemical Tables, 1982 Supplement.

49. J. M. Oakes, M. E. Jones, V. M. Bierbaum, and G. B. Ellison, J. Phys. Chem. 87, 4810 (1983).

50. K. E. McCulloh and V. H. Dibeler, J. Chem. Phys. 64, 4445 (1976).

51. D. R. Herschbach, Discuss. Faraday Soc. 55, 233 (1973); R. A. Marcus, J. Chem. Phys. 62, 1372 (1975).

52. S. A. Safron, N. D. Weinstein, D. R. Herschbach, and J. C. Tully, Chem. Phys. Lett. 12, 564 (1972).

53. W. B. Miller, S. A. Safron, and D. R. Herschbach, Faraday Discuss. Chem. Soc. 44, 108 (1967).

54. C. A. Arrington, W. Brennen, G. P. Glass, J. V. Michael, and H. Niki, J. Chem. Phys. 43, 525 (1965).

55. W. M. Shaub, T. L. Burks, and M. C. Lin, Chem. Phys. 45, 455 (1980).

56. Chapter 3; A. M. Schmoltner, P. M. Chu, R. J. Brudzynski,

and Y. T. Lee, J. Chem. Phys., in press.

57. A. R. W. McKellar, P. R. Bunker, T. J. Sears, K. M. Evenson, R. J. Saykally, and S. R. Langhoff, J. Chem. Phys. 79, 5251 (1983).

58. J. Bargon, K. Tanaka, and M. Yoshimine, in: (Symposium on) Computational Methods in Chemistry, J. Bargon, editor, (Plenum, New York, 1980), p. 239.

59. C. C. Hayden, D. M. Neumark, K. Shobatake, R. K. Sparks, and Y. T. Lee, J. Chem. Phys. 76, 3607 (1982).

60. T. H. Dunning, L. B. Harding, A. F. Wagner, G. C. Schatz, and J. M. Bowman, Science 240, 453 (1988).

2.7. Figures

Figure Captions

Fig. 1 Schematic top view of the crossed molecular beam apparatus. Shown are the source, differential pumping chambers and interaction chamber as well as the rotatable mass spectrometer detector. Dashed lines indicate the directions of the supersonic reactant beams and products entering the detector.

Fig. 2 Laboratory angular distribution of the $HCC^{18}O$ product (m/e=43). Angles are measured from the oxygen atom beam. Scattered points: measured data points; dashed line: fit.

Fig. 3 Mass spectrum determined for the ketenyl radical.

Fig. 4 Simulated angular distributions for channel (1a) at $HCCO^+$, solid curve, and channel (1b) at CO^+, dashed curve, using the results of the present experiment including dynamical information, ionization cross sections and fragmention probabilities, but ignoring the component of ketenyl radical fragmenting into CO^+ in the dashed curve.

Fig. 5 Newton diagrams of beam velocities and contour diagrams of product flux for CO from channel (1a) and for HCCO from channel (1b).

Fig. 6 Time-of-flight spectra for products at m/e=43

($HCC^{18}O^+$) at four different laboratory angles. Solid lines: fits, scaled to the data for each angle separately.

Fig. 7 Time-of-flight spectra for products at m/e=30 ($C^{18}O^+$) at four different laboratory angles. Solid lines: fits for components due to channel (1a); dashed lines: fits for components due to channel (1b). Calculated curves are scaled to the data for each angle and each channel separately.

Fig. 8 Translational energy distributions ($P(E_T)$) for channels (1a) and (1b).

Fig. 9 Center-of-mass angular distributions ($T(\theta)$) for channels (1a) and (1b).

Fig. 10 Schematic energy diagram for the reaction of $O(^3P)$ with acetylene. The values for the energy levels were taken to be the "best estimates" in Ref. 32.

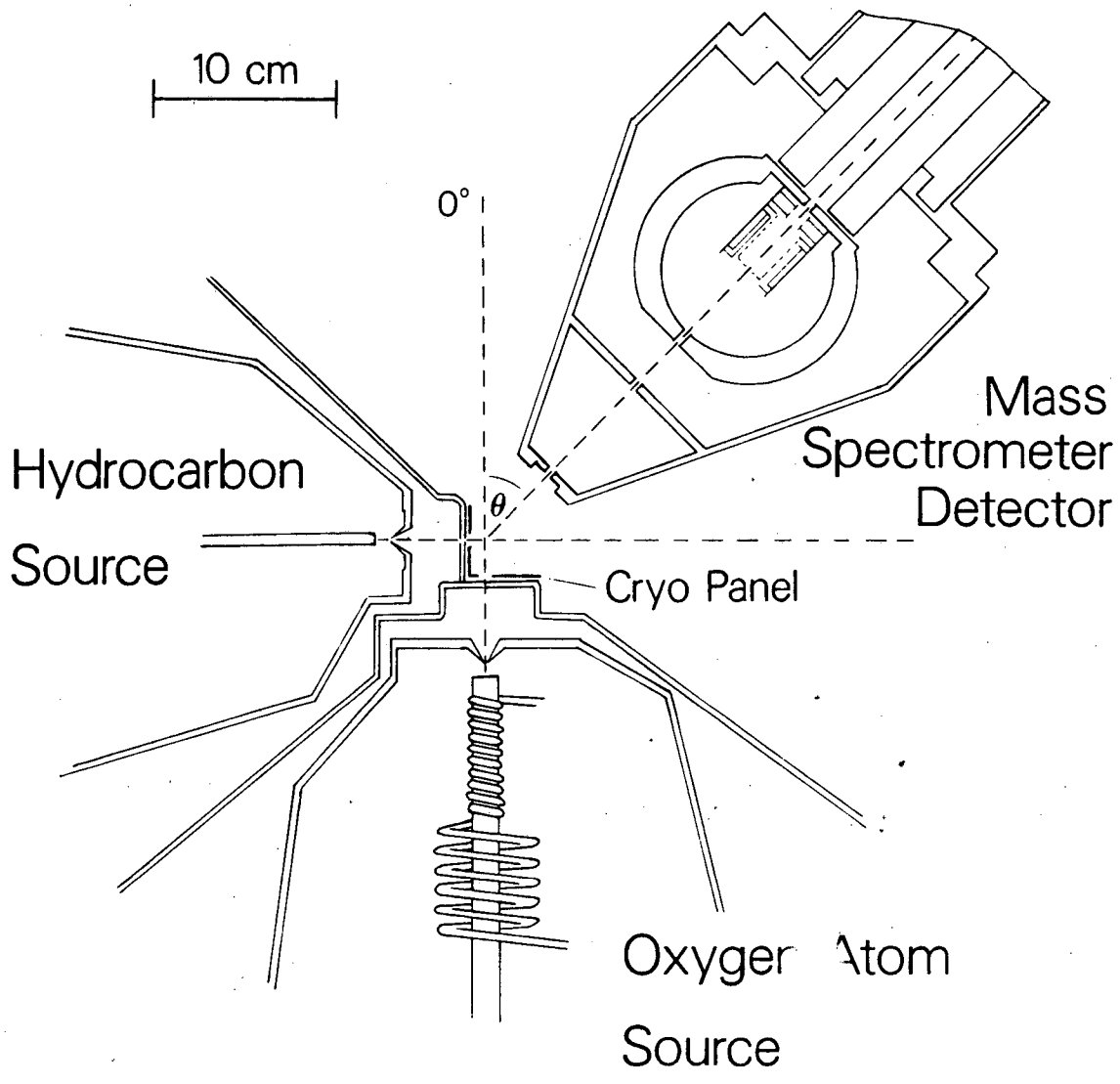
10 cm
0°
θ
Mass
Spectrometer
Detector
Hydrocarbon
Source
Cryo Panel
Oxygen Atom
Source
XBL 892-678A

Fig. 1

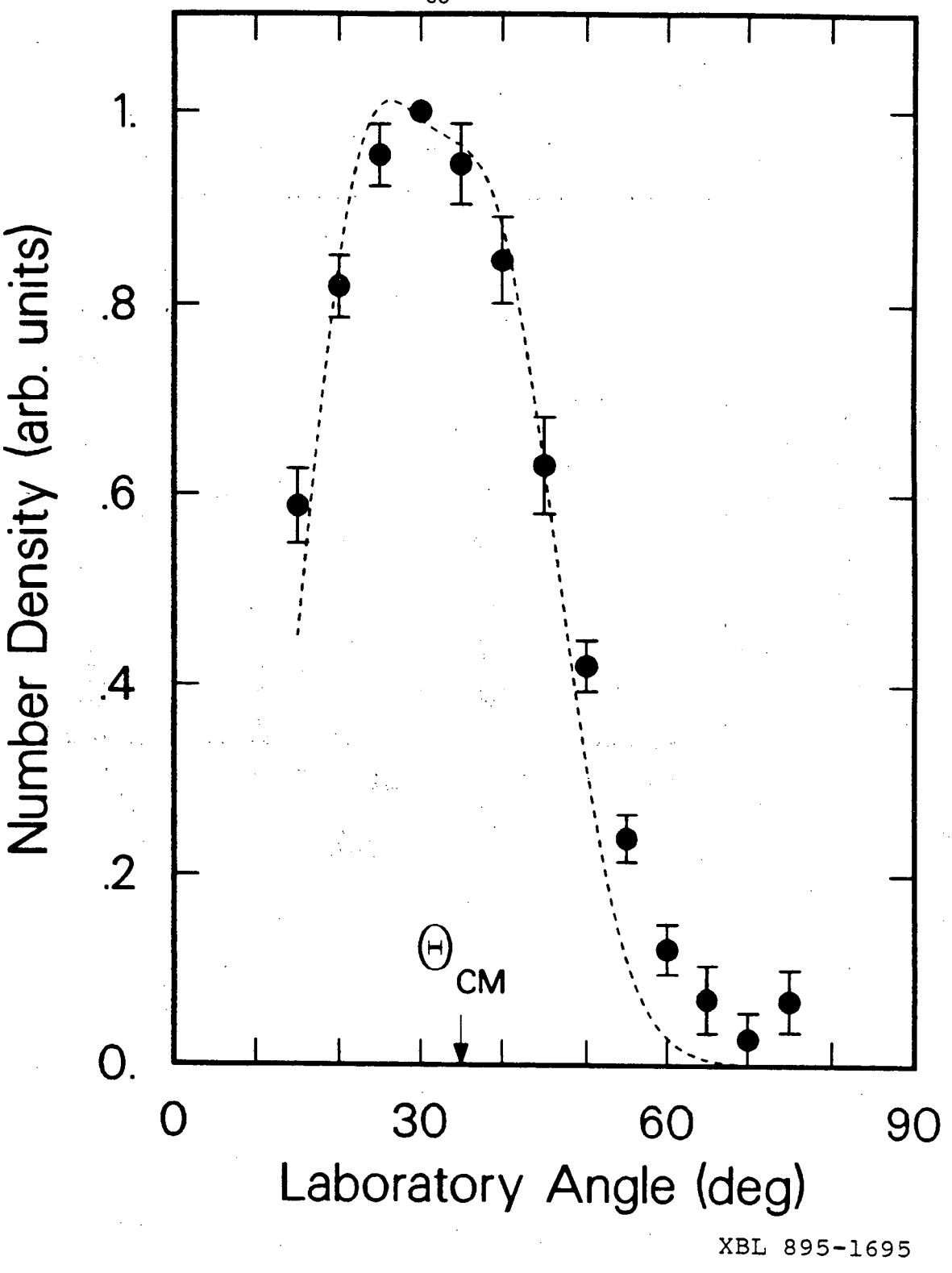

XBL 895-1695

Fig. 2

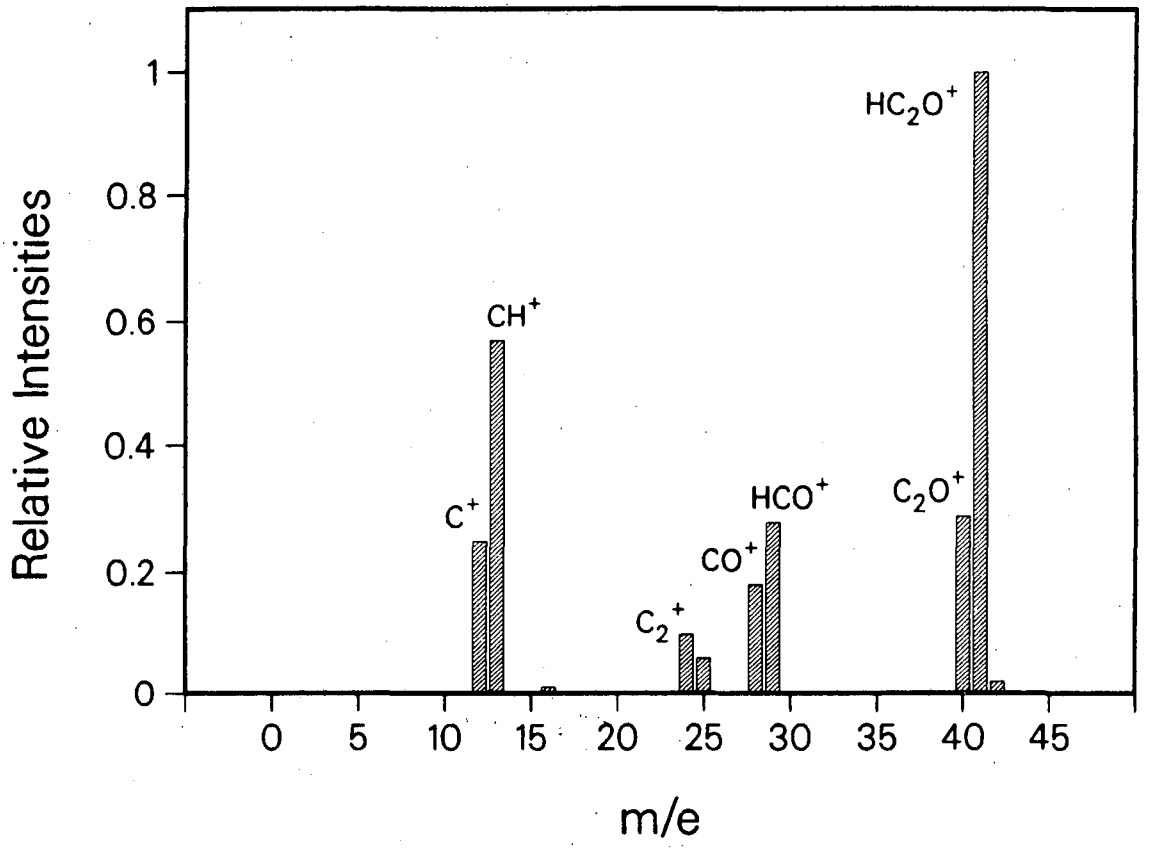

XBL 895-1694

Fig. 3

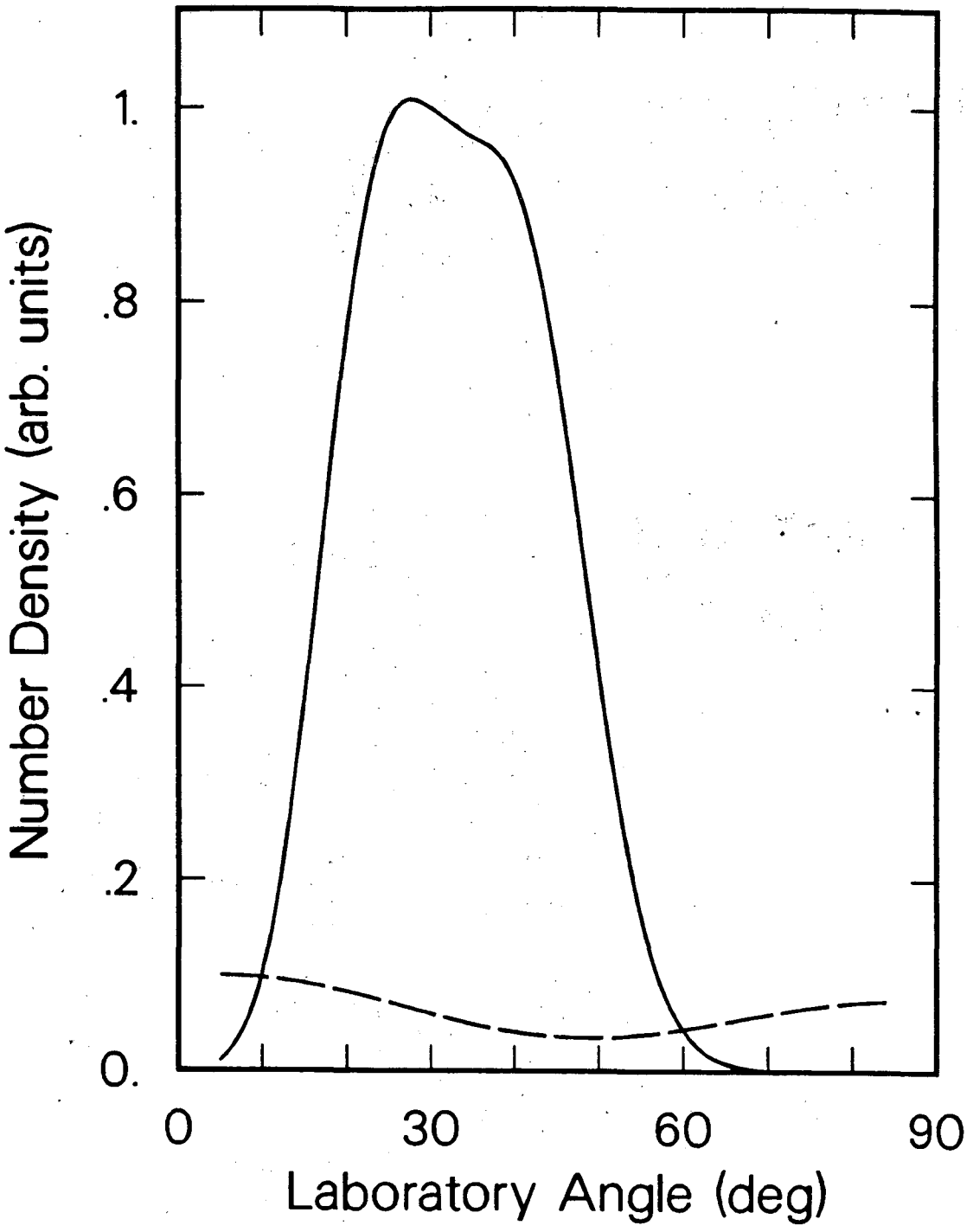

XBL 897-2675

Fig. 4

$O(^3P) + C_2H_2 \rightarrow$

$H + \underline{HCCO}$

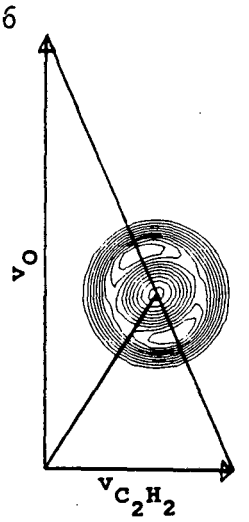

$O(^3P) + C_2H_2 \rightarrow$

$CH_2 + \underline{CO}$

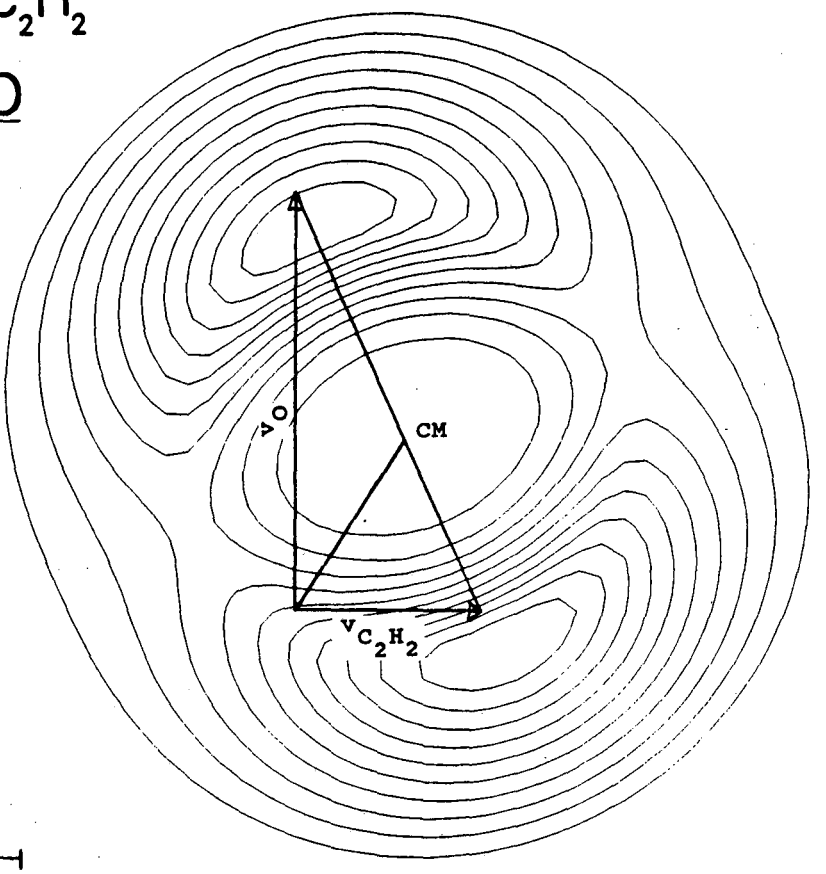

XBL 896-2105

Fig. 5

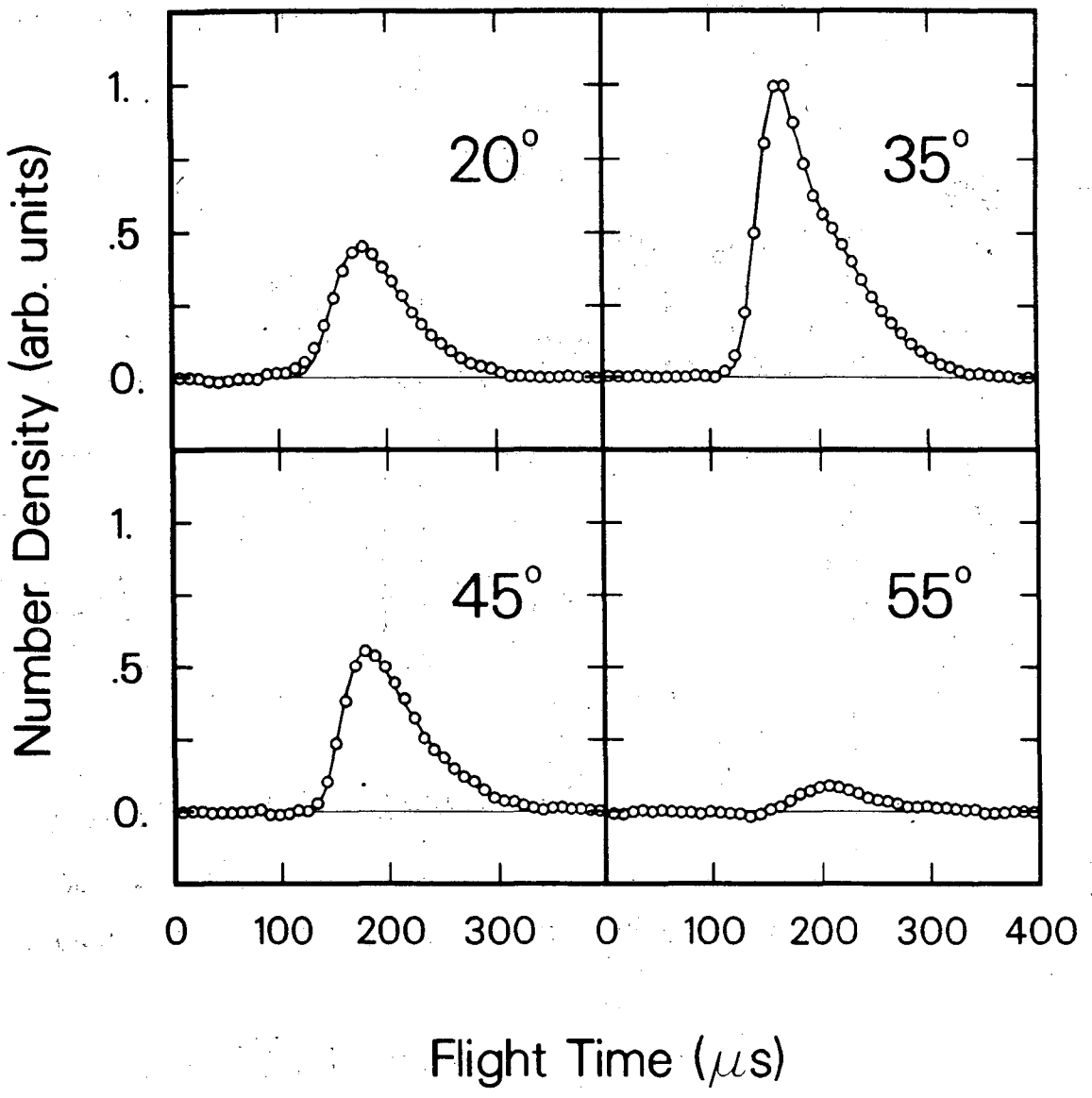

XBL 895-1696

Fig. 6

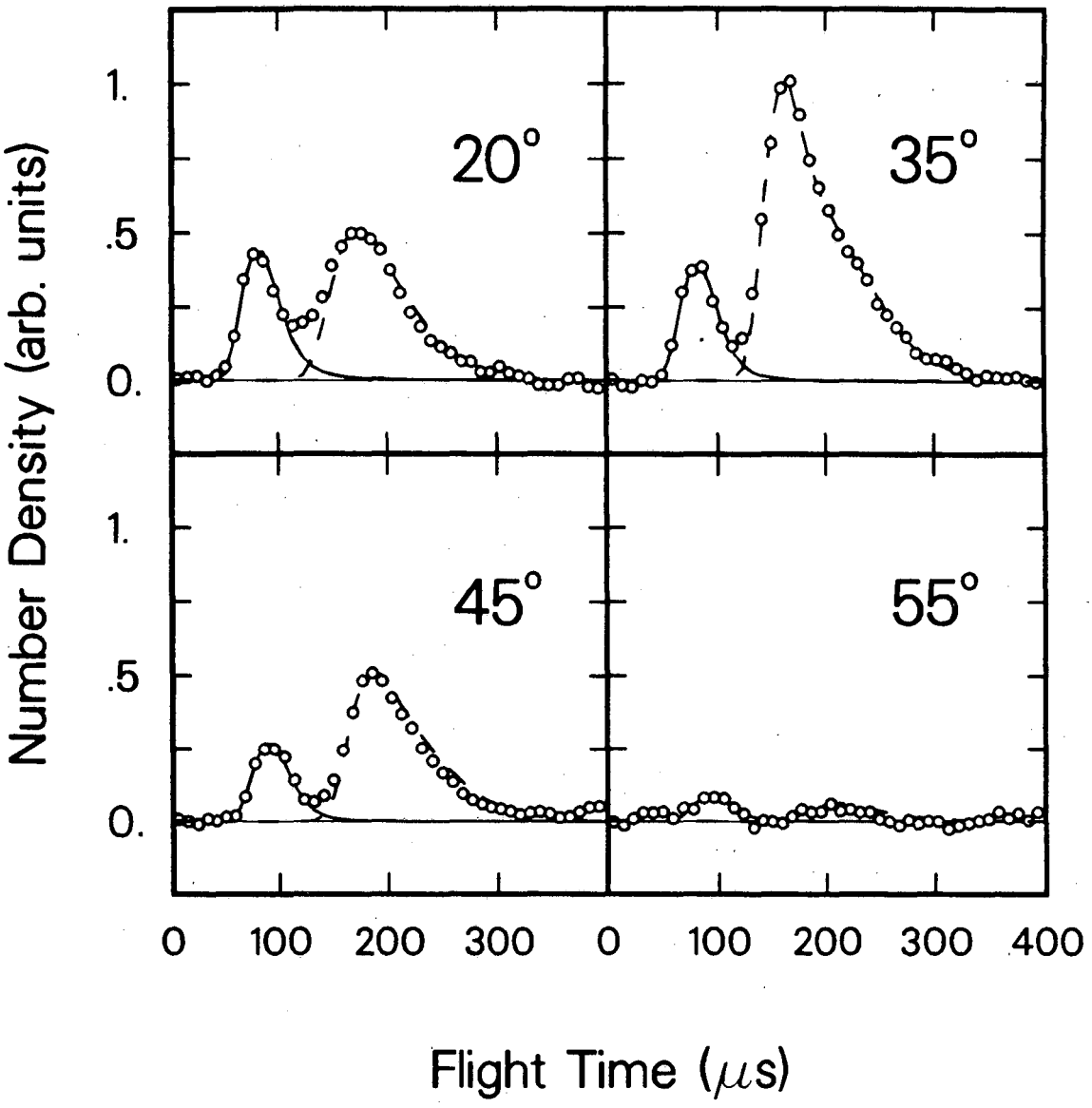

XBL 895-1697

Fig. 7

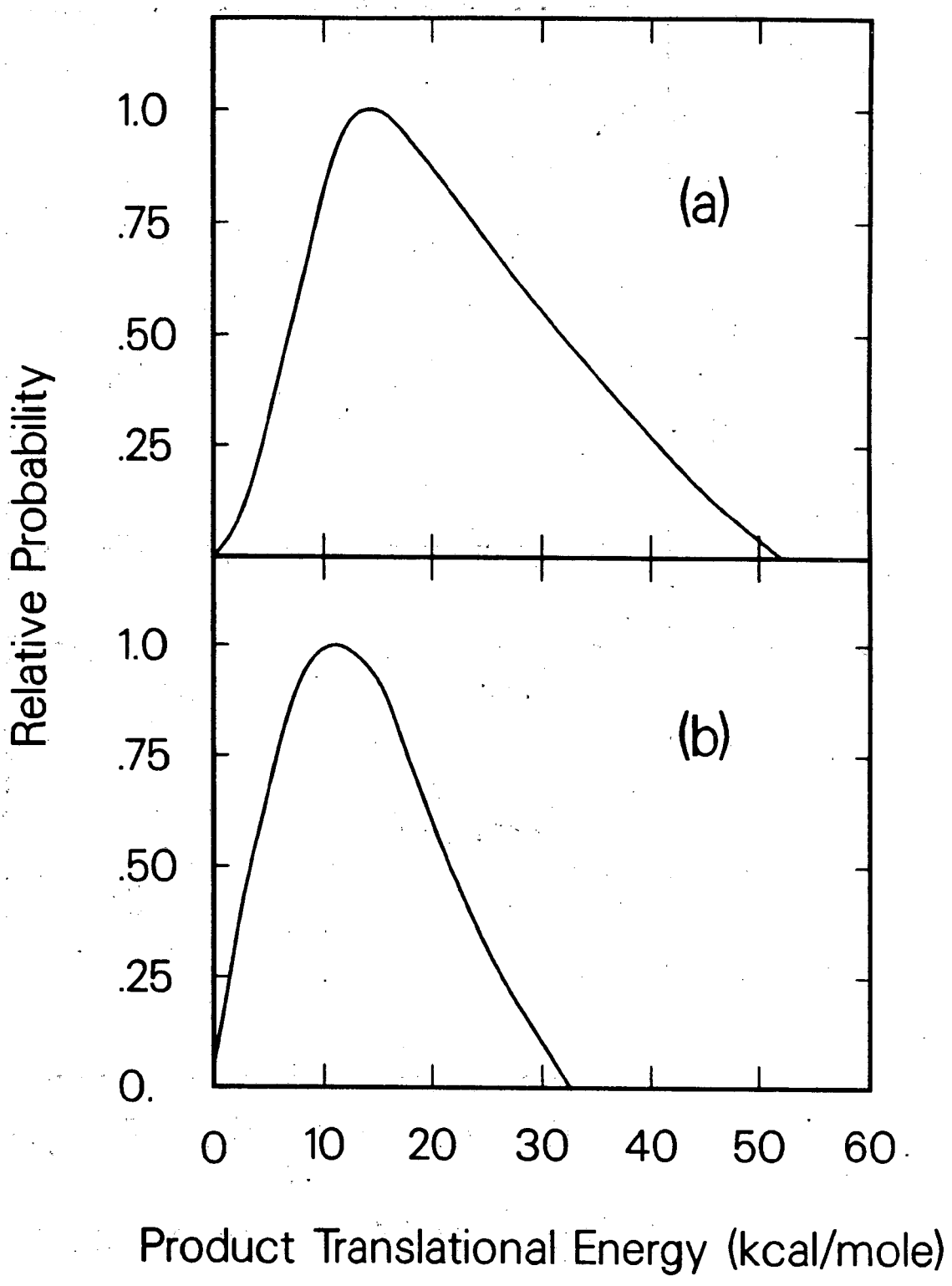

XBL 895-1699

Fig. 8

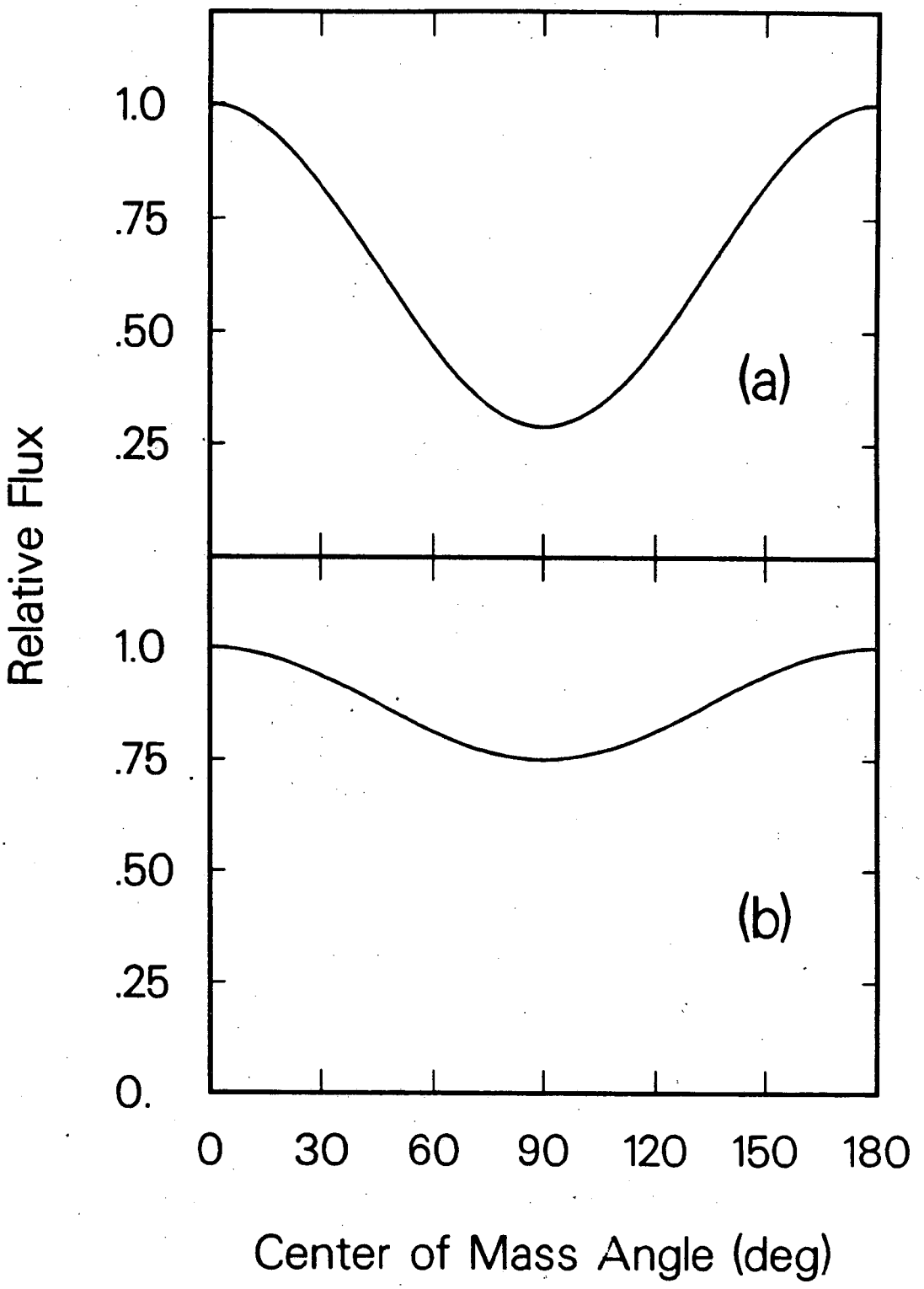

XBL 895-1698

Fig. 9

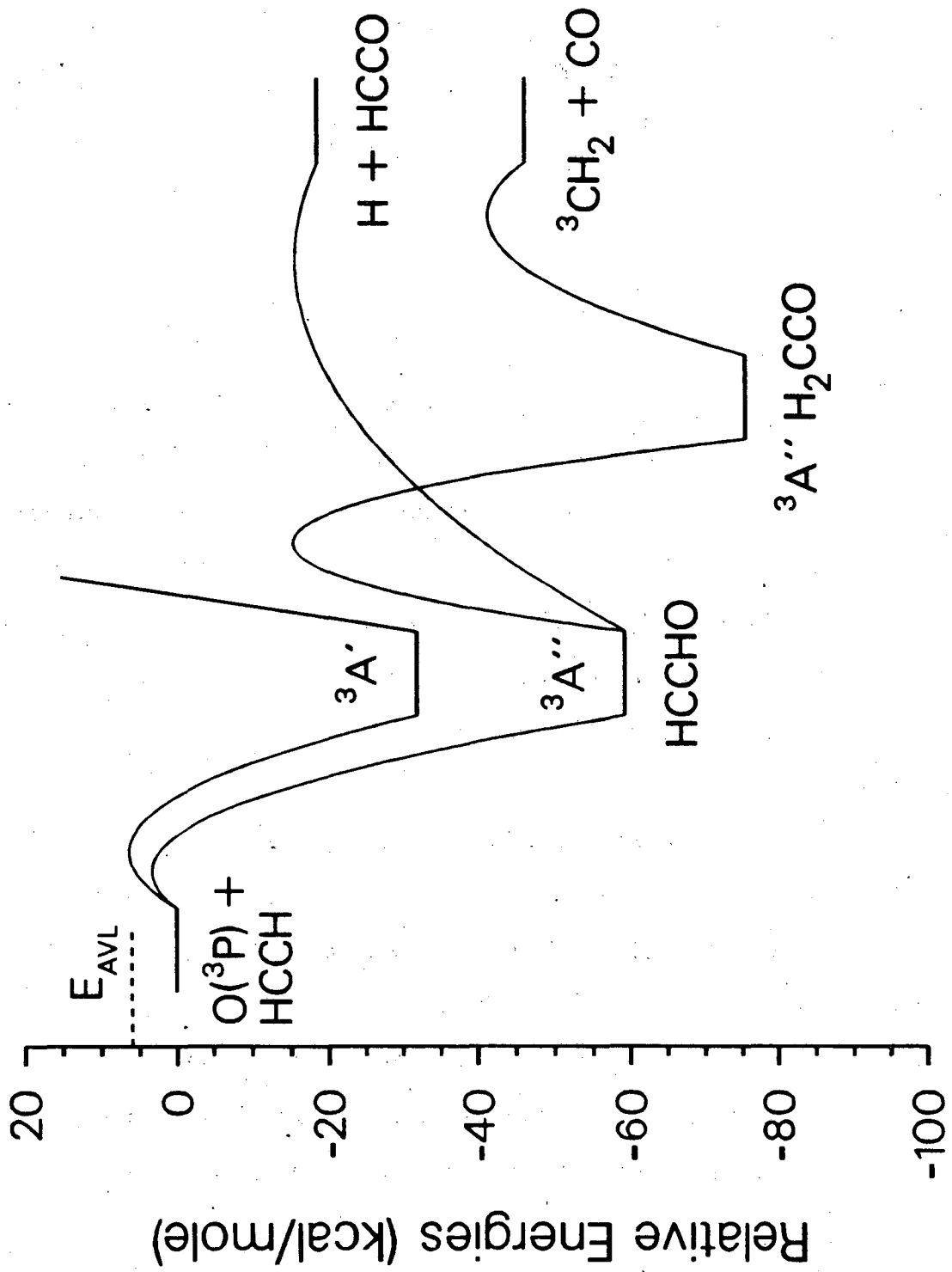
Relative Energies (kcal/mole)
20
0
-20
-40
-60
-80
-100
E_{AVL}
$O(^3P)$ + HCCH
$^3A'$
$^3A''$
HCCHO
$^3A''$ H_2CCO
H + HCCO
$^3CH_2$ + CO
XBL 895-1700

Fig. 10

CHAPTER 3

CROSSED MOLECULAR BEAM STUDY OF THE REACTION $O(^3P) + C_2H_4$

3.1. Introduction

The reaction of $O(^3P)$ with ethylene plays an important role not only in the combustion of ethylene itself, but also for many other fuels since ethylene is an important intermediate in the combustion of methane,[1,2] larger aliphatic hydrocarbons,[3] and aromatics.[4] In ethylene flames, the fuel consumption by oxygen atoms plays a crucial role[2,5-7] although the reaction of ethylene with OH radicals appears to dominate, particularly at higher temperatures.[6,7]

Modeling calculations are used extensively to describe combustion systems. Westbrook[7] has developed a comprehensive mechanism for ethylene combustion which has been extended and successfully applied to many kinds of experimental conditions.[6,8] For calculations of this kind, detailed knowledge of all the primary chemical processes involved, their rate coefficients, and the identity of all reaction channels are essential.

Good agreement has been obtained for the rate coefficient of the overall reaction of $O(^3P)$ with C_2H_4 over a large range of

temperatures.[9] The Arrhenius plots are definitely curved and good fits are obtained by using double-exponential expressions.

The identity of the primary reaction products and their relative importance has been a subject of considerable controversy for many years. However, a clear picture seems to be emerging from various recent experimental investigations. We present here the results of a new molecular beam investigation which can provide an answer to the question of the major primary reaction channels and the reason for some of the apparent contradictions.

Previous work on the $O(^3P) + C_2H_4$ reaction was reviewed recently.[10] The following reactions have been considered as possible primary channels:

$$O(^3P) + C_2H_4 \rightarrow CH_3 + CHO \qquad (1a)$$

$$O(^3P) + C_2H_4 \rightarrow H + CH_2CHO \qquad (1b)$$

$$O(^3P) + C_2H_4 \rightarrow H_2 + CH_2CO \qquad (1c)$$

$$O(^3P) + C_2H_4 \rightarrow CH_2 + CH_2O \qquad (1d)$$

$$O(^3P) + C_2H_4 \rightarrow C_2H_4O \qquad (1e)$$

$$O(^3P) + C_2H_4 \rightarrow OH + C_2H_3 \qquad (1f)$$

Cvetanovic[11,12] suggested a mechanism of electrophilic addition of the oxygen atom in the ^3P state to one of the olefinic carbon atoms, followed by rearrangement or fragmentation of the initially formed triplet diradical $(CH_2CH_2O)^{\ddagger}$. Intersystem Crossing (ISC) to the ground state

singlet surface and stabilization of the adduct through collisions, channel (1e), was indeed observed in rare gas matrices[13,14] and in the gas phase at high pressure.[15,16] Eusuf and Wagner[15] found only acetaldehyde at pressures of 20-80 atm., whereas Bley et al.[16] detected both acetaldehyde and ethylene oxide at pressures of 4-70 atm. Vinyl alcohol was found only in the matrix study by Hawkins and Andrews,[14] but was possibly due to the reaction of $O(^1D)$ in that experiment.

In the absence of stabilizing collisions, the intermediate diradical or its rearrangement products undergo fragmentation. Although some early work[17] suggested channel (1d), the formation of formaldehyde and methylene, to be the major primary route, most authors[11,18-21] found channel (1a), formation of methyl radical and formyl radical, to be dominant. From the stoichiometric balance, Cvetanovic[18] suggested the existence of additional channels: the formation of hydrogen atom and the vinoxy radical C_2H_3O, channel (1b), and the formation of molecular hydrogen and ketene, channel (1c), although ketene was not detected as a product in their experiment. The high-intensity molecular beam experiments with mass spectrometric detection carried out later by Gutman and coworkers[20] and Blumenberg et al.[21] did identify (1c) as a minor channel, accounting for about 5% of the products.

Channel (1f), abstraction of H to form OH and vinyl radical, is endothermic by approx. 6 kcal/mole[22] and is assumed to proceed without an intermediate collision complex, but with a

barrier of about 12 kcal/mole.[23] It was never observed directly but is assumed to play an important role at higher temperatures[7] and may explain the origin of the curvature in the $O(^3P) + C_2H_4$ Arrhenius plots and the two exponential terms in the rate expression.[9]

While it appeared that agreement had been reached that channel (1a), formation of CH_3 and CHO, was the dominant process in the $O(^3P) + C_2H_4$ reaction, more recent experimental and theoretical results led to a different conclusion. A molecular beams experiment conducted in our laboratory[24] firmly established channel (1b), formation of H atoms and C_2H_3O, as an important primary process from the measurements of product angular distributions. This was the first investigation of the $O(^3P) + C_2H_4$ reaction under truly single collision conditions, where primary reaction products could be identified without any of the complications caused by secondary processes in bulk phase studies. Even though the dominant product was detected at the mass-to-charge ratio m/e=42 ($C_2H_2O^+$), it was assigned to the vinoxy radical. In another crossed molecular beam experiment, Clemo et al.[25,26] also detected the vinoxy radical and obtained a threshold value of 1.2±0.7 kcal/mole for this process.

Spectroscopic information about the vinoxy radical became available from an LIF experiment by Inoue and Akimoto[27] and UV absorption[28] and was used by Kleinermanns and Luntz[29] and Hunziker et al.[28] to identify vinoxy as a product in the $O(^3P) + C_2H_4$ reaction.

Ab initio calculations for the structure and energetics of vinoxy were performed[30,31] and it was determined[31,32] that of the two possible resonance structures, formylmethyl (with the unpaired electron centered on the carbon atom) actually dominates.

Channel (1a), formation of CH_3 + CHO, was not observed in the earlier crossed molecular beam experiment,[33] which was attributed to the fact that this channel requires a 1,2-hydrogen migration in the triplet diradical adduct. The barrier for this process would be higher than the internal energy of the complex.[34] ISC was thought to be slow in a molecule that small.[24] However, CHO was observed using UV absorption by Hunziker et al.[28] and using laser magnetic resonance (LMR) by Temps and Wagner[35] in the same system. Hunziker et al.[28] suggested a mechanism whereby ISC in the diradical could be induced by collisions, followed by facile 1,2-hydrogen migration on the singlet surface and subsequent C-C-bond rupture. The CHO yields of Temps and Wagner[35] indeed showed a decrease with decreasing pressure in the range of approx. 1-4 Torr.

In order to resolve the question of the pressure dependence of the reaction mechanism and branching ratios, experiments were conducted over a large pressure range by many research groups as summarized in Table I. These results suggest that the branching ratio between channel (1a) and (1b) is relatively insensitive to the pressure over a large pressure range (30 mTorr - 760 Torr), and that these channels are about equally important. Although

in all cases secondary reactions had to be taken into account, the low pressure experiments appeared to present mounting evidence that channel (1a) is not a result of collision-induced ISC. The question whether ISC in diradical intermediates can effectively compete with channel (1b) under collision free conditions, can be answered definitively by an improved crossed molecular beam experiment.

The problems arising with this particular reaction in a crossed beam experiment are twofold: First, due to the unfavorable kinematics, as discussed below, products from channel (1a) are expected to be much harder to detect than products from channel (1b) because of a broad and unstructured angular distribution which results in low detector signal at a given angle. Second, for mass spectrometric detection, the coincidence of the expected major product fragments for channel (1a) at m/e=15, 28, and 29 with major background peaks presents difficulties. By using $^{18}O_2$ and an improved experimental arrangement, we have overcome these problems and reinvestigated the $O(^3P) + C_2H_4$ reaction. Since we were able to measure a branching ratio for the $O(^3P) + C_2H_2$ reaction[39] which was in good agreement with other recent investigations, we are confident that our method can be used to determine the branching ratio for $O(^3P) + C_2H_4$ under single collision conditions as well.

3.2. **Experimental**

The experimental setup has been described in detail recently.[39] Briefly, continuous supersonic molecular beams of oxygen atoms and ethylene were crossed at an angle of 90° in a high vacuum chamber. Scattered species were detected using a triply differentially pumped mass spectrometer equipped with an electron-impact ionizer, quadrupole mass filter, and Daly ion detector. The entire mass spectrometer was rotatable in the collision chamber around the intersection point of the two molecular beams.

The high pressure supersonic oxygen atom beam source employed in these experiments was described in detail by Sibener et al.[40] 400 to 600 Torr of a 5% O_2 in Ne mixture were expanded through 0.10-0.25 mm diameter quartz nozzles. The dissociation of O_2 was induced by a radio frequency discharge, and oxygen atoms in their ground (^3P) state were generated. The supersonic ethylene beam was formed by expanding pure ethylene gas at a backing pressure of 200 Torr through a nozzle of 0.15 mm diameter which was held at room temperature.

The peak velocities of the oxygen atom beam were between 1.8 and 2.1×10^5 cm/s with speed ratios around 5 and the peak velocity of the ethylene beam was 8.6×10^4 cm/s with a speed ratio of about 6, resulting in most probable collision energies of approximately 6 kcal/mole.

The measurement of the reaction products was carried out in

two different ways: First, the laboratory angular distributions of products at several ion masses were measured while modulating one of the beams for background subtraction. Typically, 6-8 angular scans were obtained for each m/e value, with total counting times of 6-16 min per angle. Second, time-of-flight (TOF) distributions were recorded at several laboratory angles and for several masses using the cross-correlation method.[41] Total accumulation times for the TOF-measurements ranged from a few minutes to several hours depending on the signal intensity of the particular ion.

For the TOF measurements in the present experiment, an important improvement to the standard arrangement[42] was achieved by increasing the angular spread of the hydrocarbon beam and reducing the number of differential pumping regions for the hydrocarbon beam from three to two, enabling the source to be moved closer to the interaction region, which resulted in an increase of approximately a factor of fifty in signal intensity.

The ethylene was obtained from Matheson with a stated purity of 99.99% min. and oxygen/neon mixtures were purchased from Matheson and Airco and had a stated minimum purity of 99.99% and 99.995%, respectively. $^{18}O_2$ with a stated isotopic purity of 95% minimum was kindly provided by Los Alamos National Laboratory and was mixed with neon of 99.995% stated minimum purity purchased from Airco. All gases were used without further purification.

3.3. **Results and Analysis**

Even though the ions produced in the mass spectrometer detector fragment extensively and the interference from large amounts of nonreactively (elastically and inelastically) scattered reactants and carrier gas must be accounted for, positive identification of the primary reaction products is possible by identifying common features in different spectra for establishing parent-daughter ion relationships, and from the requirement that the total mass and the linear momentum of the reaction products need to be conserved.

Cross-correlation TOF was obtained at several different angles at the m/e ratios of 12, 13, 14, 15, 16, 24, 25, 26, 27, 28, 29, 30, 31, 32, 40, 41, 42, and 43 using ^{16}O, corresponding to the ions C^+, CH^+, CH_2^+, CH_3^+, O^+, C_2^+, C_2H^+, $C_2H_2^+$, $C_2H_3^+$, CO^+ or $C_2H_4^+$, CHO^+ or $^{13}C^{12}CH_4^+$, CH_2O^+, CH_3O^+, O_2^+, C_2O^+, C_2HO^+, $C_2H_2O^+$, and $C_2H_3O^+$ or $^{13}C^{12}CH_2O^+$ respectively; and at the m/e ratios 18, 27, 30, 31, 43 and 44 using ^{18}O, corresponding to the ions $^{18}O^+$, $C_2H_3^+$, $C^{18}O^+$, $CH^{18}O^+$, $C_2H^{18}O^+$, and $C_2H_2{}^{18}O^+$, respectively. Angular distributions were measured at m/e ratios of 12, 13, 14, 15, 16, 27, 28, 29, 30, 32, 41, and 42 using ^{16}O only. No measurements could be taken at m/e=1 and 2 in the present experiment.

A forward-convolution method was used for the analysis in order to find the product translational energy distribution,

$P(E_T)$, and the angular distribution, $T(\theta)$, in the center-of-mass (CM) frame. $P(E_T)$ and $T(\theta)$ were assumed to be independent of each other. Furthermore, the relative cross-sections were assumed to be independent of the collision energy within the range of collision energies in this experiment. From the $P(E_T)$ and $T(\theta)$ functions, laboratory angular distributions and TOF spectra were calculated and averaged over beam velocities, collision angles, the detector acceptance angle and the length of the ionizer in the mass spectrometer and then scaled to the experimental data. The distributions were altered and the calculations repeated until a best fit to the experimental data was found. For maximum flexibility, the $P(E_T)$ trial functions were not confined to a particular functional form. The $T(\theta)$ functions on the other hand were represented as linear combinations of Legendre polynomials.

Major fragments of the vinoxy radical, the product of channel (1b), are expected at m/e=14, 15, 24, 25, 26, 28, 29, 40, 41, 42, and 43 using ^{16}O. The products of channel (1a) are expected to yield major fragments of m/e=29 and 28 for CHO, and 15 and 14 for CH_3. However, problems arise in measuring these particular masses in our experiment as mentioned earlier. We used ^{18}O to measure spectra of $C^{18}O^+$ and $CH^{18}O^+$ at m/e=30 and 31.

The m/e=42 data shown in Figs. 1 and 2 originate from a daughter ion produced in the ionization of the vinoxy radical. In the laboratory angular distribution of m/e=42 shown in Fig.

1, the circles represent measured data points, and the dashed line represents a best fit, as discussed below. The error bars correspond to 95% confidence intervals. The maximum count rates were approximately 40 counts/s. For this set of data, drifts in the detection probability or the beam intensities were accounted for by scaling all measured points to the value at the reference angle which was chosen to be 40°. The direction of the oxygen atom beam is defined as 0°. Fig. 2 shows TOF data for m/e=42 at four different laboratory angles together with the best fit obtained.

We chose to monitor m/e=42 for channel (1b) even though the parent mass of the vinoxy radical is m/e=43. It was found that the signal at that m/e was significantly lower, namely only about 3% of m/e=42, the major vinoxy radical fragment. M/e=43 distributions were measured and found to be superimposable on the m/e=42 distributions after appropriate scaling. The fact that very little signal (only slightly more than expected from the isotopic abundance of ^{13}C in $C_2H_2O^+$) was found at the parent mass of the vinoxy radical is not surprising since in previous studies using electron impact ionization[43] or photoionization[44] with mass spectrometric detection the parent ion of the vinoxy radical was not observed.

From the analysis of angular distributions and TOF spectra containing components arising from fragments of the vinoxy radical ion, it was possible to extract information on its ionizer cracking pattern. This was done for CH_2^+, CH_3^+, CO^+,

CHO^+, C_2O^+, C_2HO^+, $C_2H_2O^+$, and $C_2H_3O^+$. For the other masses this was not possible, due to the predominance of nonreactively scattered signal, and the corresponding fragmentation yields for vinoxy radical had to be estimated from comparison with published mass spectra[45] of related compounds. The mass spectrum of vinoxy radical obtained in this manner is shown in Fig. 3.

In comparing those features of the TOF spectra at different m/e values at a laboratory angle of 35° that correspond to vinoxy radical fragments, we noted that the peak shapes at different masses differed from one another. Particularly in the m/e=15 (CH_3^+) and m/e=31 ($HC^{18}O^+$) spectra (Fig. 4), a distinct dip (as compared to m/e=42, Fig. 2) was found at flight times corresponding to product with very small velocities in the CM frame, or velocities near to the velocity of the CM of the system in the laboratory frame. This could be explained by assuming that those $C_2H_3O^+$-ions having a large amount of internal energy (and therefore a small amount of relative translational energy) preferentially fragment into m/e=42 ($C_2H_2O^+$) by breaking a C-H bond instead of a C-C bond. Alternatively, the m/e=42 signal could stem from two different reactive channels, the vinoxy radical being the predominant source. Another channel could give rise to a product with very low velocity in the CM-frame which corresponds to that part of the m/e=42 signal that is "missing" in the m/e=15 and m/e=31 spectra. A possible minor channel producing signal at m/e=42 is

the production of acetyl radical and hydrogen atom from the decomposition of the CH_3CHO intermediate,

$$O(^3P) + C_2H_4 \rightarrow H + CH_3CO \qquad (1g)$$

and will be discussed later. The effect of this phenomenon on the determination of the vinoxy fragmentation pattern is small.

The $P(E_T)$ and $T(\theta)$ distributions obtained for channel (1b) are shown in the lower panels of Figs. 5 and 6, respectively. The translational energy distribution, $P(E_T)$, was found to be very broad, peaking at about 8 kcal/mole and extending to about 30 kcal/mole. The average energy release is about 13 kcal/mole. The CM angular distribution, $T(\theta)$, is almost isotropic but shows a small amount of preferential backward scattering (with respect to the O-atom beam) of the product. These distributions fit both the angular distribution and the TOF-spectra simultaneously, as shown in Figs. 1 and 2. The agreement is good in both cases. By considering the angular distributions and TOF data separately, it was found that an isotropic distribution would actually fit the angular distribution better, whereas the TOF data suggest stronger backward scattering. In any case, the deviations from isotropy are small.

The maximum of the translational energy distribution (lower panel in Fig. 5) of 30 kcal/mole which is actually about 7.5 kcal/mole higher than the calculated total available energy using a collision energy of 6.2 kcal/mole and the value of 16.3

kcal/mole for the exothermicity calculated by C. F. Melius.[23] Because of the CM to laboratory frame transformation Jacobian, our data analysis procedure is very sensitive to the shape of the $P(E_T)$ curve at low energies but considerably less sensitive to the distribution at higher energies, therefore no definite conclusion on the value of the exothermicity can be drawn from our data.

In addition, all m/e=42 TOF-spectra show an additional fast component (see Fig. 2). The wider tails in the angular distribution also reflect the existence of this fast component. Reaction of ethylene dimers with oxygen atoms, reactions of trace amounts of $O(^1D)$, or additional reaction channels, such as (1c), could produce products at velocities on the order of those observed here. Consequently, the fast edge of the m/e=42 features identified with vinoxy radical was somewhat obscured resulting in additional uncertainty in the high energy part of the $P(E_T)$ distribution.

In our search for signal from the products of channel (1a), the formation of methyl and formyl radicals, we relied mostly on the data obtained using ^{18}O in order to be able to distinguish the CO^+ and the CHO^+ signal from the ambient background. However, an additional difficulty lies in the kinematics of this channel. A heavy particle, such as the vinoxy radical, which is recoiling from a very light particle, like a hydrogen atom, has a very small velocity in the CM frame since the CM velocities are inversely proportional to the fragment masses as a result of

momentum conservation. A small CM velocity is reflected by an angular distribution that peaks sharply near the angle of the CM in the laboratory frame as seen in the vinoxy distribution, Fig. 1. In the case of an exothermic reaction producing pairs of product molecules with comparable masses, such as CH_3 and CHO, the CM velocities for both particles will be large even for small releases of available energy into kinetic energy, resulting in products spread over a wide angular range in the laboratory frame, causing low signal levels at all angles, and only part of the products can be detected within the detector angular range.

The differences in the kinematic relations between the two channels are illustrated in Fig. 7, which shows contour diagrams of product flux for CHO from channel (1a) and for C_2H_3O from channel (1b). The flux distributions in Fig. 7 represent the final results of the analysis as discussed below.

Because of the difficulties resulting from the unfavorable kinematics of channel (1a), Buss et al.[24] were not able to see evidence for its occurrence. In the present experiment, angular distribution measurements at m/e=30 ($C^{18}O^+$) or 31 ($HC^{18}O^+$) were not attempted, since it was found to be impossible to extract meaningful information from our earlier experiments on the analogous case of the O + C_2H_2 reaction.[39]

The problems of not being able to measure laboratory angular distributions are not very serious, however, since the reaction is expected to go through a long lived complex and TOF

data will provide a great deal of dynamical information. Whereas fast and widely scattered products are difficult to discern in angular distribution measurements, they are easily identifiable in the TOF spectra, since the signal is accumulated in only a few channels. Fig. 8 shows data at four different angles for m/e=30 using ^{18}O and the upper panel of Fig. 4 shows the TOF spectrum obtained for m/e=31 using ^{18}O at 35°. Two different components can be distinguished in the spectra - the slower one has a shape similar to the m/e=42 spectra and can be identified as a daughter ion of vinoxy radical, and the faster component can be identified as stemming from CHO, the product of reaction channel (1a).

It should be noted that the TOF spectra at 20° and 35° for m/e=15, 30 and 31 shown in Figs. 4 and 8 were corrected for an experimental artifact which was described in detail in the previous chapter[39] and has no effect on the results of the data fitting procedure.

From the analysis of the fast components of the TOF spectra, the $P(E_T)$ and $T(\theta)$ distributions shown in the upper panels of Figs. 5 and 6, respectively, were obtained. The translational energy distribution for channel (1a) extends out to the total available energy (34 kcal/mole for this channel) with a peak at about 6 kcal/mole (corresponding to 18% of the total available energy) and an average translational energy of about 12 kcal/mole. While the general features of this distribution are well defined by our data, some uncertainty

remains in the exact shape, particularly in the high energy part, as a result of noise in the data and incomplete separation of the two components in the m/e=30 and 31 TOF spectra.

The best fit CM angular distribution ($T(\theta)$) shown in the upper panel of Fig. 6 is strongly forward-backward peaked. The condition of symmetry about 90° was imposed, as discussed below, to reflect the existence of a long-lived intermediate. However, since a substantial fraction of products gets scattered outside the detector scanning range, as mentioned earlier, the shape of $T(\theta)$ for channel (1a) is much more uncertain. The effect of the choice of the $T(\theta)$ for this channel on the branching ratio is, in fact, small - if an isotropic CM angular distribution was assumed instead of a forward-backward peaking one, the branching ratio changed only by about 2%.

We also made an attempt to find the other product of channel (1a), methyl radical, and measured TOF distributions at m/e=15 and 14 at 35°. The spectrum at m/e=14 was dominated entirely by a fragment of nonreactively scattered ethylene, but the spectrum at m/e=15 (lower panel in Fig. 4) clearly shows three different contributions: the slowest part can be identified with a fragment of vinoxy radical (even though the shape is different, as discussed above), the middle feature is due to fragmentation of nonreactively scattered ethylene, and the fastest part possibly corresponds to CH_3 from reaction (1a). The long-dashed line corresponding to the fastest feature in Fig. 4 was calculated using the dynamical information obtained

for channel (1a) from an analysis of the m/e=30 data and scaled to fit the experimental data. The comparison between calculation and data suggests that the fast feature is indeed due to CH_3 from channel (1a). However, the intensity derived from the fast feature in the m/e=15 data would correspond to a much larger branching ratio (favoring channel 1a) than calculated from the analysis of the m/e=30 data. Therefore, the fast feature is probably only partly due to this product and partly due to other unidentified sources.

The analysis procedure yields relative total cross-sections σ_a^0 and σ_b^0 for each of the reaction channels through the scaling of calculated distributions to the measured spectra.[46] Since the absolute intensities of the molecular beam, the exact size of the collision volume, and the detection efficiency are not known, absolute reaction cross-sections can not be directly derived in our experiment. However, these parameters do not change during the course of an experiment, and therefore the branching ratio between two reaction channels can be calculated from the ratio of the relative cross-sections corrected for the ionization cross-sections and fragmentation patterns for the products. The branching ratio R, defined as the ratio of the total reaction cross-sections σ_a and σ_b for channels (1a) and (1b) is obtained as follows:

$$R = \frac{\sigma_a}{\sigma_b} = \frac{\sigma_a^0}{\sigma_b^0} \times \frac{Q_{vinoxy}}{Q_{CHO}} \times \frac{f_{vinoxy}^{42}}{f_{CHO}^{30}} .$$

Here σ_a^0 and σ_b^0 are the apparent cross-sections derived from the signal at m/e=30 and 42, Q_{vinoxy} and Q_{CHO} are the ionization cross-sections approximated using the method of Fitch and Sauter[47] and f_{CHO}^{30} and f_{vinoxy}^{42} are the fractions of $CH^{18}O$ and C_2H_3O which yield ions of m/e=30 and 42, respectively, upon ionization. The mass spectrum of CHO and the vinoxy radical (Fig. 3) were constructed from angular distributions and TOF data for major fragments and from estimates of minor fragments using the well known mass spectra of related compounds.[45]

The TOF measurements at different angles were performed under slightly different conditions, but great care was taken to check the experimental conditions by frequently alternating between the different products monitored. In this case we had to switch between ^{18}O and ^{16}O. The number densities for both beams were found to be identical. A value for R was thus calculated for the data at 20°, 35°, 45° and 55° separately. The results are R(20°)=2.4, R(35°)=2.9, R(45°)=2.4, and R(55°)=2.5. The good agreement in these values is considered somewhat fortuitous in view of the results obtained for the two channels in the O + acetylene system,[39] where a much larger scatter for the values of the branching ratio was found under equivalent conditions.

Three main sources contribute to the error in the determination of the branching ratio. The experimentally derived quantity σ_a^0/σ_b^0 contains errors due to fluctuations in

the detection efficiency and errors due to uncertainty in the $P(E_T)$ and $T(\theta)$ distributions, particularly for channel (1a). The overall error of σ_a^0/σ_b^0 is estimated at about 25%. The correction factor Q_{vinoxy}/Q_{CHO} is estimated to be reliable to about 20% since an empirical method was used[47] whose applicability to polyatomic radicals has not been tested. The fragmentation patterns for C_2H_3O and CHO were measured, but are associated with the same uncertainties all quantitative measurements in our system carry. The uncertainty of the factor $f_{vinoxy}^{42}/f_{CHO}^{30}$ is estimated to be about 20% as well. The overall result for the branching ratio R is therefore 2.5±0.9.

3.4. **Discussion**

The results of our crossed molecular beam experiment clearly demonstrate the occurrence of the two major reaction channels (1a) and (1b). Channel (1b) has been identified in previous crossed molecular beam experiments[24-26] and confirmed repeatedly since. In this new investigation, we were able to observe channel (1a) under single collision conditions. Thus the apparent discrepancy between bulk phase studies which in the majority support the predominance of channel (1a) and molecular beam experiments has been resolved.

The fact that vinoxy radical undergoes extensive fragmentation upon electron impact ionization provides a

possible explanation for earlier results where ketene was thought to be a major product[20,21] based on the appearance of product peaks at m/e=42. In addition, signal at m/e=15 and 29 could be due to either the products of channel (1a) or fragments of vinoxy radical, and m/e=29 could also represent some $C_2H_5^+$ from the fast reaction of hydrogen atoms with ethylene in the high pressure reactors.[48]

The analysis of our experiment did not yield absolute cross sections, but only the ratio of the relative cross sections for channels (1a) and (1b), which was found to be 2.5±0.9. Under the assumption that no other reaction channel contributes, this would correspond to 71% (62-77%) of the reaction following channel (1a) and 29% (23-38%) following channel (1b). It is not clear to what extent the use of ^{18}O affects the rate of ISC and thus the branching ratio. The occurrence of additional reaction channels can not be excluded; however, it appears to be established that channels (1a) and (1b) are the major ones under conditions of relatively small collision energies or low temperatures. In several recent investigations, absolute branching fractions for either channel (1a) or (1b) have been obtained (see Table I). Our results are in qualitative agreement with these recent measurements. It is important to note that no indication of a pressure dependence of the branching fractions was found in previous investigations and that the crossed molecular beam results presented here confirm that processes (1a) and (1b) are indeed primary reaction steps

and not a consequence of secondary collisions of reaction intermediates. Therefore our data show that the mechanism suggested by Hunziker et al.[28] in which it was assumed that collisions were necessary for ISC to occur does not need to be invoked.

The temperature dependence of the branching ratio was studied only by Smalley et al.[36] who found a slight decrease (i.e., more H production) at temperatures up to 769 K. We did not measure the dependence of the cross sections and the branching ratio on collision energy. The collision energies used in the present experiment were much higher than those in a thermal experiment, and the agreement of our results with the recent room-temperature experiments indicates that the dependence of the branching ratios on temperature is probably small. This appears to be reasonable, since for both channels the rate determining step is addition of the $O(^3P)$ atom to the ethylene molecule.

Whereas sophisticated spectroscopic techniques might be more successful in determining the exact values of the branching fractions for the various channels, the strength of the molecular beam technique lies in the unambiguous identification of such elementary reaction steps in the absence of secondary collisions.

A large amount of theoretical work has been done on both the triplet and singlet C_2H_4O potential energy surfaces. This information greatly facilitates understanding experimental

results. Fig. 9 schematically shows parts of the triplet (solid lines) and singlet (dashed lines) C_2H_4O surface taken mainly from calculations by C. F. Melius.[23]

The $O(^3P)$ atoms follow an out-of-plane approach during which the CCO-plane constitutes the plane of symmetry.[49] The reaction leads, via a small entrance channel barrier, to a triplet diradical CH_2CH_2O. There actually exist two pairs of states of this diradical with very similar energies (lying within a few kcal/mole),[49,50] where the two states in a pair can interconvert by rotation about the C-C bond with a barrier of only about 0.6 kcal/mole.[50] As indicated in Fig. 9, the approach following A" symmetry leads to the lower pair of states, whereas the approach following A' symmetry leads to the higher lying pair. Diradicals in the two lower energy states can react along several different pathways, e.g. elimination of a hydrogen atom to form vinoxy radical or 1,2-H migration to form triplet acetaldehyde which in turn would dissociate, with barriers of several kcal/mole, to CH_3 and CHO. It was suggested[28] that the energetically higher lying pair of states can either react to form the first excited electronic state (A^2A') of vinoxy radical or undergo ISC. The (A^2A') state was found to be 23 kcal/mole higher in energy than the ground state $(X^2A")$[28] and is therefore energetically inaccessible in our experiment.

The pathway forming (ground state) vinoxy radical in our experiment shows a maximum release of translational energy

approximately equal to the calculated available energy (lower panel in Fig. 5). In addition, the fact that the distribution peaks well away from zero is indicative of an exit channel barrier[51] which is in agreement with the calculations as well. The CM angular distribution $T(\theta)$ found in our experiment does not show a clear predominance of forward or backward peaked product which would be indicative of a direct reaction, but it is not completely isotropic or forward-backward symmetric either. These results could suggest that the lifetime of the triplet diradical is not much longer than a rotational period.

The translational energy distribution obtained from the analysis of the present experiment is in agreement with distributions found in earlier molecular beam experiments: Baseman[52] reported $P(E_T)$ functions for channel (1b) at nominal collision energies of 5.4 and 8.3 kcal/mole, respectively, which display essentially the same features as the one reported here. Clemo et al.[26] reported a distribution with a broad peak at around 11 kcal/mole and a sharp cutoff at 19 kcal/mole. Baseman[52] found that the experiment at 8.3 kcal/mole collision energy could be fit using CM angular distributions $T(\theta)$ with sideways or slight forward peaking. Clemo et al.[26] reported a $T(\theta)$ that was close to isotropic but slightly favored forward scattering.

In contrast to channel (1b), the formation of CH_3 and CHO, channel (1a), appears to be an unlikely process on the triplet potential energy surface, since a 1,2-hydrogen migration in the

diradical intermediate has a prohibitively high barrier according to ab initio calculations. The results of C. F. Melius[23] place this barrier at about 9 kcal/mole above the total available energy in our experiment. Tunneling corrections could not explain the high rate of reaction. The fact that channel (1a) is greatly enhanced in the case of the $O(^3P) + C_2D_4$ reaction[53] indicates that tunneling is not responsible. Therefore a different pathway must be responsible for the formation of CH_3 and CHO. Only rapid ISC from a triplet to a singlet diradical can explain the observations. On the singlet surface, there is no barrier expected for the 1,2-H migration to form ground state (singlet) CH_3CHO and also no significant exit channel barrier for the C-C bond rupture to form CH_3 + CHO.[54]

For a simple bond rupture reaction of a polyatomic molecule without an exit channel barrier, a translational energy distribution peaking at zero energy would be expected, whereas an exit channel barrier usually results in a $P(E_T)$ peaking well away from zero, as for instance in the case of channel (1b). The $P(E_T)$ distribution we obtained for channel (1a) (upper panel in Fig. 5) shows a peak at about 6 kcal/mole which represents a relatively small fraction (18%) of the total available energy, but clearly does not correspond to a typical simple bond rupture case. A possible explanation for this phenomenon arises from the release of some of the rotational energy of the reaction intermediates into the translational energy of products. The orbital angular momentum $J=24\hbar$ corresponding to the impact

parameter of approximately 0.7Å (obtained from the geometry of the transition state, Ref. 49) is converted into rotational angular momentum of the complex. After H-migration, the C-C bond stretches and subsequently breaks. During that process, some fraction of the rotational energy of the complex is expected to be converted into translational energy of the fragments. However, since the exit impact parameter is expected to be much larger than the impact parameter of the reactants, the amount of that energy is not likely to be more than 1 kcal/mole and can not explain the peak of the $P(E_T)$ at 6 kcal/mole. Consequently, there appears to be a small exit channel barrier for this C-C bond rupture process.

The comparison of these results with the $O(^3P)$ + acetylene reaction shows that the translational energy distributions for the $O + C_2H_4 \rightarrow CH_3 + CHO$ and the $O + C_2H_2 \rightarrow CH_2 + CO$ channels are qualitatively different; in the latter case a broader distribution peaking at 27% of the total available energy was found,[39] indicating a relatively large barrier. The barrier for C-C bond rupture in $^3CH_2CO$ was calculated to be about 34 kcal/mole.[23,55] The acetylene reaction, in contrast to the ethylene case, is indeed thought to proceed mostly on the triplet surface.[55]

For channel (1a), we imposed forward-backward symmetry on the center-of-mass angular distribution $T(\theta)$ (upper panel of Fig. 6), which corresponds to the assumption that the precursor of $CH_3 + CHO$, presumably $^1CH_3CHO$, has a lifetime significantly

longer than a rotational period, estimated to be about 2ps. Even though this is not an unambiguous result of the data analysis, the data for channel (1a) were found to be compatible with this assumption. It is supported by the conclusion of Bley et al.[16] that the lifetime of the addition complex, which is stabilized as acetaldehyde at high pressures, is of the order of 10^{-11}s. It is possible that the decay of the triplet diradical through the competition of H-elimination and ISC takes place on a time scale shorter than or on the order of a rotational period, while the lifetime of $^1CH_3CHO$ formed through ISC and H-migration is considerably larger.

The energies of the four triplet diradical states considered by Dupuis et al.[49] and Yamaguchi et al.[50] were found to be very similar to those of the four singlet diradicals. More recent results[54] indicate a singlet state lying about 12 kcal/mole lower than the triplet diradical. It was suggested[50] that ISC would be facile in this system since spin-orbit coupling should be efficient because of the orthogonality of the p-type orbitals in the diradical. Recent unpublished results (Ref. 26 in Ref. 38) indicate that the two surfaces indeed come close to each other at some points along the reaction coordinate, facilitating the conversion. However, no ISC rates have been calculated. Thus branching ratios for the major channels have not been evaluated theoretically and cannot be compared with the experimental results. As mentioned earlier, there might be a small difference in the ISC rate between

$C_2H_4{}^{18}O$ and $C_2H_4{}^{16}O$.

Apart from the two major reaction channels (1a) and (1b) discussed above, several other exothermic pathways are possible. Vibrationally hot adduct, acetaldehyde or ethylene oxide, could only be considered as a reaction intermediate in our experiment; RRKM calculations[56] indicate that, without stabilization through collisions, none of these highly excited molecules could survive for several hundred microseconds to reach the detector in our experiment.

The formation of formaldehyde and triplet methylene, channel (1d), was found to account for 6±3% of the products by Bley et al.[16] using LMR detection of CH_2 radicals. Endo et al.[38] found that CH_2O was formed mainly by secondary reactions, but possibly a small amount was being formed in a primary reaction step. Peeters and Vinckier[57] suggested that reaction (1d) is the predominant source of CH_2 in ethylene flames. According to theory[23] (Fig. 9), the barrier for CH_2-elimination from the triplet diradical is about 9 kcal/mole higher than that for H-elimination to form vinoxy radical. From this the ratio of reaction (1d) to (1b) is expected to be small. In our experimental data, no evidence was found for the occurrence of this channel. A small amount of CH_2O may have gone undetected, however.

The formation of ketene and molecular hydrogen, reaction (1c), although not considered to be a major channel in the recent literature, deserves some consideration. On the triplet

surface, ketene could be formed by 1,1-H_2-elimination from the diradical. Such elimination processes typically have substantial barriers. However, in this particular case the barrier could be exceptionally low in view of the comparatively low barrier for H-elimination.[23] To our knowledge, no theoretical calculation has been undertaken for this special case. Even if the barrier is several kcal/mole higher than that for H-elimination, a certain fraction of the molecules could react according to this pathway.

Another pathway to ketene proceeds through the singlet diradical. In this case, again, no ab initio calculations are available that could answer the question of the existence and magnitude of a barrier for the 1,1-H_2-elimination process. However, Melius' calculations show a possibility that this process occurs with at most a very small barrier on the singlet surface.[58] The alternative route, the 4-center H_2-elimination from acetaldehyde, is expected to have a very high barrier. If it does not greatly exceed the threshold for C-C-bond rupture, then 1,2-H_2-elimination has to be considered as a minor reaction pathway. In Fig. 9 this possibility is indicated.

The question arises, whether the signal that we attribute to vinoxy radical could be partly or entirely due to the formation of ketene. Considering first the triplet case, from the estimated exothermicity,[59] which is 18 kcal/mole larger than that for the H + vinoxy channel, and the likely existence of a barrier, we would expect a considerable translational energy

release. These assumptions could not fit the m/e=42 data. In addition, the component of the signal at m/e=15 (CH_3^+) which shows essentially the same features as the m/e=42 distributions, could not be explained by invoking this channel. Furthermore, spectroscopic identification[27,28,32] leaves no doubt that vinoxy indeed occurs as a major primary product in the $O(^3P) + C_2H_4$ reaction. However, the possibility can not be excluded that a small fraction of our m/e=42 signal is due to ketene.

In the case of the reaction forming ketene on the singlet surface where more energy will be available, an even larger release of translational energy is expected if the dynamics is determined by repulsive forces. As a result, this channel would be expected to manifest itself in very fast components in the TOF spectra. Such fast components were indeed found in the m/e=42 spectra, and they are possibly in part due to the formation of ground state ketene and molecular hydrogen. However, without further experiments, this assignment can not be made with certainty.

Additional pathways that are conceivable are the formation of hydrogen atom and acetyl radical, CH_3CO - channel (1g) - or hydrogen atom and vinoxy radical via the singlet surface, i.e. as dissociation products of highly vibrationally excited acetaldehyde. Simple RRKM calculations[56] indicate that the ratio $(CH_3 + CHO):(CH_3CO + H):(CH_2CHO + H)$ would be about 1:0.05:0.0025. These numbers strongly depend on the values for the dissociation thresholds, but it is likely that a small

amount of acetyl radical is formed. Because the process is a simple bond rupture, a small amount of translational energy is expected in the fragments. Such a signal could possibly be hidden under the vinoxy signal in our m/e=42 data. In fact, the different shapes of the relevant parts of the m/e=42, 15, and 31 data as discussed above could indicate two separate sources of m/e=42 product. Thus, that part of the m/e=42 signal which corresponds to very low velocities in the center-of-mass frame and which is partly absent in the m/e=15 spectra could be due to acetyl radical. So far, acetyl has escaped spectroscopic detection in the O + ethylene reaction, possibly because the radical lacks accessible electronic transitions.[60]

This clearly does not exhaust the list of thermodynamically possible channels in the C_2H_4O system. For instance, Donaldson and Sloan[61] suggested the channel

$$O(^3P) + C_2H_4 \rightarrow [C_2H_4O]^{\ddagger} \rightarrow H + CO + CH_3 \qquad (1h)$$

as a possible source of vibrationally excited CO.

It is also of interest to compare the products of the $O(^3P)$ + C_2H_4 reaction with the products of the photodissociation of acetaldehyde. If internal conversion of the initially prepared electronically excited state is fast, then the products of photodissociation and of chemically activated acetaldehyde at similar excitation energies should be similar. The photodissociation of acetaldehyde has been studied extensively[62]

in the wavelength region 240-340 nm. Three reaction channels have been observed:

$$CH_3CHO \xrightarrow{h\nu} CH_3 + CHO \qquad (2a)$$

$$CH_3CHO \xrightarrow{h\nu} CH_3CO + H \qquad (2b)$$

$$CH_3CHO \xrightarrow{h\nu} CH_4 + CO \qquad (2c)$$

Channels (2a) and (2b) correspond to channels (1a) and (1g), respectively, but channel (2c) has no equivalent in the $O(^3P)$ + C_2H_4 reaction, since CH_4 was not detected among the major products in any previous experiment. It is questionable, however, whether channel (2c) constitutes a primary reaction channel at all, since the barrier for this process was calculated to be 8 kcal/mole above the dissociation threshold for $CH_3CHO \rightarrow CH_3 + CHO$.[63] In order to gain further insight into the dynamics of the C_2H_4O system, we attempted to study the photodissociation of acetaldehyde in a molecular beam at 248 and 193 nm. In preliminary experiments we found that the absorption cross sections at these wavelengths under molecular beam conditions are too small to observe photodissociation products.

Future research is expected to shed more light on minor reaction channels. At this point, it appears that a consensus has been reached on the mechanism and the identity of the primary products of the $O(^3P)$ + C_2H_4 reaction.

A fairly thorough understanding of these reactions is of central importance for the description of complex combustion

systems. The inclusion of channel (1b) in model calculations might have important effects since an additional source of H atoms is introduced. Although a large amount of spectroscopic information is available for the vinoxy radical,[27,32,60,64] its application to direct measurements of concentration profiles in complicated systems has not been developed so far. At present, little is known about reactions of vinoxy radical, except for its reaction with molecular oxygen.[65]

3.5. **Conclusions**

Using the crossed molecular beam technique, the occurrence of two major channels in the reaction of ground state oxygen atoms and ethylene under single collision conditions was confirmed, namely formation of methyl radical and formyl radical (channel (1a)) and formation of hydrogen atom and vinoxy radical (channel (1b)). Upon formation of a triplet diradical from the addition of $O(^3P)$ to ethylene, two competitive processes of approximately equal importance are responsible for the fast decay of the triplet diradicals. One of the processes is the direct elimination of a hydrogen atom to form vinoxy radicals and the other is ISC from the triplet to a singlet diradical. Most of the singlet diradicals are first transformed into highly vibrationally excited acetaldehyde through 1,2-H migration and these molecules fragment in a time much longer than the

rotational period of 2 ps. The vibrationally excited singlet acetaldehyde decays mostly into CH_3 and CHO. A value for the branching ratio σ_a/σ_b of 2.5±0.9 was determined which is in approximate agreement with other recent determinations.

In addition to these two major channels, our experiment also provides evidence for the formation of acetyl radical and hydrogen atoms, a minor dissociation channel from vibrationally excited CH_3CHO. Furthermore there is possibly a minor channel forming ketene on the singlet potential energy surface.

3.6. References

1. J. N. White and W. C. Gardiner, Jr., J. Phys. Chem. 83, 562 (1979).
2. J. Warnatz, H. Bockhorn, A. Möser and H. W. Wenz, Nineteenth Symposium (International) on Combustion (Combustion Institute, Pittsburgh, 1982), p. 197.
3. C. K. Westbrook and F. L. Dryer, Eighteenth Symposium (International) on Combustion (Combustion Institute, Pittsburgh, 1981), p. 749.
4. K. Brezinsky, Prog. Energy Combust. Sci. 12, 1 (1986).
5. C. P. Fenimore and G. W. Jones, Ninth Symposium (International) on Combustion (Combustion Institute, Pittsburgh, 1963), p. 597.
6. C. K. Westbrook, M. M. Thornton, W. J. Pitz, and P. C. Malte, Twenty-Second Symposium (International) on Combustion (Combustion Institute, Pittsburgh), in press.
7. C. K. Westbrook, F. L. Dryer, and K. P. Schug, Nineteenth Symposium (International) on Combustion (Combustion Institute, Pittsburgh, 1982), p. 153.
8. J. M. Levy, B. R. Taylor, J. P. Longwell, and A. F. Sarofim, Nineteenth Symposium (International) on Combustion (Combustion Institute, Pittsburgh, 1982), p. 167; C. K. Westbrook, F. L. Dryer, and K. P. Schug, Combust. Flame 52, 299 (1983); M. Cathonnet, F. Gaillard, J. C. Boettner, P. Cambray, D. Karmed, and J. C. Bellet, Twentieth Symposium

(International) on Combustion (Combustion Institute, Pittsburgh, 1985), p. 819.

9. K. Mahmud, P. Marshall, and A. Fontijn, J. Phys. Chem. 91, 1568 (1987); R. B. Klemm, F. L. Nesbitt, E. G. Skolnik, J. H. Lee, and J. F. Smalley, J. Phys. Chem. 91, 1574 (1987); and references therein.

10. R. J. Cvetanovic and D. L. Singleton, Rev. Chem. Int. 5, 183 (1984).

11. R. J. Cvetanovic, J. Chem. Phys. 23, 1375 (1955).

12. R. Cvetanovic, Adv. Photochem. 1, 115 (1963).

13. A. N. Ponomarev, Kinet. i Kat. 7, 237 (1966).

14. M. Hawkins and L. Andrews, J. Am. Chem. Soc. 105, 2523 (1983).

15. M. Eusuf and H. Gg. Wagner, Ber. Bunsenges. Phys. Chem. 76, 437 (1972).

16. U. Bley, P. Dransfeld, B. Himme, M. Koch, F. Temps, and H. Gg. Wagner, Twenty-Second Symposium (International) on Combustion (Combustion Institute, Pittsburgh), in press.

17. L. I. Avramenko, R. V. Kolesnikova, and G. I. Savinova, Izv. Akad. Nauk SSSR, Ser. Khim. 1, 36 (1963); A. A. Westenberg and N. deHaas, Twelfth Symposium (International) on Combustion (Combustion Institute, Pittsburgh, 1969), p. 289.

18. R. J. Cvetanovic, Can. J. Chem. 33, 1684 (1955).

19. J. M. Brown and B. A. Thrush, Trans. Faraday Soc. 63, 630 (1967); H. Niki, E. E. Daby, and B. Weinstock, Twelfth

Symposium (International) on Combustion (Combustion Institute, Pittsburgh, 1969), p. 277; J. T. Herron and R. D. Penzhorn, J. Phys. Chem. 73, 191 (1969); I. T. N. Jones and K. D. Bayes, J. Am. Chem. Soc. 94, 6869 (1972).

20. J. Kanofsky and D. Gutman, Chem. Phys. Lett. 15, 236 (1972); J. R. Kanofsky, D. Lucas, and D. Gutman, Forteenth Symposium (International) on Combustion (Combustion Institute, Pittsburgh, 1973), p. 285; F. J. Pruss, Jr., I. R. Slagle, and D. Gutman, J. Phys. Chem. 78, 663 (1974).
21. B. Blumenberg, K. Hoyermann, and R. Sievert, Sixteenth Symposium (International) on Combustion (Combustion Institute, Pittsburgh, 1977), p. 841.
22. A. M. Wodtke, E. J. Hintsa, J. Somorjai, and Y. T. Lee, submitted to Isr. J. Chem.
23. C. F. Melius, unpublished results.
24. R. J. Buss, R. J. Baseman, G. He, and Y. T. Lee, J. Photochem. 17, 389 (1981).
25. A. R. Clemo, F. E. Davidson, G. L. Duncan, and R. Grice, Chem. Phys. Lett. 84, 509 (1981).
26. A. R. Clemo, G. L. Duncan, and R. Grice, Trans. Faraday Soc. 2, 78, 1231 (1982); 79, 637 (1983).
27. G. Inoue and H. Akimoto, J. Chem. Phys. 74, 425 (1981).
28. H. E. Hunziker, H. Kneppe, and H. R. Wendt, J. Photochem. 17, 377 (1981).
29. K. Kleinermanns and A. C. Luntz, J. Phys. Chem. 85, 1966 (1981).

30. E. S. Huyser, D. Feller, W. T. Borden, and E. R. Davidson, J. Am. Chem. Soc. 104, 2959 (1982).

31. M. Dupuis, J. J. Wendoloski, and W. A. Lester, Jr., J. Chem. Phys. 76, 488 (1982).

32. Y. Endo, S. Saito, and E. Hirota, J. Chem. Phys. 83, 2026 (1985).

33. Further analysis of the results obtained in the crossed molecular beam experiment (Ref. 52) showed that because of the unfavorable kinematic relations and the high detector background at m/e=29 (CHO^+), the failure to detect the CHO product could only indicate an upper limit of 50% on the contribution of this channel.

34. W. A. Lester, Jr., M. Dupuis, T. J. O'Donnell, and A. J. Olson, in: Frontiers of Chemistry, K. J. Laidler, Editor (Pergamon Press, Oxford, 1982).

35. F. Temps and H. Gg. Wagner, Max-Planck-Institut für Strömungsforschung, Bericht 18/1982.

36. J. F. Smalley, F. L. Nesbitt, and R. B. Klemm, J. Phys. Chem. 90, 491 (1986).

37. U. C. Sridharan and F. Kaufman, Chem. Phys. Lett. 102, 45 (1983).

38. Y. Endo, S. Tsuchiya, C. Yamada, E. Hirota, and S. Koda, J. Chem. Phys. 85, 4446 (1986).

39. Chapter 2; A. M. Schmoltner, P. M. Chu, and Y. T. Lee, J. Chem. Phys., in press.

40. S. J. Sibener, R. J. Buss, C. Y. Ng, and Y. T. Lee, Rev.

Sci. Instrum. 51, 167 (1980).

41. K. Sköld, Nucl. Instrum. Methods 63, 114 (1968); V. L. Hirschy and J. P. Aldridge, Rev. Sci. Instrum. 42, 381 (1971); G. Comsa, R. David, and B. J. Schumacher, Rev. Sci. Instrum. 52, 789 (1981).

42. Y. T. Lee, J. D. McDonald, P. R. LeBreton, and D. R. Herschbach, Rev. Sci. Instrum. 40, 1402 (1969).

43. K. O. McFadden and C. L. Currie, J. Chem. Phys. 58, 1213 (1973); F. Huisken, D. Krajnovich, Z Zhang, Y. R. Shen, and Y. T. Lee, J. Chem. Phys. 78, 3806 (1983).

44. R. B. Klemm, personal communication.

45. Atlas of Mass Spectral Data, E. Stenhagen, S. Abrahamsson, and F. W. McLafferty, editors, Vol. 1 (Wiley, New York, 1969).

46. R. J. Buss, Ph. D. Thesis, University of California, Berkeley, 1979; App. 2 of this thesis.

47. W. L. Fitch and A. D. Sauter, Anal. Chem. 55, 832 (1983).

48. J. Y. Park, P. F. Sawyer, M. C. Heaven, and D. Gutman, J. Phys. Chem. 88, 2821 (1984).

49. M. Dupuis, J. J. Wendoloski, T. Takada, and W. A. Lester, Jr., J. Chem. Phys. 76, 481 (1982).

50. K. Yamaguchi, S. Yabushita, T. Fueno, S. Kato, and K. Morokuma, Chem. Phys. Lett. 70, 27 (1980).

51. S. A. Safron, N. D. Weinstein, D. R. Herschbach, and J. C. Tully, Chem. Phys. Lett. 12, 564 (1972). D. R. Herschbach, Discuss. Faraday Soc. 55, 233 (1973); R. A. Marcus, J.

Chem. Phys. 62, 1372 (1975).

52. R. J. Baseman, Ph. D. thesis, University of California, 1982.

53. S. Koda, Y. Endo, E. Hirota, and S. Tsuchiya, J. Phys. Chem. 91, 5840 (1987).

54. Y. Takahara, K. Yamaguchi, and T. Fueno, Book of Abstracts, Third Symposium on Chemical Reactions, Tokyo University, June 3-5, 1987.

55. L. B. Harding and A. F. Wagner, J. Phys. Chem. 90, 2974 (1986).

56. P. J. Robinson and K. A. Holbrook, Unimolecular Reactions (Wiley, London, 1972).

57. J. Peeters and C. Vinckier, Fifteenth Symposium (International) on Combustion (Combustion Institute, Pittsburgh, 1975), p. 969.

58. C. F. Melius, personal communication.

59. The heat of formation of ketene was measured by Nuttal et al. (R. L. Nuttal, A. H. Laufer, and M. V. Kilday, J. Chem. Thermodynamics 3, 167 (1973)), and was recently confirmed independently by the determination of the ketene dissociation threshold (W. H. Green, I.-C. Chen, C. B. Moore, Ber. Bunsenges. Phys. Chem. 92, 389 (1988); I.-C. Chen, W. H. Green, Jr., and C. B. Moore, J. Chem. Phys. 89, 314 (1988)) and measurement of the heat of formation of methylene (K. E. McCulloh and V. H. Dibeler, J. Chem. Phys. 64, 4445 (1976)). The value for the triplet ketene energy

was taken from the calculations of Ref. 23.

60. M. E. Jacox, Chem. Phys. 69, 407 (1982).

61. D. J. Donaldson, J. J. Sloan, J. Chem. Phys. 77, 4777 (1982); Can. J. Chem. 61, 906 (1983).

62. N. Goldstein and G. H. Atkinson, Chem. Phys. 105, 267 (1986); F. Stoeckel, M. D. Schuh, N. Goldstein, and G. H. Atkinson, Chem. Phys. 95, 135 (1985); B. M. Stone, M. Noble, and E. K. C. Lee, Chem. Phys. Lett. 118, 83 (1985); A. Horowitz, C. J. Kershner, and J. G. Calvert, J. Phys. Chem. 86, 3094 (1982); A. Horowitz and J. G. Calvert, J. Phys. Chem. 86, 3105 (1982); and References therein.

63. J. S. Yadav and J. D. Goddard, J. Chem. Phys. 84, 2682 (1986).

64. L. F. DiMauro, M. Heaven, T. A. Miller, J. Chem. Phys. 81, 2339 (1984).

65. D. Gutman, H. H. Nelson, J. Phys. Chem. 87, 3902 (1983); K. Lorenz, D. Rhäsa, R. Zellner, B. Fritz, Ber. Bunsenges. Phys. Chem. 89, 341 (1985).

3.7. Tables

Table I: Recent experiments on the relative contributions of channels (1a), (1b), and (1d).

Ref.	%(1a)	%(1b)	%(1d)	total pressure	method
28	52-58	36±4	-	40-760 Torr	photochemical modulation spectroscopy
36	-	27±5	-	50-100 Torr	resonance fluorescence
37	-	79±14	-	0.4-6 Torr	resonance fuorescence
38	50±10	40±10	-	30 mTorr	microwave spectroscopy
16	44±15	50±10	6±3	3-53 Torr	LMR, ESR

3.8. Figures

Figure Captions

Fig. 1 Laboratory angular distribution for products at m/e=42 ($C_2H_3O^+$). Angles are measured from the oxygen atom beam. Scattered points: measured data points; dashed line: fit.

Fig. 2 Time-of-flight spectra for products at m/e=42 ($C_2H_3O^+$) at four different laboratory angles. Scattered points: data; solid lines: fits, scaled to the data for each angle separately.

Fig. 3 Mass spectrum determined for the vinoxy radical.

Fig. 4 Time-of-flight spectra for products at m/e=31 ($HC^{18}O^+$) and m/e=15 (CH_3^+) at 35°. Upper panel: m/e=31. Scattered points: data; dashed lines: fits for components due to channel (1a), large dashes, and channel (1b), small dashes; solid line: sum of the fits for channels (1a) and (1b). Lower panel: m/e=15. Scattered points: data; dashed lines: fits for components due to channel (1a), large dashes, and channel (1b), small dashes; dash-dotted line: contribution of nonreactively scattered ethylene; solid line: sum of the fits for channels (1a) and (1b) and nonreactive scattering contribution. Calculated curves and nonreactively scattered contribution are

scaled to the data for each angle and each channel separately.

Fig. 5 Translational energy distributions, $P(E_T)$, for channels (1a) and (1b).

Fig. 6 Center-of-mass angular distributions, $T(\theta)$, for channels (1a) and (1b).

Fig. 7 Newton diagrams of beam velocities and contour diagrams of product flux for CHO from channel (1a) and C_2H_3O from channel (1b).

Fig. 8 Time-of-flight spectra for products at m/e=30 ($C^{18}O^+$) at four different laboratory angles. Scattered points: data; dashed lines: fits for components due to channel (1a); dotted lines: fits for components due to channel (1b); solid lines: sum of the fits for channels (1a) and (1b). Calculated curves are scaled to the data for each angle and each channel separately.

Fig. 9 Schematic energy diagram for the reaction of $O(^3P)$ with ethylene. Solid lines: triplet surface; dashed lines: singlet surface.

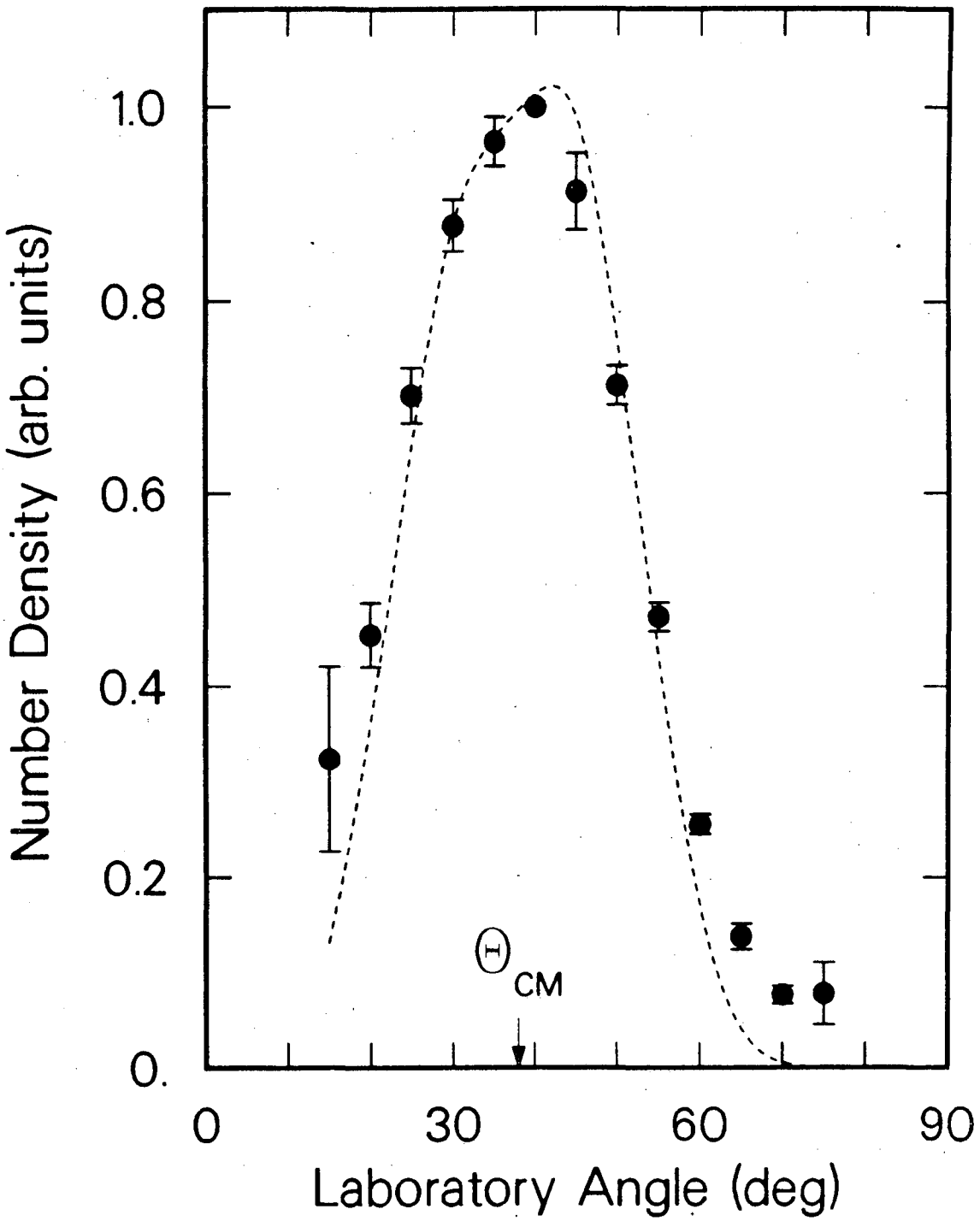
Number Density (arb. units)
1.0
0.8
0.6
0.4
0.2
0.
0
30
60
90
Laboratory Angle (deg)
Θ CM
XBL 896-2106

Fig. 1

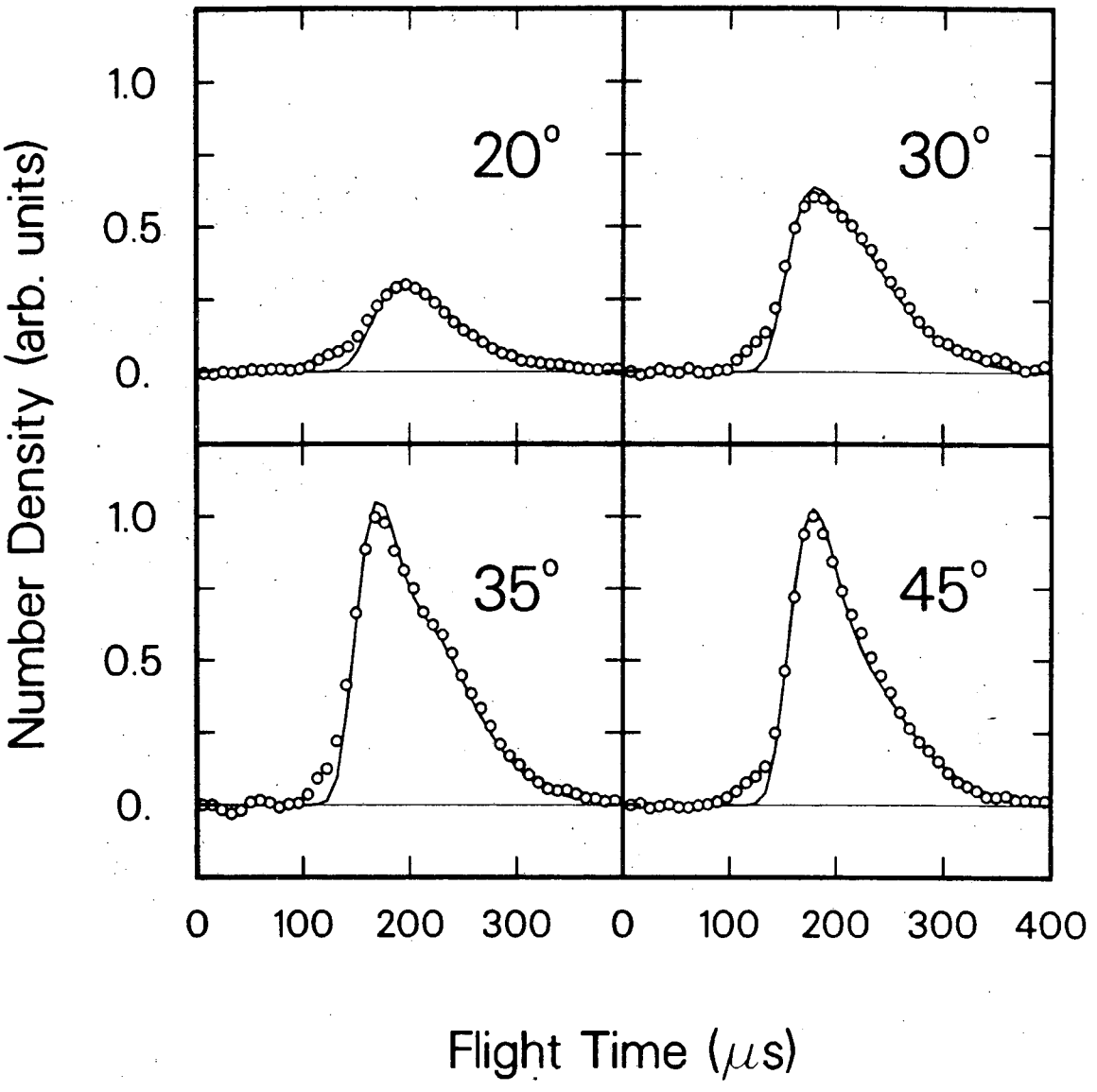

XBL 896-2107

Fig. 2

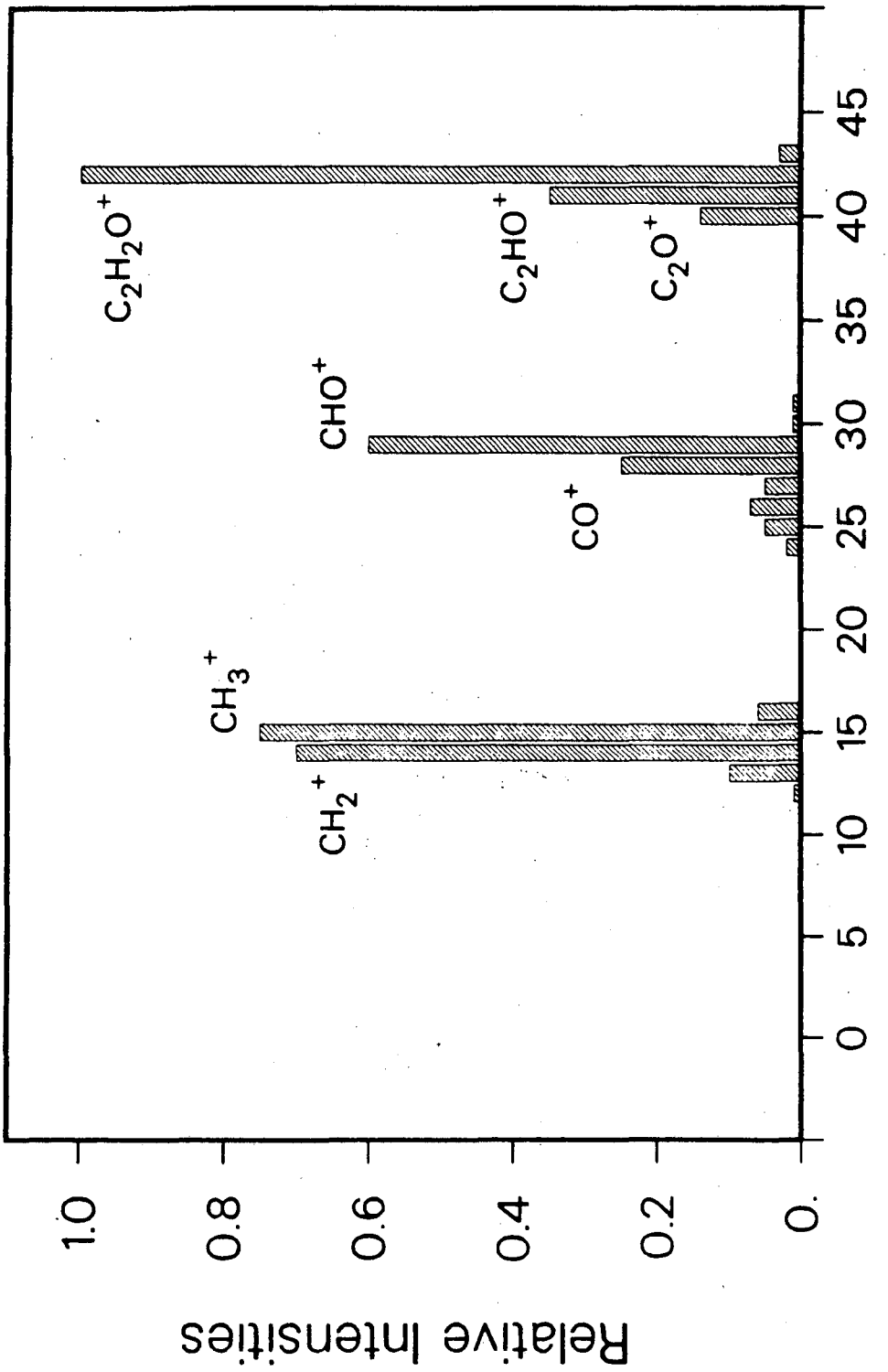

XBL 896-2111

Fig. 3

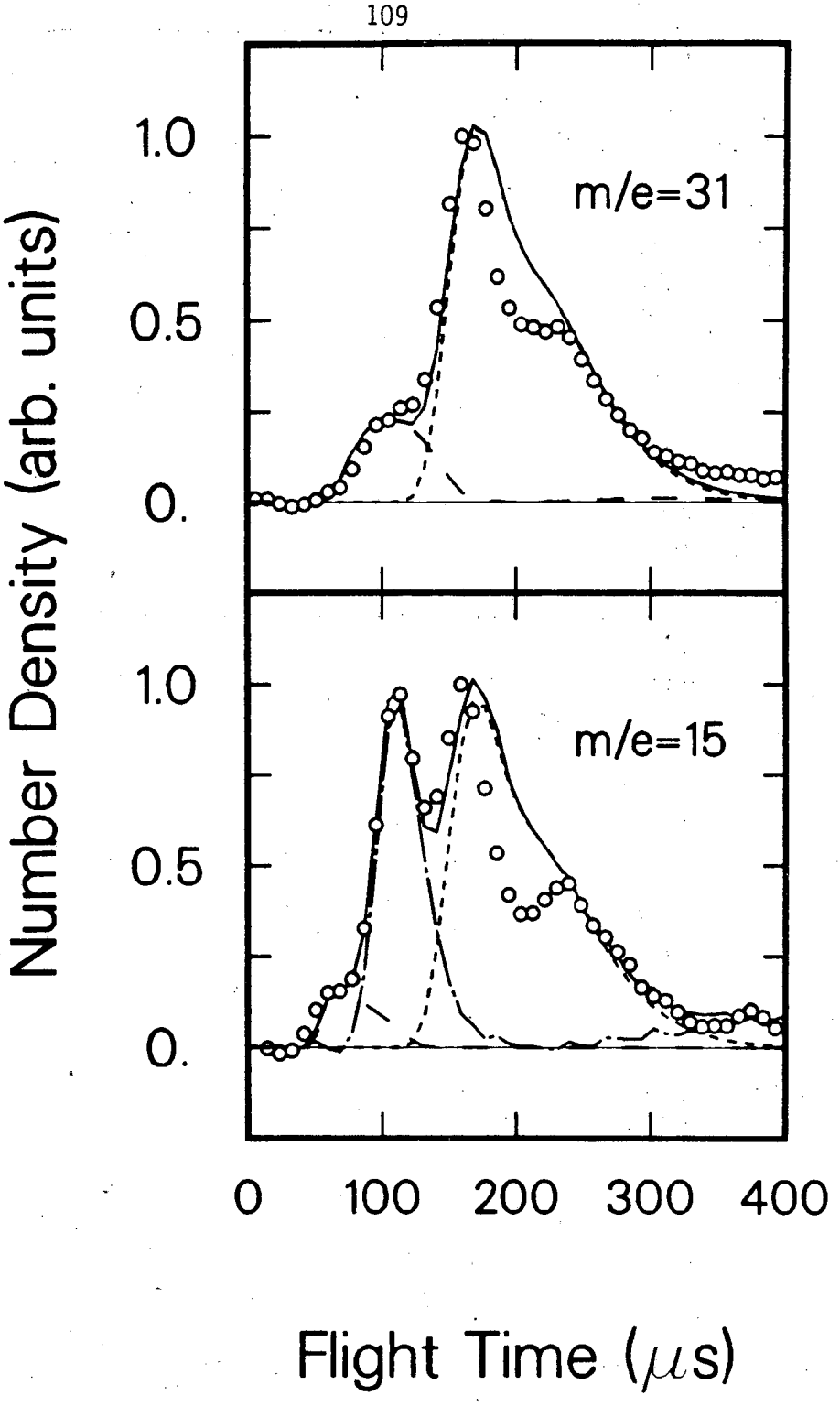

XBL 896-2108

Fig. 4

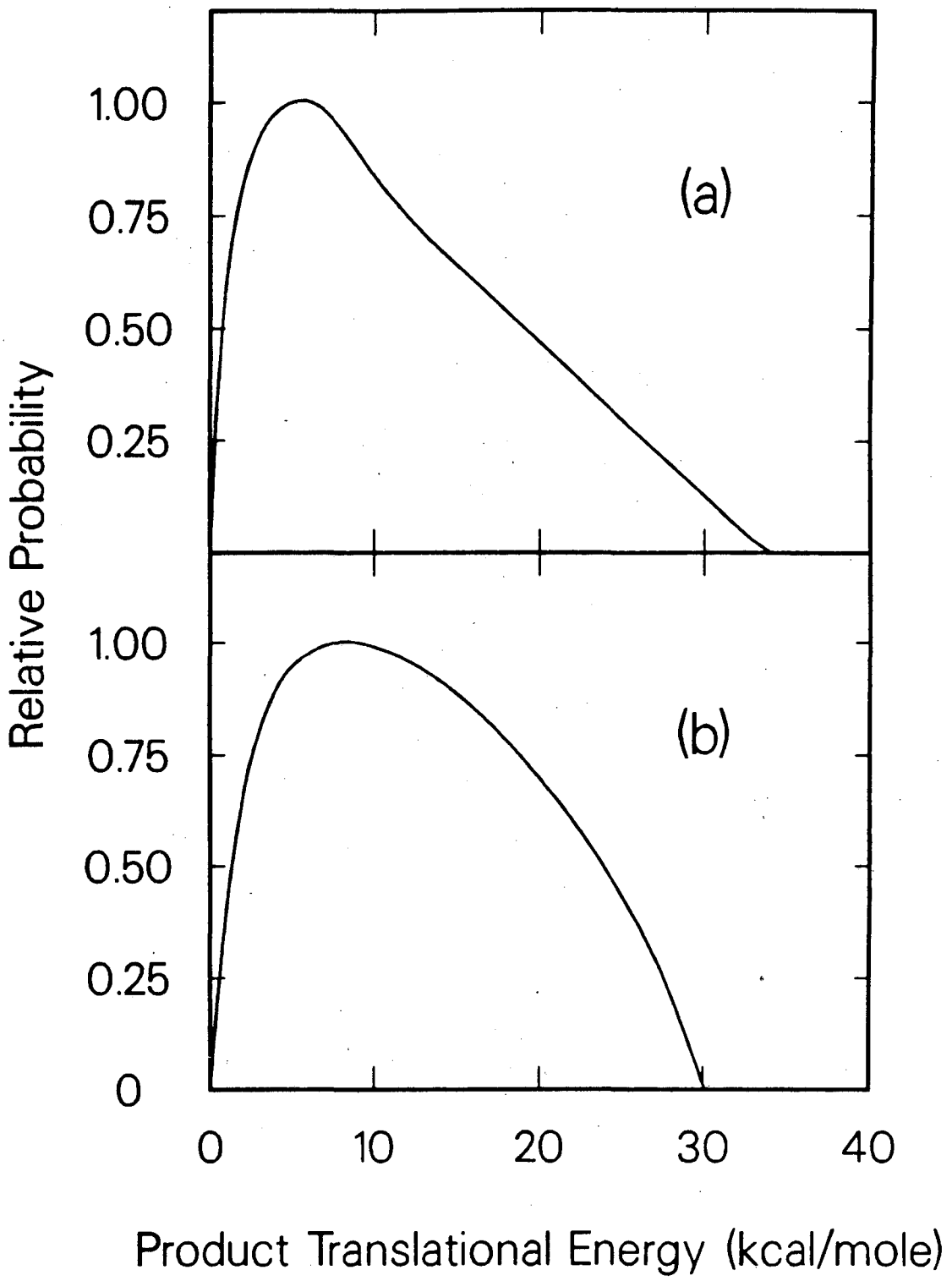
1.00
0.75
0.50
0.25
(a)
1.00
0.75
0.50
0.25
0
(b)
Relative Probability
0
10
20
30
40
Product Translational Energy (kcal/mole)
XBL 896-2113

Fig. 5

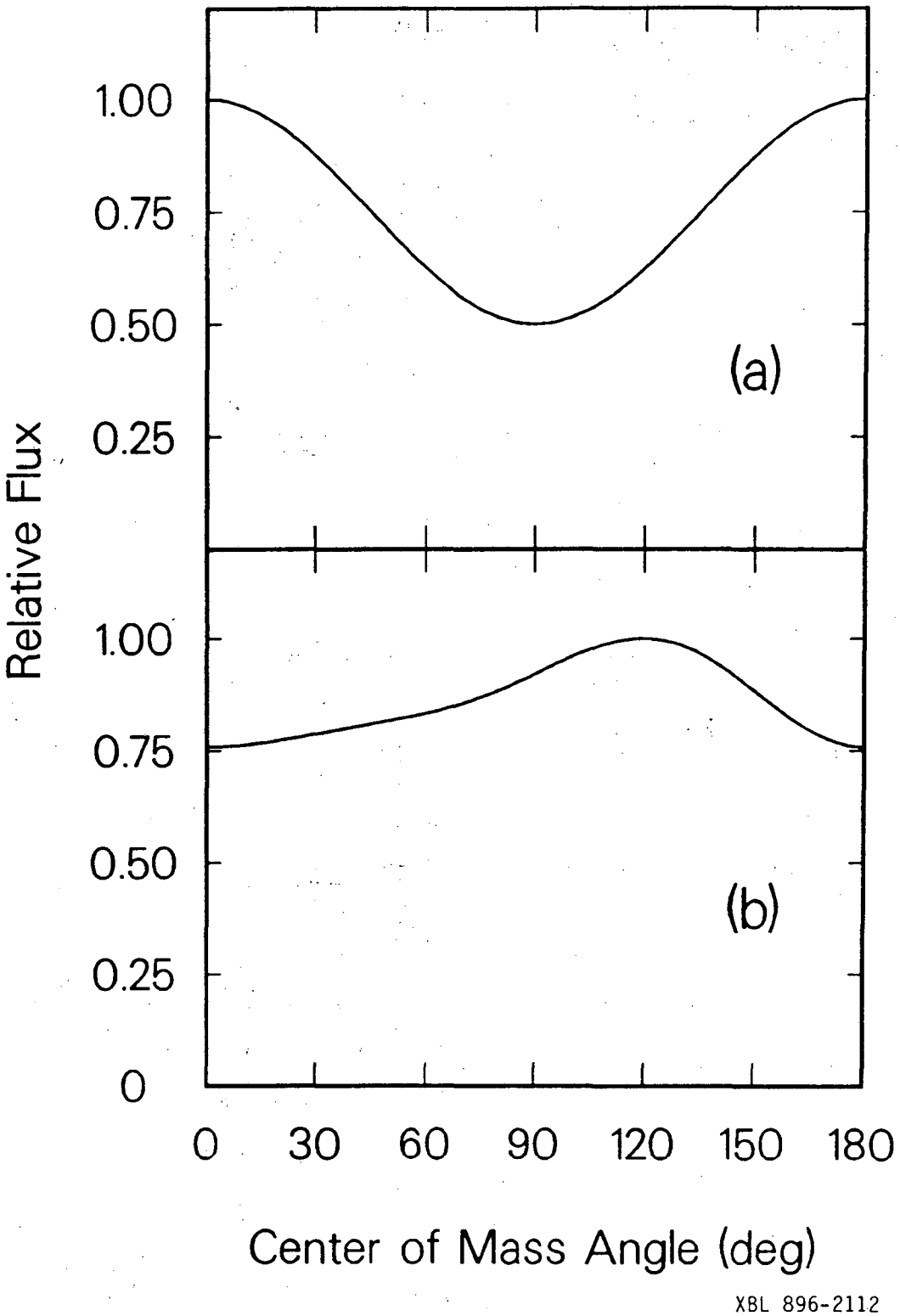
1.00
0.75
0.50
0.25
(a)
1.00
0.75
0.50
0.25
(b)
0
Relative Flux
0
30
60
90
120
150
180
Center of Mass Angle (deg)
XBL 896-2112

Fig. 6

$O(^3P) + C_2H_4 \rightarrow$

$H + \underline{C_2H_3O}$

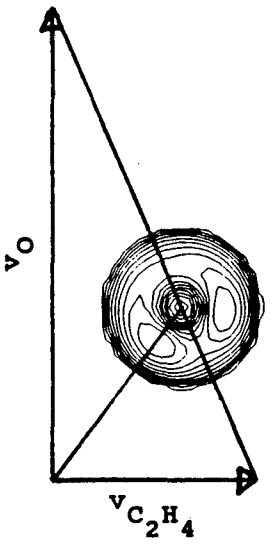

$O(^3P) + C_2H_4 \rightarrow$

$CH_3 + \underline{HCO}$

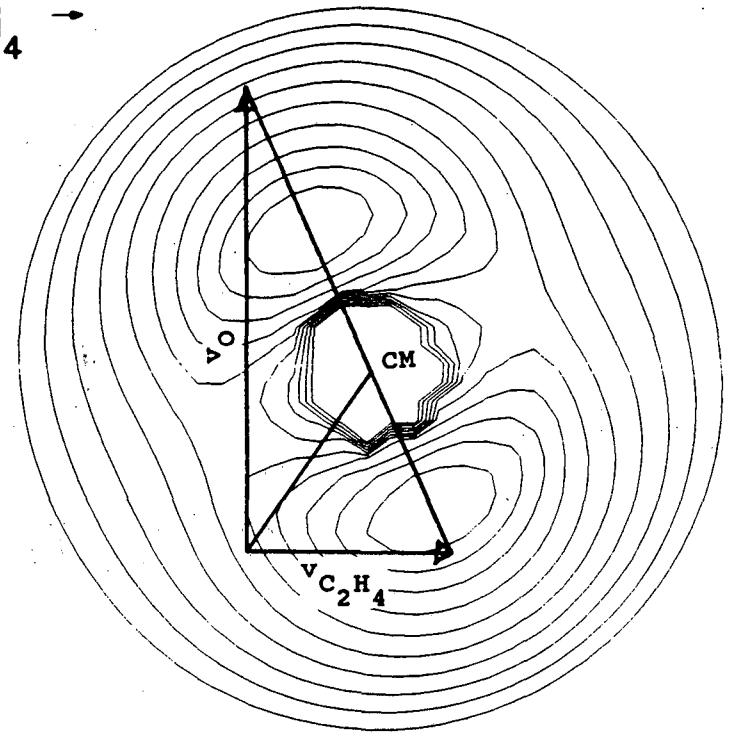

$1x10^5$ cm/s

XBL 896-2104

Fig. 7

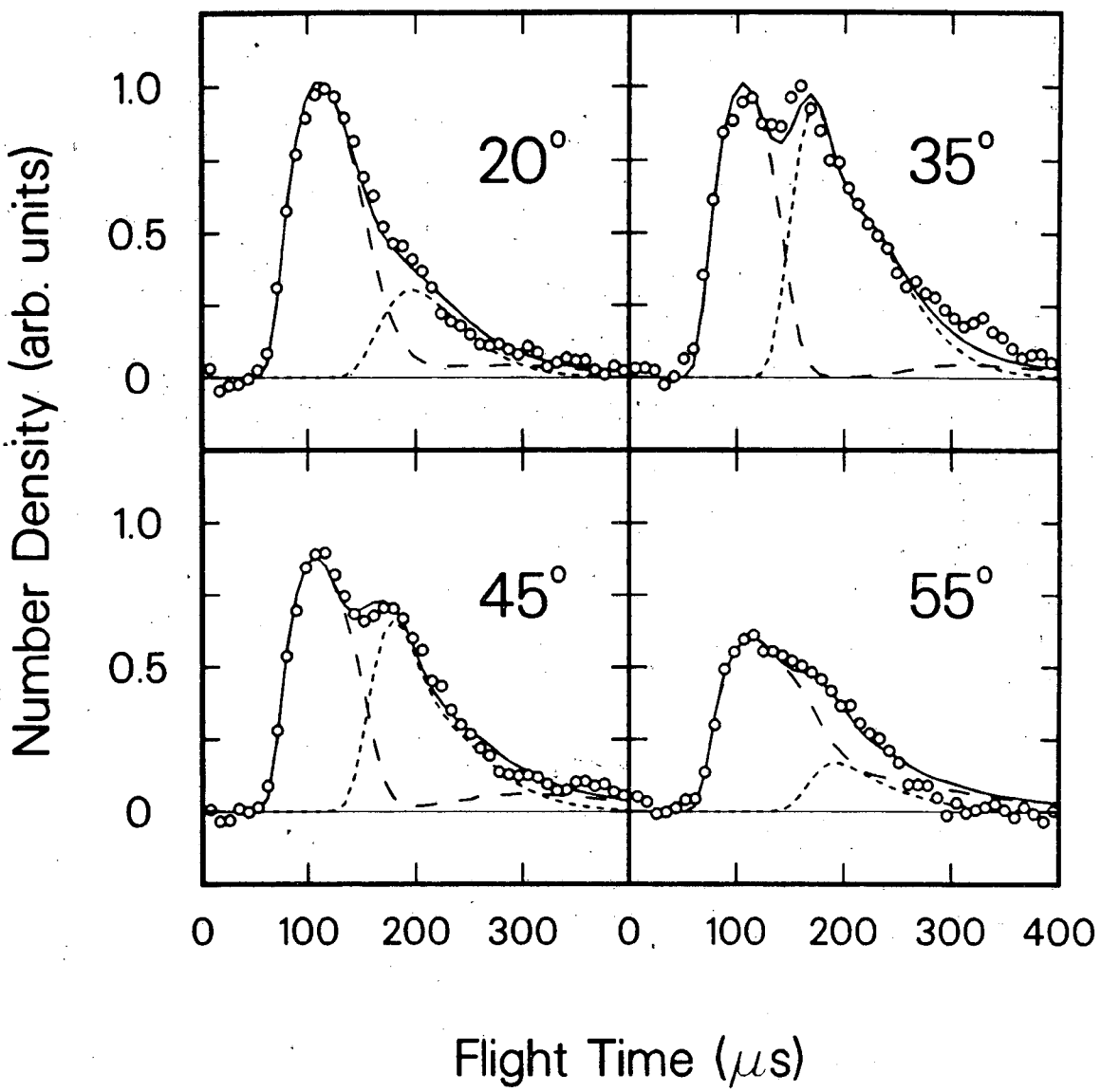

XBL 896-2109

Fig. 8

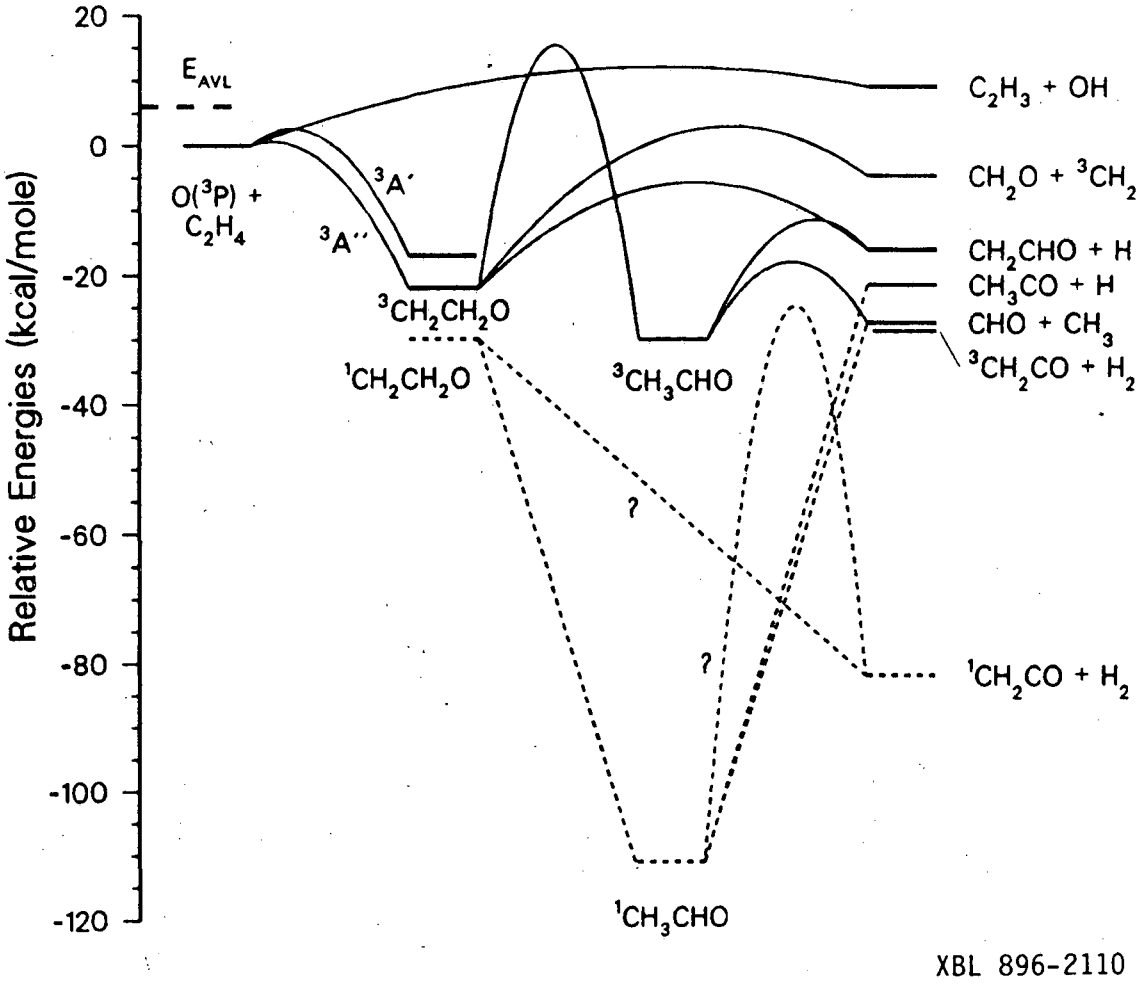
20
0
-20
-40
-60
-80
-100
-120
Relative Energies (kcal/mole)
E_{AVL}
$O(^3P) + C_2H_4$
$^3A'$
$^3A''$
$^3CH_2CH_2O$
$^1CH_2CH_2O$
$^3CH_3CHO$
$^1CH_3CHO$
?
?
$C_2H_3 + OH$
$CH_2O + {}^3CH_2$
$CH_2CHO + H$
$CH_3CO + H$
$CHO + CH_3$
$^3CH_2CO + H_2$
$^1CH_2CO + H_2$
XBL 896-2110

Fig. 9

CHAPTER 4

CROSSED MOLECULAR BEAM STUDY OF THE REACTION $O(^3P)$ + ALLENE

4.1. Introduction

The reactions of hydrocarbons with atoms or radicals are of particular importance in combustion chemistry, since they are often responsible for the consumption of the fuel molecules in flames. The reactions of ground state (^3P) oxygen atoms with a variety of simple hydrocarbons have been studied in this laboratory.[1-4] Here we present our recent results for the reaction of $O(^3P)$ with allene.

Two isomers of C_3H_4, allene and methylacetylene, have been identified as intermediates in the combustion of acetylene[5] and aromatic hydrocarbons.[6] The reaction of allene with oxygen atoms has been studied extensively[7-12] and the rate constant of this reaction has been determined.[11,13] However, questions remain regarding the mechanism of the reaction and the identity of the primary products.

The accepted general mechanism for reactions of $O(^3P)$ with unsaturated hydrocarbons[14] involves electrophilic addition to the double or triple bond. In the case of allene, the oxygen atom is thought to add to the central carbon atom[10] forming a

triplet diradical, the oxyallyl radical (**1**), which subsequently undergoes ring closure and intersystem crossing (ISC) to form singlet cyclopropanone (**2**). The highly excited cyclopropanone molecule then decomposes into carbon monoxide and ethylene:

$$O(^3P) + C_3H_4 \rightarrow C_2H_4 + CO \qquad (1a)$$

The results of several previous investigations[9-11] indicate that (1a) constitutes the predominant reaction channel.

1 **2** **3** **4**

However, this does not appear to be the exclusive path in the $O(^3P)$ + allene reaction. Acrolein (**3**) was identified as a minor product in the gas phase[10] and this species as well as its isomers cyclopropanone (**2**) and allene oxide (**4**) were recently detected in a cryogenic matrix as products of the $O(^3P)$ + allene reaction.[7] A channel producing hydrogen atoms and C_3H_3O (1b) was studied by Aleksandrov et al.[12] in a flow tube experiment using resonance fluorescence detection:

$$O(^3P) + C_3H_4 \rightarrow C_3H_3O + H \qquad (1b)$$

The complete mechanism of the $O(^3P)$ + allene reaction is

expected to be very complex. Attack of the oxygen atom to either the central or the terminal carbon atom has to be considered. Products can be formed on the initially accessed triplet potential energy surface, or ISC to a singlet state can lead to different sets of products. ISC is required for the formation of the stabilized (singlet) addition products cyclopropanone, allene oxide, or acrolein, and is expected to be facilitated in solid matrices. However, ISC in an isolated vibrationally excited C_3H_4O reaction intermediate is also likely to be fast, since this was found to be the case in the even smaller C_2H_4O diradical, the intermediate in the reaction of $O(^3P)$ with ethylene.[4]

The comparison with the $O(^3P)$ + ethylene reaction furthermore suggests the occurrence of hydrogen elimination from the triplet C_3H_4O diradical (channel 1b), in analogy to the formation of vinoxy radical and hydrogen atoms, channel (2a):

$$O(^3P) + C_2H_4 \rightarrow H + CH_2CHO \qquad (2a)$$

We indeed found evidence for channel (1b) in the $O(^3P)$ + allene reaction.

Our attempts to detect the products of reaction (1a), carbon monoxide and ethylene, were initially not successful due to background problems at m/e=28 (CO^+) and the interference of nonreactive scattering. However, the difficulties were overcome by using ^{18}O, and time-of-flight (TOF) spectra for $C^{18}O$ were

obtained at m/e=30.

We also searched for additional product channels. As a possible alternative route on the triplet surface, channel (1c), the formation of ketene and triplet methylene following attack of the central carbon atom was considered:

$$O(^3P) + C_3H_4 \rightarrow CH_2CO + {}^3CH_2 \qquad (1c)$$

Ketene was found in the matrix studies.[7] In our experiments, the detection of the methylene radical or the ketene parent proved to be extremely difficult due to the predominance of nonreactive (elastic and inelastic) signal at m/e=14 and 42. No unambiguous evidence for ketene was found.

If ISC is fast and hydrogen atom migration is facile on the singlet surface, as was found to be the case in the $O(^3P)$ + ethylene reaction,[4] additional channels are possible. Addition of oxygen to the terminal carbon atom leads to the diradical (**5**).

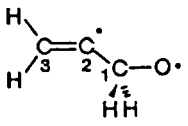

5

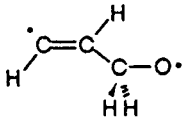

6

C_1-C_2 bond rupture in (**5**) would lead to the formation of vinylidene and formaldehyde, channel (1d):

$$O(^3P) + C_3H_4 \rightarrow CH_2C: + CH_2O \qquad (1d)$$

Subsequently, vinylidene can easily rearrange to acetylene.[15] Alternatively, hydrogen migration from C_3 in (**5**) to form (**6**) followed by C_1-C_2 bond rupture can lead to the formation of acetylene and formaldehyde, channel (1e):

$$O(^3P) + C_3H_4 \rightarrow C_2H_2 + CH_2O \qquad (1e)$$

The fact that formaldehyde was found in the matrix studies[7] suggests processes (1d) or (1e) as minor channels.

Hydrogen migration in (**5**) to acrolein (**3**) followed by C_1-C_2-bond rupture could result in vinyl radical and formyl radical, channel (1f):

$$O(^3P) + C_3H_4 \rightarrow C_2H_3 + CHO \qquad (1f)$$

Collisional stabilization of acrolein constitutes channel (1g):

$$O(^3P) + C_3H_4 \rightarrow [CH_2{=}CH{-}CHO]^{\ddagger} \xrightarrow{M} CH_2{=}CH{-}CHO \qquad (1g)$$

Acrolein was detected in gas phase experiments[10] as well as in cryogenic matrices.[7] Table 1 summarizes energetically possible reaction channels considered for the $O(^3P)$ + allene reaction.

Numerous theoretical investigations at both the semi-empirical and ab initio levels have been performed on various

parts of the singlet and triplet C_3H_4O-surfaces. The focus of much of the work, especially the earlier studies, was on the relative energies of the isomers cyclopropanone, allene oxide, and oxyallyl radical, and on the question of the stability of cyclopropanone.[24,25,27-35] In addition, the mechanisms of the thermal and photochemical decomposition of cyclopropanone and of the isomerization of cyclopropanone to allene oxide were investigated.[36-39] Recent ab initio calculations,[40] stimulated by our experimental work, focussed on the energetics and geometries of the two different modes of oxygen atom approach to allene on the triplet surface and the decomposition routes (1a) and (1b). Chiu and Abidi[41] specifically addressed the question of ISC from triplet oxyallyl to singlet cyclopropanone.

The goal of our work has been to explore the reaction of $O(^3P)$ with allene in the gas phase under single collision conditions. Of particular interest in this system is the question of competition between decomposition on the triplet surface and triplet→singlet ISC under collision free conditions. The results indicate that similarities with the model system $O(^3P)$ + ethylene exist, but also that interesting additional processes take place.

4.2. **Experimental**

The experimental setup has been described in detail

recently.[3] Briefly, a universal crossed molecular beam apparatus[42] was used, where two continuous supersonic molecular beams were crossed at 90° in a high vacuum chamber. The detector consisted of a differentially pumped mass spectrometer equipped with an electron-impact ionizer, quadrupole mass filter, and Daly scintillation ion counter and was rotatable in the collision chamber around the intersection region of the two molecular beams.

The high pressure supersonic oxygen atom beam source employed in these experiments was described by Sibener et al.[43] We used mixtures of 5% O_2 in Ne for all experiments. Only ground state (^3P) oxygen atoms were formed under our experimental conditions.[3] The gas mixture, at pressures from 400 to 600 Torr, was expanded through a quartz nozzle whose diameter varied between 0.10 and 0.25 mm. The dissociation of O_2 was induced by a radio frequency discharge.

The supersonic allene beam was formed by expanding a mixture of 5% allene in helium at a backing pressure of 200-350 Torr through a nozzle of 0.15 mm diameter which was held at room temperature (for the TOF experiments) or heated to about 80°C (for the angular distribution measurements).

The peak velocities of the oxygen atom beam were between 1.8 and 2.1×10^5 cm/s with speed ratios around 5 and the peak velocity of the allene beam was 1.45×10^5 cm/s with a speed ratio of about 11, resulting in most probable collision energies of 7-8 kcal/mole.

The measurement of the reaction products was carried out in two different ways: First, angular distributions of several masses were measured by modulating one of the beams for background subtraction. Typically, 12 angular scans were obtained for each m/e value, with total counting times of 20 min per angle. Second, TOF distributions were recorded at several laboratory angles and for several masses using the cross-correlation technique.[44] Total accumulation times for the TOF measurements ranged from a few minutes to about two hours depending on the angle and the m/e monitored.

The allene was obtained from Matheson with a stated purity of 95% min. GC/MS analysis was performed on the allene and no impurities were found in detectable amounts. Oxygen/neon mixtures were purchased from Matheson and Airco and had a stated minimum purity of 99.99% and 99.995%, respectively. $^{18}O_2$ with a stated isotopic purity of 95% minimum was kindly provided by Los Alamos National Laboratory and was mixed with neon of 99.995% stated minimum purity purchased from Airco. All gases were used without further purification.

4.3. **Results and Analysis**

Angular distributions for the reaction $O(^3P)$ + allene were measured at various masses, however, meaningful reactive scattering data could be obtained only at m/e=53 (C_3HO^+) and 54

($C_3H_2O^+$). At these masses, only one channel contributes to the signal: the formation of C_3H_3O, reaction (1b). At many other masses of interest, such as m/e=42 (parent mass of ketene) or m/e=14 (parent mass of methylene and major fragment of ketene), fragment ions produced in the dissociative ionization of nonreactively scattered reactants predominate. In the case of m/e=28 (parent mass of both CO and ethylene, major fragment of many species), a large inherent detector background interferes with the measurements.

The angular distribution of m/e=53 is shown in Fig. 1. The direction of the oxygen atom beam corresponds to a laboratory angle of 0°. The error bars represent 95% confidence intervals. The maximum count rates were approximately 8 counts/s. The angular distribution of m/e=54 was found to be superimposable on the m/e=53 distribution after appropriate scaling, but the count rate at this mass was considerably lower. A distinct peak was found whose maximum occurs at an angle close to the direction of the center-of-mass (CM) of the system. Thus the C_3H_3O radical product, recoiling from a light H atom, has a comparatively small CM velocity, and is confined to a small angular range in the laboratory frame, as can be seen in Fig. 1.

When a pair of products with similar or identical masses are produced, such as in the case of the formation of carbon monoxide and ethylene, both products have the same and relatively large velocities in the CM coordinate system and are therefore scattered over a very large angular range even at

translational energies of only a few kcal/mole. The scanning range of the detector can only probe part of such distributions. Because of this large spread the fraction of the products detected at any particular angle is small, further limiting the chances of obtaining meaningful data.

Because of these difficulties and because the reaction is expected to go through a long lived complex with an expected forward-backward symmetric angular distribution, we focussed our efforts on the measurement of TOF spectra. They provide a significant amount of dynamic information and allow us to distinguish features due to different reactive and nonreactive channels. Due to extensive fragmentation in the electron-impact ionizer, signal is often detected at many different ion masses for each product. Parent/daughter-ion relationships can be established by identifying the corresponding features in spectra at different masses.

Cross-correlation TOF spectra were obtained at several different angles at the m/e ratios of 14, 25, 26, 27, 28, 29, 30, 31, 32, 40, 41, 42, 52, 53, 54, and 55 using ^{16}O, corresponding to the ions CH_2^+, C_2H^+, $C_2H_2^+$, $C_2H_3^+$, CO^+ or $C_2H_4^+$, CHO^+, CH_2O^+, CH_3O^+, O_2^+, $C_3H_4^+$ or C_2O^+, $^{13}C^{12}C_2H_4^+$ or C_2HO^+, $^{13}C_2{}^{12}CH_4^+$ or $C_2H_2O^+$, C_3O^+, C_3HO^+, $C_3H_2O^+$, and $C_3H_3O^+$, respectively; and at the m/e ratios 30, 31, and 55 using ^{18}O, corresponding to the ions $C^{18}O^+$, $CH^{18}O^+$, and $C_3H^{18}O^+$, respectively.

It should be noted that the TOF spectra at m/e=29 and 30

shown in Figs. 2 and 3 were corrected for an experimental artifact which was described in detail in our previous paper[3] and has no effect on the results of the data fitting procedure. The signal appearing at flight times of over 300 μs at 50°, 60°, and 70° is also a result of this artifact.

A forward-convolution method was used for the analysis of the reactive scattering data. The FORTRAN code was based on versions used previously.[45] The goal of the analysis was to find the product translational energy distribution, $P(E_T)$, and the angular distribution in the center-of-mass (CM) frame for the reactions, $T(\theta)$. $P(E_T)$ and $T(\theta)$ were assumed to be independent of each other. Furthermore, within the narrow spread of reactant collision energies in our experiment, the relative cross-sections were assumed to be independent of the collision energy. From the $P(E_T)$ and $T(\theta)$ functions, laboratory angular distributions and TOF spectra were calculated and averaged over beam velocities and collision angles as well as the detector acceptance angle and the length of the ionizer and then scaled to the experimental data. This was repeated until a best fit to the experimental data was found. For maximum flexibility, the $P(E_T)$ trial functions were not confined to a particular functional form. The $T(\theta)$ functions on the other hand were represented as linear combinations of Legendre polynomials.

4.3.1. $\underline{C_3H_3O + H \text{ channel}}$

M/e=53 was identified as a fragment of C_3H_3O, a product of channel (1b). TOF data for m/e=53 are shown in Fig. 4. The solid lines through the data in Figs. 1 and 4 represent the best fit. The relatively poor fit of the angular distribution at smaller angles could be due to the nonreactive scattering of impurities coming from the beams.

The translational energy distribution $P(E_T)$, shown in the upper panel of Fig. 5, and the CM angular distribution $T(\theta)$, shown in the upper panel of Fig. 6, fit both the TOF data and the angular distribution simultaneously. The $P(E_T)$ distribution for this channel is very broad, extending to 25 kcal/mole, which corresponds to the total available energy of the system, namely the sum of collision energy, exothermicity (16 kcal/mole[46]), and internal energy left in the allene molecules after the supersonic expansion. Both the energy of maximum probability and the average energy in this distribution are around 12 kcal/mole. The $T(\theta)$ (see Fig. 6) is almost isotropic but shows slight backward peaking with respect to the oxygen beam. The deviation from isotropy for this channel is small and probably insignificant.

The TOF spectra of m/e=52, 53, and 54 showed identical features, m/e=53 having the highest count rates. At m/e=55, the parent mass of C_3H_3O, no peak was found. The data at m/e=55 obtained with ^{18}O were equivalent to the data at m/e=53 using ^{16}O. Furthermore, components due to the fragmentation of $C_3H_3O^+$

could be identified at m/e=29 (CHO^+), m/e=30 ($C^{18}O^+$), and m/e=31 ($CH^{18}O^+$). Fig. 2 shows these components as the slowest features (dashed line, small dashes) at 50°, 60°, and 70° for m/e=29, and Fig. 3 for m/e=30. The fact that no signal was observed at the parent mass of C_3H_3O, m/e=55, is not too surprising since in the case of the O + ethylene reaction (2a) the major fragment of vinoxy radical was found to be at m/e=42, and only very little signal was observed at m/e=43, the parent of vinoxy radical.[2,4] The mass spectrum of ketenyl radical HCCO, on the other hand, was found to peak at its parent mass m/e=41 under the same conditions.[3]

4.3.2. <u>CO + C_2H_4 channel</u>

As mentioned in the introduction, extensive efforts to detect the products of channel (1a), carbon monoxide and ethylene, were initially not successful because of a number of experimental difficulties. The background problems at m/e=28 were overcome by using ^{18}O, enabling us to detect $C^{18}O^+$ at m/e=30.

Fig. 3 shows the m/e=30 TOF spectra at five different laboratory angles. In all five spectra, a sharp and fast feature, which peaks around 55 μs, was identified with $C^{18}O$ from channel (1a). The chain-dashed lines in Fig. 3 represent the best fit for this assumption. The translational energy distribution $P(E_T)$ used is shown in Fig. 7. The CM angular distribution $T(\theta)$ is shown in the lower panel of Fig. 6. The

$P(E_T)$ distribution for this channel peaks around 32 kcal/mole and the average translational energy is about 40 kcal/mole. A minimum translational energy of about 15 kcal/mole was observed. It should be noted, however, that the exact shape of this distribution could not be determined from the available data. The fit is not very sensitive to the fast edge of the distribution due to the lack of sufficient resolution for products arriving at the detector in a very short time. It is clear, however, that in this case the distribution does not extend to the total available energy of approximately 126 kcal/mole. The precise determination of the minimum translational energy suffers from the fact that the contributions of the different components of the CO^+ signal can not be separated easily.

The CM angular distribution could not be determined with great certainty since a large fraction of the CO product is scattered outside the detector scanning range. As can be seen in Fig. 3, the signal at m/e=30 is of comparable size at all angles measured, indicating a flat laboratory angular distribution resulting from a fairly isotropic CM angular distribution. The best fit was obtained using the $T(\theta)$ shown in the lower panel of Fig. 6, which is forward-backward symmetric and slightly forward-backward peaking. The deviations from isotropy are probably insignificant in this case, as well.

The m/e=30 data at 50°, 60°, and 70° also show slow features (centered around 160 μs) deriving from channel (1b), as

mentioned above. Furthermore, all five angles show an additional component with intermediate velocities. The step at flight times of around 70 μs in each of the five spectra clearly suggests the presence of a third channel.

4.3.3. CHO + C_2H_3 channel

The nature of the product or products from which the signal at intermediate velocities (see Fig. 3) originates, could not be determined unambiguously. Both the m/e=30 data ($C^{18}O^+$) and the m/e=29 data (CHO^+) show this component at all angles measured.

Since the reaction channel (1b) was found in striking similarity to the $O(^3P)$ + C_2H_4 reaction, it appears very likely that an analogous reaction to

$$O(^3P) + C_2H_4 \rightarrow CHO + CH_3 \qquad (2b)$$

could occur in the case of allene as well. This channel would involve a 1,2-hydrogen migration from the carbon atom to which the oxygen atom is bonded and subsequent C_1-C_2 bond rupture. At the collision energies of typical molecular beams experiments, this process is only possible if T↦S ISC occurs in the initially formed diradical. In the allene case, the product of this hydrogen migration would be acrolein, and the fragments formyl radical and vinyl radical. Even though neither of these two radicals was identified as a product of the $O(^3P)$ + allene reaction previously, acrolein has been identified in both gas

phase and matrix experiments.[7,10]

As can be seen from the fits in Figs. 2 and 3, the production of formyl + vinyl radicals through reaction (1f) can account for the remainder of the reactive scattering signal. The $P(E_T)$ used for this fit (lower panel of Fig. 5) peaks at 5 kcal/mole and has an average translational energy of about 11 kcal/mole and a maximum translational energy of 30 kcal/mole, corresponding to approximately the maximum available energy for this channel. As for the CO + C_2H_4 channel, the CM angular distribution $T(\theta)$ could not be determined accurately for (1f). It appears that a forward-backward symmetric, strongly forward-backward peaked distribution fit the data best.

4.3.4. Other channels

The identification of the features in the TOF spectra (Figs. 2 and 3) which peak at flight times around 100 μs with CHO from channel (1f) is not unambiguous. Alternatively, we were able to fit this signal using a combination of other channels, such as the formation of ketene and triplet methylene, channel (1c), and the formation of formaldehyde and C_2H_2, channel (1d) or (1e).

The total available energy for channel (1c) is approximately 30 kcal/mole. Even when a $P(E_T)$ extending to the total available energy was used, the TOF distributions calculated for this process could not account for all the remaining signal in the TOF spectra after channel (1a) and (1b)

had been considered. An additional faster component was needed. This can be provided by channel (1d) or (1e) - or channel (1f). We considered (1e) as a possible minor channel since a small peak was observed at m/e=30 using ^{16}O (CH_2O^+). However, the data at m/e=30 using ^{16}O were too noisy to determine the origin of this peak.

Using a combination of contributions from channels (1c) and (1e), the faster part of the signal at m/e=29 (CHO^+) and the intermediate part of the signal at m/e=30 ($CH^{18}O^+$) could be reproduced well. Thus the occurrence of either of these channels is in agreement with our data, as is a combination of them and channel (1f). If (1f) is a major channel and the others are also occurring to some extent, then the $P(E_T)$ and $T(\theta)$ distributions we are reporting for that channel are uncertain to some degree.

4.3.5. Alternative interpretations

It should be noted that the data that were assigned to the C_3H_3O + H channel (1b) could be fitted equally well with the assumption of the formation of a hydrogen molecule and propadienone:

$$O(^3P) + C_3H_4 \rightarrow CH_2{=}C{=}C{=}O + H_2 \qquad (1h)$$

This channel would be analogous to the formation of ketene and molecular hydrogen in the $O(^3P)$ + ethylene case, reaction (2c),

$$O + C_2H_4 \rightarrow CH_2CO + H_2 \qquad (2c)$$

(2c) is possibly a minor channel in the $O(^3P)$ + ethylene system. The occurrence of channel (1h) cannot be excluded on the basis of our data. However, we are confident that at least most of the signal at m/e=53 and other fragments is indeed due to channel (1b).

If all the signal at m/e=53 would indeed be due to a fragment of CH_2CCO, then the $P(E_T)$ required would be a broad distribution like that for channel (1b), but peaking at 6 kcal/mole. This number appears to be too low for a channel forming closed shell products. In such a case strong repulsions are expected as soon as the new bonds are formed leading to a considerable release in translational energy. It therefore seems much more likely that the product observed at fragments $C_3H_2O^+$ and smaller stems from channel (1b).

An alternative interpretation is also possible for the fast feature which was assigned to channel (1a). The formation of formaldehyde and acetylene, channel (1e), is exothermic by about 75 kcal/mole. If channel (1e) would occur with a translational energy release of up to the available energy with a distribution peaking around 50-60 kcal/mole, then the fast features in all spectra at m/e=30 could be accounted for. However, if formaldehyde were formed, it would be expected to fragment into CH_2O^+ (m/e=30) and CHO^+ (m/e=29) to a significant degree. As

can be seen in Fig. 2, the fast feature is absent in the m/e=29 data, and the same is true for the m/e=30 data taken using ^{16}O (not shown) which showed no clear peaks at all.

It appears unlikely that channel (1e) constitutes a major pathway, since in none of the previous $O(^3P)$ + allene experiments significant amounts of formaldehyde were detected, whereas all investigators reported large amounts of carbon monoxide and ethylene. This, however, does not exclude the possibility of channel (1e) as a minor pathway.

4.3.6. Branching Ratios

The crossed molecular beam method does not yield absolute reaction cross sections readily; however, relative cross sections can be determined. Using the method described in detail in Ref. 3, the branching ratio between different reaction channels can then be evaluated. In order to do so, the relative ionization cross sections for the products as well as the ion fragmentation patterns are required. In this case, the total ionization cross sections were calculated using an empirical method.[47] The fragmentation pattern of CO was taken from the literature.[48] For HCO, the two major fragments were measured at m/e=29 (HCO^+) and 30 ($C^{18}O^+$). For C_3H_3O, some of the major fragments in the mass spectrum could be measured, m/e=29 being the largest, followed by m/e=53. The TOF spectra at m/e=26 and particularly m/e=27 indicated large signals due to cracking of C_3H_3O, but quantitative evaluation proved to be not feasible

because of the predominance of contributions from nonreactively scattered allene, and estimates of the contributions to the mass spectrum had to be made. The contributions of the remaining masses were taken to be the same as those for the ionization of acrolein.[48]

The branching ratio between channel (1a) and (1b) R_{ab}, defined as the ratio between the relative reaction cross sections σ_a and σ_b, was thus calculated to be approximately 4. The error limits on this number are large due to incomplete knowledge of the fragmentation pattern of the vibrationally excited $C_3H_3O^+$, the large uncertainty in the $P(E_T)$ caused by incomplete separation of the different reactive contributions to the measured spectra and uncertainties of the fit, as well as uncertainties arising from the empirical determination of the ionization cross sections. However, our data clearly indicate that channel (1a) has a significantly higher probability of occurring than channel (1b), which is in agreement with the earlier assumptions about the importance of channel (1a).[9-11]

Assuming that all the signal with flight times between those of channel (1a) and (1b) stems from channel (1f), formation of vinyl and formyl radicals, a relative cross section for this channel can be calculated as well. $R_{fa} = \sigma_f/\sigma_a$ was determined to be approximately 4, implying that channel (1f) is the major reaction pathway. This result must be interpreted with caution, since the assignment of the signal exclusively to

channel (1f) can not be done with certainty. This is also in contradiction to the previous results[9-11] which indicate that the formation of CO and ethylene is the single most important channel. However, it is very likely that the radical products went undetected in the earlier experiments or reacted further to the final products observed.

4.4. Discussion

Table 1 lists several of the energetically accessible reaction channels considered in the O + C_3H_4 reaction system, and Figs. 8 and 9 schematically show the triplet and singlet potential energy surfaces involved in the reactions studied. There are large uncertainties in some of the energy levels and particularly in most of the barrier heights.

The initial step in the reaction is electrophilic addition of the oxygen atom to either the central or the terminal carbon atom. The potential for the terminal carbon attack channel is expected to resemble that for $O(^3P)$ addition to C_2H_4. This is confirmed by ab initio MCSCF calculations performed by Huang and Lester.[40] The entrance channel barrier for the terminal carbon attack was calculated to be 23.5 kcal/mole which is clearly too high, since reaction was observed at lower collision energies, 8 kcal/mole and less. Similarly, the energy levels calculated for the intermediates and products are likely to be too high. In

fact, the triplet adduct (**5**) was found to be less stable than the reactants when double zeta or double zeta + polarization basis sets were used, but more stable for a single zeta basis set. In analogy to the results by Dupuis et al.[49,50] who used similar methods in a study of the O + C_2H_4 system, it can be expected[40] that CI corrections would reduce the calculated values by about 15 kcal/mole. (The O + C_2H_4 entrance channel barrier was calculated[49] to be 16 kcal/mole, but is actually very small.[51]).

The resulting diradical (**5**) has a plane of symmetry but is not planar. The C_1-O bond has partial double bond character and the C_2-C_3 double bond remains intact.[40]

H elimination from (**5**) leads to allenyloxy (α-formyl-vinyl) radical (**7**). The barrier for this process has not been calculated, but is likely to be similar to that for the CH_2CH_2O → CH_2CHO + H reaction, or about 18.5 kcal/mole.[18] The C_1-O and C_2-C_3 distances are shorter than the C_1-C_2 distance,[40] indicating a double bond character for the C_1-O and C_2-C_3 bonds. Thus a cis- and a trans-isomer of (**7**) can be distinguished:

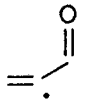

7a

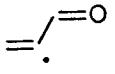

7b

The data we obtained on the ionizer cracking pattern of (**7**) show large ion signals at m/e=29 (CHO^+) and m/e=26 and 27 ($C_2H_2^+$

and $C_2H_3^+$) similar to the fragmentation of acrolein,[48] indicating a relatively weak C_1-C_2 bond.

Our data suggest significant similarities between channel (1b) and the $O(^3P) + C_2H_4 \rightarrow H + C_2H_3O$ reaction (2a). The translational energy distribution we obtained is very similar to that in the ethylene case, but clearly broader. The maximum translational energy corresponds roughly to the available energy calculated assuming the same exothermicity as channel (2a) for $O(^3P)$ + ethylene. The CM angular distribution was found to be isotropic, again very similar to the ethylene case.

For the oxygen atom attacking the central carbon atom of allene, a lower entrance channel barrier than for the terminal carbon attack was calculated by Huang and Lester,[40] namely 16.7 kcal/mole. Again, this value must actually lie considerably lower, since reaction (1a) was observed at thermal energies.[9-11]

The oxygen atom approach toward the central carbon atom can be visualized as follows: the two oxygen p-orbitals, each containing one unpaired electron, interact with the two π-orbitals of allene which are orthogonal to each other. The two allene π-bonds are (partially) replaced by a C-O σ-bond and a C-O π-bond, respectively. This is confirmed[40] by the lengthening of the C-C bonds as the O comes closer. At the same time, the C-C-C backbone bends, and the hydrogen atoms move into the C-(CO)-C plane. The final C-C and C-O bond lengths indicate partial double bond character. Assuming no ISC occurs, triplet oxyallyl (**1**) is formed. Its energy was calculated[40] to be 23.5

kcal/mole lower than $O(^3P)$ + allene.

Twenty years ago, Hoffmann[35] had already predicted the ground state of oxyallyl to be a triplet. Recently, Osamura et al.[52] calculated the structures of several low lying singlet and triplet states of oxyallyl. The ground state ($^3B_2$) and the first excited state ($^1A_1$) were found to be only 6 kcal/mole apart.

Oxyallyl was postulated as an intermediate in various reactions, such as the isomerization of cyclopropanone to allene oxide[53] or the racemization of substituted cyclopropanones,[54] however, it could never be established experimentally.[23,55] Cyclopropanone, on the other hand, has been synthesized and its chemistry is well studied,[56] and detailed spectroscopic information has become available.[7,23,57]

Triplet → singlet ISC has to take place in order for cyclopropanone to be formed from triplet reactants. A process where orbital angular momentum and spin are changed simultaneously can provide the mechanism for efficient ISC.[40,41] Several electronic states of oxyallyl which are close in energy possibly facilitate the conversion. Sevin et al.[37] have determined the approximate position of a crossing point at $\leq$ 55 kcal/mole above the ground state of cyclopropanone, using ab initio calculations without complete geometry optimization.

The decomposition of cyclopropanone has received much attention. The calculations by Sevin et al.[37] indicate that the lowest energy pathway from ground state cyclopropanone is

actually C_2-C_3 bond scission, resulting in the oxyallyl diradical. This is in accord with the experimental results of Rodriguez et al.[23] who found that the thermal reaction produced no volatile substances but only a polymer. C_1-C_2 scission on the other hand requires a higher activation energy (about 80 kcal/mole) and an additional 15 kcal/mole to overcome the barrier to completely dissociate the molecule.[37]

The photochemical reaction, on the other hand, following excitation to the $^1n\pi^*$ state, should proceed along the C_1-C_2 scission/CO extrusion channel, since the barrier for this was found[37] to be considerably lower than for C_2-C_3 bond scission. A surface crossing is required to reach the ground states of the products CO and C_2H_4. The results of the ab initio calculations by Yamabe et al.[38] indicate that this process is "bent-in-plane", where the C-C-C-O plane continues to be the plane of symmetry. It is possible that channel (1a) involves the triplet or singlet $n\pi^*$ state of cyclopropanone, rather than the ground state.

Lin et al.[9] measured the distributions of CO vibrational energy in the reactions of $O(^3P)$ with allene and methylacetylene. In the case of the allene reaction, excitation up to v=7 was found for CO, corresponding to a Boltzmann vibrational temperature of 5100±100K or an average vibrational energy of 6.8 kcal/mole. These values were found to be consistent with a statistical model where the energy in the cyclopropanone is completely randomized, and assuming CO and

C_2H_4 are so loosely bound that they could rotate freely. This is in agreement with the theoretical result[37,38] that the dissociation is not a one-step process with a tight transition state but proceeds through an open $\cdot CO\text{-}CH_2\text{-}CH_2\cdot$ diradical.

The results of our experiments suggest that in channel (1a) a large amount of energy is channelled into translation, indicating a repulsive interaction upon separation of the products. Ab initio calculations[37,38] indeed predict a large exit barrier.

An alternative pathway leading to the products CO and C_2H_4 through terminal carbon attack can be envisioned[58] as a hydrogen transfer from CHO to the vinyl radical in the process of acrolein decomposition. The additional barrier for this process can be expected to be small in view of the large exothermicity of the CO + C_2H_4 production.

While ab initio calculations already provide a great deal of information on channels (1a) and (1b), little work has been done on any of the other channels mentioned above. In particular, oxygen atom attack on the terminal carbon followed by 1,2-hydrogen migration to acrolein has not been considered. However, the occurrence of channel (1g), formation of acrolein, has been observed in condensed phase[7] and high pressure gas phase[10] experiments. No information is available on the hydrogen migration barrier, but it can be assumed that it would be high on the triplet surface. In analogy to the C_2H_4/O system, ISC is expected to occur followed by facile 1,2-hydrogen

migration on the singlet surface. Fueno and co-workers suggest no barrier for 1,2-hydrogen migration in the $^1C_2H_4O$ case.[59]

The singlet/triplet splittings in CH_2CH_2O were found to be less than 3 kcal/mole[49] and about 6 kcal/mole for the two lowest states of oxyallyl,[52] suggesting a similarly small value for C_3H_4O.

Under single collision conditions the highly excited acrolein could not survive for hundreds of microseconds required to reach our detector, but will fragment instead. Rupture of the C_1-C_2 bond, leading to vinyl and formyl radicals, was found to be the major channel in the mercury sensitized decomposition[60] and the UV-photodissociation[61] of acrolein. Shinohara and Nishi[61] reported a translational energy distribution for the 193 nm photodissociation of acrolein which is qualitatively similar to our $P(E_T)$ shown in the lower panel of Fig. 5. Their distribution, obtained by a direct inversion method from the TOF data, peaks at about 10 kcal/mole and extends to 60 kcal/mole. Their experiment was insensitive to low energy products ($\leq$2 kcal/mole) due to geometric constraints. Furthermore, two-photon processes clearly play a role in their experiment. The authors[61] suggest $S_2 \rightarrow S_1$ internal conversion followed by fragmentation as the major dissociation mechanism at 193 nm.

The translational energy distribution obtained for channel (1f) from our data (lower panel of Fig. 5) peaks at about 5 kcal/mole and is very similar to that obtained for channel (2b)

in the O + C_2H_4 reaction.[4] The fact that the distribution does not peak at 0 kcal/mole translational energy but instead at a small, but finite value indicates that there is probably a small barrier to the C-C bond rupture process in both cases. Thus the dynamics of channel (1f) appears to be very similar to the corresponding channel in the O + C_2H_4 reaction.

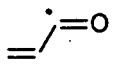

8

As indicated in Fig. 8, hydrogen atom elimination from acrolein has to be considered as a reaction route. According to the thermodynamical data compiled in Table 1, elimination of the aldehydic hydrogen to form the acrolyl radical (**8**), channel (1i), should be the lowest energy pathway. (**8**) would be indistinguishable from (**7**) in our experiment. From the branching ratio calculations mentioned earlier, it appears that hydrogen elimination from acrolein is less probable than C-C-bond rupture, channel (1f). Some of the thermodynamic values in Table 1 are associated with error limits of several kcal/mole, making the relative energetics of the acrolein dissociation channels uncertain. In addition, possible barrier heights for these simple bond rupture channels are not known, making it difficult to predict the predominant reaction path.

Some of the C_3H_3O in our experiment could be formed on the

singlet rather than the triplet surface. The broad $P(E_T)$ (upper panel of Fig. 5) suggests the possibility of more than one source of this product. Furthermore, the maximum translational energy in the upper panel of Fig. 5 is not very well determined due to the limited energy resolution of this experiment. $P(E_T)$ distributions including translational energies beyond 25 kcal/mole could fit the C_3H_3O data equally well.

The possibility of forming ketene and triplet (or singlet) methylene, channel (1c), as well as other channels, have not received any theoretical attention either. Thus it is not known whether the formation of ketene and formaldehyde, which were found in the matrix studies,[7] is the result of a primary process or secondary reactions.

Channel (1h), the formation of propadienone by elimination of molecular hydrogen from C_1 of the adduct (**5**), in analogy to the formation of ketene and hydrogen from the reaction of $O(^3P)$ with ethylene, has not been considered previously. Propadienone has been synthesized recently[62] and has received much attention since unexpectedly the C-C-C-O chain was found to be bent.[63]

Other parts of the C_3H_4O surfaces have been calculated, such as allene oxide - cyclopropanone rearrangement pathways.[24,31] However, no information regarding this process could be gained from our data.

4.5. Summary

The crossed molecular beam experiment conducted under single collision conditions produced detailed information on major reaction channels of the $O(^3P)$ + allene reaction. Previously the major reaction channel was thought to be (1a), the formation of carbon monoxide and ethylene, and evidence for the occurrence of this process was found in our experiments also. In addition, we identified unambiguously channel (1b), formation of hydrogen atom and allenyloxy (formyl-vinyl) radical (**8**). Further, we determined the branching ratio between channel (1a) and (1b) to be approximately 4.

Our data suggest at least one additional major channel, tentatively identified as (1f), formation of vinyl and formyl radicals from fragmentation of vibrationally excited acrolein. Other reaction paths are possible, however, they can not be distinguished in our data.

While channels (1b) and (1f) suggest large similarities between the reaction of $O(^3P)$ atoms with allene and with ethylene, channel (1a) is specific to allene.

4.6. References

1. S. J. Sibener, R. J. Buss, P. Casavecchia, T. Hirooka, and Y. T. Lee, J. Chem. Phys. 72, 4341 (1980); R. J. Baseman, R. J. Buss, P. Casavecchia, and Y. T. Lee, J. Am. Chem. Soc. 106, 4108 (1984).
2. R. J. Buss, R. J. Baseman, G. He, and Y. T. Lee, J. Photochem. 17, 389 (81).
3. A. M. Schmoltner, P. M. Chu, and Y. T. Lee, J. Chem. Phys., in press.
4. A. M. Schmoltner, P. M. Chu, R. J. Brudzynski, and Y. T. Lee, J. Chem. Phys., in press.
5. K. H. Homann, J. Warnatz, and C. Wellmann, Sixteenth Symposium (International) on Combustion (Combustion Institute, Pittsburgh, 1977), p. 853; K. H. Homann and H. Schweinfurth, Ber. Bunsenges. Phys. Chem. 85, 569 (1981); K. H. Homann and Ch. Wellmann, Ber. Bunsenges. Phys. Chem. 87, 609 (1983).
6. J. D. Bittner and J. B. Howard, Eighteenth Symposium (International) on Combustion (Combustion Institute, Pittsburgh, 1981), p. 1105.
7. K. A. Singmaster and G. C. Pimentel, J. Mol. Structure 194, 215 (1989).
8. K. A. Singmaster and G. C. Pimentel, J. Mol. Structure, in press.
9. M. C. Lin, R. G. Shortridge, and M. E. Umstead, Chem. Phys.

Lett. 37, 279 (1976).

10. J. J. Havel, J. Am. Chem. Soc. 96, 530 (1974).

11. P. Herbrechtsmaier and H. G. Wagner, Ber. Bunsenges. Phys. Chem. 76, 517 (1972).

12. E. N. Aleksandrov, V. S. Arutyunov, and S. N. Kozlov, Kinet. Katal. 21, 1327 (1980).

13. R. Atkinson and J. N. Pitts, Jr., J. Chem. Phys. 67, 2492 (1977); W. S. Nip, D. L. Singleton, and R. J. Cvetanovic, Can. J.Chem. 57, 949 (1979).

14. R. Cvetanovic, Adv. Photochem. 1, 115 (1963).

15. A. C. Scheiner and H. F. Schaefer III, J. Am. Chem. Soc. 107, 4451 (1985).

16. M. W. Chase, Jr., C. A. Davies, J. R. Downey, Jr., D. J. Frurip, R. A. McDonald, and A. N. Syverud, J. Phys. Chem. Ref. Data 14 (1985), Supplement No. 1: JANAF Thermochemical Tables, Third Edition.

17. J. B. Pedley, R. D. Naylor, and S. P. Kirby, Thermochemical Data of Organic Compounds (Chapman and Hall, London, 1986).

18. C. F. Melius, to be published.

19. R. L. Nuttal, A. H. Laufer, and M. V. Kilday, J. Chem. Thermodynamics 3, 167 (1973).

20. A. M. Wodtke, E. J. Hintsa, J. Somorjai, and Y. T. Lee, submitted to Isr. J. Chem.

21. M.-C. Chuang, M. F. Foltz, and C. B. Moore, J. Chem. Phys. 87, 3855 (1987).

22. Z. B. Alfassi and D. M. Golden, J. Am. Chem. Soc. 95, 319

(1973).

23. H. J. Rodriguez, J.-C. Chang, and T. F. Thomas, J. Am. Chem. Soc. 98, 2027 (1976).

24. A. Liberles, A. Greenberg, and A. Lesk, J. Am. Chem. Soc. 94, 8685 (1972).

25. J. F. Liebman and A. Greenberg, J. Org. Chem. 39, 123 (1974).

26. E. Block, R. E. Penn, M. D. Ennis, T. A. Owens, and S.-L. Yu, J. Am. Chem. Soc. 100, 7436 (1978).

27. O. Kikuchi, H. Nagata, and K. Morihashi, J. Mol. Structure (Theochem) 124, 261 (1985).

28. P. M. Lahti, A. R. Rossi, and J. A. Berson, J. Am. Chem. Soc. 107, 2273 (1985).

29. L. J. Schaad and B. A. Hess, Jr., J. Org. Chem. 46, 1909 (1981).

30. R. C. Bingham, M. J. S. Dewar, and D. H. Lo, J. Am. Chem. Soc. 97, 1302 (1975).

31. M. E. Zandler, C. E. Choc, and C. K. Johnson, J. Am. Chem. Soc. 96, 3317 (1974).

32. A. Liberles, S. Kang, and A. Greenberg, J. Org. Chem. 38, 1922 (1973).

33. J. F. Olsen, S. Kang, and L. Burnelle, J. Mol. Structure 9, 305 (1971).

34. N. Bodor, M. J. S. Dewar, A. Harget, and E. Haselbach, J. Am. Chem. Soc. 92, 3854 (1970).

35. R. Hoffmann, J. Am. Chem. Soc. 90, 1475 (1968).

36. J. V. Ortiz, J. Org. Chem. 48, 4744 (1983).

37. A. Sevin, E. Fazilleau, and P. Chaquin, Tetrahedron 37, 3831 (1981).

38. S. Yamabe, T. Minato, and Y. Osamura, J. Am. Chem. Soc. 101, 4525 (1979).

39. D. M. Hayes, C. A. Zeiss, and R. Hoffmann, J. Phys. Chem. 75, 340 (1971).

40. S. Y. Huang, Ph. D. Thesis, University of California, Berkeley, 1988; S. Y. Huang and W. A. Lester, Jr., to be published.

41. Y.-N. Chiu and M. S. F. A. Abidi, J. Phys. Chem. 86, 3288 (1982).

42. Y. T. Lee, J. D. McDonald, P. R. LeBreton, and D. R. Herschbach, Rev. Sci. Instrum. 40, 1402 (1969).

43. S. J. Sibener, R. J. Buss, C. Y. Ng, and Y. T. Lee, Rev. Sci. Instrum. 51, 167 (1980).

44. K. Sköld, Nucl. Instrum. Methods 63, 114 (1968); V. L. Hirschy and J. P. Aldridge, Rev. Sci. Instrum. 42, 381 (1971); G. Comsa, R. David, and B. J. Schumacher, Rev. Sci. Instrum. 52, 789 (1981).

45. R. J. Buss, Ph. D. Thesis, University of California, Berkeley, 1979.

46. Assumed to be same as the exothermicity of the $O(^3P) + C_2H_4 \rightarrow H + C_2H_3O$ channel in Ref. 18.

47. W. L. Fitch and A. D. Sauter, Anal. Chem. 55, 832 (1983).

48. Atlas of Mass Spectral Data, E. Stenhagen, S. Abrahamsson,

and F. W. McLafferty, editors, Vol. 1 (Wiley, New York, 1969).

49. M. Dupuis, J. J. Wendoloski, T. Takada, and W. A. Lester, Jr., J. Chem. Phys. 76, 481 (1982).

50. M. Dupuis, J. J. Wendoloski, and W. A. Lester, Jr., J. Chem. Phys. 76, 488 (1982).

51. Crossed-beams experiments (A. R. Clemo, G. L. Duncan, and R. Grice, Trans. Faraday Soc. 2, 78, 1231 (1982); 79, 637 (1983)) determined a threshold of 1.2±0.7 kcal/mole; the bulk activation energy was found to be 1.5-1.6 kcal/mole, assuming that the first term in the biexponential expression corresponds to the addition reaction (K. Mahmud, P. Marshall, and A. Fontijn, J. Phys. Chem. 91, 1568 (1987); R. B. Klemm, F. L. Nesbitt, E. G. Skolnik, J. H. Lee, and J. F. Smalley, J. Phys. Chem. 91, 1574 (1987)); and recent BAC-MP4 calculations (Ref. 18) yielded a value of 0.6 kcal/mole.

52. Y. Osamura, W. T. Borden, and K. Morokuma, J. Am. Chem. Soc. 106, 5112 (1984).

53. T. H. Chan and B. S. Ong, J. Org. Chem. 43, 2994 (1978).

54. D. B. Sclove, J. F. Pazos, R. L. Camp, and F. D. Greene, J. Am. Chem. Soc. 92, 7488 (1970).

55. S. S. Edelson and N. J. Turro, J. Am. Chem. Soc. 92, 2770 (1970).

56. N. J. Turro, Acc. Chem. Res. 2, 25 (1969).

57. J. M. Pochan, J. E. Baldwin, and W. H. Flygare, J. Am.

Chem. Soc. 90, 1072 (1968); W. J. M. van Tilborg, Tetrahedron Letters 7, 523 (1973); P. C. Martino, P. B. Shevlin, and S. D. Worley, J. Am. Chem. Soc. 99, 8003 (77).

58. C. F. Melius, pers. comm.

59. Y. Takahara, K. Yamaguchi, and T. Fueno, Book of Abstracts, Third Symposium on Chemical Reactions, Tokyo University, June 3-5, 1987.

60. A. G. Harrison and F. P. Lossing, Can. J. Chem. 37, 1696 (1959).

61. H. Shinohara and N. Nishi, J. Chem. Phys. 77, 234 (1982).

62. R. F. C. Brown, F. W. Eastwood, and G. L. McMullen, J. Am. Chem. Soc. 98, 7421 (1976); R. F. C. Brown, R. W. Eastwood, and G. L. McMullen, Aust. J. Chem. 30, 179 (1977); O. L. Chapman, M. D. Miller, and S. M. Pitzenberger, J. Am. Chem. Soc. 109, 6867 (1987).

63. R. D. Brown, P. D. Godfrey, R. Champion, and D. McNaughton, J. Am. Chem. Soc. 103, 5711 (1981); J. Am. Chem. Soc. 104, 6167 (1982); L. Farnell and L. Radom, Chem. Phys. Lett. 91, 373 (1982).

4.7. Tables

Table 1. Exothermicities ($\Delta H^{o}_{f,298}$) for various $O(^3P)$ + allene reaction channels

Reaction	Exothermicity (kcal/mole)	Sources
(1a) $O + C_3H_4 \rightarrow C_2H_4 + CO$	-119.4	a,b
(1b) $O + C_3H_4 \rightarrow CH_2{=}C{\cdot}{=}CHO + H$	-18.5	c
(1c) $O + C_3H_4 \rightarrow CH_2CO + {}^3CH_2$	-24.6	a,b,d
(1d) $O + C_3H_4 \rightarrow CH_2{=}C{:} + CH_2O$	-39.5	a,b,e
(1e) $O + C_3H_4 \rightarrow HC{\equiv}CH + CH_2O$	-79.0	a,b
(1f) $O + C_3H_4 \rightarrow C_2H_3 + CHO$	-25	a,b,f,g
(1g) $O + C_3H_4 \rightarrow$ acrolein	-123.2	a,b,h
$O + C_3H_4 \rightarrow$ cyclopropanone	-101.7	a,b,i
$O + C_3H_4 \rightarrow$ allene oxide	-80	j
(1h) $O + C_3H_4 \rightarrow CH_2{=}C{=}C{=}O + H_2$	-82	k
(1i) $O + C_3H_4 \rightarrow CH_2{=}CH{-}CO + H$	-36	a,b,i

(a) Ref. 16, (b) Ref. 17, (c) assumed to be the same as for reaction (2a) (Ref. 18), (d) Ref. 19, (e) Ref. 18, (f) Ref. 20, (g) Ref. 21, (h) Ref. 22, (i) Ref. 23, (j) allene oxide is assumed to lie about 22 kcal/mole higher in energy than cyclopropanone, see Refs. 24-27, (k) taken to be the same as for reaction (2c) (Ref. 18).

4.8. Figures

Figure Captions

Fig. 1 Laboratory angular distribution of the C_3H_3O product at m/e=53 (C_3HO^+). Angles are measured from the oxygen atom beam. Scattered points: measured data points; dashed line: fit.

Fig. 2 Time-of-flight spectra for products at m/e=29 (HCO^+) at four different laboratory angles. Dashed lines (short dashes): fits for components due to channel (1b); dashed lines (long dashes): fits for components due to channel (1f); solid lines: sum of the fits for channels (1b) and (1f). Calculated curves are scaled to the data for each angle and each channel separately.

Fig. 3 Time-of-flight spectra for products at m/e=30 ($C^{18}O^+$) at five different laboratory angles. Dashed lines (short dashes): fits for components due to channel (1b); dashed lines (long dashes): fits for components due to channel (1f); chain-dashed lines: fits for components due to channel (1a); solid lines: sum of the fits for the individual channels. Calculated curves are scaled to the data for each angle and each channel separately.

Fig. 4 Time-of-flight spectra for products at m/e=53 (C_3HO^+)

at three different laboratory angles. Solid lines: fits, scaled to the data for each angle separately.

Fig. 5 Translational energy distributions $P(E_T)$ for channels (1b), upper panel, and (1f), lower panel.

Fig. 6 Center-of-mass angular distributions $T(\theta)$ for channels (1b), upper panel, and (1a), lower panel.

Fig. 7 Translational energy distribution $P(E_T)$ for channel (1a).

Fig. 8 Schematic energy diagram for the terminal carbon attack channels in the reaction of $O(^3P)$ with allene. Solid lines: triplet surfaces; dashed lines: singlet surfaces.

Fig. 9 Schematic energy diagram for the central carbon attack channels in the reaction of $O(^3P)$ with allene. Solid lines: triplet surfaces; dashed lines: singlet surfaces.

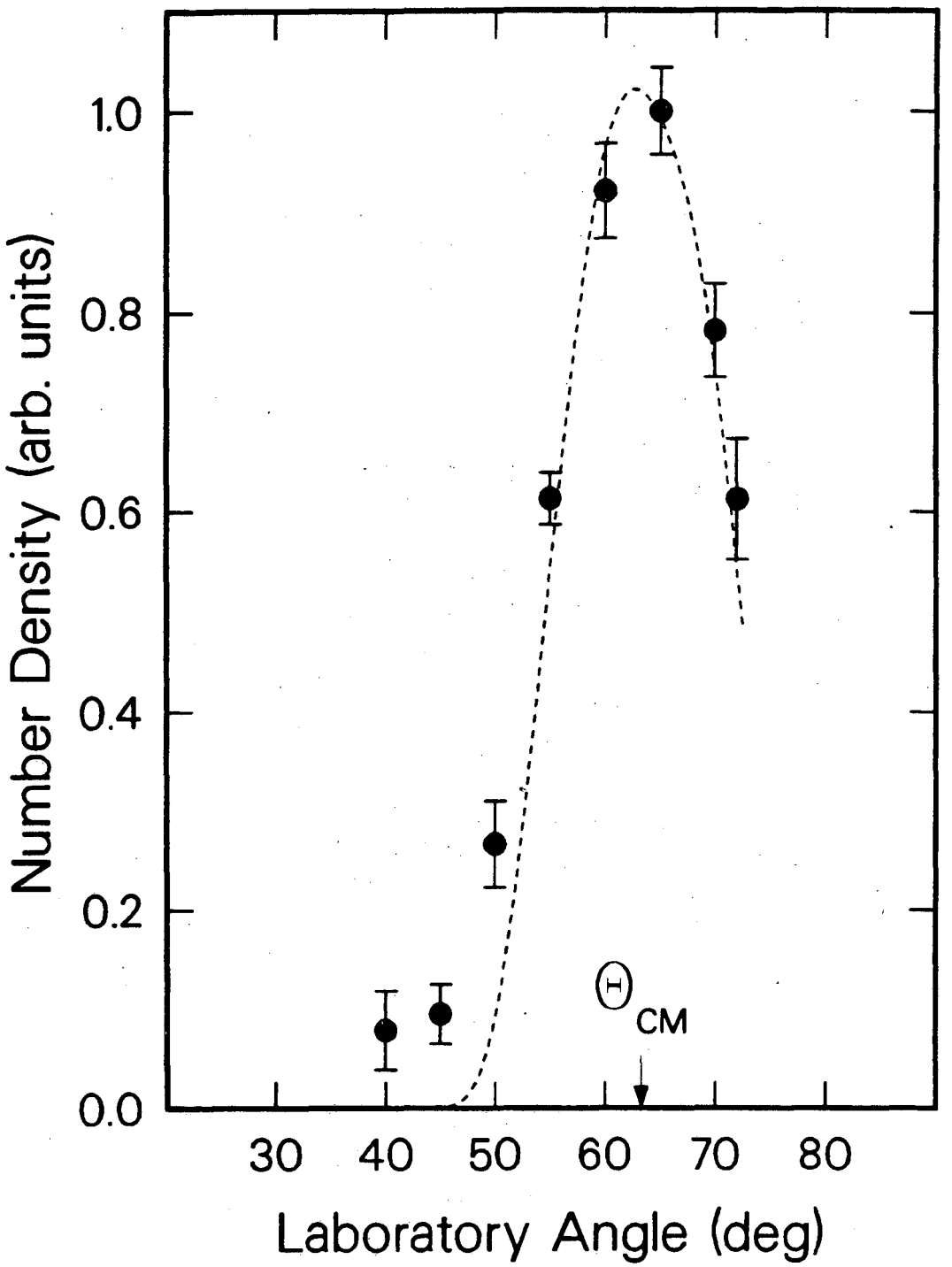

XBL 899-3194

Fig. 1

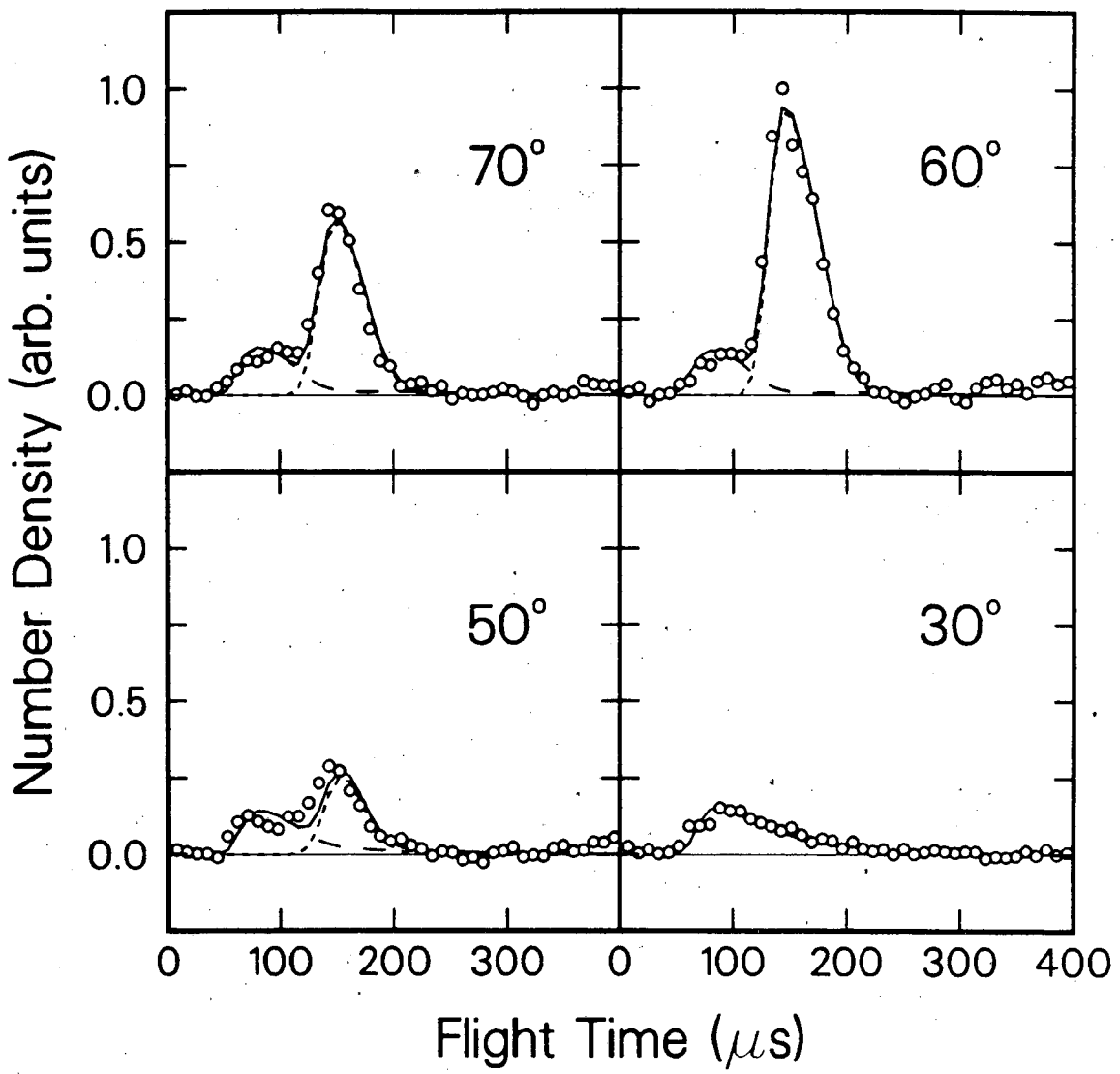

XBL 899-3198

Fig. 2

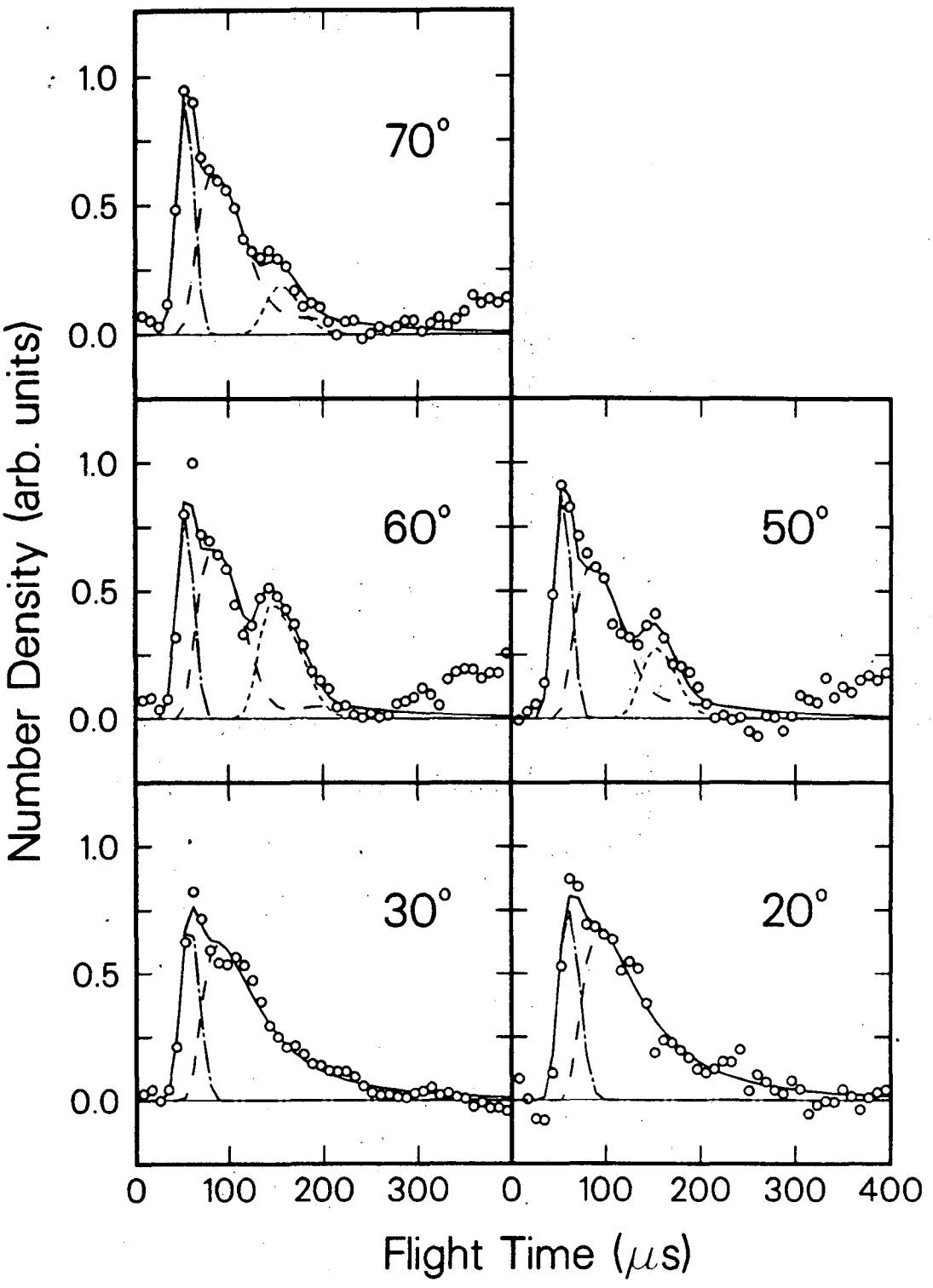
70°
60°
50°
30°
20°
1.0
0.5
0.0
Number Density (arb. units)
0
100
200
300
400
Flight Time (μs)
XBL 899-3200

Fig. 3

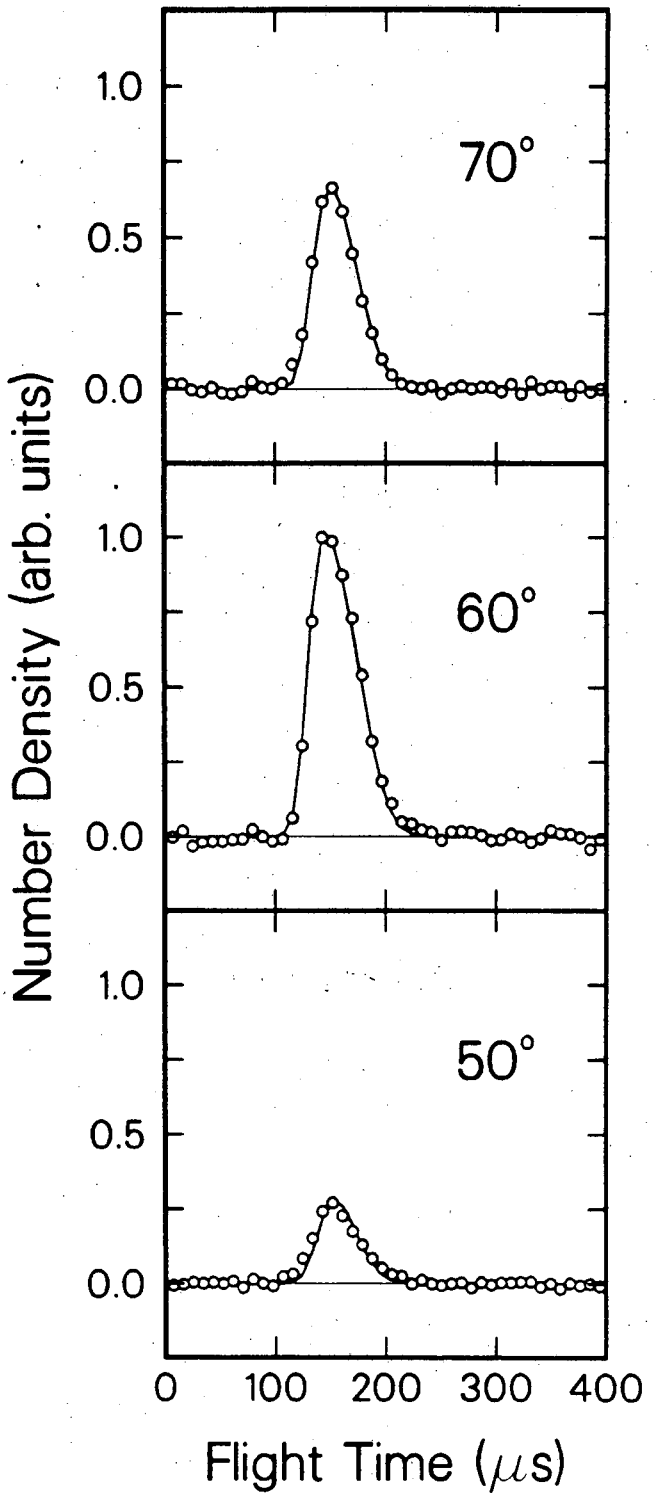

XBL 899-3199

Fig. 4

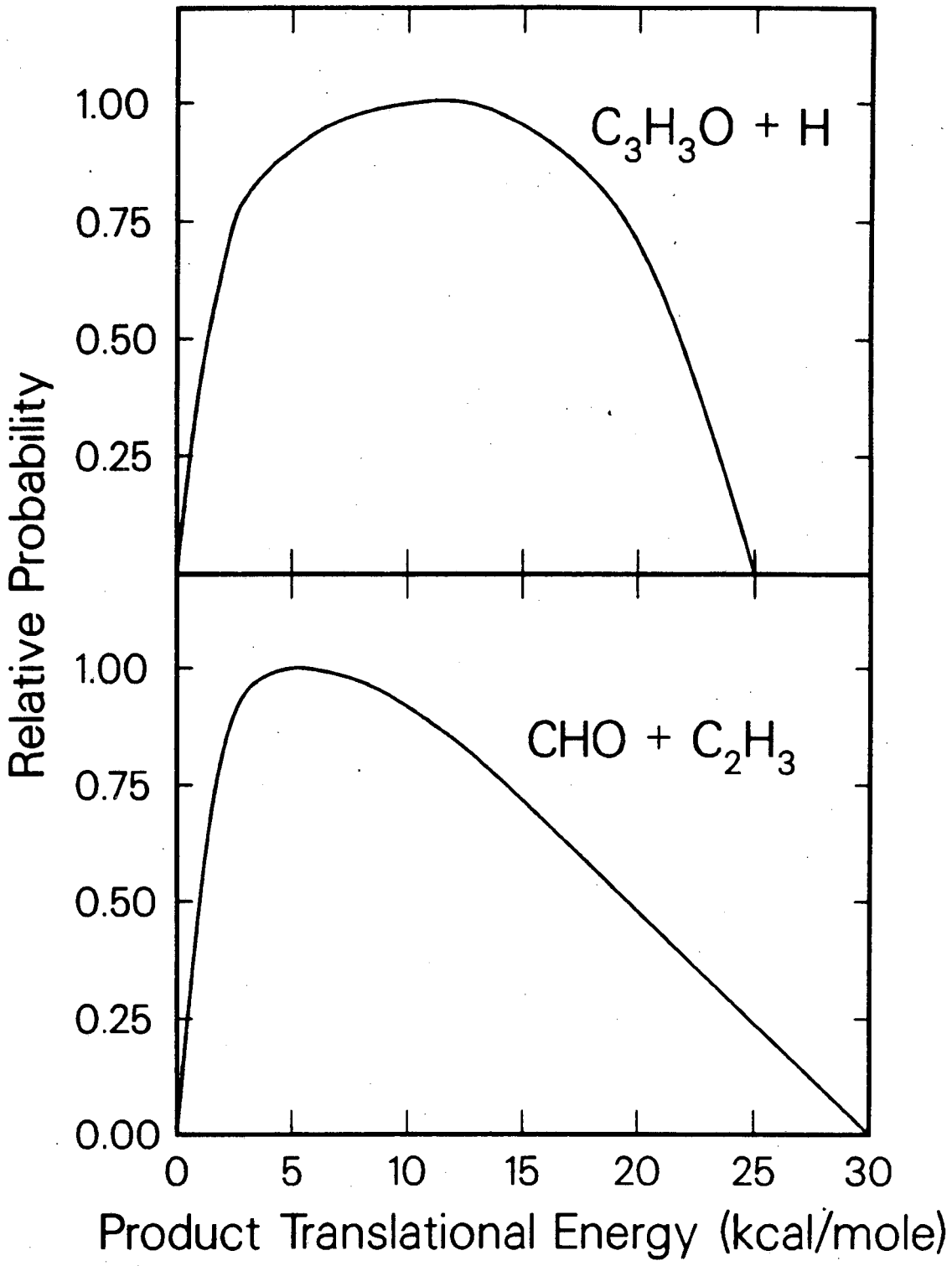

XBL 899-3196

Fig. 5

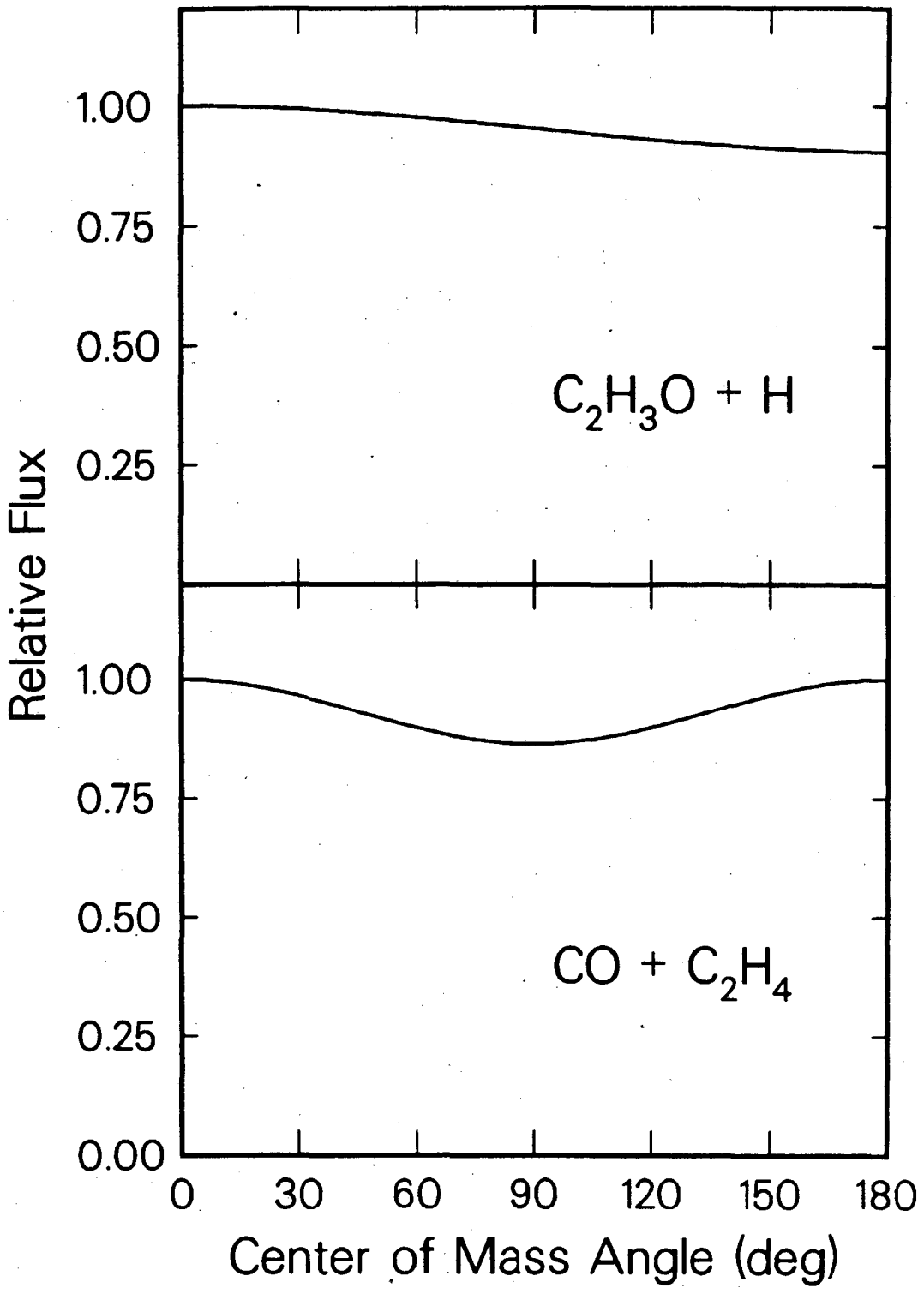

XBL 899-3195

Fig. 6

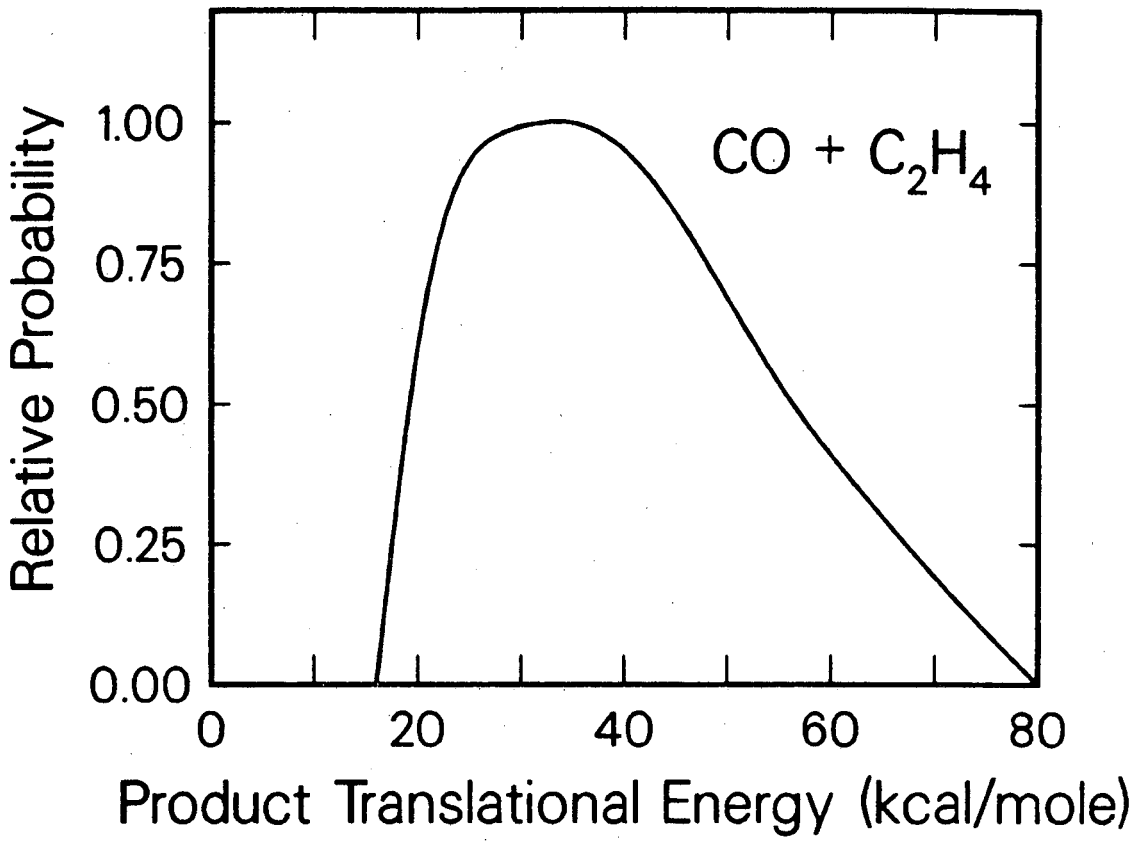

XBL 899-3197

Fig. 7

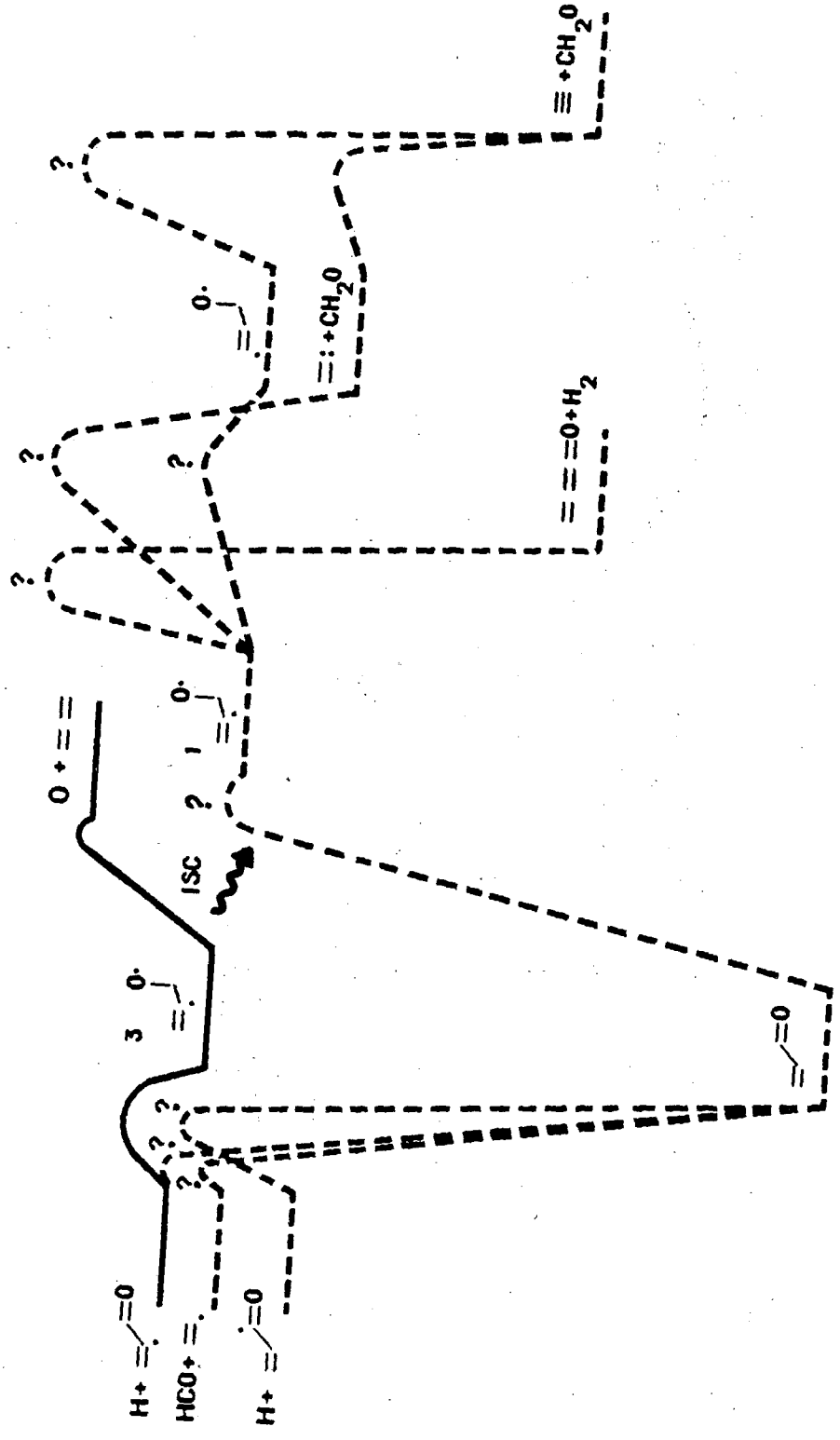

XBL 899-3202

Fig. 8

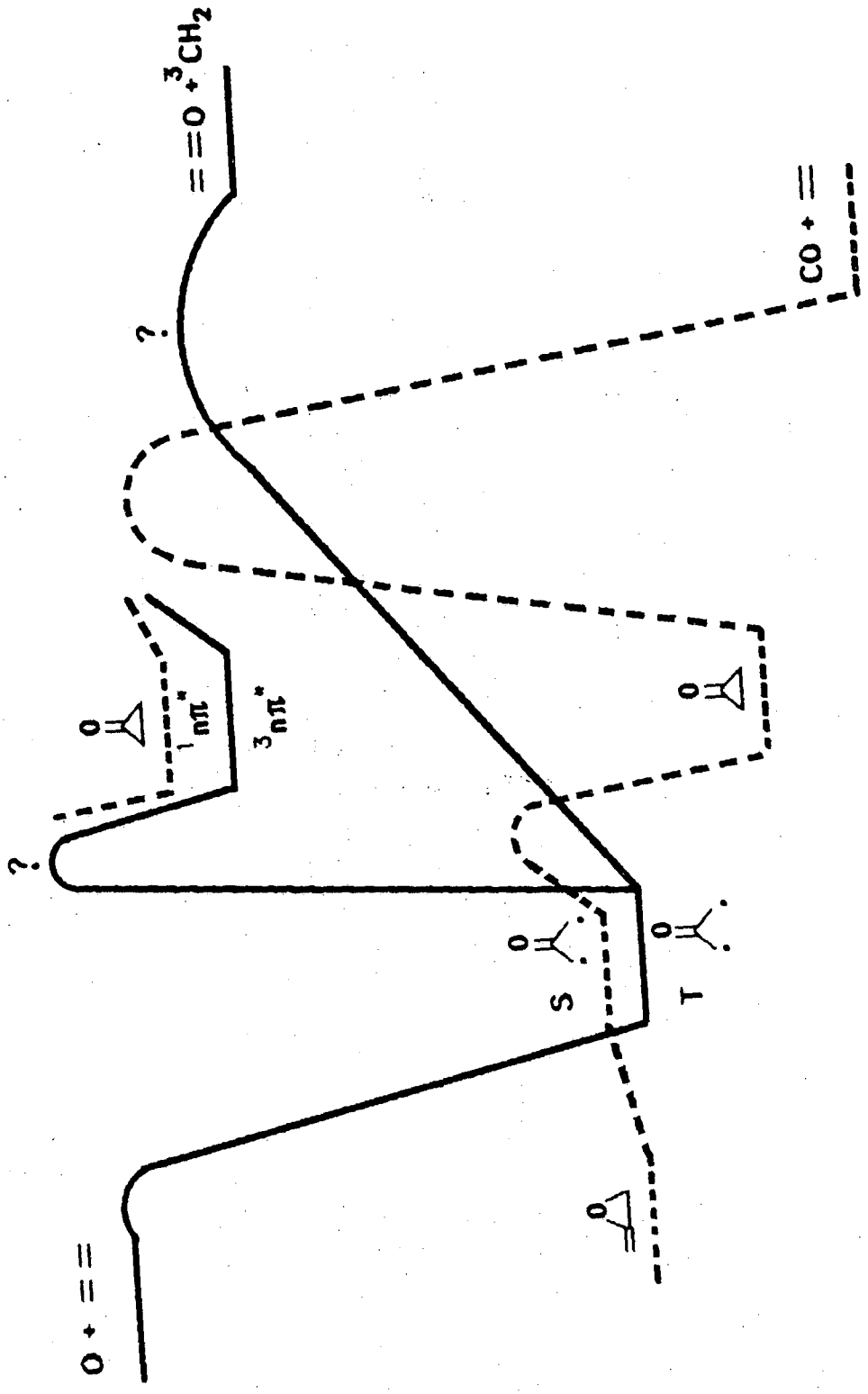

XBL 899-3201

Fig. 9

4.9. EPILOGUE: PHOTODISSOCIATION OF CYCLOBUTANONE

The example of the $O(^3P)$ + allene reaction shows how a seemingly simple question can lead to the examination of complicated potential energy surfaces and reaction pathways. In such a case it is always valuable to access the same potential energy surface or surfaces from different initial conditions or reactants. For instance, the process of forming ethylene and carbon monoxide from $O(^3P)$ and allene presumably proceeds through cyclopropanone as an intermediate. It would be interesting to study the cyclopropanone decomposition using photochemical instead of chemical activation and compare the dynamic features with those of the $O(^3P)$ + allene reaction. The UV photodissociation of cyclopropanone has been studied by Rodriguez et al.[1] Unfortunately it would be impossible to try this experiment in a molecular beam machine because of the instability of the molecule at room temperature.

Photodissociation of acrolein, another C_3H_4O isomer, has been studied by several authors.[2-4] Shinohara and Nishi[2] found CHO and C_2H_3 to be the products in a molecular beam experiment with fixed 90° detection geometry. Fujimoto et al.[3] measured the CO vibrational distribution and concluded that carbon monoxide is most likely a primary product. No other channels could be investigated. Gardner et al.[4] studied several photodecomposition channels of acrolein in air after excitation with 313 and 334 nm light, and found evidence for the primary

processes forming CO + C_2H_4, CO + CH_3CH (singlet and triplet), CH_2=CH + CHO, and CH_2=CHCO + H.

Unsubstituted allene oxide, another C_3H_4O isomer, has been identified experimentally only recently in a cryogenic matrix[5] and is probably very unstable.

Although the decarbonylation of cyclopropanone can not be studied directly by molecular beam photodissociation, similar reactions of higher cyclic ketones are amenable to this type of investigation. Cyclobutanone, cyclopentanone, and cyclohexanone are commercially available and their photochemistry has been studied extensively. The general mechanisms are thought to involve α-C-C-bond cleavage followed by decomposition of the diradical.[6] At least one channel includes the formation of CO.

In the case of cyclobutanone (CB), two major dissociation pathways were identified:

$$C_4H_6O \rightarrow CH_2{=}CH_2 + CH_2{=}C{=}O \qquad (1a)$$

$$C_4H_6O \rightarrow CO + C_3H_6 \qquad (1b)$$

(1a) is referred to as the C_2-channel and (1b) as the C_3-channel. Most of the C_3H_6 product is cyclopropane. Propene is being formed as an isomerization product of cyclopropane.[7] The propene/cyclopropane ratio reflects the internal energy distribution of the C_3-fragment.[8]

Thermal decomposition of CB only produced ethylene and ketene, channel (1a).[9] Photosensitization experiments with

singlet and triplet benzene[10] suggest that channel (1a) represents the singlet and (1b) the triplet decay channel of CB.

E. K. C. Lee and co-workers[11] have studied the decomposition of CB excited to the $n\pi^*$ state extensively. The ratio between the C_2 and the C_3-channel as a function of excitation energy[8,12] yields detailed information on the decay processes. The mechanism can be summarized as follows: At low excitation energy primarily $S_1 \rightarrow T_1$ intersystem crossing takes place, followed by decomposition to cyclopropane and CO; at higher energies ($\approx$1000 cm^{-1} of vibrational excitation) $S_1 \rightarrow S_0$ internal conversion starts to set in followed by decomposition into ethylene and ketene.

Some questions remain about the involvement of collisions[13], and a molecular beam experiment could give a definitive answer to the question of the branching ratio between the primary reaction channels under collisionless conditions, ideally as a function of wavelength. However, a high intensity tunable UV light source would be required for this experiment.

Even though mass spectrometric detection is a very versatile tool for detecting molecules and radicals, problems arise in this particular experiment since the products of both channels have the same mass ratios: Both ethylene and CO have mass 28 amu, and cyclopropane (which could not be distinguished from propene) and ketene have mass 42 amu. If the translational energy release for both channels is similar, difficulties are expected in separating the two contributions. However, a close

look at the fragmentation patterns[14] shows that certain masses could be chosen to distinguish between the different products. For instance, m/e=27 or 26 would only come from ethylene (and possibly C_3H_6), but not CO; m/e=39 would only come from C_3H_6, not from ketene.

An experiment was performed in our laboratory by Eric Hintsa and Prof. Yehuda Haas[15] using 193 nm excitation. With that wavelength the second absorption band (≈180-205 nm) of CB is accessed, which is considerably stronger ($\epsilon \approx 1600$ lmol/cm)[16] than the first one and has been assigned to a $\pi^* \leftarrow n'$ transition.[17]

TOF spectra were measured at m/e=26, 29, and 41. M/e=26 was assigned to ethylene fragments and m/e=41 to a ketene fragment. The signal at m/e=29 was weak and resembled that at m/e=41. Preliminary analysis showed that the data were compatible with the assumption of channel (1a) dominating, indicating a singlet pathway.

Later we investigated the photodissociation at 308 nm. The absorption coefficient for the $\pi^* \leftarrow n$ excitation (≈230-320 nm) is small ($\epsilon \approx 8$ lmol/cm).[18] The supersonic molecular beam was formed by bubbling approximately 200 Torr of N_2 through CB held at 0°C. The nozzle was heated to about 117°C. The excimer laser was run at 100 Hz and produced an output of about 80 mJ/pulse and was focussed at the interaction zone. Time-of-flight data were taken at 20° at m/e=14, 26, 29, 39, 41 and 42. 500,000 Laser shots were averaged for all masses except m/e=14.

Due to the small absorption cross section the signal levels were extremely low, peaks being evident only at m/e=26, 39, and 41.

M/e=39 can only represent a fragment of cyclopropane, whereas m/e=41 could stem from either cyclopropane or ketene. The TOF distribution at m/e=41 was faster and narrower than that of m/e=39, indicating that both channels (1a) and (1b) were occurring. The signal at m/e=26 could arise from fragments of ethylene or cyclopropane. The signal at this mass was even faster than m/e=41, indicating that ethylene was its (major) source. A crude analysis was done and is shown in Fig. 1 together with the data. The translational energy distribution $P(E_T)$ for channel (1a) peaks at approximately 30 kcal/mole, whereas the $P(E_T)$ for channels (1b) peaks at about 20 kcal/mole.

We thus established that both decomposition channels are taking place under molecular beam conditions following 308 nm excitation, however, much more signal averaging would be required in order to obtain data of sufficient quality to allow the determination of detailed dynamical features. The chances of measuring cross sections as a function of excitation wavelength are pretty slim as long as no tunable high power laser sources are available for this wavelength region.

References

1. H. J. Rodriguez, J.-C. Chang, and T. F. Thomas, J. Am. Chem. Soc. 98, 2027 (1976).
2. H. Shinohara and N. Nishi, J. Chem. Phys. 77, 234 (1982).
3. G. T. Fujimoto, M. E. Umstead, and M. C. Lin, J. Chem. Phys. 82, 3042 (1983).
4. E. P. Gardner, P. D. Sperry, and J. C. Calvert, J. Phys. Chem. 91, 1922 (1987).
5. K. A. Singmaster and G. C. Pimentel, submitted to J. Mol. Structure.
6. H. A. J. Carless and E. K. C. Lee, J. Am. Chem. Soc. 92, 6683 (1970).
7. R. F. Klemm, D. N. Morrison, P. Gilderson, and A. T. Blades, Can. J. Chem. 43, 1934 (1965); R. J. Campbell, E. W. Schlag, and B. W. Ristow, J. Am. Chem. Soc. 89, 5098 (1976).
8. K. Y. Tang and E. K. C. Lee, J. Phys. Chem. 80, 1833 (1976).
9. M. N. S. Das, F. Kern, T. D. Coyle, and W. D. Walters, J. Am. Chem. Soc. 76, 6271 (1954).
10. H. O. Denschlag and E. K. C. Lee, J. Am. Chem. Soc. 89, 4795 (1967); J. Am. Chem. Soc. 90, 3628 (1968).
11. E. K. C. Lee, Acc. Chem. Res. 10, 319 (1977), and Refs. therein.
12. J. C. Hemminger, C. F. Rusbutt, and E. K. C. Lee, J. Am.

Chem. Soc. 93, 1867 (1971).

13. J. C. Hemminger and E. K. C. Lee, J. Chem. Phys. 56, 5284 (1972).

14. Atlas of Mass Spectral Data, E. Stenhagen, S. Abrahamsson, and F. W. McLafferty, editors, Vol. 1 (Wiley, New York, 1969).

15. E. J. Hintsa, Y. Haas, and Y. T. Lee, unpublished results.

16. A. Udvarhazi and M. A. El-Sayed, J. Chem. Phys. 42, 3335 (1965).

17. R. F. Whitlock and A. B. F. Duncan, J. Chem. Phys. 55, 218 (1971); E. E. Barnes and W. T. Simpson, J. Chem. Phys. 39, 670 (1963).

18. S. W. Benson and G. B. Kistiakowski, J. Am. Chem. Soc. 64, 80 (1942); W. D. Chandler and L. Goodman, J. Mol. Spectr. 35, 232 (1970).

Figure Caption

Fig. 1 Time-of-flight spectra at m/e=26 ($C_2H_2^+$), 41 (C_2HO^+ and $C_3H_5^+$), and 39 ($C_3H_3^+$). Solid line: preliminary fit assumung m/e=26 and 41 are entirely due to channel (1a) and m/e=39 is entirely due to channel (1b).

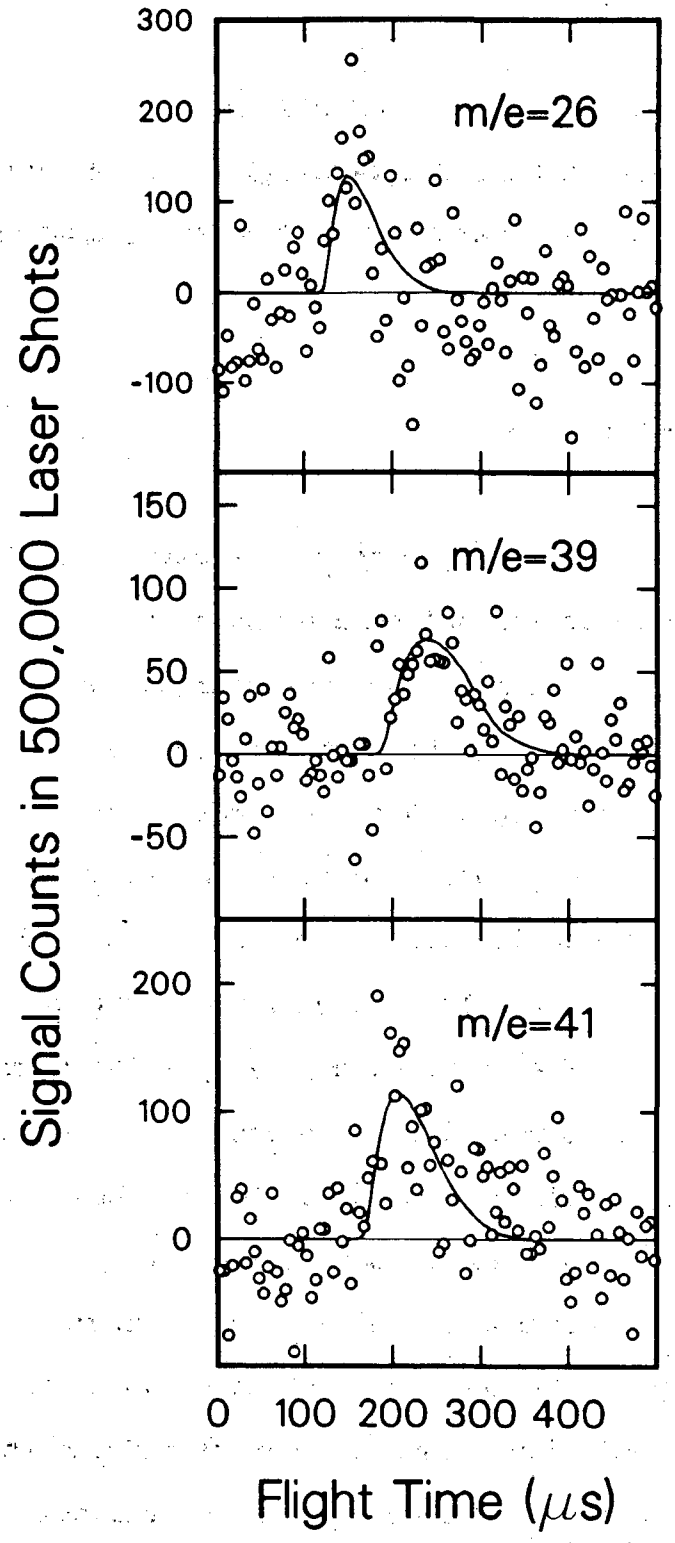

XBL 899-3203

Fig. 1

CHAPTER 5

IR MULTIPHOTON DISSOCIATION OF ANISOLE: PRODUCTION AND DISSOCIATION OF PHENOXY RADICAL

5.1. Introduction

The infrared multiphoton dissociation (IRMPD) of polyatomic molecules has been established as an excellent experimental technique for studying unimolecular dissociation processes of polyatomic molecules. The fast intramolecular energy distribution that occurs after absorption of many IR photons makes it possible to use intense IR radiation to prepare hot ground state molecules similar to those prepared by thermal excitation.[1-3] Since IR multiphoton absorption can take place under collision free conditions, detailed information about unimolecular decomposition processes of molecules can be obtained in experiments using a molecular beam.

The technique used in our laboratory, photofragmentation translational spectroscopy with mass spectrometric detection, is particularly well suited for the unambiguous identification of primary dissociation products and for studying the dissociation dynamics from the measurements of product angular and velocity distributions.

The thermal decomposition of anisole has been studied

repeatedly,[4-7] and the only primary dissociation channel identified was cleavage of the weak[8,9] O-CH_3 bond to form the methyl radical and the phenoxy radical.

$$C_6H_5\text{-}O\text{-}CH_3 \xrightarrow{h\nu} C_6H_5O\cdot + \cdot CH_3 \qquad (1)$$

At temperatures above 1000K the unimolecular decomposition of the phenoxy radical into carbon monoxide and the cyclopentadienyl radical was observed.[4,5,10] Colussi et al.[10] suggested a mechanism for phenoxy radical decomposition involving a bridged C_6H_5O species (Scheme 1). This mechanism is compatible with the low A-factor and low activation energy for the process obtained by Lin and Lin.[5]

The phenoxy radical is an important intermediate in the combustion of aromatic hydrocarbons.[11] The reaction of oxygen atoms with benzene leads to the production of the phenoxy radical and phenol,[12] and the decomposition of phenol in turn produces phenoxy radicals. The reaction of molecular oxygen with the phenyl radical was postulated as an additional pathway for the production of the phenoxy radical.[13]

One of the goals of our recent investigations has been to find efficient and clean ways of producing phenoxy radicals and to study the dynamics of their decomposition. In our IRMPD experiments, we did find that production of the phenoxy radical was the only primary channel of anisole decomposition. At conditions of high laser fluence, the secondary decomposition of

some of the phenoxy radicals was observed.

5.2. **Experimental**

The apparatus used in this experiment has been described in detail previously.[14] Briefly, a supersonic molecular beam was crossed at 90° with the output of a pulsed CO_2-laser. Time-of-flight (TOF) spectra of the photodissociation products were recorded using a mass spectrometer detector consisting of an electron-impact ionizer, quadrupole mass filter, and Daly ion counter. Rotation of the differentially pumped molecular beam source around the axis defined by the laser beam allowed the angle between molecular beam and detector to be varied.

A continuous supersonic beam of anisole was formed by bubbling helium or nitrogen through anisole held at 20°C. The gas mixture at a total pressure of 100-150 Torr was passed through heated lines into the beam source. The nozzle had an aperture of 125 μm diameter and was held at 150° or 200° in order to prevent the formation of molecular clusters in the expansion. Typical beam velocities for He-seeded beams were $1.45\text{-}1.65\times10^5$ cm/s, with speed ratios of about 8-10. The beam velocity distributions were measured using the time-of-flight method.

Two different pulsed CO_2 lasers were used. The earlier experiments were performed using a Gentec DD-250-B TEA CO_2

laser, the later ones using a Lumonics TEA-820 CO_2 laser. The laser radiation was focused into the interaction region using a 25 cm focal length ZnSe lens. The spot sizes were estimated from burning patterns on tape and paper. With the Gentec Laser, fluences were estimated to be 8-17 J/cm^2 with laser spot sizes of approximately 1 mm^2, with the Lumonics Laser fluences of up to 27 J/cm^2 over about 4 mm^2. These values have considerable uncertainties, however, since the laser output power was measured in different ways in the two sets of experiments, and furthermore the determination of the spot sizes from the burning patterns is rather inaccurate.

The best yield was observed at the P(26) line of the 001-020 band at 1041 cm^{-1}. The fundamental frequency of the O-CH_3 stretch was determined[15] to lie at 1039 cm^{-1} and is most likely responsible for the initial absorption at this wavelength.

For a given laboratory angle, TOF spectra were recorded for each laser shot. The signal was accumulated in a multichannel scaler triggered by the laser pulse. Dwell times of 1-5 μs/channel were used. The data acquisition and storage was handled by an LSI-11 laboratory computer.

Anisole was obtained from Matheson and was degassed in several freeze-pump-thaw cycles. A GC-MS analysis revealed a minor impurity of benzoic acid (about 0.3%). This impurity was found not to interfere in our experiments, as its vapor pressure is considerably lower than that of anisole.

5.3. **Results and Analysis**

Even though the product molecules or radicals fragment extensively upon ionization in the mass spectrometer, parent-daughter-ion relationships can be established by identifying common features in the TOF spectra for different mass-to-charge ratios (m/e). Corresponding fragment pairs can be identified using the constraint of momentum conservation in the center-of-mass coordinate system.

TOF spectra were measured at laboratory angles between 6° and 50° at m/e=15, 28, 29, 30, 31, 39, 65, 75, 76, 77 and 93, corresponding to the ions CH_3^+, CO^+, CHO^+, CH_2O^+, CH_3O^+, $C_3H_3^+$, $C_5H_5^+$, $C_6H_3^+$, $C_6H_4^+$, $C_6H_5^+$, and $C_6H_5O^+$. The parent ion of the expected product of anisole decomposition, phenoxy radical, has a mass of 93 amu. Major fragments were found at m/e=39, 65 and others, with m/e=39 showing the highest count rate. TOF spectra are shown in Figs. 1-6.

Figs. 1 and 2 show data taken in the first set of experiments using the Gentec laser at low fluence, while Figs. 3-6 represent data taken at higher laser fluence using the Lumonics CO_2-laser. The spectra of m/e=39, 65 and 93 at 8° (Figs. 1 and 2) show only one feature which is the same for all three masses except for a small shift due to the flight time of the ions through the quadrupole mass spectrometer, which is a

function of the ion m/e. This feature in the TOF spectra can be identified as the phenoxy radical. The corresponding second fragment, methyl radical, was detected at m/e=15 and the TOF distribution is shown in Fig. 1. TOF spectra of m/e=39 at three different laboratory angles are shown in Fig. 2.

In contrast to these results, the TOF spectra obtained in the second set of experiments show an additional feature. The comparison of the spectra at m/e=39, 65, and 93 (Figs. 3 and 4) reveals the occurrence of two different reaction channels: The slower feature in all three spectra again corresponds to the phenoxy radical, while the faster feature at m/e=39 and 65 can be identified with the decomposition product of the phenoxy radical, the cyclopentadienyl radical. Methyl radical was again detected at m/e=15, and the TOF spectra at three different laboratory angles are shown in Fig. 5. Despite the high detector background at m/e=28, we were able to obtain a TOF spectrum at m/e=28 as well (Fig. 3). The detection of very fast CO at m/e=28 corroborates the identification of the fast feature in the m/e=39 and 65 spectra with the secondary dissociation products of phenoxy radical. Fig. 4 shows TOF spectra of m/e=39 at six different laboratory angles, illustrating the relative contributions of the two channels at different angles. At angles of 20° and larger, only secondary product can be observed.

The appearance of the photodissociation products in the laboratory frame is illustrated in the Newton diagram shown in

Fig. 7. Short velocity vectors originating at the tip of the beam velocity vector represent the center of mass velocity of the phenoxy radical recoiling from the methyl radical. The kinetic energy corresponding to this velocity is the maximum energy for this channel as determined by the analysis below. The smaller circle in Fig. 7 represents the trace of the termination points of the possible resultant laboratory velocity vectors arising from the addition of the molecular beam velocity to the center of mass velocities. The larger arrows and circle represent the velocity of the cyclopentadienyl radical recoiling from carbon monoxide in the secondary decomposition of the phenol radical. Again, the maximum kinetic energy from the data analysis which is discussed below was used to determine the velocity shown. In the sequential decomposition process, a collection of primary and secondary circles would appear, each corresponding to particular primary and secondary velocities. Also shown in this diagram are several source-detector angles. If a resultant velocity vector falls on one of these lines, then that fragment will be detected at this angle. As can be seen from Fig. 7, the primary phenoxy radical will not be seen at laboratory angles of 20° and higher, whereas the secondary cyclopentadienyl radical may be detected beyond 40°.

The data of m/e=65 and 93 in Fig. 3 show slow components (arriving later than approximately 400 μs) that were not accounted for in the data analysis. These slow features did not originate from the photodissociation of anisole in the beam.

They were identified as resulting from time-dependent desorption of anisole molecules from laser heating of a cold surface in the vacuum chamber and did not interfere with the analysis of the IRMPD signal.

A forward convolution method was used in the analysis of the data in order to determine the translational energy distribution of the reaction products, $P(E_T)$.[16] From a trial input distribution, TOF distributions were calculated and averaged over beam velocities, the finite dimensions of the interaction zone, and the finite size of the ionizer and compared with the experimental data. The trial $P(E_T)$ was then adjusted and the process repeated until a best fit was obtained. The angular distributions of the products in the center-of-mass frame were found to be isotropic as expected. The solid lines in Figs. 1-6 represent the fits to the data. The $P(E_T)$ distributions for the primary channel under the two different experimental conditions are shown in Fig. 8, and the $P(E_T)$ for the secondary dissociation is shown in Fig. 9.

The translational energy distributions for the primary product phenoxy radical from the two different sets of experiments (Fig. 8) are almost identical. Both distributions peak at 3 kcal/mole and extend to about the same maximum value, 17 and 18 kcal/mole, respectively. The differences are small but real. For the conditions of smaller laser fluence in the earlier experiments, the $P(E_T)$ is slightly narrower and the average recoil energy is 4.4 kcal/mole, while for higher laser

fluence the distribution is somewhat wider and the average recoil energy is about 5.0 kcal/mole.

The recoil energy distributions in both cases are fairly well characterized since different TOF spectra are sensitive to different parts of the $P(E_T)$. The data for the phenoxy radical at larger angles (12-15°) reflect the high energy tail of the distribution. The fits of the m/e=15 distributions at small angles, on the other hand, are particularly sensitive to the low energy part of the $P(E_T)$.

It has to be emphasized that in all cases the spectra stemming from methyl radical and those stemming from phenoxy radical could be fit with the same recoil energy distributions. However, the minimum recoil energy required for phenoxy to reach the detector at 6° is 2.2 kcal/mole (for a typical beam velocity), whereas the minimum recoil energy required for methyl to reach the detector at 10° is only 0.2 kcal/mole. Thus it is possible that the $P(E_T)$ distributions for the two fragments deviate at very small recoil energies because of the secondary decomposition of some highly vibrationally excited (and thus slow) phenoxy radicals.

The $P(E_T)$ for the secondary reaction, Fig. 9, shows a threshold value of 8 kcal/mole and a maximum energy release of 48 kcal/mole. These values probably have uncertainties of about 2 kcal/mole.

A set of experiments was performed at different laser powers and thus different laser fluences. Fig. 6 shows the TOF

spectra for m/e=39 at 13°, and in Fig. 10 the relative contributions of the two channels are plotted as a function of laser fluence. It can be seen that the relative importance of the secondary channel decreases roughly with decreasing laser fluence. The lowest fluence in this experiment was 5 J/cm^2, which is lower than the value for the earlier set of data, but secondary decomposition was still observed. This shows that either the absolute values for the laser fluence for the two different experiments are not very accurate, or that the temporal structure of these two lasers is sufficiently different so that the comparison becomes difficult. Fig. 10 illustrates that phenoxy radicals formed from anisole molecules at lower levels of internal excitation (at lower laser fluence) still undergo secondary decomposition.

5.4. **Discussion**

Several conclusions can be drawn from the recoil energy distributions obtained from this experiment. The only primary process, dissociation into phenoxy radical and methyl radical, shows the same characteristics for both conditions studied. The fact that the translational energy release in the formation of phenoxy and methyl radicals at higher laser fluence does not differ substantially from that of lower laser fluence indicates that the high rate of dissociation of vibrationally excited

anisole is limiting the further absorption of IR photons. The phenoxy radicals which were produced in the earlier part of the laser pulse continue to absorb IR photons and dissociate into cyclopentadienyl radicals and carbon monoxide.

The fact that the translational energy distributions peak at a small but finite value suggests the existence of a barrier in the $C_6H_5O-CH_3$ dissociation. This is in contrast to simple bond rupture processes which previous investigations of IRMPD[17] have demonstrated to result in translational energy distributions that peak at 0 energy in accordance with the predictions of statistical theory.[18] A barrier for the bond rupture process considered here could result from the electronic rearrangement associated with the partial C-O double bond character in the phenoxy radical. This also explains the fact that in the reverse reaction of methyl radicals with phenoxy radicals the methyl prefers to attach to the o- and p-positions of the benzene ring rather than the oxygen atom.[19]

The secondary process, decomposition of the phenoxy radical to the cyclopentadienyl radical (C_5H_5) and carbon monoxide, has a large barrier. Lin and Lin[5] obtained an activation energy of 44.0±0.9 kcal/mole for this process. The large energy release (up to 48 kcal/mole) in the secondary process is indicative of the barrier for this reaction. The dissociation of phenoxy radical to cyclopentadienyl and carbon monoxide is 20 kcal/mole endothermic.[9,20] The known thermochemistry of the present system is summarized in Fig. 11.

Our results therefore indicate that the IRMPD of anisole is a possible and convenient way of producing phenoxy radicals. No other primary products were observed, and with sufficient control of the laser fluence, secondary products could be prevented. UV photodissociation of anisole at 248 or 193 nm, on the other hand, which has been used as a source of phenoxy radicals,[21] was studied in our laboratory as well, and a number of different primary reaction channels were identified[22] indicating possible difficulties in the application of this method in the investigation of the kinetics of phenoxy radical reactions.

5.5. **Conclusions**

In the IRMPD of anisole the only primary decomposition channel occurring is rupture of the weak[8,9] O-CH_3 bond forming phenoxy and methyl radicals. The recoil energy distribution suggests the existence of an exit barrier for this dissociation channel. Under higher laser fluence conditions, the secondary dissociation of the phenoxy radical was observed. The large recoil energy release is in accordance with the existence of a sizable exit barrier for this process as determined by Lin and Lin.[5]

5.6. References

1. P. A. Schulz, Aa. S. Sudbo, D. J. Krajnovich, H. S. Kwok, Y. R. Shen, and Y. T. Lee, Ann. Rev. Phys. Chem. 30, 379 (1979).
2. M. N. R. Ashfold and G. Hancock, Gas Kinetics and Energy Transfer 4, 73 (1980).
3. I. Oref and B. S. Rabinovitch, Acc. Chem. Res. 12, 166 (1979).
4. A. G. Harrison, L. R. Honnen, H. J. Dauben, and F. P. Lossing, J. Am. Chem. Soc. 82, 5593 (1960).
5. C.-Y. Lin and M. C. Lin, Int. J. Chem. Kinet. 17, 1025 (1985); C.-Y. Lin and M. C. Lin, J. Phys. Chem. 90, 425 (1986).
6. J. C. Mackie, K. R. Doolan, and P. F. Nelson, J. Phys. Chem. 93, 664 (1989).
7. M. M. Suryan, S. A. Kafafi, and S. E. Stein, J. Am. Chem. Soc. 111, 1423 (1989).
8. S. Paul and M. H. Back, Can. J. Chem. 53, 3330 (1975).
9. D. F. McMillen and D. M. Golden, Ann. Rev. Phys. Chem. 33, 493 (1982).
10. A. J. Colussi, F. Zabel, and S. W. Benson, Int. J. Chem. Kinet. 9, 161 (1977).
11. K. Brezinsky, Prog. Energy Combust. Sci. 12, 1 (1986).
12. S. J. Sibener, R. J. Buss, P. Casavecchia, T. Hirooka, and Y. T. Lee, J. Chem. Phys. 72, 4341 (1980).

13. C. Venkat, K. Brezinsky, and I. Glassman, Nineteenth Symposium (International) on Combustion (Combustion Institute, Pittsburgh, 1982), p. 143.

14. A. M. Wodtke and Y. T. Lee, J. Phys. Chem. 89, 4744 (1985).

15. W. J. Balfour, Spectrochimica Acta 9, 795 (1983).

16. X. Zhao, Ph. D. Thesis, University of California, Berkeley, 1988.

17. Aa. S. Sudbo, P. A. Schulz, E. R. Grant, Y. R. Shen, and Y. T. Lee, J. Chem. Phys. 70, 912 (1979); L. J. Butler, R. J. Buss, R. J. Brudzynski, and Y. T. Lee, J. Phys. Chem. 87, 5106 (1983); E. J. Hintsa, A. M. Wodtke, and Y. T. Lee, J. Phys. Chem. 92, 5379, 1988.

18. P. J. Robinson and K. A. Holbrook, Unimolecular Reactions (Wiley, London, 1972).

19. C.-Y. Lin and M. C. Lin, Aust. J. Chem. 39, 723 (1986).

20. M. W. Chase, Jr., C. A. Davies, J. R. Downey, Jr., D. J. Frurip, R. A. McDonald, and A. N. Syverud, J. Phys. Chem. Ref. Data 14 (1985), Supplement No. 1: JANAF Thermochemical Tables, Third Edition.

21. Y. Kajii, K. Obi, N. Nakashima, and K. Yoshihara, J. Chem. Phys. 87, 5059 (1987).

22. Chapter 6.

Scheme 1.

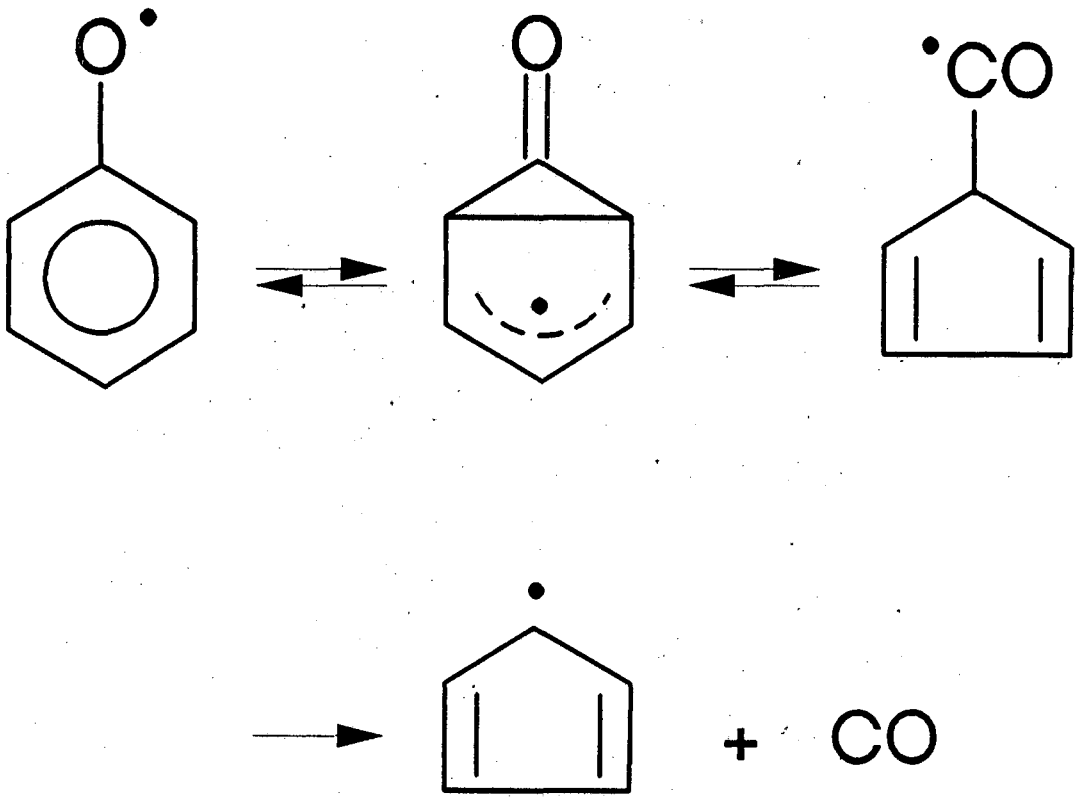

5.8. Figures

Figure Captions

Fig. 1 TOF spectra of m/e=93 and m/e=65 at 8° and m/e=15 at 15° obtained at low laser fluence.

Fig. 2 TOF spectra of m/e=39 at 8°, 12°, and 15° obtained at low laser fluence.

Fig. 3 TOF spectra of m/e=93, 65, and 28 at 10° obtained at high laser fluence.

Fig. 4 TOF spectra of m/e=39 at 6°, 10°, 13°, 20°, 30°, and 40° obtained at high laser fluence showing the primary (long dashed curve) and the secondary (short dashed curve) channels.

Fig. 5 TOF spectra of m/e=15 at 10°, 30°, and 50° obtained at high laser fluence.

Fig. 6 TOF spectra of m/e=39 at 13° obtained at five different laser fluence values: (a) 27 J/cm^2, (b) 24 J/cm^2, (c) 20 J/cm^2, (d) 13 J/cm^2, (e) 5 J/cm^2.

Fig. 7 Newton or velocity diagram illustrating primary and secondary dissociation channels. The shorter vectors originating at the tip of the beam velocity vector correspond to the primary dissociation product, the phenoxy radical. The longer vectors originating at the tip of a phenoxy radical velocity vector correspond to the secondary dissociation product, the cyclopentadienyl radical. The underlined species

indicate which is the detected fragment for each channel. At angles of 20° and larger only secondary products appear.

Fig. 8 Translational energy distributions, $P(E_T)$, for the primary dissociation channel of anisole for low laser fluence (solid curve) and high laser fluence (dashed curve).

Fig. 9 Translational energy distribution, $P(E_T)$, for the secondary dissociation channel of anisole.

Fig. 10 Plot of the relative contributions of the primary and secondary dissociation channels (in arbitrary units) in the spectra in Fig. 6 as a function of laser fluence. One estimated error bar is included.

Fig. 11 Energy diagram for the primary and secondary dissociation process in the IRMPD of anisole.

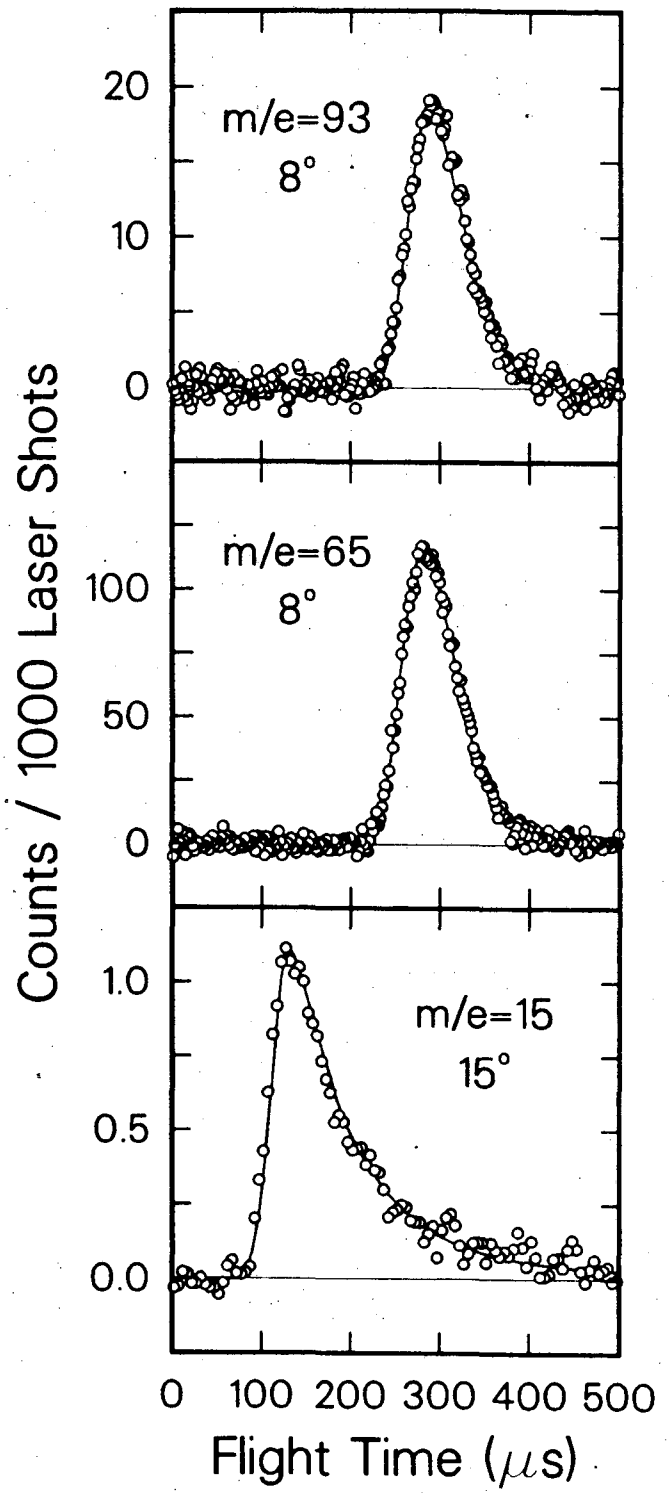

XBL 8910-3570

Fig. 1

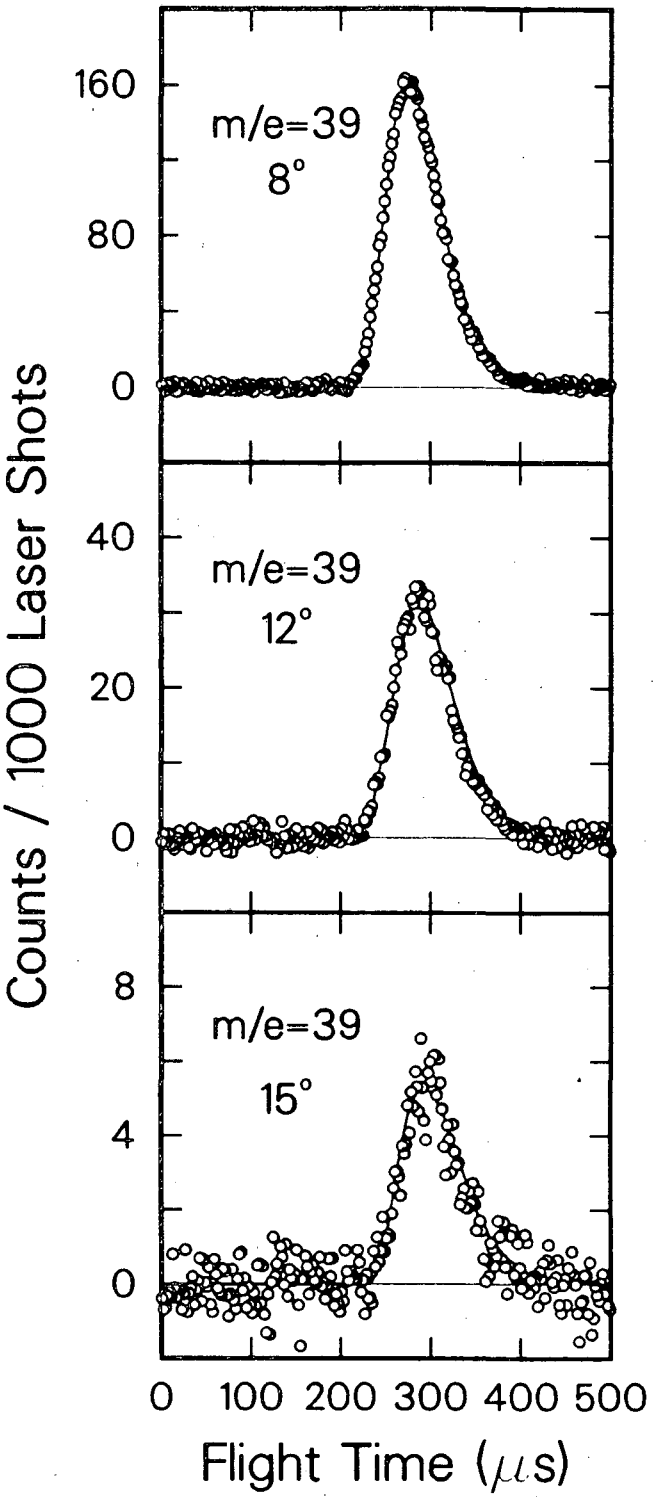

XBL 8910-3572

Fig. 2

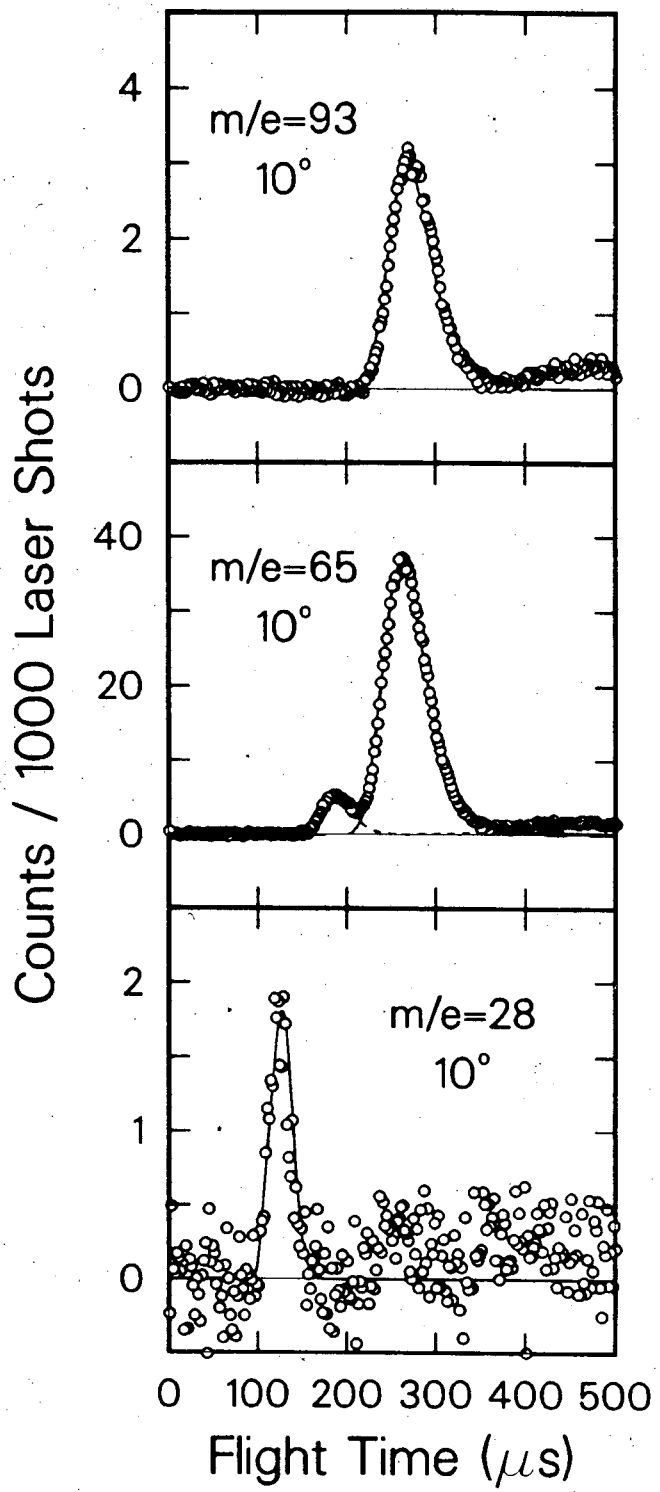

XBL 8910-3569

Fig. 3

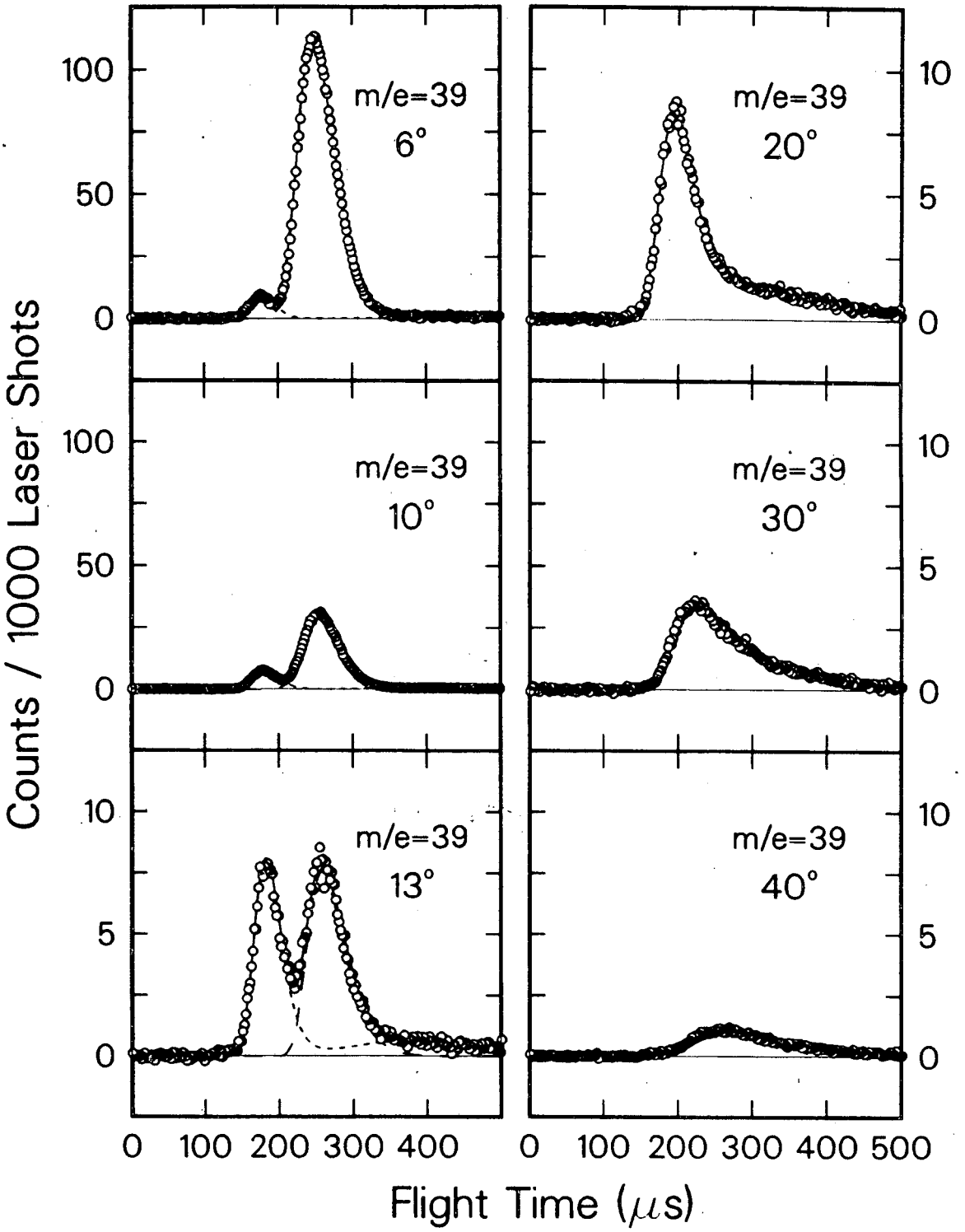

XBL 8910-3568

Fig. 4

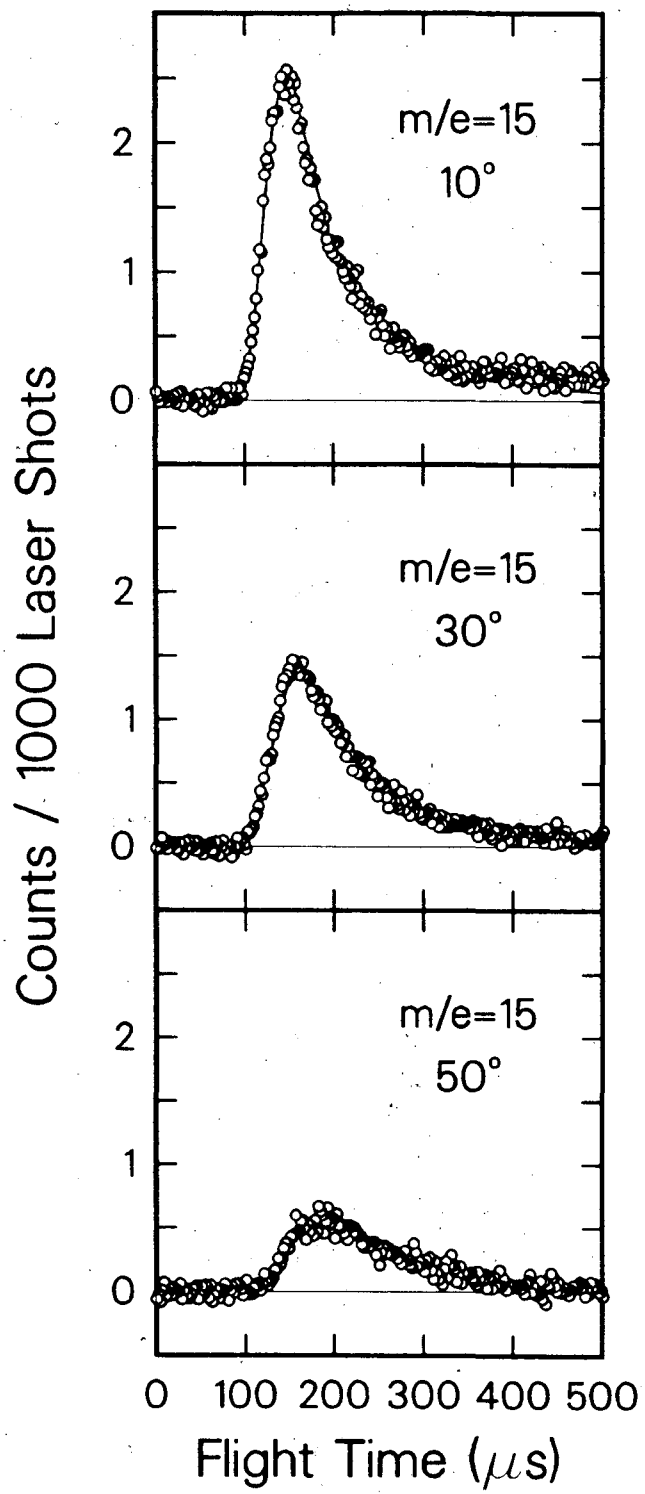

XBL 8910-3573

Fig. 5

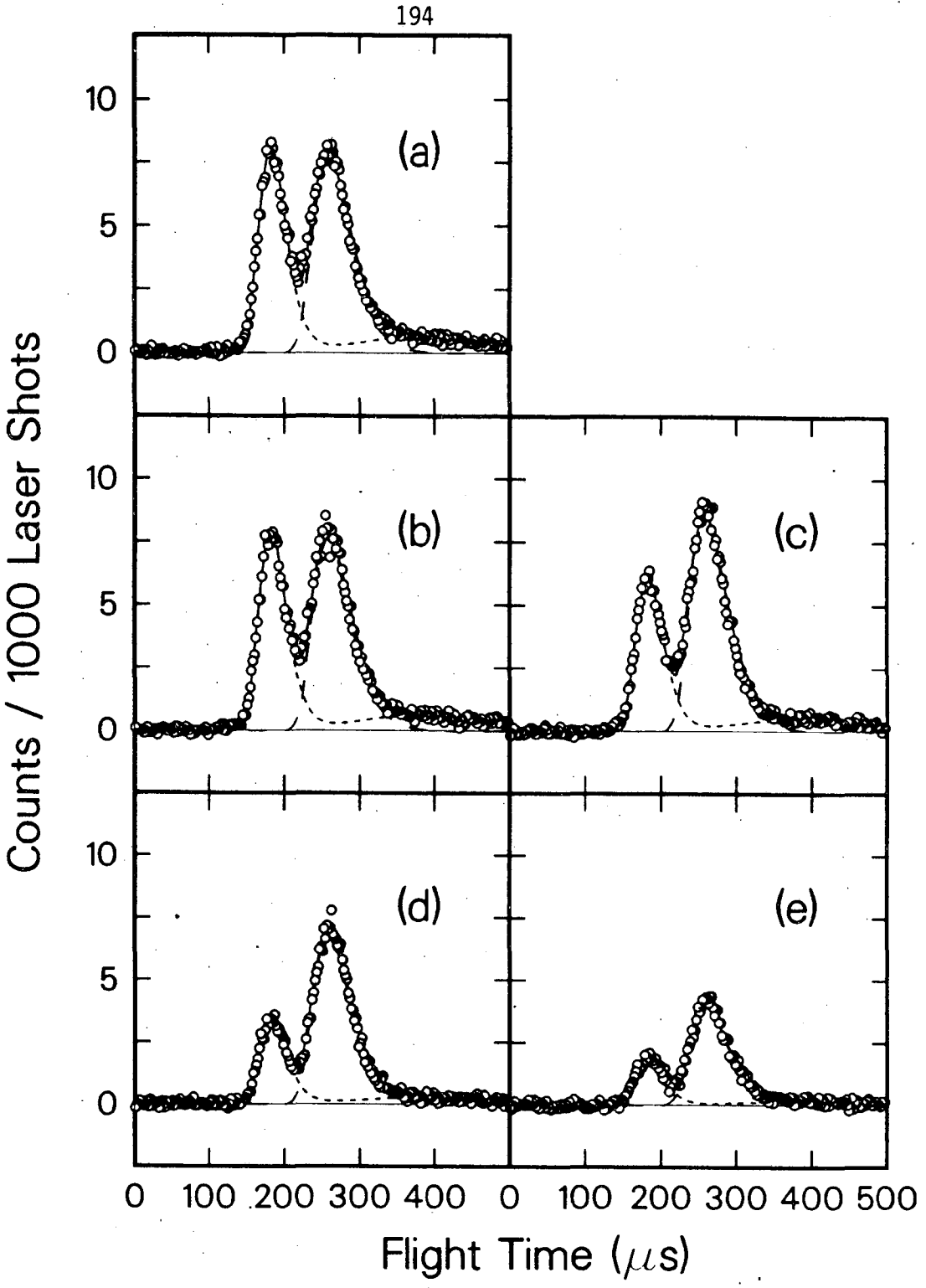

XBL 8910-3571

Fig. 6

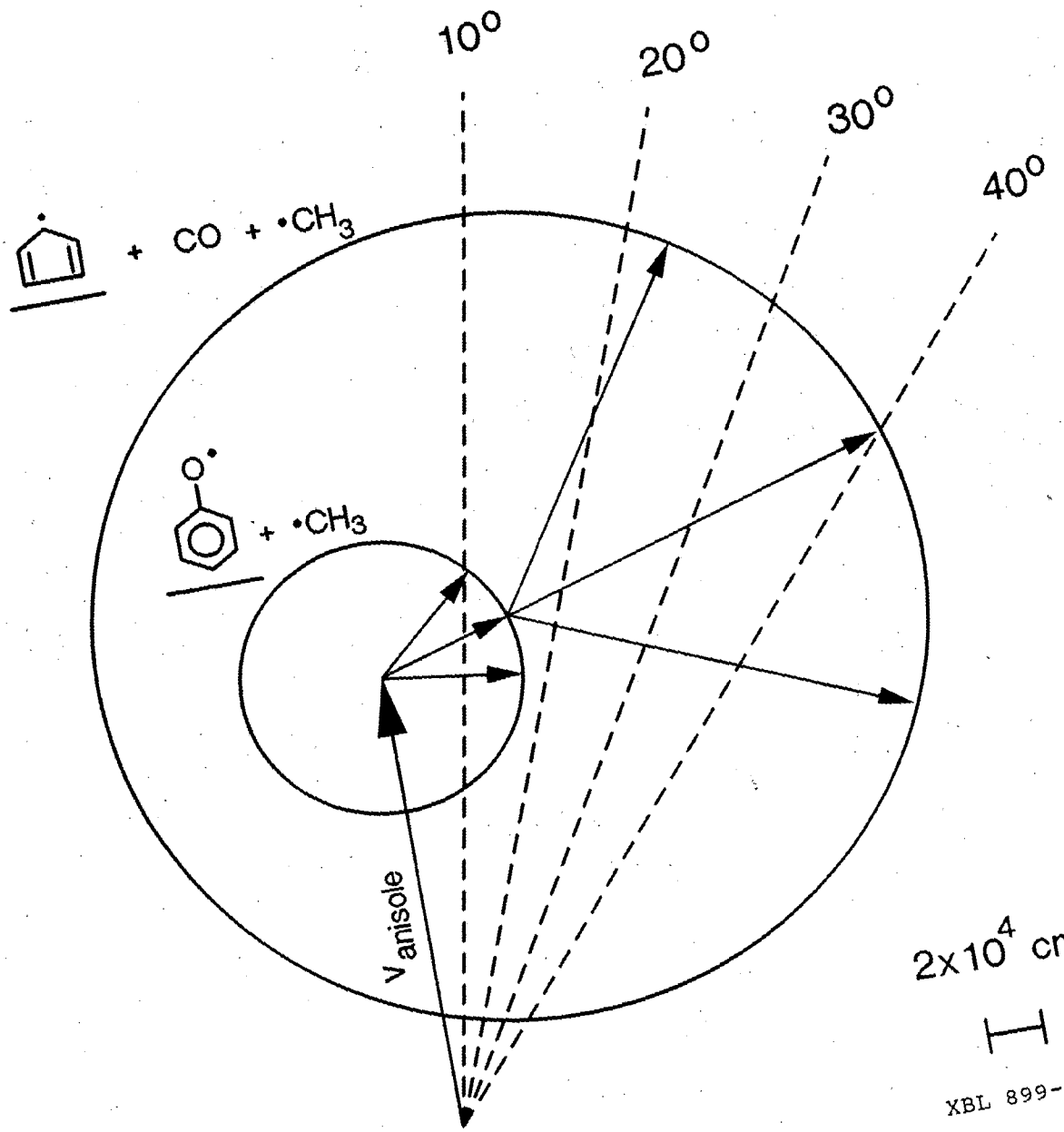

Fig. 7

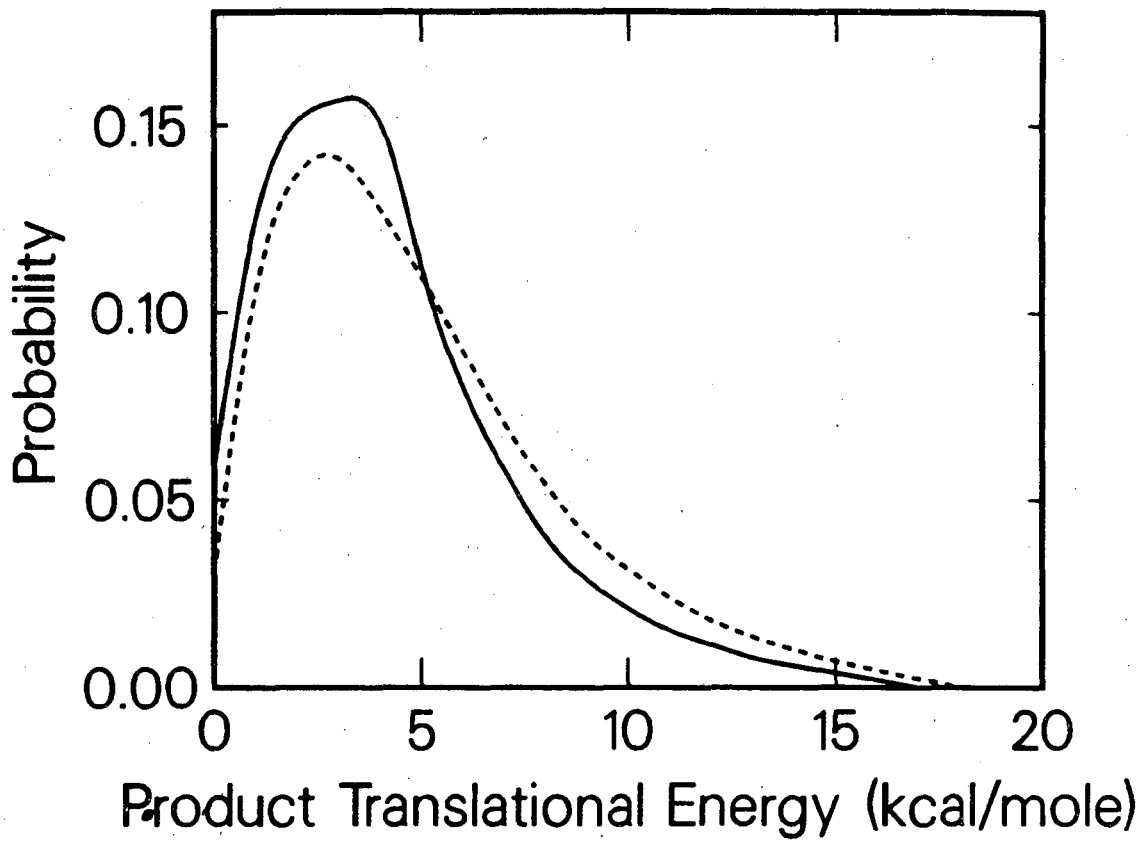

XBL 899-3205

Fig. 8

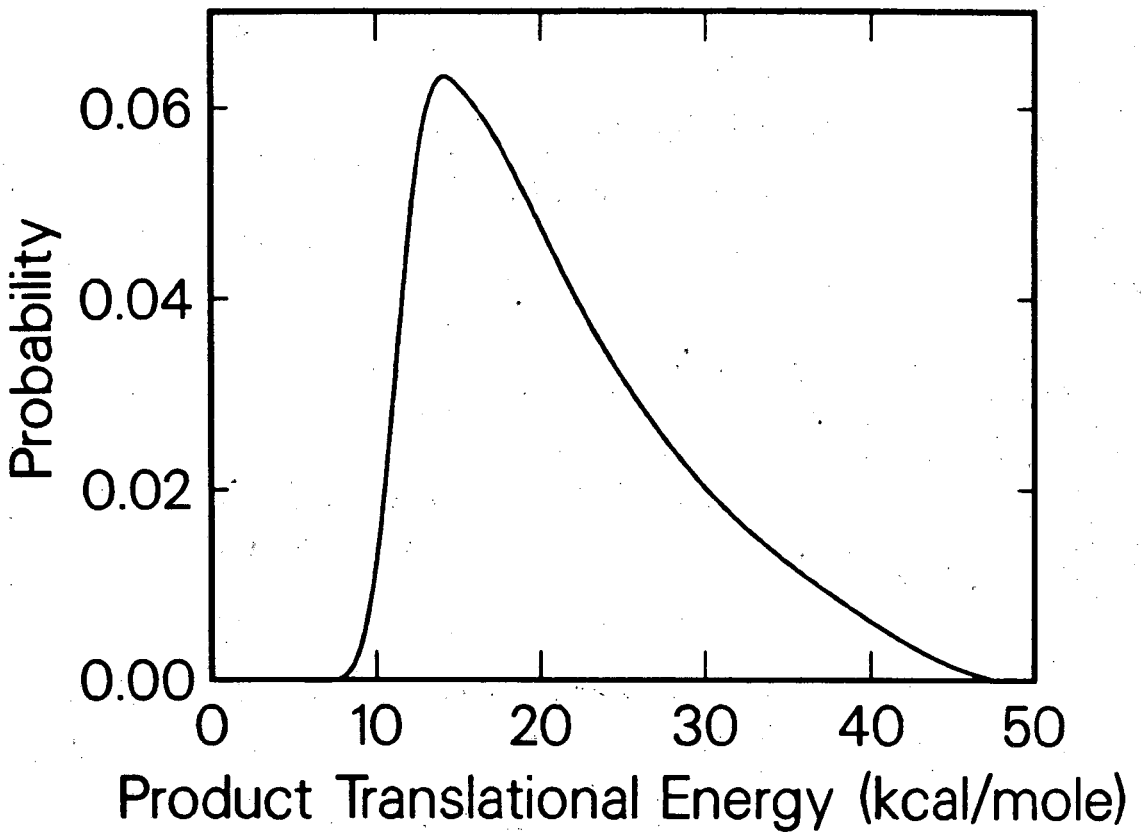

XBL 899-3204

Fig. 9

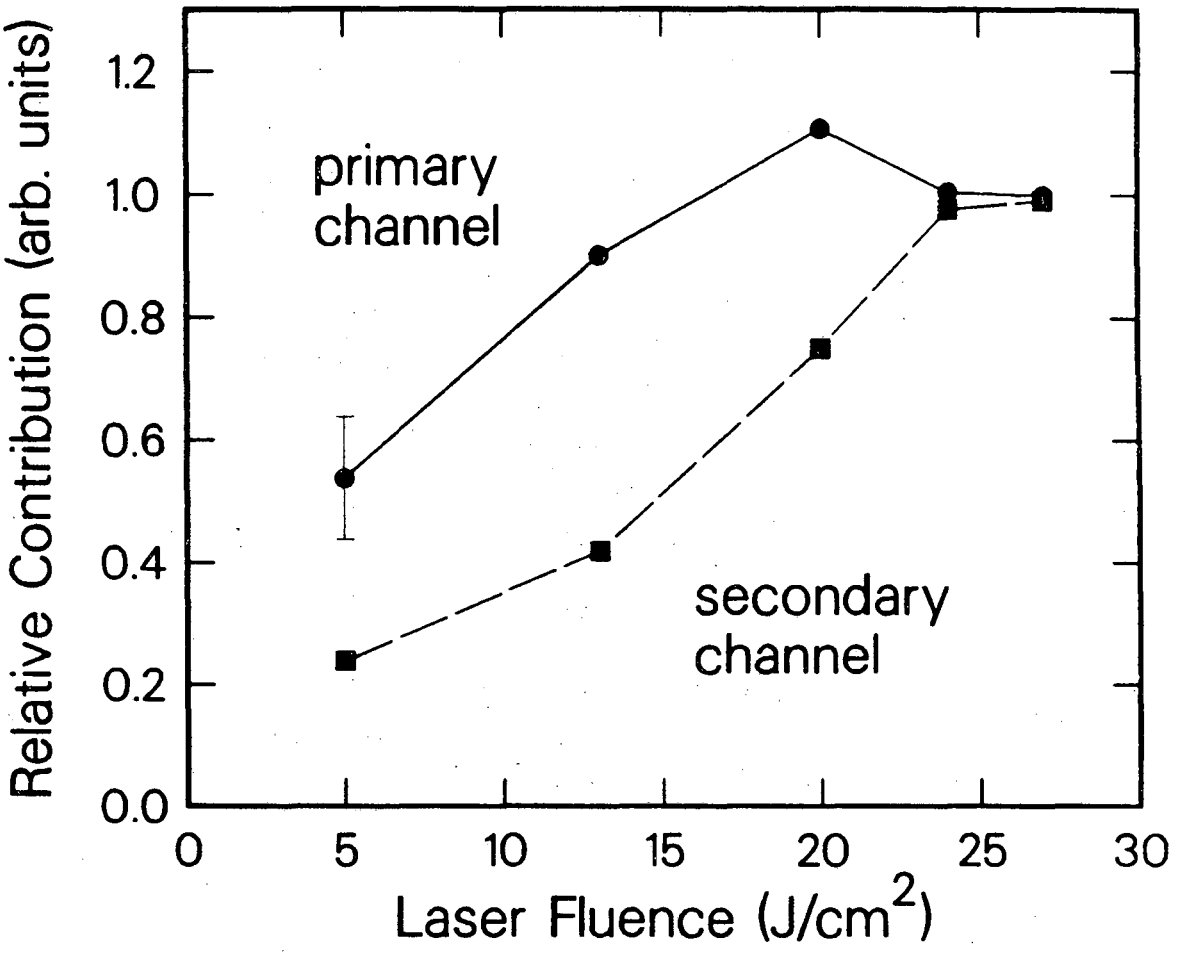

XBL 8910-3575

Fig. 10

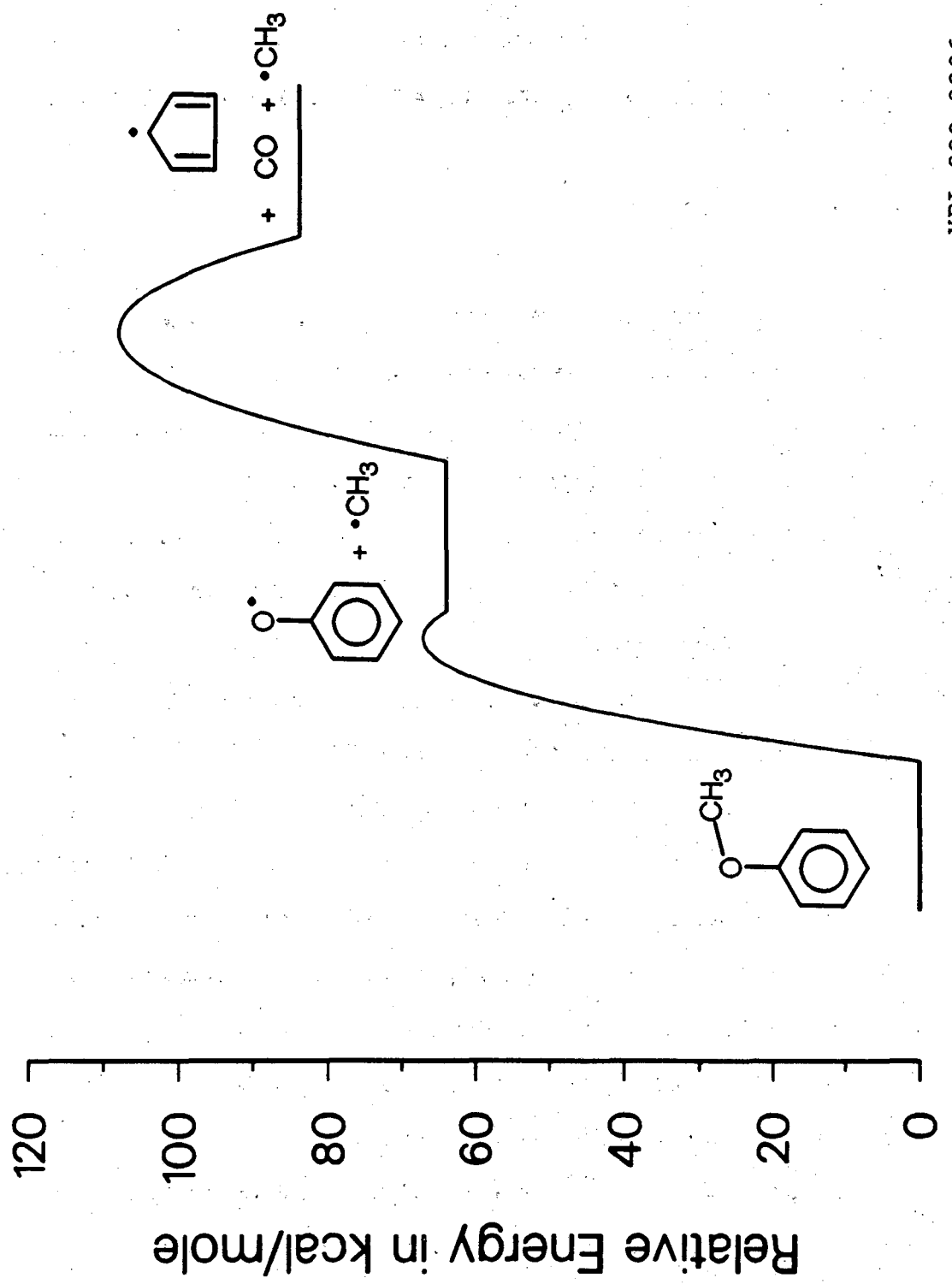
Relative Energy in kcal/mole
120
100
80
60
40
20
0
+ CO + •CH3
+ •CH3
XBL 899-3206

Fig. 11

CHAPTER 6:

DYNAMICS OF ANISOLE PHOTODISSOCIATION AT 193 nm AND 248 nm

6.1. Introduction

The photochemistry of aromatic compounds induced by UV light has been of great interest for a long time. In our laboratory, several simple aromatic compounds were studied using the technique of photofragmentation translational spectroscopy.[1,2] Anisole was chosen in the present study because of our interest in the photodissociation dynamics of phenolic compounds and the processes involved in the formation and decomposition of phenoxy radical, an important intermediate in the combustion of aromatic hydrocarbons.[3]

Cleavage of the weak[4] CH_3-OC_6H_5 bond in anisole leading to the formation of methyl and phenoxy radicals is the dissociation channel which requires the lowest energy. This was indeed found to be the only primary decomposition pathway in the thermal decomposition[5] or in IR multiphoton dissociation,[6] a process which mimics thermal dissociation processes under collision-free conditions. Reactions following UV excitation and rapid internal conversion (IC) to the highly vibrationally excited electronic ground state should include the same dissociation pathway. However, the direct excitation to a dissociative state

or predissociation can result in very different product channels.

The decomposition of the phenoxy radical to carbon monoxide and the cyclopentadienyl radical was suggested[7] to take place through an intermediate five-membered ring structure (Scheme 1). A low activation energy, 44 kcal/mole, was determined for this process.[8] Thus, if phenoxy radicals are produced with sufficient internal energy in the photodissociation of anisole, or if the phenoxy radicals subsequently absorb another photon, they will decompose.

The UV absorption spectrum of anisole has been reported[9] and the transitions have been assigned using results of CNDO/S-CI calculations of the electronic states.[10] Among two possible conformers, the planar one was found to be more stable.[11] The measured absorption cross section at 193 nm is considerably larger than that at 248 nm.[9] Absorption spectra of the phenoxy radical in the UV and visible wavelength regions have also been measured repeatedly,[12-14] and a strong absorption band was found around 240 nm.[13] Recently, Kajii et al.[15] studied the transient absorption spectra obtained following flash photolysis of phenol and anisole at 193 nm and identified two major features around 230 and 290 nm as originating from phenoxy radicals.

In our experiment, the photodissociation of anisole in a molecular beam was studied at 193 nm and 248 nm. In addition to the formation of phenoxy and methyl radicals, several different primary and secondary product channels were observed. Our

results indicate that dissociation from electronically excited states plays a major role at both wavelengths.

6.2. **Experimental**

The apparatus and the preparation of the molecular beam of anisole were described in the previous chapter. A Lambda Physik EMG 103 MSC Excimer Laser equipped with an Intelligent Laser Control to stabilize the output power was used at the 193 nm (ArF) and 248 nm (KrF) transitions. The laser radiation was focused using a 25 cm focal length fused silica lens. The spot size at the interaction region of approximately 6 mm x 1.5 mm was estimated from burning patterns on tape. Maximum output power levels were 80 mJ/pulse at 193 nm and 110 mJ/pulse at 248nm. The laser was operated at repetition rates of 50-100 Hz. All measurements were performed using unpolarized laser light. Laser power dependence studies were performed by attenuating the laser using various combinations of fine metal screens. Between 50,000 and 700,000 laser shots were accumulated for each spectrum.

6.3. **Results and Analysis**

Time-of-flight (TOF) spectra of the dissociation products

were measured at laboratory angles between 6° and 50° at a large number of mass-to-charge ratios (m/e) at both wavelengths. Some of the spectra were repeated at different laser power levels in order to identify multi-photon processes.

The variety of features observed indicate the occurrence of several competitive dissociation pathways. In addition, product molecules or radicals fragment extensively upon ionization in the mass spectrometer. However, parent-daughter-ion relationships can be established by identifying common features in the TOF spectra for different mass-to-charge ratios (m/e). Corresponding fragment pairs can be identified using the condition of momentum conservation in the center-of-mass coordinate system. The data analysis procedure was described in the previous chapter. The translational energy distributions obtained for the different channels will be presented below. The center-of-mass angular distributions were isotropic in all cases.

In the present experiment, the large number of different features observed as well as the fact that many of these overlap and can not be separated unambiguously cause difficulties in the qualitative and quantitative interpretation of the data. The different features that could be distinguished in the 193 nm and 248 nm results will be designated as I-1 through I-14 and as II-1 through II-13, respectively, and their interpretations will be discussed. Table 1 lists several possible channels and the energetics in the dissociation processes at 193 and 248 nm.

Table 2 summarizes the features described in detail below.

6.3.1. **193 nm**

6.3.1.1. Features I-1 and I-2. A narrow and fast peak (centered at flight times of about 190 μs at 10°) is easily identified at m/e=93, 92, 91 ($C_6H_5O^+$, $C_6H_4O^+$, and $C_6H_3O^+$), see Figs. 1-2, as well as m/e=65 ($C_5H_5^+$) and many other masses of C_5H_5-fragments. The occurrence of this feature, designated as I-1, at these masses suggests the phenoxy radical as its source. At m/e=93 (Fig. 1) this is probably the only feature, which facilitates the analysis. Data at three different angles were obtained for m/e=93 and all these spectra could be fit using the assumption of reaction (1):

$$C_6H_5\text{-}O\text{-}CH_3 \xrightarrow{h\nu} C_6H_5O\cdot + \cdot CH_3 \qquad (1)$$

The translational energy found for this process, shown in Fig. 3, has a minimum value of approximately 30 kcal/mole, a peak at 45 kcal/mole, and a maximum of about 63 kcal/mole. The maximum available energy for (1) is 85 kcal/mole (Table 1). The assignment of this product to the phenoxy radical is supported by the fact that the fastest peak (feature I-2) at m/e=15, 14, and 13 (CH_3^+, CH_2^+, and CH^+), see Fig. 4, peaking at about 75 μs at 10°, can be identified with the corresponding methyl radical fragment.

It should be noted that all phenoxy radicals having an internal energy of more than 44 kcal/mole can further decompose into carbon monoxide and cyclopentadienyl radical,[8] reaction (2):

$$C_6H_5O\cdot \longrightarrow C_5H_5\cdot + CO \qquad (2)$$

In the present case, if methyl radicals are produced in the ground state, more than 44 kcal/mole internal energy corresponds to a translational energy of less than 41 kcal/mole. Of course some of the available energy will be channeled into excitation of the methyl radical, and that is the reason why some phenoxy radicals are stable even in the cases where the translational energy only amounts to 30 kcal/mole. The energetics of the primary and possible secondary dissociation channels are illustrated in Fig. 5.

The origin of features I-1 and I-2 could be either a direct dissociation from an excited state, or the dissociation of vibrationally excited ground state anisole molecules formed by the internal conversion of electronically excited molecules. In the latter case, however, a translational energy distribution peaking at lower values would be expected. It is conceivable that all slower phenoxy radicals, having a larger internal energy, spontaneously dissociate further, and only the fast ones are detected. The corresponding signal at m/e=15 should reflect the primary dissociation channel completely. It was found that

the m/e=15 data are compatible with the assumption of only some additional slower primary product, which is not detected as phenoxy radical but instead decomposes further, but the peak of the translational energy still has to be at approximately 40 kcal/mole in order to fit the m/e=15 data.

No clear evidence was found for secondary products, CO and C_5H_5, originating from such comparatively fast primary phenoxy radicals. It thus appears unlikely that large amounts of phenoxy radicals which spontaneously decompose are being produced in this channel. The most likely source of features I-1 and I-2 is direct dissociation of anisole into fast phenoxy and methyl radicals from an electronically excited state.

6.3.1.2. Features I-3 and I-4. Feature I-3 is the most prominent one in many spectra at 10°, particularly at m/e=65 (see Figs. 6-7) and its fragments (m/e=36-39, 48-52, 60-64) but it also occurs at m/e=92, 91, and 90, and possibly at m/e=93. Several interpretations for this feature are possible. Its mass spectrum suggests the phenoxy radical as its origin. A fit of feature I-3 (at 10° and 20°) using this assumption is possible with a translational energy distribution peaking at approximately 8 kcal/mole and extending to about 20-30 kcal/mole (Figs. 3,8). However, as was argued before, phenoxy radicals which are that slow should have enough internal energy to decompose before they are able to reach the detector. On the other hand, this energy could have been channeled into

electronic excitation of either products. The energy of this excited state would be around 15,000-25,000 cm^{-1}. The energy of the lowest excited state of the methyl radical is not known,[21] but is most likely higher than that.[22] For the phenoxy radical, Roebber[13] and Pullin and Andrews[14] found an absorption band around 25,200 cm^{-1} which could correspond to an excited state that is accessed in our experiment. An optically inaccessible state could also be responsible. The striking differences in the mass spectra of features I-1 and I-3 indicate large differences in the internal energy of the two moieties.

Other possible reaction channels responsible for feature I-3 are (3), the expulsion of $O(^1D)$, or (4), the expulsion of $^1CH_2$. These processes would be the reverse of the well-known insertion of singlet oxygen atoms[23] or methylene radicals[24] into single bonds.

$$C_6H_5\text{-}O\text{-}CH_3 \xrightarrow{h\nu} C_6H_5\text{-}CH_3 + O(^1D) \qquad (3)$$

$$C_6H_5\text{-}O\text{-}CH_3 \xrightarrow{h\nu} C_6H_5\text{-}OH + {}^1CH_2 \qquad (4)$$

Reaction (3) appears to be an unlikely candidate since the remaining available energy would be only 14 kcal/mole and thus the feature cannot be fit satisfactorily complying with this constraint. An additional clue comes from the mass spectrum of this product. Even though the mass spectra of phenol,[25] toluene,[25] and phenoxy radical produced in the IR multiphoton

dissociation of anisole[6] are very similar (see Fig. 9), a very important observation is that toluene lacks significant fragmentation into m/e=29, 30, and 31. However, these masses are clearly fragments of feature I-3.

Reaction (4) with an available energy of 52 kcal/mole, provides a possible explanation. A peak at m/e=93 would be expected from phenol, but is probably absent for feature I-3, moreover, the signal at m/e=92 and 91 is low also. However, no definite conclusions can be drawn from the mass spectrum in this respect, since it is well known that fragmentation patterns can depend strongly on the internal energy of the molecule.[26]

The search for the corresponding second fragment yields no clear answer, either. Under the assumption of channel (1), a peak at m/e=15 is calculated that does not fit the observed features in the spectrum entirely, but can be considered a possible component, and will be denoted feature I-4 (See Figs. 4, 10). The m/e=14 (CH_2^+) spectrum is basically similar to the m/e=15 (CH_3^+) spectrum, suggesting no major additional channel. The signal at m/e=16 (O^+) is low, furthermore it has a component faster than that expected for $O(^1D)$. Overall, m/e=16 appears to be mostly due to a fragment of CO because of the similarity to the m/e=28 (CO^+) spectrum. Alternatively, an isomer of phenoxy radical could be formed which loses its excess internal energy through emission of a photon.

In summary, the origin of feature I-3 could not be identified unambiguously. Possible sources are electronically

excited metastable phenoxy radical, phenol being formed in reaction (3), or perhaps a radiatively stabilized isomer of the phenoxy radical.

The fits presented in Figs. 6 and 7 assumed a channel producing phenoxy radicals as the origin of feature I-3, and the translational energy distributions used are shown in Figs. 3 and 8, respectively. The $P(E_T)$ distributions in these two cases are slightly different (particularly in the high energy tail) since they were optimized in combination with different additional channels. Because of the overlap with the other features, their exact shape can not be determined from our experiment.

6.3.1.3. Features I-5 and I-6. Another prominent feature, designated as I-5, which peaks at about 130 μs at 10°, is found at m/e=30, 29, 15, 14, and 13 (See Figs. 4, 10 and 11). This combination of masses suggests a species containing one carbon atom, one oxygen atom, and at least three hydrogen atoms as the source. Possible decomposition channels therefore are:

$$C_6H_5\text{-}O\text{-}CH_3 \xrightarrow{h\nu} C_6H_5\cdot + CH_3O\cdot \qquad (5)$$

$$C_6H_5\text{-}O\text{-}CH_3 \xrightarrow{h\nu} C_6H_4 + CH_3OH \qquad (6)$$

Channel (6) represents a 4-center elimination of a methanol molecule from anisole forming benzyne. If methanol were the product, fragments would be expected at m/e=32 and 31 (CH_3OH^+

and CH_3O^+) as well, but were not found in significant amounts. However, the fragmentation pattern of vibrationally excited methanol could be considerably different from that of cold molecules. The available energy for channel (5) is about 48 kcal/mole, but it was found that much more translational energy, about 65 kcal/mole, is required for fitting this feature, see Fig. 12, indicating that methanol is produced rather than methoxy radicals. The translational energy distribution was found to peak around 12 kcal/mole, implying an exit channel barrier.

The corresponding second product, benzyne, was detected as feature I-6 at m/e=76 and 75, where it constitutes the faster part of the spectra (centered at about 200 μs), see Fig. 13.

6.3.1.4. Features I-7 and I-8. At first glance, the signal at m/e=28 (see Fig. 14) appears to be due to feature I-5, however, a close inspection reveals significant differences. The m/e=28 distribution has components distinctly faster than feature I-5. Therefore the major part of the m/e=28 signal constitutes a separate feature, denoted as I-7, with a peak at around 120 μs at 10°. Another indication for the different origin of features I-5 and I-7 is the fact that the peak in the m/e=28 spectrum is about 80 counts/laser shot, whereas the peak at m/e=29 is about 6 counts/laser shot. If both m/e=28 and m/e=29 were fragments of the same product, such as methanol, m/e=28 would not be expected to dominate so strongly.

The most likely source of feature I-7 is carbon monoxide produced in the secondary decomposition of phenoxy radicals. The other product of this process, the cyclopentadienyl radical, is expected to appear as fast signal at m/e=65 and the masses of its fragments. Such a signal is indeed found in the m/e=65 spectra (see Figs. 6-7). At 10°, a component even faster than feature I-1 can be distinguished and is denoted as feature I-8. At 20°, 30°, and 40°, this feature, denoted I-8, becomes more apparent. Feature I-1 disappears at angles larger than 30°, and feature I-3 disappears at angles larger than 20°. Laser power dependence studies indicate that no multiphoton processes are involved.

The analysis of features I-7 and I-8 under the assumption that they both originate from the same secondary dissociation process presents difficulties, primarily due to the fact that the vibrationally excited phenoxy radicals which are assumed to lead to the observed secondary products could not be detected, since they dissociate before reaching the detector. They could be produced from the highly vibrationally excited anisole formed by internal conversion. After absorption of a 193 nm photon (148 kcal/mole) and $C_6H_5O-CH_3$ bond rupture (63 kcal/mole), 85 kcal/mole of excess energy would be partitioned between the phenoxy radicals and the methyl radicals. A large fraction of this energy would get channelled into the vibrational excitation of phenoxy and most phenoxy radicals thus could overcome the 44 kcal/mole decomposition barrier.

In order to fit both feature I-7 and I-8 simultaneously, a very slow primary process (maximum translational energy about 3 kcal/mole) and a relatively fast secondary process (maximum translational energy more than 60 kcal/mole, peak at about 15 kcal/mole) are needed (see Fig. 3). The slower the primary process assumed, the better the fit. When a faster primary process was assumed, the calculated spectra for m/e=65 were too fast.

A comparison with the translational energy distribution found for the primary $C_6H_5O-CH_3$ bond rupture process in the IR multi-photon dissociation (IRMPD) of anisole[6] can give an indication for what the primary $P(E_T)$ should look like. Surprisingly, the translational energy release in the IRMPD case was larger (the $P(E_T)$ peaked at 3 kcal/mole and extended to about 18 kcal/mole) than what appears to be required in the analysis of the data at 193 nm excitation, even though the energy absorbed by each anisole molecule is substantially larger in the latter case. The fact that the $P(E_T)$ in the IRMPD experiment[6] had a peak at a few kcal/mole rather than at zero energy indicates the existence of a barrier to dissociation. This should also be reflected as a peak away from zero in the $P(E_T)$ for the primary dissociation following UV-excitation and IC. The present data do not allow a definite conclusion on the existence of such a peak in the primary $P(E_T)$. However, if it exists, it would be at an energy considerably smaller than 3 kcal/mole.

The upper panel of Fig. 3 shows a very slow $P(E_T)$ distribution which was assumed to represent the IC channel. No primary phenoxy product corresponding to this $P(E_T)$ was found, instead it was assumed that all of the highly vibrationally excited phenoxy radicals decompose. The translational energy distribution for this process is shown in the lower panel of Fig. 3. The secondary $P(E_T)$ peaks at about 16 kcal/mole and extends to over 60 kcal/mole. Fig. 6 shows the fits obtained for feature I-8 in the m/e=65 data using these assumptions and the upper panel in Fig. 14 the corresponding curve for feature I-8 at m/e=28.

Attempts were made to fit the secondary dissociation with translational energy distributions for the secondary process that depended on the translational and thus vibrational energy of the primary product. However, no improvements in the fits could be achieved.

6.3.1.5. Features I-9 and I-10. These apparent discrepancies could be resolved by assuming the existence of an additional dissociation channel producing CO directly from anisole, such as process (7):

$$C_6H_5\text{-}O\text{-}CH_3 \xrightarrow{h\nu} C_5H_5\text{-}CH_3 + CO \qquad (7)$$

In order for this process to occur directly, the methyl group has to migrate to a position on the aromatic ring,

possibly followed by a rearrangement to a methyl-substituted 5-membered ring system with subsequent decarbonylation (Scheme 2). This sequence of rearrangements resembles that suggested for the unimolecular decomposition of phenol,[27] with the methyl group instead of the phenolic hydrogen migrating.

The energy available to the products of this process would be about 132 kcal/mole. It was assumed that at least the fast part of the m/e=28 data is due to this channel, since particularly the fast edge could not be fit satisfactorily with the assumption of reaction (2). For reaction (7), a translational energy distribution peaking at about 15 kcal/mole and extending to about 35 kcal/mole (Fig. 8) was used to obtain the fit for the m/e=65 data shown in Fig. 7 and simultaneously for m/e=28 as shown in the lower panel of Fig. 14. The faster part of the m/e=28 data that was identified with CO from this channel will be denoted as feature I-9. The corresponding second fragment, the methyl-cyclopentadiene, could not be identified with any salient feature in any of the TOF spectra. At 10°, the peak of the spectrum due to the methyl-cyclopentadiene was calculated to be at about 200 μs, which indicates that such a feature could be hidden under features I-1, I-3 and I-8 at m/e=65 and its fragments, and is denoted as feature I-10 in the m/e=65 spectra (Fig. 7) for illustrative purposes.

6.3.1.6 Feature I-11. The slowest part of the m/e=15, and more

notably the m/e=14 and 13 spectra (Figs. 4 and 10), will be denoted as feature I-11. Several explanations are possible for this feature. First, it could originate from slow methyl radicals being formed along with the phenoxy radicals in the electronic ground state dissociation which was discussed above. Even if none of the phenoxy radicals reach the detector because of secondary decomposition, it should be possible to detect the corresponding methyl radicals. Feature I-11 in the m/e=15, 14, and 13 data could indeed be fit using the very low translational energy release (Fig. 3) that was assumed for the primary dissociation leading to the secondary features I-7 and I-8.

On the other hand, it is possible that feature I-11 arises from the ionizer fragmentation of larger species such as the phenoxy radical or possibly methyl-cyclopentadiene, if channel (7) indeed occurs.

6.3.1.7 Feature I-12. A small signal is found at m/e=15, 14, and 13 at flight times around 90 μs at 10° which lies between features I-2 and I-5 in the spectrum (see Figs. 4 and 10, feature I-12 not indicated). Laser power dependence studies showed that this feature most likely arises from a multi-photon process. It is not clear which primary reaction, if any, is responsible for producing the precursor to this secondary product. It is unlikely that the phenoxy radical would produce methyl, but other possible primary products discussed above could be the source, such as toluene, methyl-cyclopentadiene, or

methanol. Alternatively, an additional primary reaction channel could be responsible such as the elimination of H atoms or H_2 from anisole. These channels were found to take place in the UV photodissociation of benzene,[1] and they would most likely go undetected in the present experiment, since the resultant heavy fragment would get scattered only to very small laboratory angles.

6.3.1.8 Features I-13 and I-14. In the spectra at m/e=29, 30, and 31, an additional feature, I-13, can be distinguished which is centered at flight times of about 180 μs at 10° and lies between features I-3 and I-5. The position of feature I-13 is similar to that of feature I-1, however, it becomes clear in the fitting procedure that the assumption of an additional channel significantly improves the fits of the spectra at m/e=29, 30, and 31. Channel (5), the formation of methoxy and phenyl radicals, provides a possible explanation. The counterpart of the methoxy radical, the phenyl radical, could then be responsible for feature I-14, centered at about 250 μs in the m/e=76 and 75 spectra (see Fig. 13). The position and shape of feature I-14 somewhat resembles that of feature I-1, and it is possible that fragmentation of phenoxy radicals into m/e=76 and 75 occurs additionally.

No accurate determination of the translational energy distribution for this channel was possible, but it can be said that the translational energy release is relatively small, with

a maximum energy of 5 kcal/mole, and a peak at about half of that. If this channel occurred as a simple bond rupture process with no barrier on the ground state surface following IC of the excited state of anisole, the translational energy distribution should peak at zero. Not enough is known about this channel to determine its mechanism, and its relative importance is probably very small.

6.3.1.9 Other Features. Fig. 15 shows the spectra of C_5^+, C_4^+, and C_3^+ (m/e=60, 48, and 36) at 10° which illustrate these additional fast features. A very fast component was found at around 50 μs at 10° at m/e=39, 38, 37, and 36 ($C_3H_3^+$-C_3^+) suggesting additional channels producing secondary decomposition products of cyclopentadienyl radicals and/or other larger species. No data were taken for the C_2-fragments (except m/e=28 which could contain contributions from ethylene molecules), but the data for the C_4-fragments, particularly m/e=50, 49, and 48, also show an additional fast component. In fact, even the C_5 fragments, particularly m/e=62, 61 and 60 ($C_5H_2^+$, C_5H^+, and C_5^+), apparently contain components faster than feature I-8, which is due to the formation of cyclopentadienyl radical in a secondary process.

No detailed analysis of these additional reaction channels involved was attempted. These processes are possibly due to multiple photon absorption by anisole or absorption by the primary products and subsequent dissociation.

6.3.2. 248 nm

Many features in the TOF-spectra obtained from the photodissociation at 248 nm are similar to those in the 193 nm dissociation, but also a number of differences were found. In particular, many of the spectra in the 248 nm experiment contain features which show a laser power dependence indicating that more than one photon is involved. In the case of the 193 nm experiment, this was only observed for feature I-12 in the m/e=15 spectra.

6.3.2.1. Features II-1 and II-2. At m/e=93, 92, 91, 65 and all other typical C_5H_5-fragment masses, a fast feature (II-1), centered at flight times of about 210 μs at m/e=93, was observed (see Figs. 16-18) which appears to correspond to feature I-1 in the 193 nm experiment. It could indeed be fit with the assumption of reaction (1), the formation of phenoxy and methyl radicals. Similar to the case of I-1, the translational energy release (see Fig. 19) is large, and a minimum translational energy value of 8 kcal/mole was found. This value, however, is not very well defined because of the overlap with feature II-3, as discussed later. The value of 8 kcal/mole in fact corresponds to the energy at which the onset of secondary dissociation of the phenoxy radical into the cyclopentadienyl radical and carbon monoxide becomes energetically possible,

again suggesting the possibility that more slow phenoxy than observed is actually produced which does not reach the detector but instead dissociates spontaneously. As before, the spectra of the corresponding second fragment, the methyl radical, can provide an answer to this question. The fast feature in the m/e=15, 14 and 13 spectra (see Fig. 20), designated as II-2 and centered at about 90 μs, can be identified with the methyl radicals originating from the same process as feature II-1. The fit to feature II-2 reveals that no significant amounts of slow methyl radicals - and thus phenoxy radicals - are being produced in this channel. Therefore it appears that features II-1 and II-2 originate from the direct dissociation of an electronically excited state of anisole.

6.3.2.2. Features II-3 and II-4. At the same ion masses as feature II-1, a slower component is found (centered at about 250 μs at m/e=65), which is designated as feature II-3 (see Figs. 16-18). Similarities between this feature and I-3 exist, but also marked differences, such as the mass spectrum - feature I-3 produces little or no signal at m/e=93, whereas II-3 clearly does - and the power dependence. The relative contribution of II-3 compared to II-1 increases with increasing laser power, as shown in Fig. 18, suggesting that II-3 originates from a multi-photon process, in contrast to I-3. Under the assumption that II-3 represents phenoxy radical, as its mass spectrum suggests, a translational energy distribution was obtained that peaks at

about 7 kcal/mole and extends to approximately 11 kcal/mole (see Fig. 19). The exact shape of this distribution, particularly the high energy limit, is not well defined by the experimental data due to the partial overlap of features II-1 and II-3 in all the spectra in which they occur. This comparatively low translational energy release is surprising in view of the finding that most likely a two-photon process is responsible for this feature, leaving about 167 kcal/mole of available energy for the phenoxy and methyl radicals. The explanation could again come from the assumption of the involvement of an electronically excited state of the phenoxy radical or possibly the methyl radical.

Other possibilities for the interpretation of this feature exist, in analogy to those discussed for feature I-3 in the 193 nm experiment, such as reaction (4), the formation of phenol and $^1CH_2$. Channel (3), the formation of toluene and $O(^1D)$, is energetically possible only as a multi-photon process at 248 nm (see Table 1), but is a very unlikely source of feature II-3 since no significant amounts of toluene, whose parent mass is 92 amu, are expected to be detected at m/e=93.

In contrast to the case of the 193 nm experiment, somewhat clearer evidence was found for slower methyl radical stemming from reaction (1) and corresponding to feature II-3. The laser power dependence studies on the m/e=15 spectrum at the laboratory angle of 10° (upper panels of Fig. 20) show that the slower part of the m/e=15 spectra is comprised of at least two

components, with the contribution of the faster part increasing with increasing laser power. This part of the m/e=15 spectra (denoted II-4, centered at about 120 μs) could represent the slower CH_3 + phenoxy radical channel.

6.3.2.3. Features II-5 and II-6. The m/e=65 TOF spectrum at 10° and high laser power (Fig. 18) shows an additional fast component centered at flight times of about 170 μs (feature II-5). This component becomes very prominent at 20° where it is well separated from feature II-1, and at 30° and 40° it constitutes the only component (Fig. 17). In the TOF spectra of smaller fragments of $C_5H_5^+$, e.g. m/e=36-39, the relative contribution of this channel is considerably larger. Power dependence studies of m/e=65 and 36 show clearly that a two-photon process is responsible for this channel. The most likely source is secondary photodissociation of phenoxy radical.

The corresponding second fragment of this dissociation process, carbon monoxide, should appear in the TOF spectrum at m/e=28 (CO^+), see Fig. 21. In contrast to the 193 nm case, the intensity of the m/e=28 spectrum is more similar to that of m/e=29 and 30, although still higher. The shape of the m/e=28 distribution suggests several components contributing to the signal. The fastest part could be identified with carbon monoxide from the secondary decomposition of phenoxy radicals and will be denoted as feature II-6, centered at flight times of about 110 μs.

A satisfactory fit to both the fast $C_6H_5^+$ (and fragments) and fast CO^+ components is obtained by assuming that the phenoxy radical which comprises feature II-1 is the source of the secondary products. In a two-photon process, the total energy available to the products is 147 kcal/mole. Out of that, an average of about 22 kcal/mole is channeled into translational energy of the primary products, and the remainder is distributed between translation of the secondary products (Fig. 19) and vibrational excitation of all fragments. The translational energy distribution obtained for the secondary products peaks at about 25 kcal/mole and extends beyond 60 kcal/mole. The secondary $P(E_T)$ was assumed to be independent of the translational and thus vibrational energy of the primary product.

6.3.2.4. Features II-7 and II-8. A very prominent feature in the spectra obtained in the 193 nm experiments, I-4, was identified with methanol and was observed at m/e=30, 29, 15, 14 and 13. It can be expected that a similar channel occurs in the case of 248 nm dissociation. An indication for this is found in feature II-7, centered at about 150 μs, which was identified as a component in the TOF spectra at m/e=13, 14, 15, 28, 29, and 30 (See Figs. 20 and 21). This feature could be fit assuming channel (6), the formation of methanol and benzyne, as its origin. The translational energy for this channel (see Fig. 22) was found to peak at about 7 kcal/mole with a maximum of about

28 kcal/mole. A very accurate determination of this distribution was not possible because of the overlap with other features, such as II-9 and II-11 which will be discussed later.

A feature due to benzyne (C_6H_4) stemming from the same reaction channel could be identified as well and is denoted II-8. It appears in the TOF spectra at m/e=76, 75, and 74 ($C_6H_4^+$, $C_6H_3^+$, and $C_6H_2^+$), see Fig. 23, as the major slower component.

6.3.2.5. Features II-9 and II-10. A relatively slow component was observed in the spectra of m/e=29 and 30 which could not be due to channel (6). This component comprises feature II-9 and has a peak at flight times of about 210 μs. It can be interpreted as resulting from channel (5), the simple bond rupture process leading to methoxy and phenyl radicals. The spectra can be fit with the assumption of this channel occurring with a translational energy distribution that peaks at zero energy and extends to about 6 kcal/mole (Fig. 22).

A feature stemming from slow phenyl radical produced in this reaction, II-10, is calculated to be centered at about 250 μs and can be expected to be a part of the TOF spectra measured at m/e=74, 75 and 76 (Fig. 23), although no prominent structures in these spectra are associated with it.

6.3.2.6. Features II-11 and II-12. An additional fast component was found in the TOF spectra of m/e=28 and 29 which can not be explained with reactions (5) or (6) given the maximum

available energies for these channels (see Table 1). An additional channel has to be postulated. Given the energetics and the masses at which the feature occurs, a possibility appears to be the formation of formaldehyde and benzene, channel (8):

$$C_6H_5\text{-}O\text{-}CH_3 \xrightarrow{h\nu} C_6H_6 + CH_2O \qquad (8)$$

A possible mechanism for this reaction is indicated in Scheme 3: a hydrogen atom migrates from the methyl group to the o-carbon atom on the ring and subsequently displaces the $O\text{-}CH_2$ group to form benzene. If both formaldehyde and benzene are being formed in the same reaction step, large amounts of energy, 106 kcal/mole in the case of the absorption of one 248 nm-photon, become available. Thus a large release of translational energy can be expected.

Feature II-11 (centered at flight times of about 120 μs) at m/e=28, 29 and 30 (see Fig. 21) and feature II-12 (centered at flight times of about 190 μs) at m/e=74, 75, and 76 (Fig. 23) can thus be tentatively assigned to reaction (8). For the fast part of these C_6-fragments, no possible other source has been found. It should be noted, though, that feature II-11 does not constitute a major component of the spectra at m/e=30 (Fig. 21), the parent mass of formaldehyde, and feature II-12 does not appear at m/e=77. No TOF spectra were obtained at m/e=78, the parent mass of benzene. However, in view of the large energy

release expected for this channel, it is possible that extensive fragmentation in the ionizer results from the high energy content of the products of this dissociation channel.

A possible alternative path responsible for features II-11 and II-12 would be a two-photon process forming either methoxy and phenyl radicals or methanol and benzyne. The higher excitation energy could lead to the large translational energy observed. No power dependence measurements were carried out to distinguish this possibility from reaction (8). The fragmentation pattern of feature II-11 is different from that of II-7 and II-9, however, that could be a result of the very high internal excitation expected in a two-photon process.

6.3.2.7. Feature II-13. In the m/e=15, 14 and 13 TOF spectra, an additional component appears to be present between features II-2 and II-4, i.e. centered at flight times of about 110 μs, whose origin could not be identified (see Fig. 20, feature not indicated). It appears that this feature is also due to a multi-photon process and it is possibly related to feature I-9 in the 193 nm experiment.

6.3.2.8. Other features. Very fast features were found in the spectra of the C_2, C_3, and C_4-fragments, which indicate additional secondary or tertiary processes. Fig. 24 shows spectra at m/e=24 (C_2^+), m/e=36 (C_3^+), and m/e=48 (C_4^+). For the latter two, the laser power dependence was studied. The

spectra on the left represent the higher laser power. It can be concluded that the fastest features at m/e=36 and 48 result from a multiphoton process, and the same is probably true for m/e=24. It appears that m/e=48 does not contain contributions from a feature faster than II-5, however, inspection of the spectra at 20° (Fig. 25) reveal that a feature at flight times between II-1 and II-5 has to be considered at the C_4 fragments, illustrated with the spectrum at m/e=50 ($C_4H_2^+$). The comparison of the m/e=36 (C_3^+) and m/e=39 ($C_3H_3^+$) spectrum shows the additional fast component at m/e=36, whereas the m/e=39 spectrum is very similar to that at m/e=65 ($C_5H_5^+$), Fig. 17.

A possible source for these products is the decomposition of cyclopentadienyl radical into C_2- and C_3-fragments. No detailed analysis of these features has been performed.

6.4. **Discussion**

The UV photodissociation experiments described in this chapter were originally undertaken in order to study the production of phenoxy radicals, thought to take place through the dissociation of ground state anisole following UV excitation and IC, and to observe the secondary decomposition of these radicals. It was found that the UV photochemistry of anisole is much more complicated than that, and the different channels occurring could be only partially identified. For large systems

like the present one, the spectroscopic information available is much less detailed than that for many smaller molecules. The role of the different excited states as well as the electronic ground state in the photochemistry of anisole is unknown. However, the dynamical information obtained in our photofragmentation translational spectroscopy experiment for the individual channels provides indications for the types of dissociation mechanisms involved.

It is of great interest to compare the results of UV photodissociation and IRMPD experiments. In cases where UV absorption is followed by fast IC and the subsequent decomposition takes place on the ground state surface, the same factors that govern the IRMPD dynamics also determine the dissociation at higher excitation energies. If there is a sizable barrier to dissociation and the release of this exit potential energy into translation predominates the contribution from the the statistically distributed excess energy to the translational energy, then the $P(E_T)$ distributions obtained with these two different excitation methods can be very similar.[28]

6.4.1. **Production of the phenoxy radical**

The most remarkable result of our experiment is the absence of direct evidence for the production of phenoxy and methyl radicals in a ground state dissociation channel. Two different

explanations can be given for this fact. Either IC indeed does not play a significant role in the photochemistry of anisole at the wavelengths studied, or alternatively, if IC takes place, the primary products are not easily observable. If a statistical distribution of the excitation energy is assumed, the ground state dissociation channel producing phenoxy and methyl radicals is expected to involve the release of comparatively small amounts of translational energy and thus result in fairly large vibrational excitation of the products, in particular the phenoxy radical. Then most of the phenoxy radicals would dissociate further into cyclopentadienyl radicals and carbon monoxide, since the threshold for this process is only about 44 kcal/mole.[8] On the other hand, it should be possible to detect the slow methyl radicals. However, identifying a feature in the m/e=15 data with this channel proved to be difficult due to the overlap with other features.

Information on the anisole ground state dissociation process was obtained in the IR multiphoton dissociation experiment recently performed in our laboratory.[6] Only one major dissociation channel was observed, reaction (1). The translational energy distribution measured for this process showed a peak at about 3 kcal/mole, indicating the existence of an exit channel barrier. This result was in agreement with studies by Lin and Lin[29] who found that in the reaction of methyl radicals with phenoxy radicals, the methyl primarily attaches to the o- and p-positions on the ring rather than to

the oxygen atom. If the UV-induced dissociation resulted in a similar translational energy distribution, most of the phenoxy radicals would indeed have sufficient internal energy to undergo spontaneous secondary dissociation.

Even if most of the primary phenoxy radicals do not reach the detector but decay instead, the corresponding second product, methyl radicals, should be observable as slow features in the spectra of m/e=15, 14, and 13. However, neither in the spectra obtained at 193 nm nor in those at 248 nm case did we find a clearly distinguishable feature that could be associated unambiguously with the ground state dissociation producing methyl radicals, although in both cases slow parts of the m/e=15 spectra could be due to this source.

While questions remain regarding the ground state phenoxy dissociation channel, a fast dissociation channel yielding the same products was clearly identified at both wavelengths. The phenoxy radicals are responsible for features I-1 and II-1, respectively, and the matching methyl radical features are I-2 and II-2. In both cases, the translational energy distributions show a minimum translational energy value and a peak at relatively large values, but do not extend to the maximum available energy. The peak in the 193 nm reaction is at about 60% of the available energy, in the 248 nm reaction about 50%. In view of the discussion of the ground state reaction, it is concluded that these processes represent the dissociation of an excited state of anisole. This is in agreement with the

conclusions of Kajii et al.[15] that at 193 nm, the dissociation process forming phenoxy radicals occurs via predissociation from an $n-\sigma^*$ state after the excitation to a $\pi-\pi^*$ state. Ground state dissociation was ruled out by these authors based on lifetime arguments. In their experiments with perfluoro-anisole, where the lifetime of the vibrationally excited ground state should be much longer than in the unsubstituted molecule, the dissociation was found to be equally fast.

In addition, another channel was observed at both wavelengths which possibly represents reaction (1), evidenced by features I-3 and II-3, respectively. However, this interpretation remains uncertain. It is also unclear whether the same or similar processes are responsible for features I-3 and II-3. The mass spectra of the two features are similar and suggest phenoxy radical as their origin, however, the formation of phenol or other channels can not be excluded as possible sources. One notable difference between the spectra obtained at 193 nm and the 248 nm is the absence of significant fragmentation of I-3 into m/e=93.

The most important difference is that II-3 apparently results from a two-photon process, while I-3 clearly does not. For both cases, the translational energy release is comparatively low, peaking at about 6 kcal/mole in the 193 nm experiment and at about 8 kcal/mole in the 248 nm experiment. Thus, ground state dissociation into phenoxy radicals can be excluded as the source, since the phenoxy radicals would have

too much vibrational excitation to be able to survive long enough to reach the detector. A possible alternative explanation would be the formation of electronically excited phenoxy or methyl radicals. The nature of the electronic state of a product can not be determined in our crossed molecular beam experiment, except for indications in the translational energy distributions and the mass spectra of the features.

As in the case of the ground state dissociation channel, confirmation of the assignment to reaction (1) should be found in the TOF spectra of methyl radical. In the 248 nm experiment, feature II-4 could be interpreted in this manner, and in the 193 nm experiment, feature I-4 was postulated but it is probably not responsible for a major part of the m/e=15 data.

6.4.2. **Dissociation of the phenoxy radical**

The secondary dissociation of the phenoxy radical is expected to result in the formation of carbon monoxide and cyclopentadienyl radical. CO should be observable as fast signal at m/e=28, while the cyclopentadienyl radical should be responsible for fast features in the spectra of m/e=65 ($C_5H_5^+$) and its fragments. Such fast features were indeed observed at both wavelengths. A significant difference between the two experiments was that at 193 nm, the reaction responsible was identified as a single-photon process, whereas at 248 nm most

likely a two-photon process was involved. This indicates spontaneous secondary decomposition of highly vibrationally excited primary product in the first case and secondary absorption following the primary dissociation process in the latter. This view is supported by the earlier result that the phenoxy radicals exhibit an absorption maximum around 240 nm.[13,15]

In the 193 nm experiment, difficulties were encountered in fitting the data assuming that features I-7 (at m/e=28) and I-8 (at m/e=65 and fragments) originate from the same process. It had to be assumed that the primary reaction step was the dissociation according to reaction (1) with an extremely low translational energy release (maximum energy about 5 kcal/mole). Even then, the m/e=28 signal appears to have an onset faster than the calculation. Alternatively, part of the peak at m/e=28 could be due to other sources, such as reaction (7).

In the 248 experiment, several ways of fitting the data were found: In one, it was assumed that the slow feature (II-3), under the assumption that it is due to phenoxy radicals, absorbed another photon and dissociated, in another, the primary $P(E_T)$ was assumed to be identical to that in the IR experiment and the secondary $P(E_T)$ was varied. The best fit was found, however, under the assumption that the fast phenoxy (feature II-1) absorbed another photon and dissociated. This interpretation would indicate that no ground state dissociation followed by secondary decomposition of the phenoxy radicals takes place at

all. However, it is possible that some signal due to such a channel is hidden under the features discussed above.

In summary, at both wavelengths fast signal was observed at m/e=28 (CO^+) and m/e=65 ($C_5H_5^+$), indicating the occurrence of secondary dissociation of phenoxy radicals, however, the primary process or processes producing these phenoxy radicals could not be identified unambiguously.

6.4.3. **Production of methanol, methane, methoxy, and formaldehyde**

A major channel which occurs at both wavelengths was assigned to reaction (6), the formation of methanol and benzyne as a four-center elimination. This channel is represented by features I-5 and II-7, respectively. Both of these features are found at m/e=13, 14, 15, 29, 30, and probably at m/e=31. II-7 clearly constitutes a component of the m/e=28 spectrum, but in the case of I-5 this can only be assumed because of the overlap with feature I-7.

The translational energy distributions for this channel at the two wavelengths are qualitatively similar, with peaks at about 20% and 25%, respectively, of the total available energy in the 193 nm and 248 nm case. The maximum energy in the 193 nm case was found to be the total available energy, and the same was assumed for 248 nm. However, the translational energy

distribution for the methanol and the methoxy channels at 248 nm can not be determined separately, a range of combinations is possible. Consequently, the relative importance of the methanol and the methoxy channels can not be evaluated.

The channel forming methanol is most likely due to a single-photon process and was assigned to reaction (6) on grounds of the energetics and the fact that a peak in the translational energy distribution away from zero was observed which indicates an exit channel barrier. Such a barrier is definitely expected to occur for a four-center elimination process like the one required in this particular case. Most likely this channel originates from dissociation of an electronically excited state of anisole, since in the ground state dissociation the lowest energy channel, reaction (1), is expected to dominate and the formation of methanol was not observed in the IR multiphoton dissociation.[6]

If the methanol production on the excited state surface is preceded by H-migration from the o-position on the aromatic ring to the O atom, then another decay process to be considered: the formation of methane and C_6H_4O, reaction (9):

$$C_6H_5\text{-}O\text{-}\dot{C}H_3 \xrightarrow{h\nu} C_6H_4O + CH_4 \qquad (9)$$

The rearrangements presumed to occur in this process and a conceivable structure of C_6H_4O are shown in Scheme 4. The data

at both wavelengths do not provide any indication for an additional channel of this kind, however, it is possible that it takes place to a small degree and is not responsible for any of the major features, but a minor part of features I-3, II-3, etc. The structure of the C_6H_4O species remains hypothetical, and the energetics for reaction (9) can not be estimated.

The formation of methoxy and phenyl radicals, reaction (5), was postulated in the 248 nm experiment based on feature II-9 in the TOF spectra at m/e=29, 30 and 31 and it could be a component in the m/e=28 spectrum, dependent on the $P(E_T)$ assumed for the methanol channel. The $P(E_T)$ for this reaction in the 248 nm case was found to peak at zero, indicating a simple bond rupture process occurring on the ground state surface.

In the 193 nm reaction, a methoxy channel was postulated to explain feature I-13 at m/e=31, 30 and 29. The translational energy for this channel was found to peak at 2.5 kcal/mole, indicating a barrier to the C-C bond rupture, in contrast to the result above. This channel is a very minor one in the 193 nm case and its interpretation is quite uncertain.

A channel producing formaldehyde and benzene, reaction (8), was postulated for the 248 nm reaction to explain a very fast feature (II-11) at m/e=28 and 29. Signal as fast as that could not be due to the formation of methanol nor methoxy in a one-photon process for energetic reasons. A two-photon process, however, has to be considered as an alternative explanation.

The counterpart fragments in these channels, benzyne,

phenyl radicals, and benzene, contribute to the spectra at m/e=76, 75 and 74 ($C_6H_4^+$, $C_6H_3^+$, and $C_6H_2^+$). No signal was observed at m/e=77 and no data were taken at m/e=78 at both wavelengths. The phenoxy radical was found to fragment into m/e=77 in the IR experiment,[6] and it is thus possible that a small part of the signal at these masses is due to phenoxy radical fragmentation.

6.4.4. **Unobserved channels**

It should be mentioned that several dissociation channels which could be expected to occur were not observed in the present experiments. In particular, elimination of atomic or molecular hydrogen from either the aromatic ring or the methyl group could take place. Primary and secondary H- and H_2-elimination was indeed observed in the UV-photodissociation of benzene performed in our laboratory.[1] The energetic relations for these processes are included in Table 1.

If these reactions occur in the present case as well, it is very likely that their products can not be detected. Atomic or molecular hydrogen are impossible to detect in the present detector arrangement. The corresponding heavy fragments, on the other hand, could escape detection as a result of the kinematic relations, in particular in the case of a translational energy peaking at zero as was observed for the atomic hydrogen

elimination from benzene. Because of momentum conservation, the heavy fragments would travel very slowly and would therefore not be scattered significantly out of the beam. We made several attempts to overcome this problem by using slower molecular beams formed by seeding anisole in molecular nitrogen and by measuring spectra at very small laboratory angles. No indication for such a channel was found, but none of these reactions can be excluded with certainty. They could in fact be responsible for various secondary products and explain some of the unidentified features.

6.4.5. **Other channels**

Evidence for several additional channels was found, in particular subsequent dissociation processes of the primary and secondary products. These reactions are probably due to multi-photon processes, and a detailed analysis proved to be difficult, particularly in view of the remaining uncertainties regarding the nature of the primary processes. For instance, the only feature in the 193 nm experiment which was clearly identified as resulting from a multiphoton-process, I-12, and the possible equivalent in the 248 nm reaction, II-13, are likely due to a secondary dissociation process whose origin remains unclear.

At both wavelengths, very fast features were found in the

spectra of various C_2-, C_3- and C_4-fragments, indicating further decomposition of the cyclopentadienyl radical or possibly other larger products. Power dependence studies at 248 nm suggest that multi-photon processes are responsible for these channels.

6.5. Summary

In the UV photodissociation of anisole in a molecular beam at 193 and 248 nm, a variety of different dissociation channels was observed. In a direct dissociation process, phenoxy and methyl radicals are being produced. Only indirect evidence was found for the same reaction occurring in highly vibrationally excited electronic ground state molecules formed by IC after absorption.

A major channel was observed in both cases producing slow product at the phenoxy radical masses. However, this channel can not be due to the ground state dissociation process since the resulting phenoxy radicals would have too much vibrational excitation to be able to reach the detector. Possible sources for this product are dissociation of anisole yielding electronically excited fragments or alternative processes, such as the formation of phenol and $^1CH_2$, reaction (4).

Signal was observed at both wavelengths which indicates secondary dissociation of phenoxy radicals into carbon monoxide and cyclopentadienyl radicals. The primary processes

responsible for these phenoxy radicals, however, could not be identified unambiguously.

Additional channels are the production of methanol plus benzyne, methoxy plus phenyl radicals, and formaldehyde plus benzene. The methanol channel can be postulated with considerable certainty in both the 193 and the 248 nm case and probably represents dissociation from an electronically excited state. Methoxy formation appears to be of importance at 248 nm and possibly contributes at 193 nm as well. The formation of formaldehyde was postulated to explain certain fast features in the 248 nm data.

Multiphoton processes are probably responsible for further dissociation of the primary and secondary products into smaller C_2-C_4 fragments.

In summary, a large variety of channels of channels could be observed in the UV-photodissociation of anisole. Many of them could only be assigned tentatively, and additional work using as many different techniques as possible is needed to unravel the complex photochemistry of this molecule. It appears that anisole UV-photochemistry involves to a large degree the dissociation from electronically excited states and that IC does not play a major role.

6.6. References

1. A. Yokoyama, X. Zhao, E. J. Hintsa, R. E. Continetti, and Y. T. Lee, to be published.
2. M. S. Helfand, Ph. D. Thesis, University of California, Berkeley, 1989.
3. K. Brezinsky, Prog. Energy Combust. Sci. 12, 1 (1986).
4. D. F. McMillen and D. M. Golden, Ann. Rev. Phys. Chem. 33, 493 (1982).
5. A. G. Harrison, L. R. Honnen, H. J. Dauben, and F. P. Lossing, J. Am. Chem. Soc. 82, 5593 (1960); J. C. Mackie, K. R. Doolan, and P. F. Nelson, J. Phys. Chem. 93, 664 (1989); M. M. Suryan, S. A. Kafafi, and S. E. Stein, J. Am. Chem. Soc. 111, 1423 (1989).
6. Chapter 5; A. M. Schmoltner, D. S. Anex, and Y. T. Lee, manuscript in preparation.
7. A. J. Colussi, F. Zabel, and S. W. Benson, Int. J. Chem. Kinet. 9, 161 (1977).
8. C.-Y. Lin and M. C. Lin, Int. J. Chem. Kinet. 17, 1025 (1985); C.-Y. Lin and M. C. Lin, J. Phys. Chem. 90, 425 (1986).
9. H. Konschin and H. Tylli, Chem. Phys. Lett. 108, 191 (1984).
10. H. Konschin and M. Lindblad, J. Mol. Structure 104, 37 (1983).
11. H. Konschin, H. Tylli and C. Grundfelt-Forsius, J. Mol.

Structure 77, 51 (1981).

12. G. Porter and F. J. Wright, Trans. Faraday Soc. 51, 1469 (1955); E. J. Land, G. Porter and E. Strachan, Trans. Faraday Soc. 57, 1885 (1961); B. Ward, Spectrochim. Acta 24A, 813 (1968).

13. J. L. Roebber, J. Chem. Phys. 37, 1974 (1962).

14. D. Pullin and L. Andrews, J. Mol. Structure 95, 181 (1982).

15. Y. Kajii, K. Obi, N. Nakashima, and K. Yoshihara, J. Chem. Phys. 87, 5059 (1987).

16. H. M. Rosenstock, K. Draxl, B. W. Steiner, and J. T. Herron, J. Phys. Chem. Ref. Data 6, Suppl. 1, 774 (1977).

17. M. W. Chase, Jr., C. A. Davies, J. R. Downey, Jr., D. J. Frurip, R. A. McDonald, and A. N. Syverud, J. Phys. Chem. Ref. Data 14 (1985), Supplement No. 1: JANAF Thermochemical Tables, Third Edition.

18. S. K. Pollack, and W. J. Hehre, Tetrahedron. Lett. 21, 2483 (1980).

19. A. R. W. McKellar, P. R. Bunker, T. J. Sears, K. M. Evenson, R. J. Saykally, and S. R. Langhoff, J. Chem. Phys. 79, 5251 (1983).

20. S. W. Benson, Thermochemical Kinetics (Wiley-Interscience, New York, 1977).

21. G. Herzberg, Electronic Spectra and Electronic Structure of Polyatomic Molecules (Van Nostrand, New York, 1966), p. 347.

22. R. McDiarmid, Theoret. chim. Acta (Berlin) 20, 282 (1971).

23. M. C. Lin, in Potential Energy Surfaces, K. P. Lawley, editor (Wiley, New York, 1980).

24. A. H. Lauffer, Rev. Chem. Int. 4, 225 (1981).

25. Atlas of Mass Spectral Data, E. Stenhagen, S. Abrahamsson, and F. W. McLafferty, editors, Vol. 1 (Wiley, New York, 1969).

26. H.-G. Rubahn, J. P. Toennies, and M. Wilde, Chem. Phys. Lett. 120, 11 (1985), and references therein.

27. R. Cypres and B. Bettens, Tetrahedron 30, 1253 (1974).

28. X. Zhao, R. E. Continetti, A. Yokoyama, E. J. Hintsa, and Y. T. Lee, J. Chem. Phys., in press; D. S. Anex and Y. T. Lee, work on the photodissociation of tetralin, in progress.

29. C.-Y. Lin and M. C. Lin, Aust. J. Chem. 39, 723 (1986).

6.7. Tables

Table 1. Energetics for various dissociation channels at 193 and 248 nm.

channel	ΔH_f	available E		source
		193 nm	248 nm	
CH_3 + phenoxy	63	85	52	a,b,c
CH_3 + C_5H_5 + CO	84	65	32	a,b,c
CH_3OH + benzyne	87	61	28	a,d
CH_3O + phenyl	100	48	15	a,b
$O(^1D)$ + toluene	134	14	-	a,c
$^1CH_2$ + phenol	96	52	20	a,c,e
H• + ø-O-CH_2•	93	55	22	a,f
H_2 + methoxy-benzyne	98	50	17	a,g
H• + methoxy-phenyl	111	37	4	a,h
CO + methyl-cyclopentadiene	16	132	99	a,c,i
CH_2O + C_6H_6	9	139	106	a,c

(a) Ref. 16
(b) Ref. 4
(c) Ref. 17
(d) Ref. 18
(e) Ref. 19
(f) assumed to be the same as -O- → •-O- + H (b)
(g) assumed to be the same as ø → H_2 + benzyne (a,d)
(h) assumed to be the same as ø → H + ø• (b)
(i) estimated from Ref. 20

Table 2. Summary of features

1. 193 nm

I-1	fast phenoxy from excited state dissociation
I-2	fast methyl (counterpart of I-1)
I-3	slow feature at m/e= 92,91,90, 65, etc. (presumed to be an excited state or isomer of the phenoxy radical)
I-4	slow 15 (counterpart of I-3, assuming it is phenoxy)
I-5	methanol
I-6	benzyne (counterpart of I-5)
I-7	m/e=28 feature, probably secondary CO
I-8	cyclopentadienyl radical from secondary processes
I-9	CO (counterpart of I-10)
I-10	methylcyclopentadiene
I-11	very slow m/e=15 - methyl from ground state dissociation
I-12	two-photon component in m/e=15
I-13	methoxy radical
I-14	phenyl radical (counterpart of I-13)

2. 248 nm

II-1	fast phenoxy from excited state dissociation
II-2	fast methyl (counterpart of II-1)
II-3	slow phenoxy radical
II-4	slow methyl radical (counterpart of II-2)
II-5	cyclopentadienyl radical from secondary processes
II-6	CO (counterpart of II-5)
II-7	methanol
II-8	benzyne (counterpart of II-7)
II-9	methoxy radical
II-10	phenyl radical (counterpart of II-9)
II-11	formaldehyde
II-12	benzene (counterpart of II-11)
II-13	intermediate m/e=15

6.8. Schemes

Scheme 1.

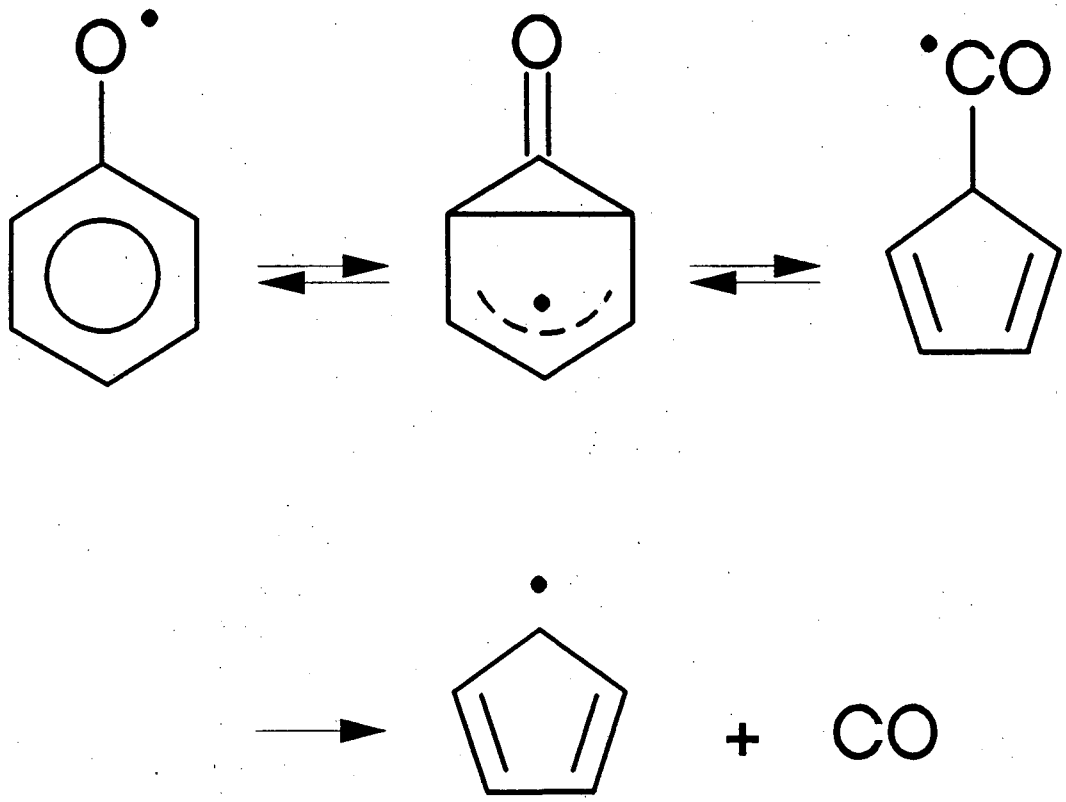

Scheme 2.

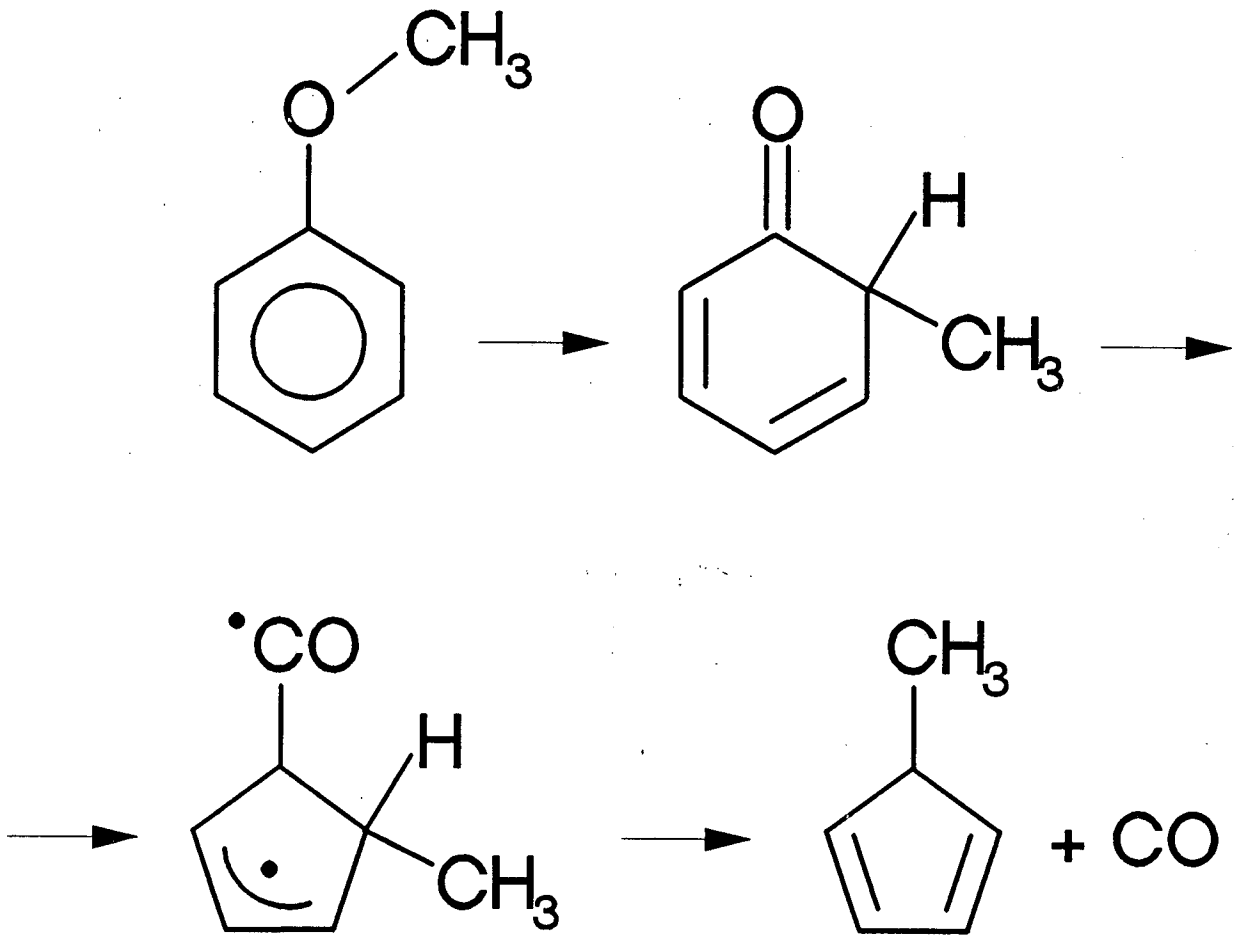

Scheme 3.

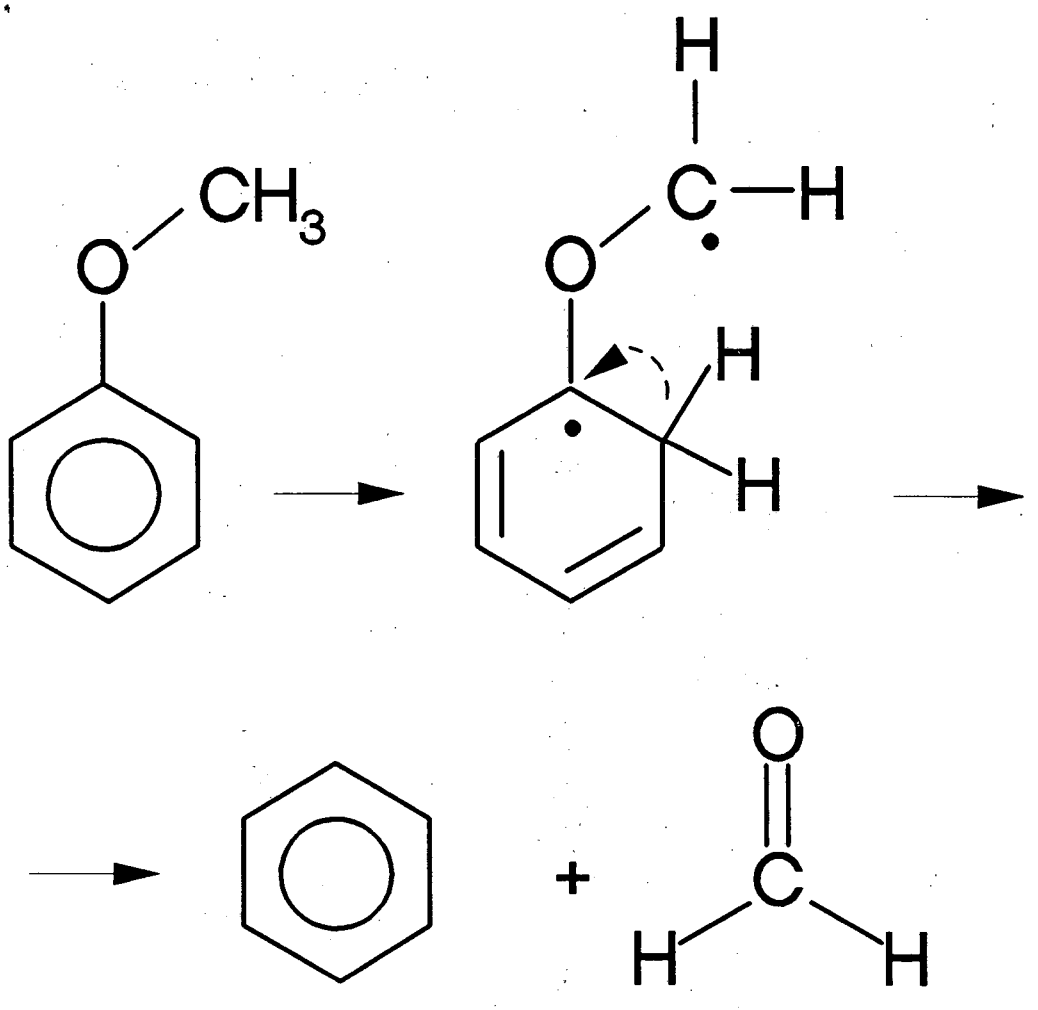

Scheme 4 .

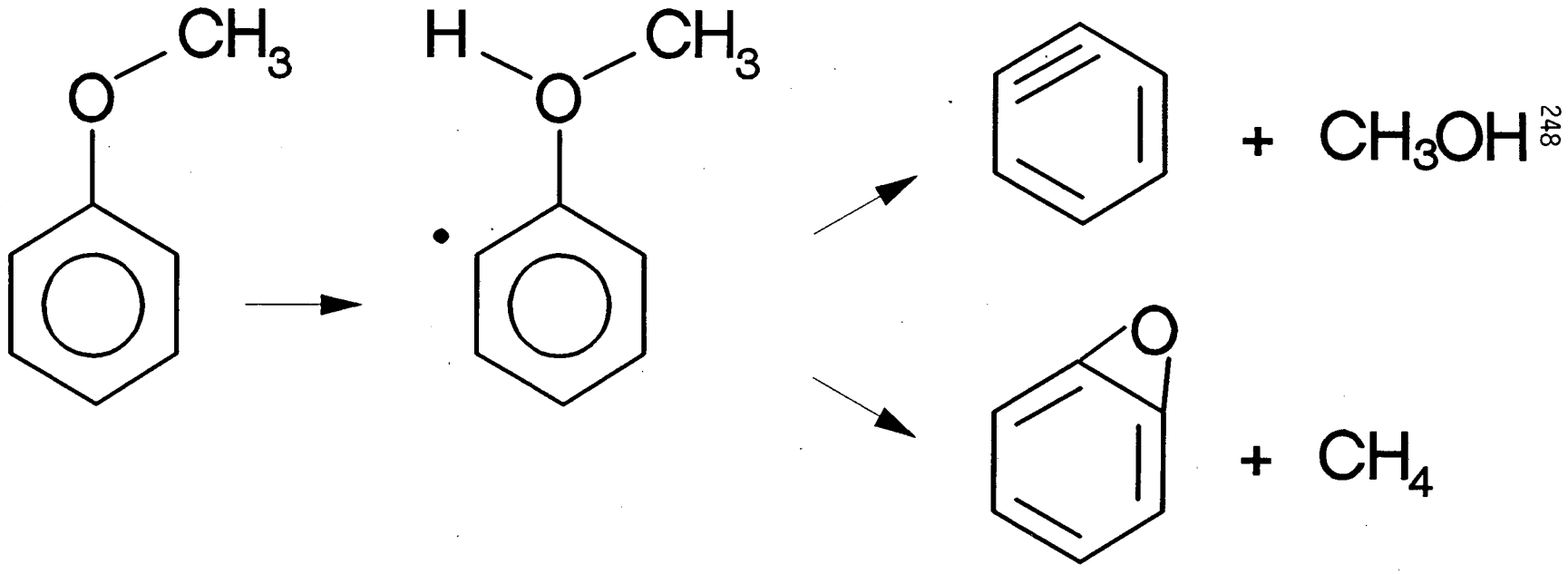

6.9. Figures

Figure captions

For all TOF spectra, the scattered points represent the data. The calculated features are shown in broken lines and identified where necessary, and the solid lines correspond to the sum of all features.

Fig. 1 TOF data at m/e=93 at three different laboratory angles obtained at 193 nm.

Fig. 2 TOF data at m/e=90, 91, and 92 at 10° obtained at 193 nm. The fits were obtained using the translational energy distributions shown in Fig. 3.

Fig. 3 Upper panel: translational energy distribution for the hypothetical ground state dissociation of anisole to phenoxy and methyl radicals; lower panel: (a) the channel responsible for features I-3 and I-4, presumed to be the formation of phenoxy and methyl radicals, (b) the secondary dissociation of the phenoxy radical from the ground state channel to form cyclopentadienyl (feature I-10) and carbon monoxide (feature I-9), (c) the excited state dissociation channel into phenoxy (feature I-1) and methyl radicals (feature I-2) at 193 nm.

Fig. 4 TOF data at m/e=15, 14, and 13 at 10° obtained at 193 nm.

Fig. 5 Schematic energy diagram illustrating the primary dissociation of anisole to phenoxy and methyl radicals and the secondary dissociation of vibrationally excited phenoxy radicals to cyclopentadienyl radicals and carbon monoxide.

Fig. 6 TOF data at m/e=65 at four different laboratory angles obtained at 193 nm. The fits were obtained using the translational energy distributions shown in Fig. 3. In these fits the relative contributions of each feature was optimized for a best fit at each angle separately.

Fig. 7 TOF data at m/e=65 at four different laboratory angles obtained at 193 nm. The fits were obtained using the translational energy distributions shown in Fig. 8. In these fits the relative contributions of each channel was assumed to be the same at all four angles.

Fig. 8 Translational energy distributions for (a) the hypothetical ground state dissociation of anisole to phenoxy and methyl radicals, (b) the channel responsible for features I-3 and I-4, presumed to be the formation of phenoxy and methyl radicals, (c) translational energy distribution for hypothetical reaction (7), (d) the secondary dissociation of the phenoxy radical from (a) to form cyclopentadienyl (feature I-10) and carbon monoxide (feature I-9), (e) the excited state dissociation channel into phenoxy

(feature I-1) and methyl radicals (feature I-2) at 193 nm.

Fig. 9 Mass spectra of feature I-3 (upper left panel), phenoxy radical formed in IR multiphoton dissociation[6] (lower left panel), phenol[25] (upper right panel), and toluene[25] (lower right panel).

Fig. 10 TOF data at m/e=15 at four different laboratory angles obtained at 193 nm.

Fig. 11 TOF data at m/e=29, 30, and 31 at 10° obtained at 193 nm.

Fig. 12 Translational energy distributions for (a) reaction (5), formation of methoxy and phenyl radicals, and (b) reaction (6), formation of methanol and benzyne at 193 nm.

Fig. 13 TOF data at m/e=75, 76, and 77 at 10° obtained at 193 nm.

Fig. 14 TOF spectrum at m/e=28 at 10° obtained at 193 nm, (a) fit assuming the processes and translational energy distributions shown in Fig. 3, (b) fit assuming the processes and translational energy distributions shown in Fig. 8.

Fig. 15 TOF data at m/e=60, 48, and 36 at 10° obtained at 193 nm.

Fig. 16 TOF data at m/e=93 at two different laboratory angles and m/e=92 and 91 at 10° obtained at 248 nm.

Fig. 17 TOF data at m/e=65 at four different laboratory angles

obtained at 248 nm.

Fig. 18 TOF data at m/e=65 at 10° at three different laser power levels (top: 0.9 W, center: 0.29 W, bottom: 0.: 0.035 W) obtained at 248 nm.

Fig. 19 Translational energy distributions for (a) the channel responsible for features II-3 and II-4, presumed to be the formation of phenoxy and methyl radicals, (b) the excited state dissociation channel forming phenoxy and methyl radicals, (c) secondary dissociation of the faster phenoxy radicals into cyclopentadiene and carbon monoxide at 248 nm.

Fig. 20 TOF data at m/e=15, 14, and 13 at 10° obtained at 248 nm; upper left panel: 3.55 W, upper right panel: 0.93 W.

Fig. 21 TOF data at m/e=28, 29, 30 and 31 at 10° obtained at 248 nm.

Fig. 22 Translational energy distributions for (a) reaction (5), formation of methoxy and phenyl radicals, (b) reaction (6), formation of methanol and benzyne, (c) reaction (8), formation of formaldehyde and benzene at 248 nm.

Fig. 23 TOF data at m/e=74, 75, and 76 at 10° obtained at 248 nm.

Fig. 24 TOF data at m/e=24, 36, and 48 at 10° obtained at 248 nm; for m/e=36 and 48 the spectrum shown on the left was taken at higher laser power than the spectrum on

the right. (M/e=36: 4.1 W and .93 W respectively; m/e=48: 3.6 W and 1.1 W respectively).

Fig. 25 TOF data at m/e=36, 39, and 50 at 20° obtained at 248 nm.

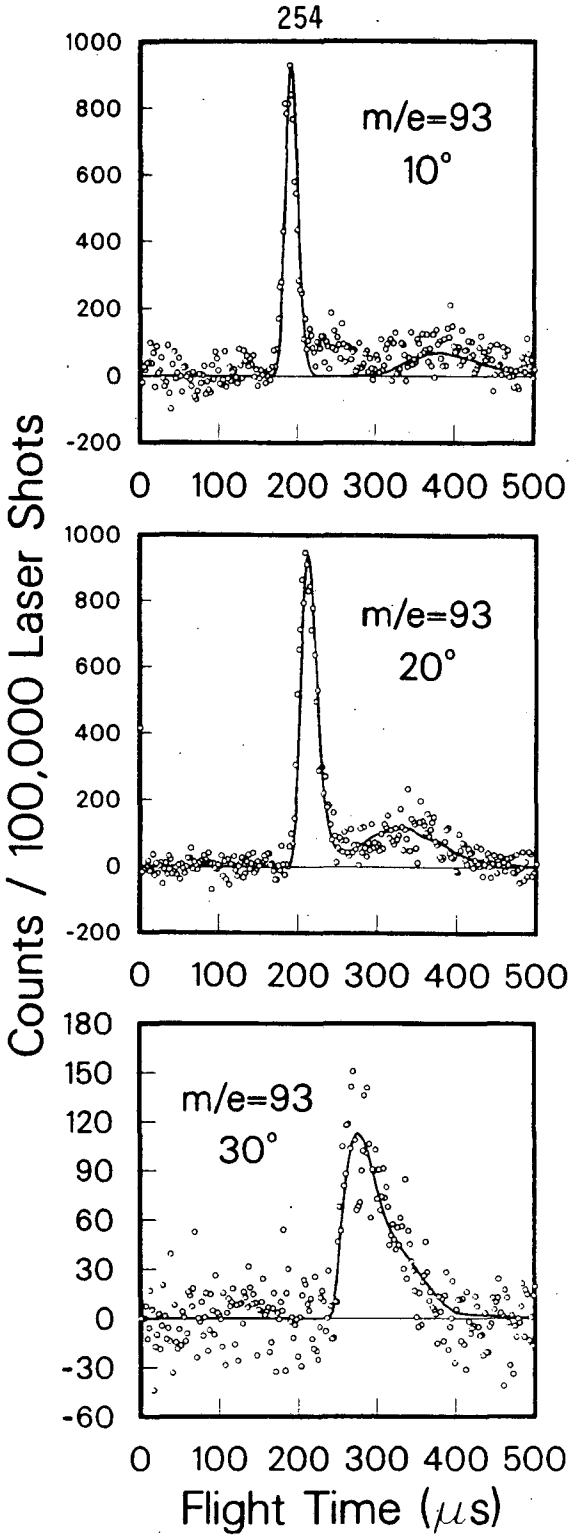

XBL 8910-3686

Fig. 1

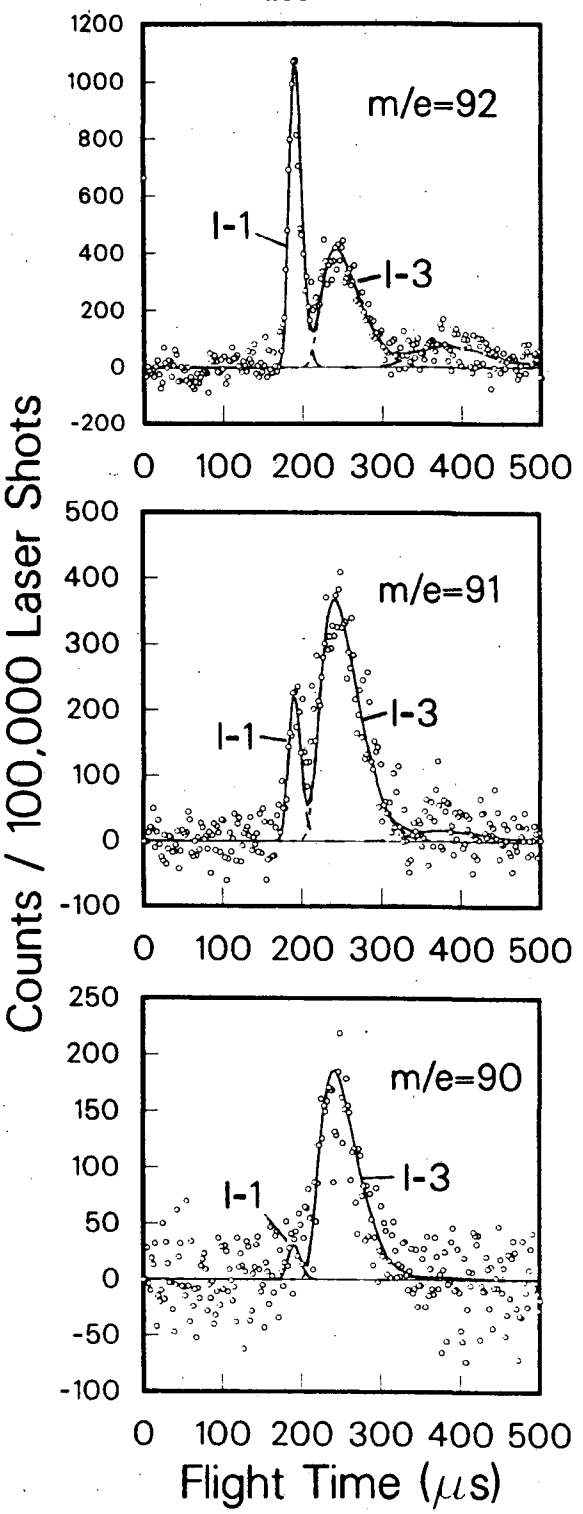
m/e=92
I-1
I-3
m/e=91
I-1
I-3
m/e=90
I-1
I-3
Counts / 100,000 Laser Shots
Flight Time (μs)
XBL 8910-3687

Fig. 2

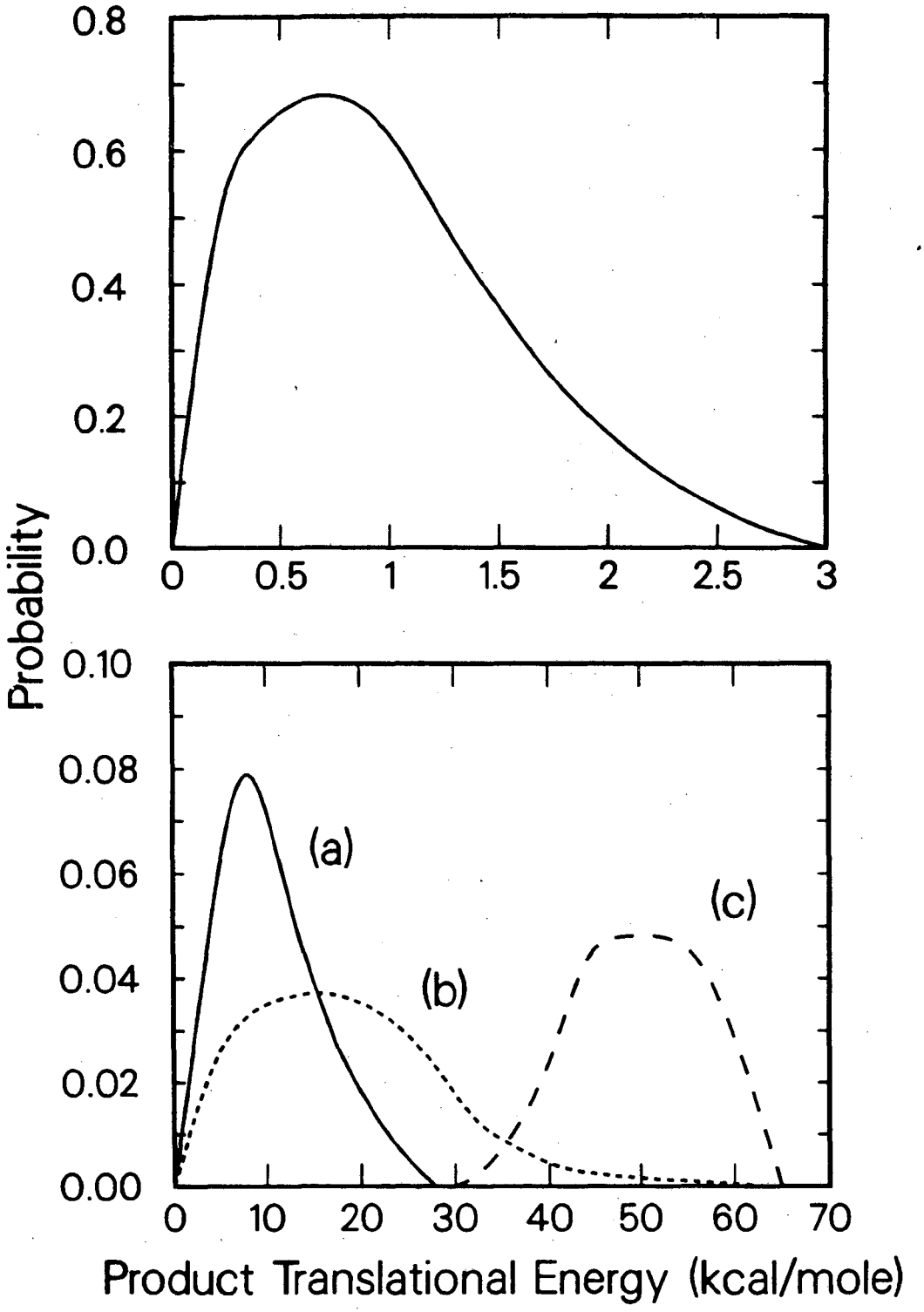

XBL 8910-3688

Fig. 3

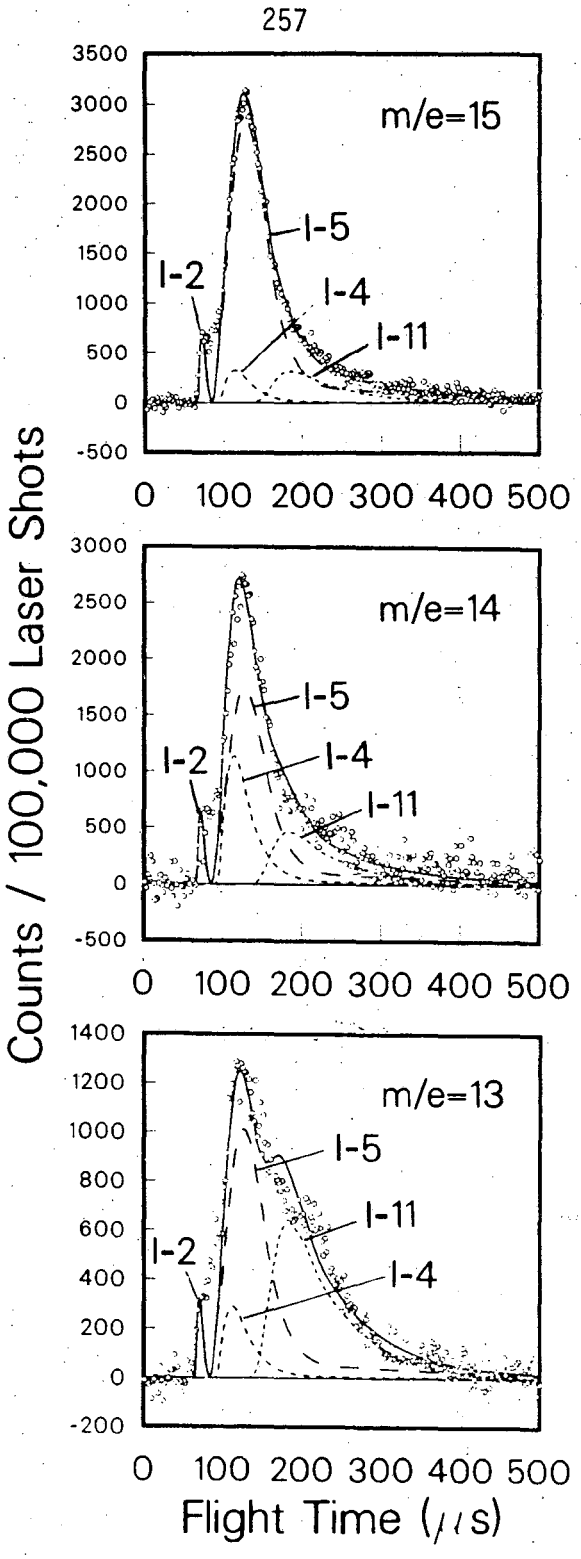
m/e=15
I-5
I-2
I-4
I-11
m/e=14
I-5
I-2
I-4
I-11
m/e=13
I-5
I-11
I-2
I-4
Counts / 100,000 Laser Shots
Flight Time (μs)
XBL 8910-3689

Fig. 4

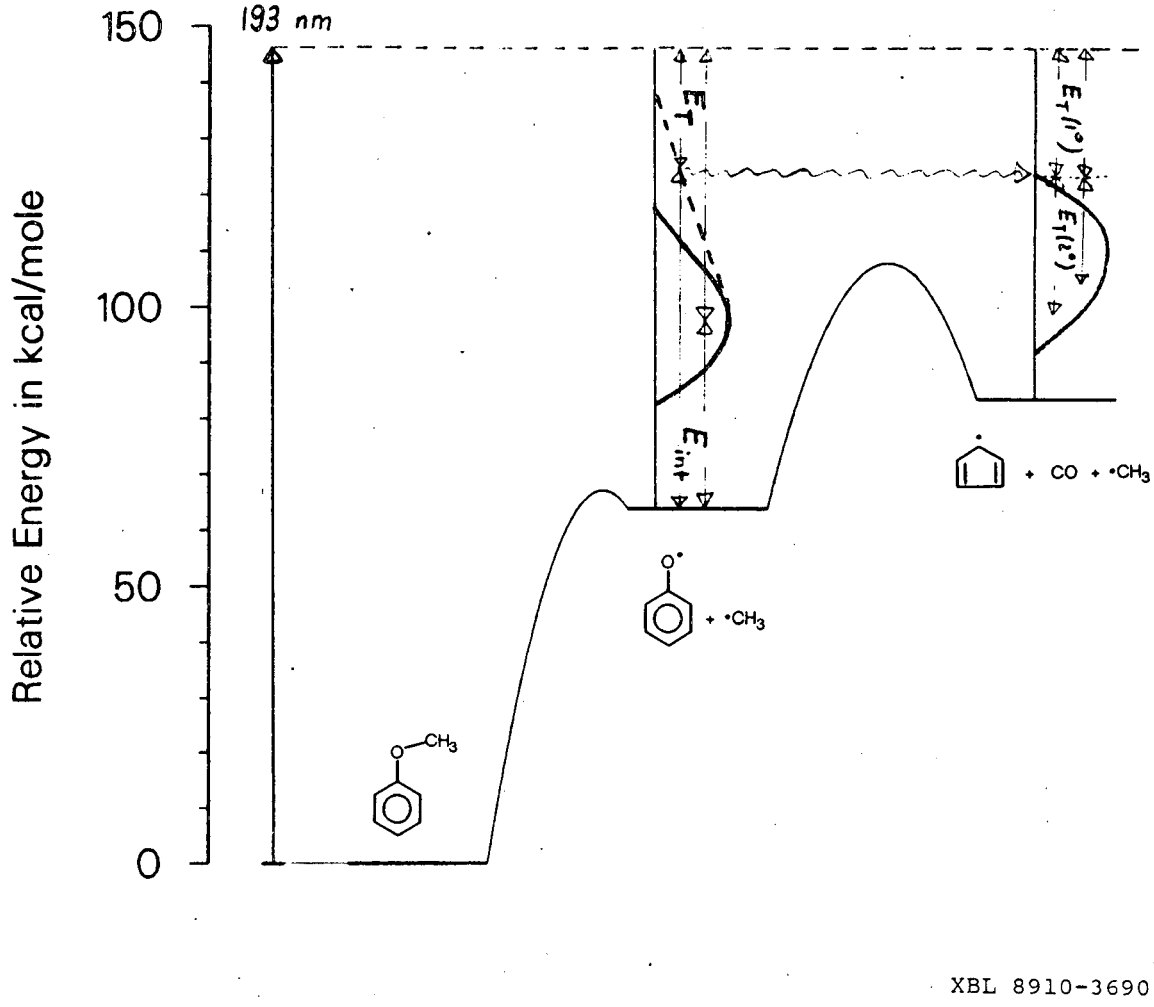

XBL 8910-3690

Fig. 5

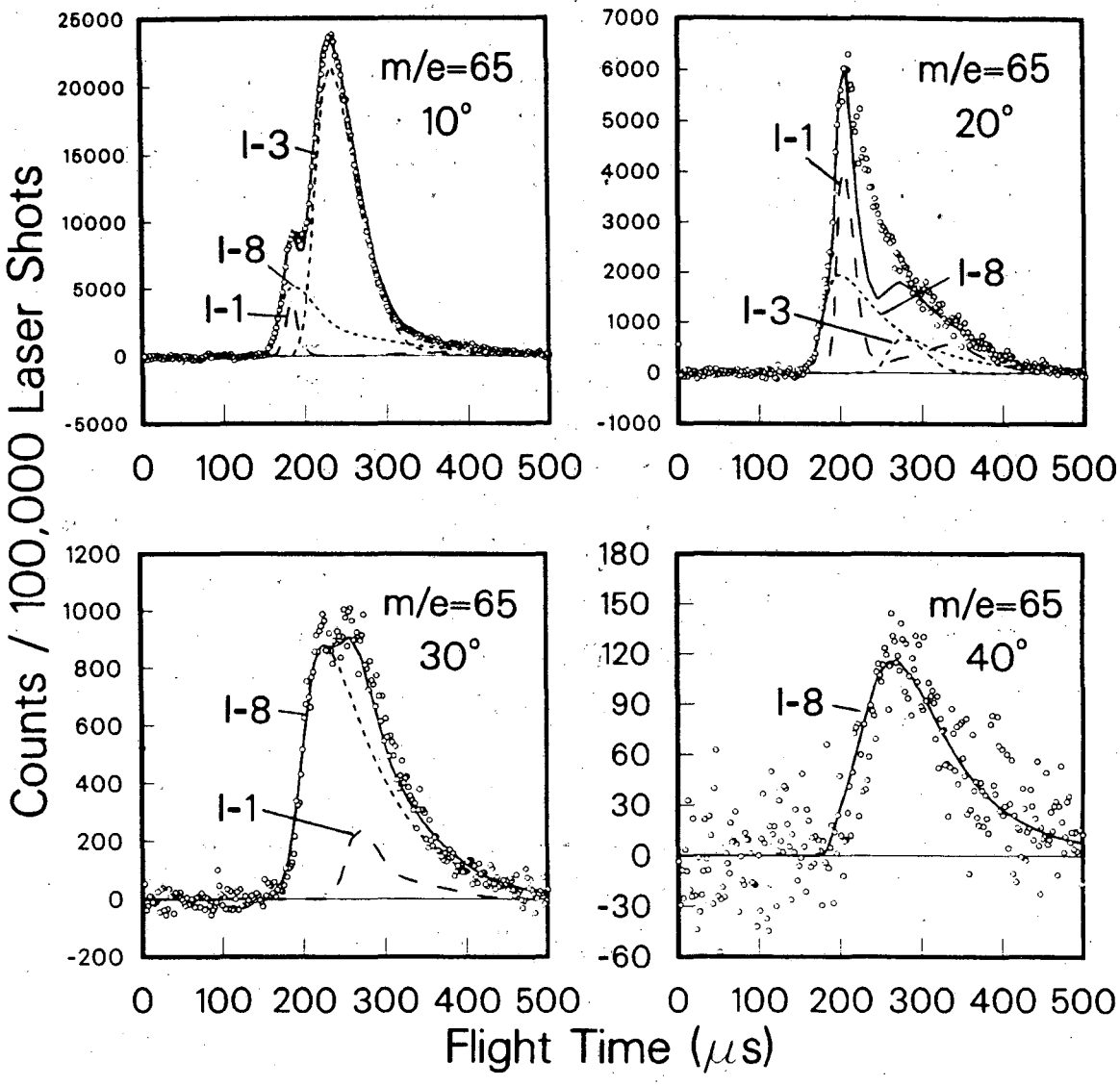

XBL 8910-3692

Fig. 6

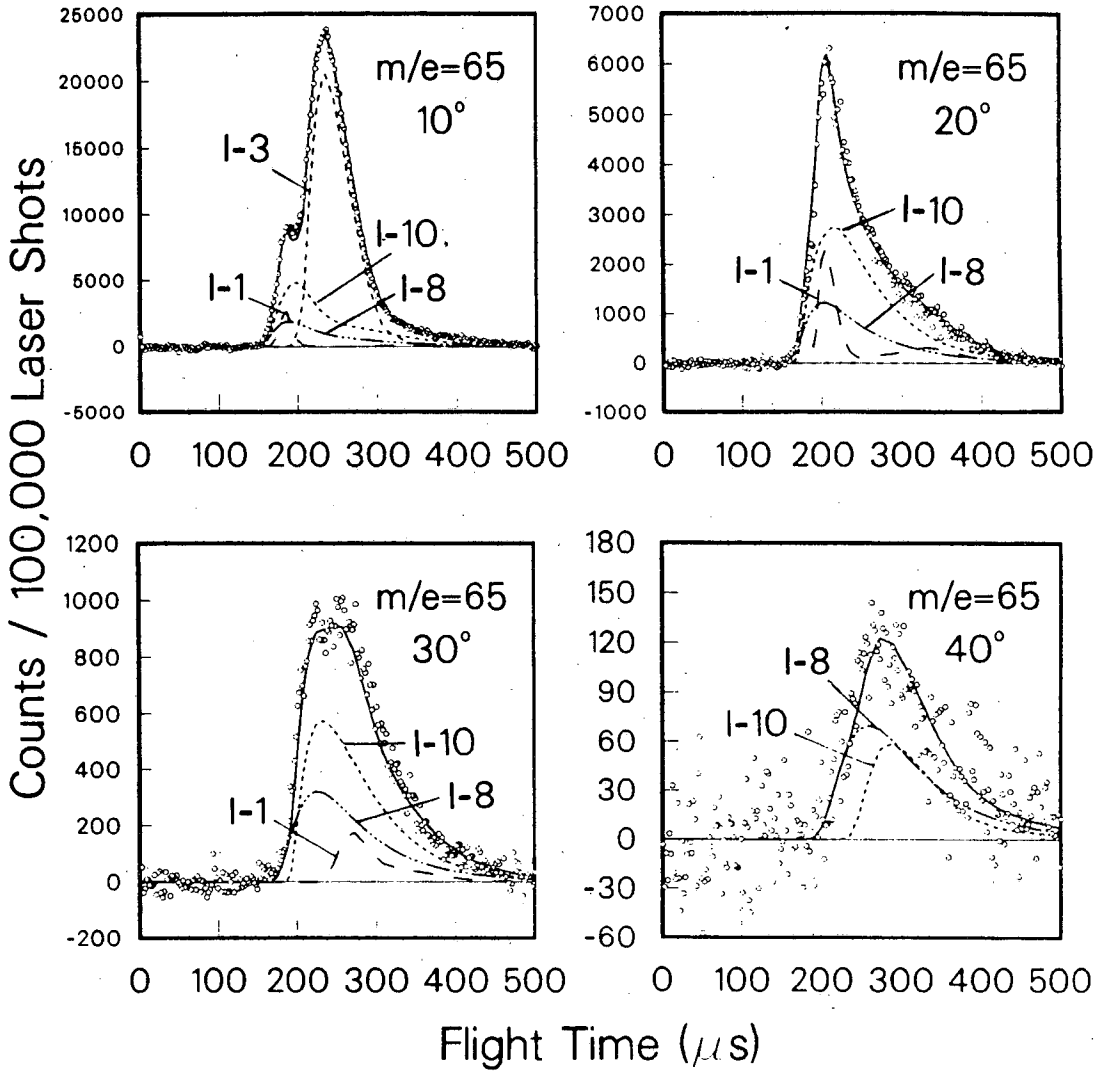

XBL 8910-3691

Fig. 7

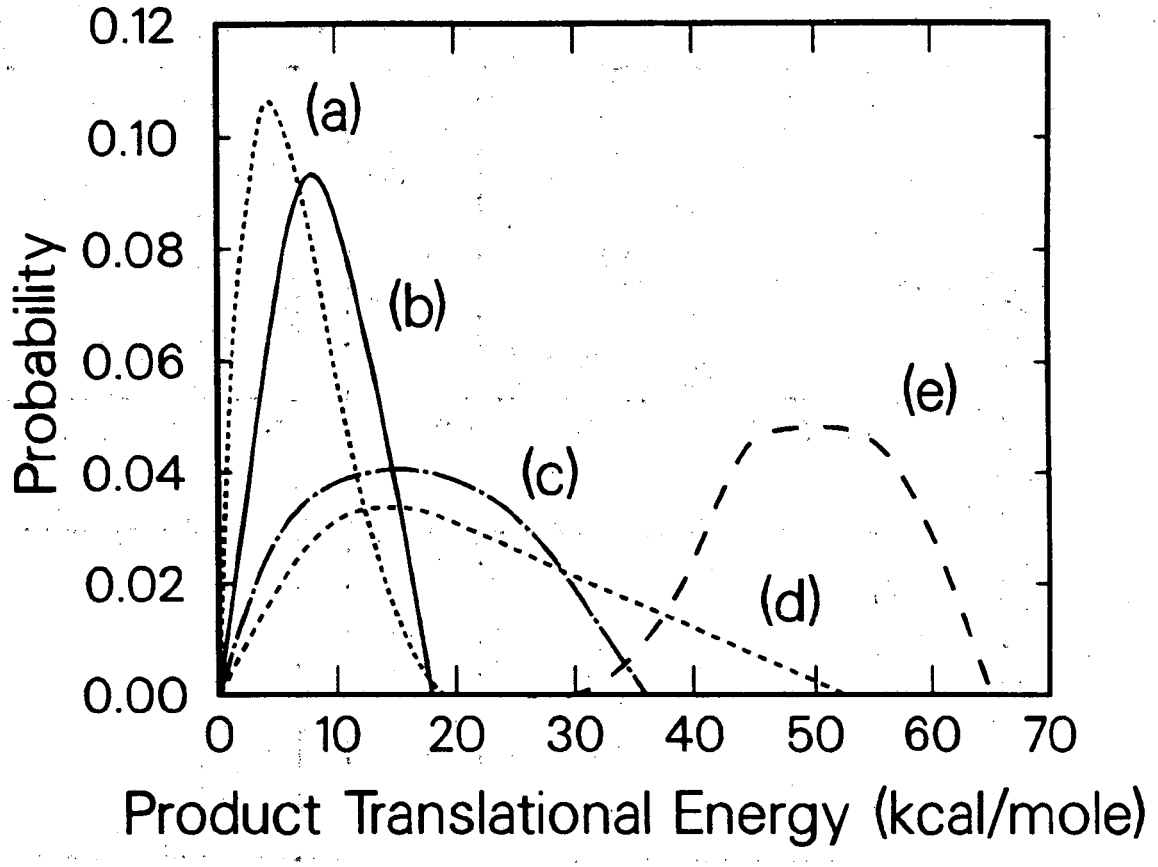

XBL 8910-3693

Fig. 8

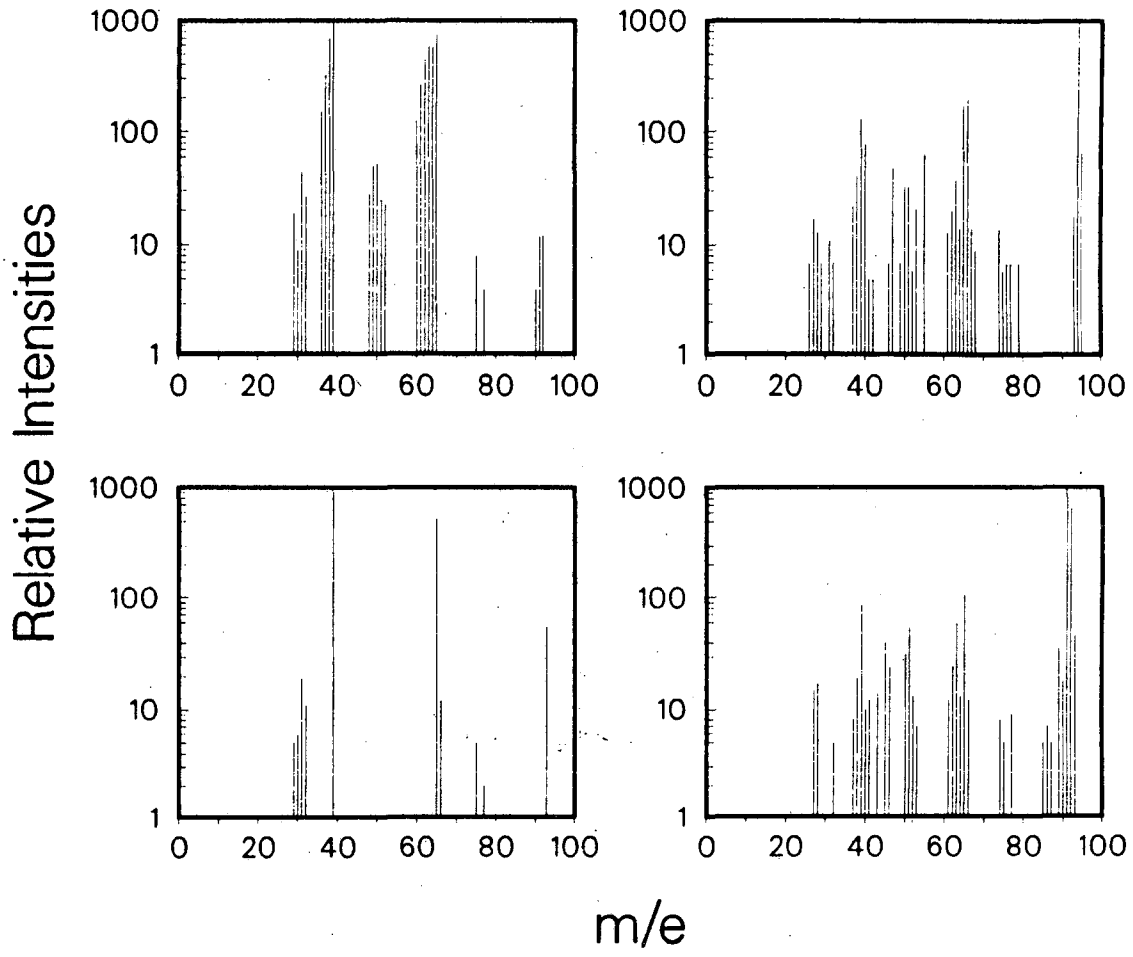

XBL 8910-3694

Fig. 9

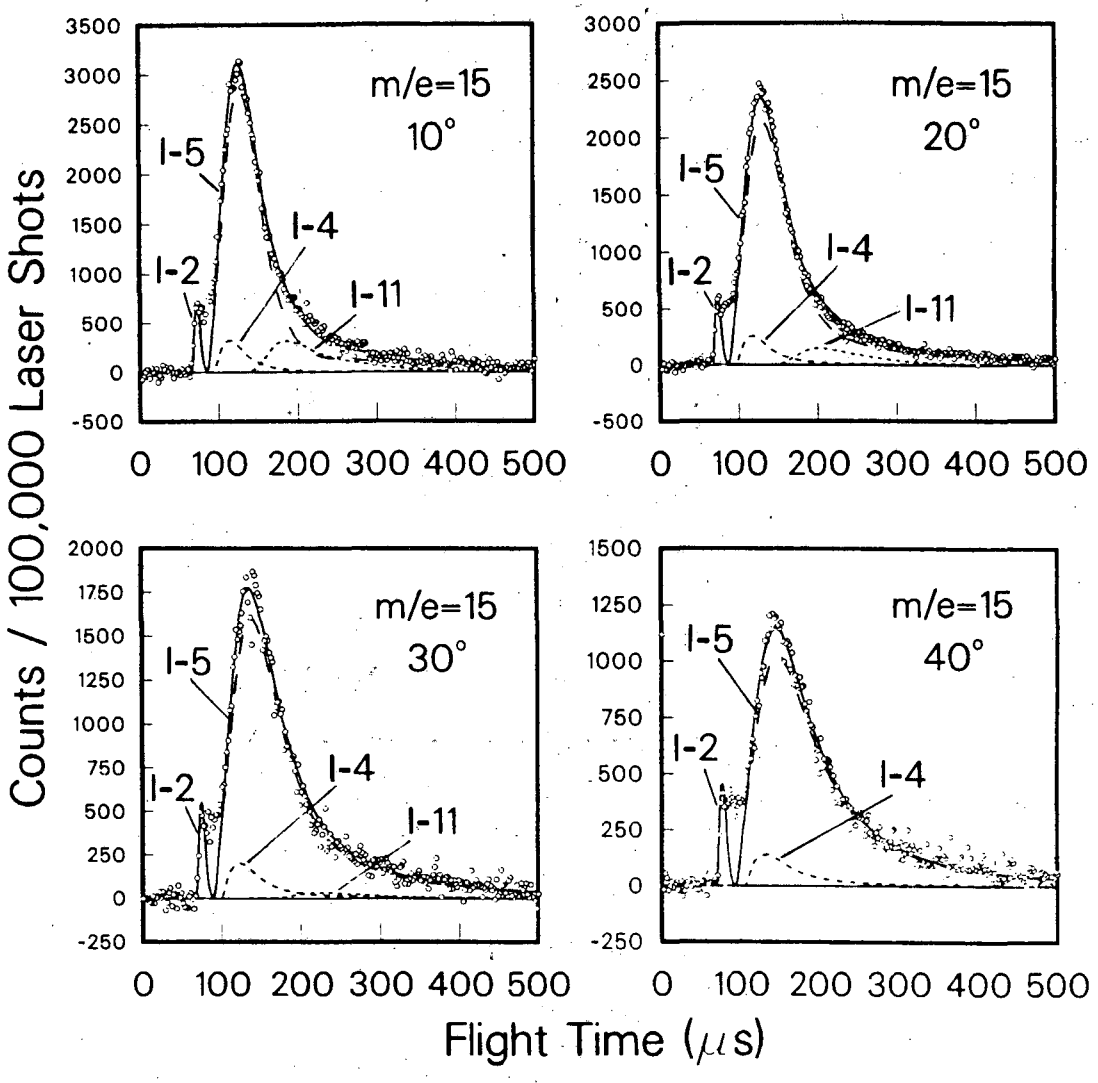

XBL 8910-3695

Fig. 10

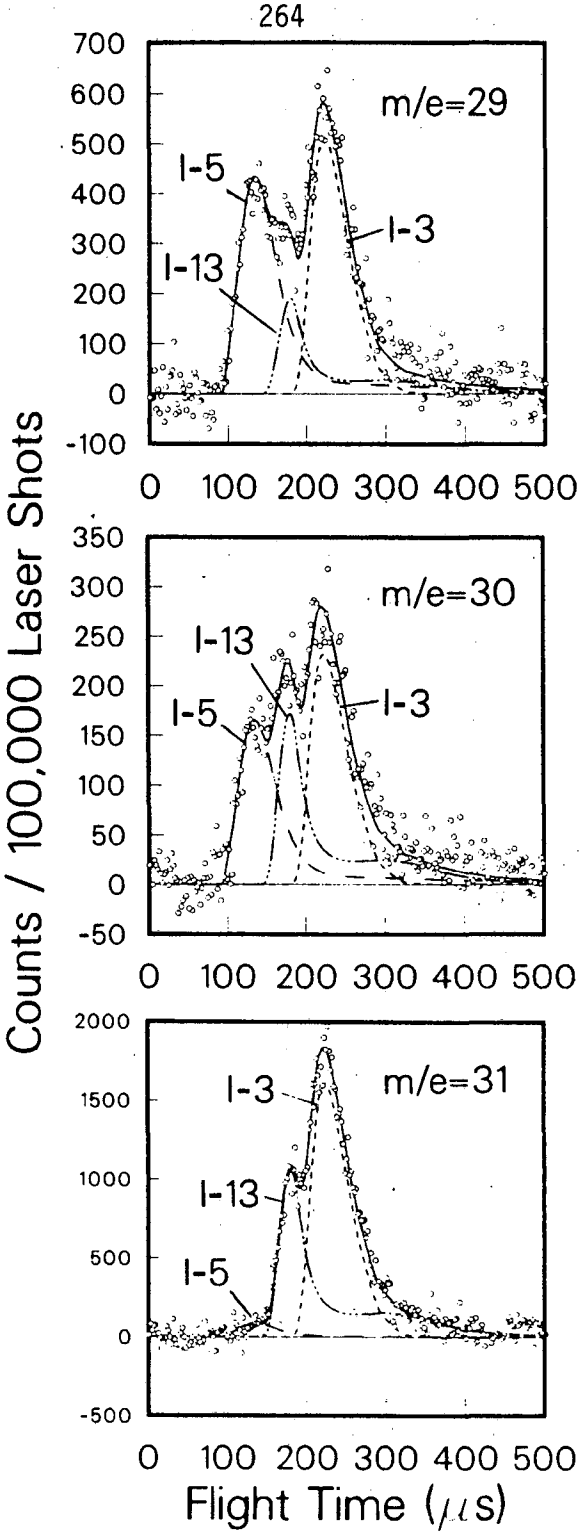

XBL 8910-3696

Fig. 11

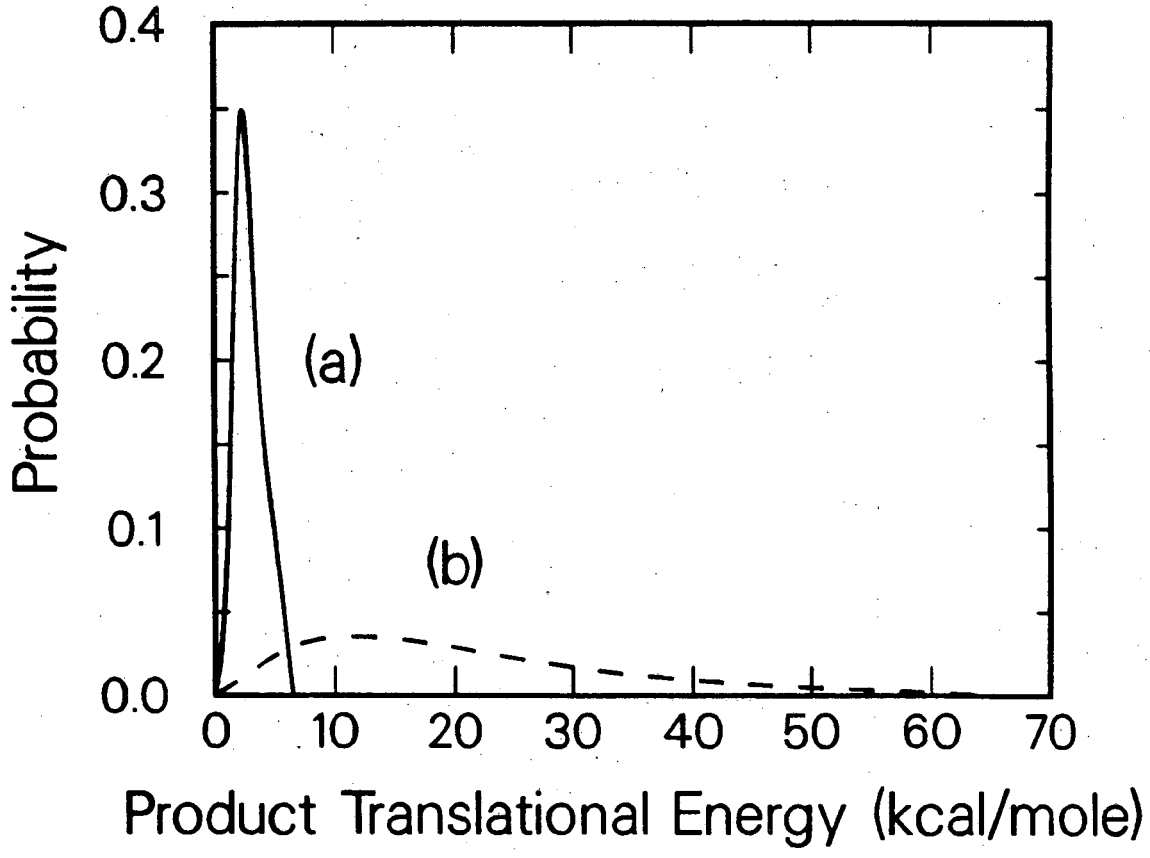

XBL 8910-3697

Fig. 12

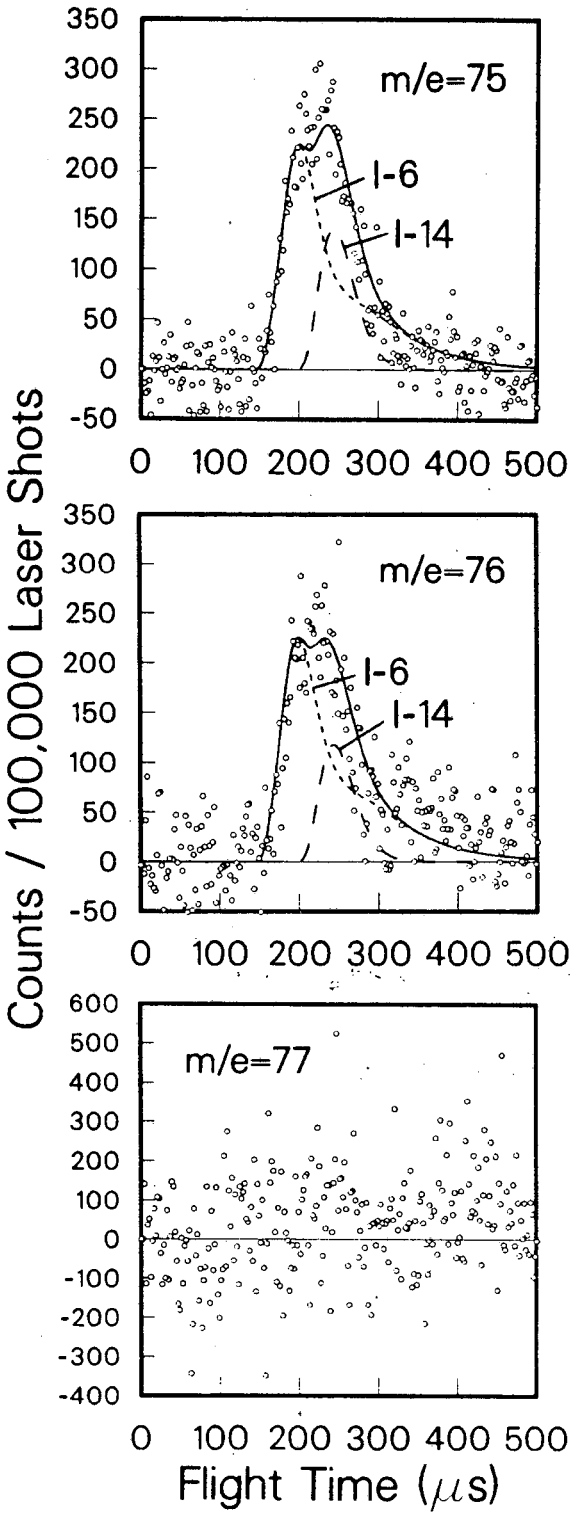

XBL 8910-3698

Fig. 13

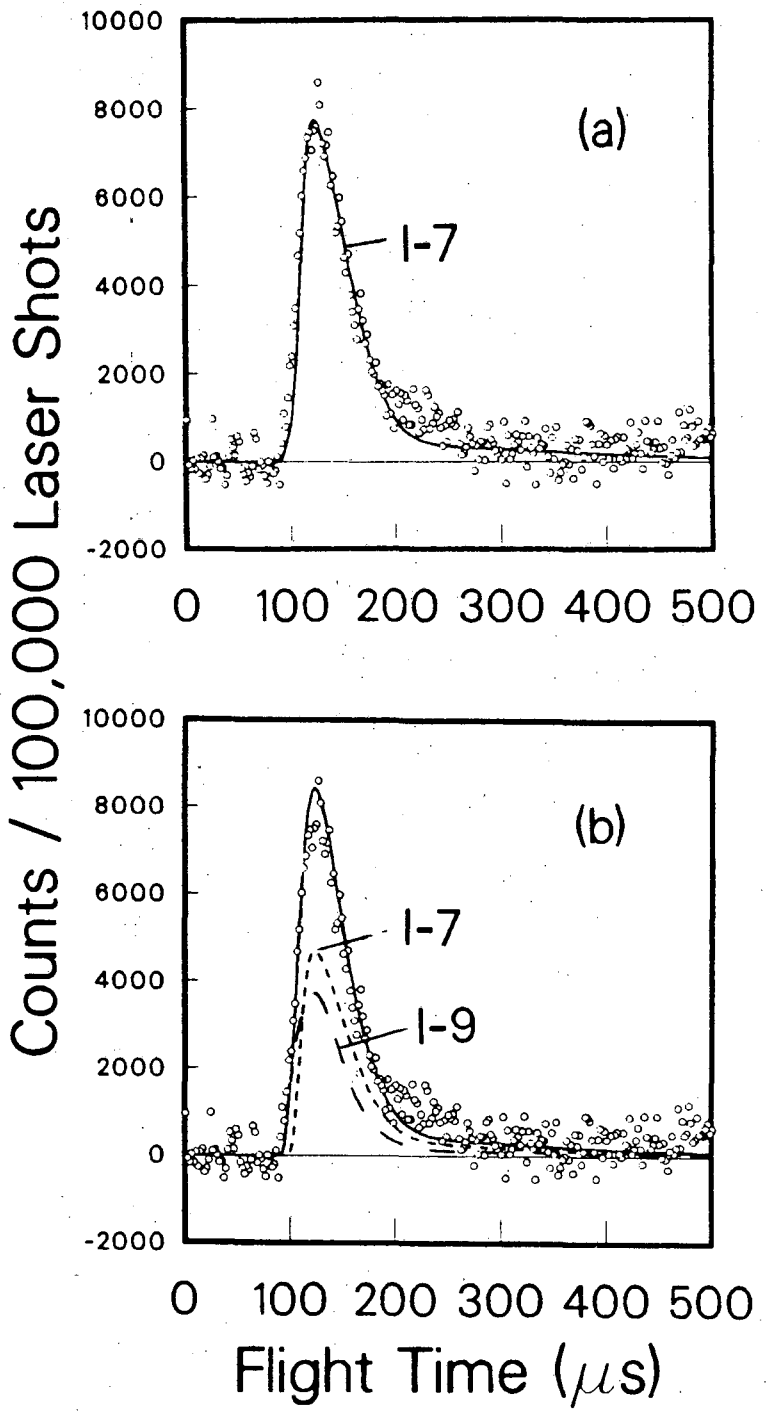

XBL 8910-3685

Fig. 14

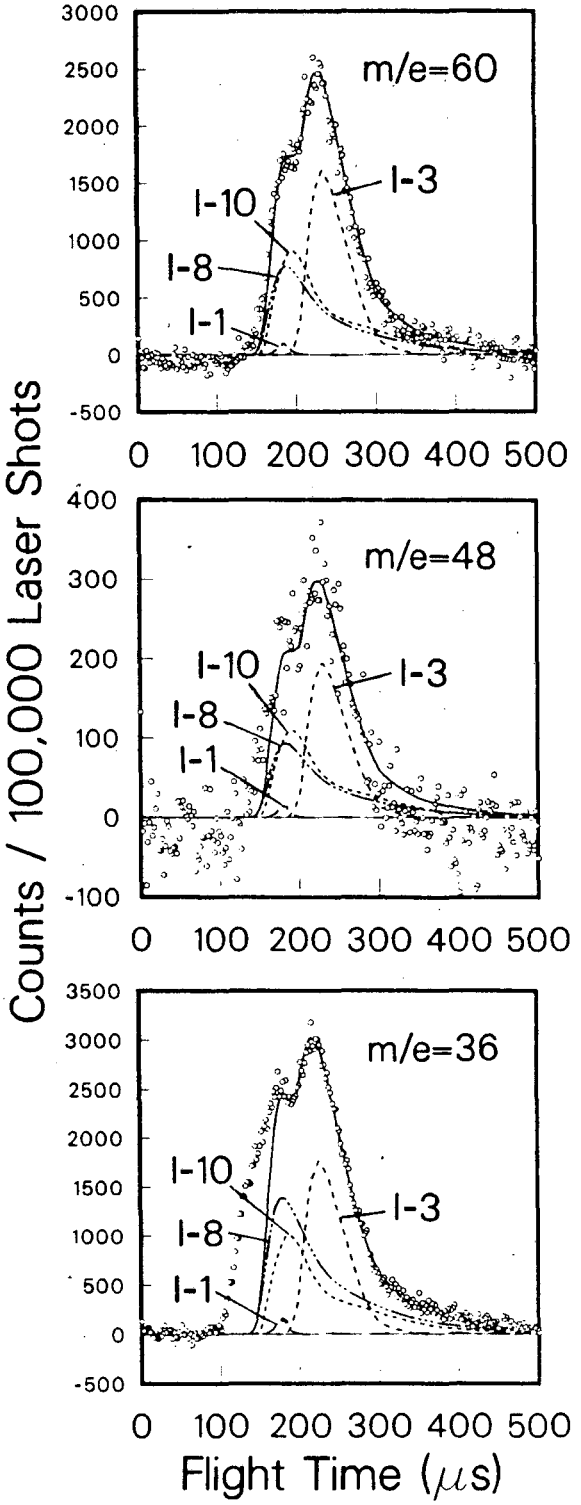

XBL 8910-3684

Fig. 15

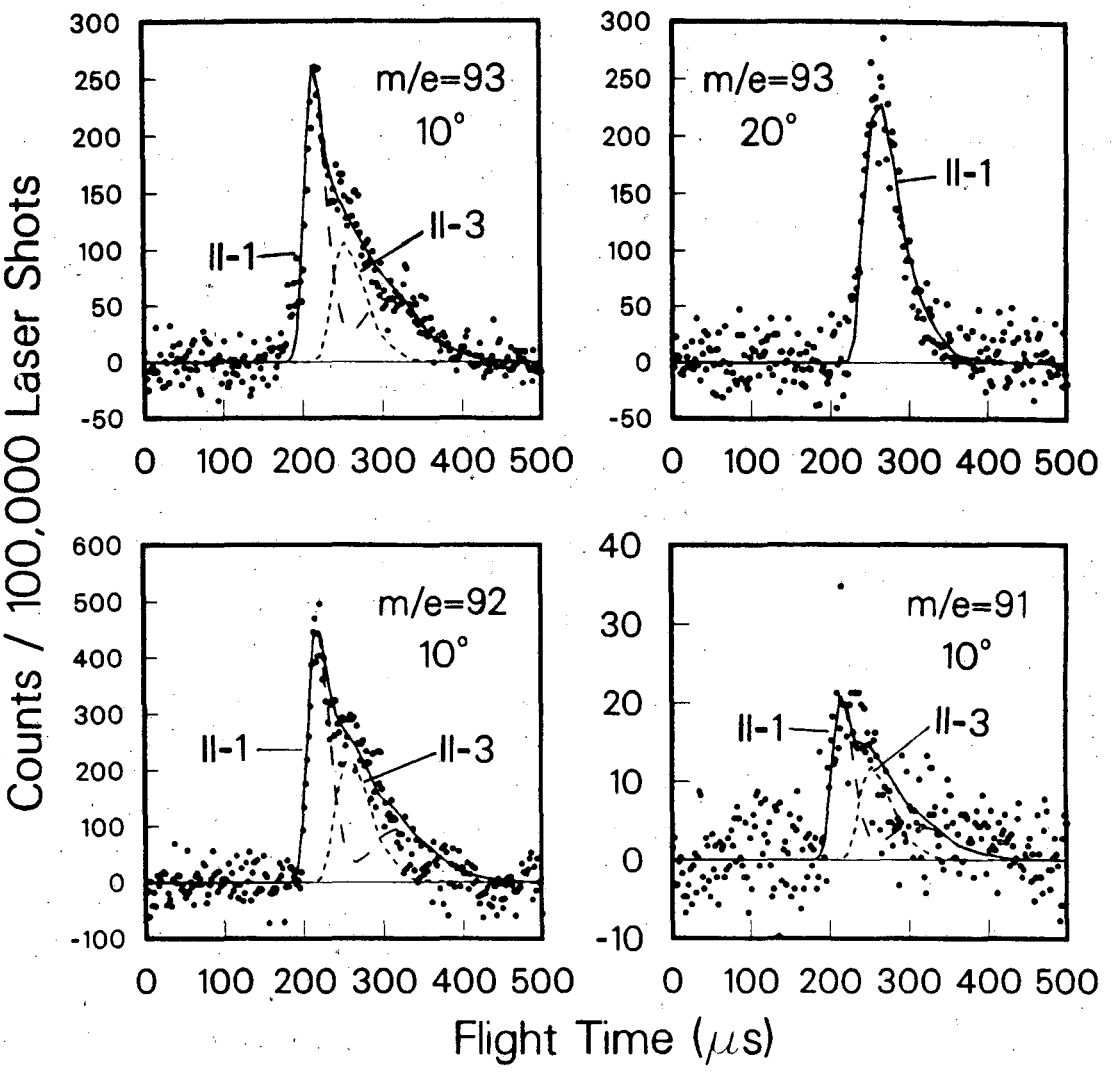

XBL 8910-3683

Fig. 16

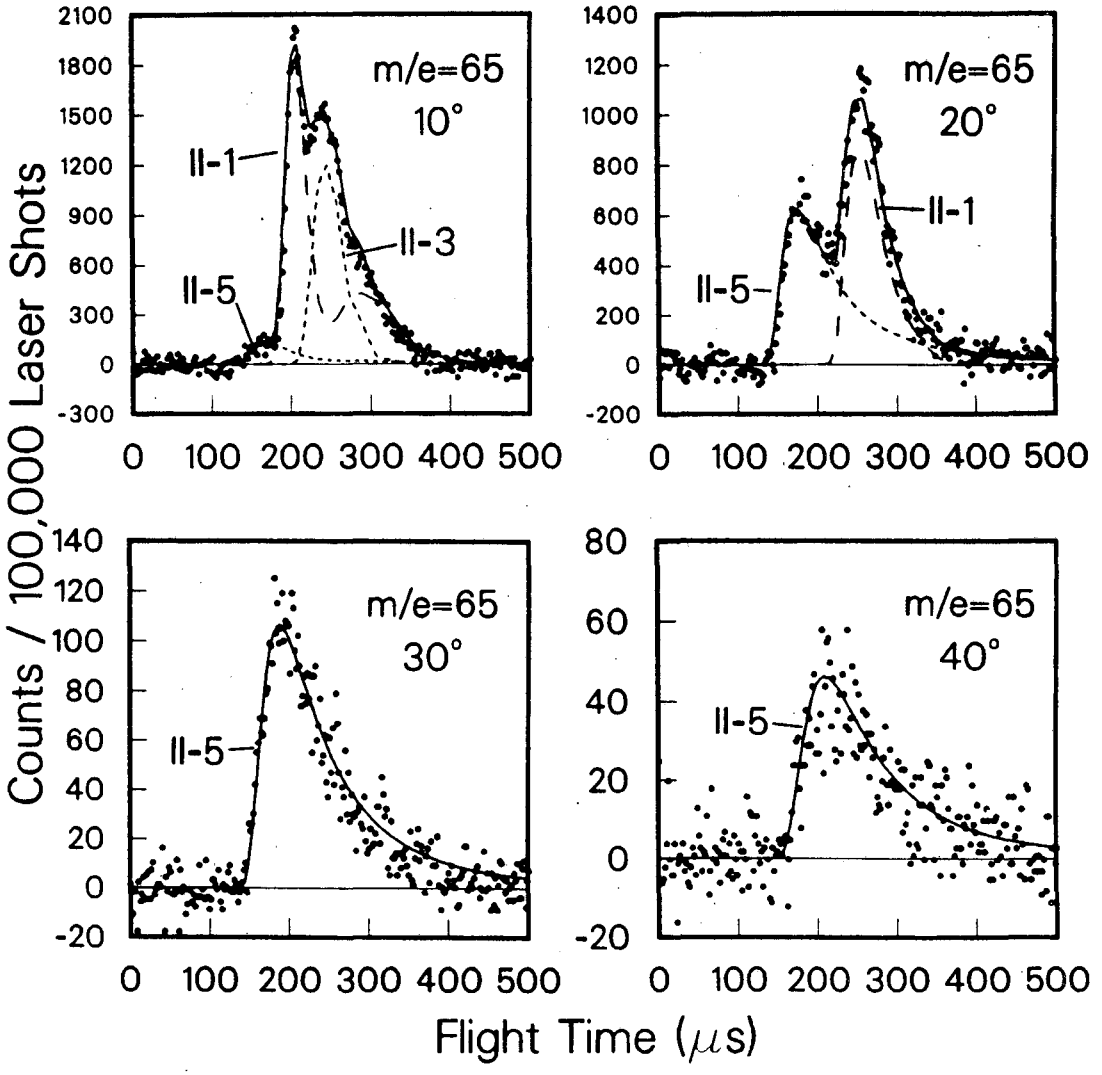
m/e=65
10°
II-1
II-3
II-5
m/e=65
20°
II-1
II-5
m/e=65
30°
II-5
m/e=65
40°
II-5
Counts / 100,000 Laser Shots
Flight Time (μs)
XBL 8910-3682

Fig. 17

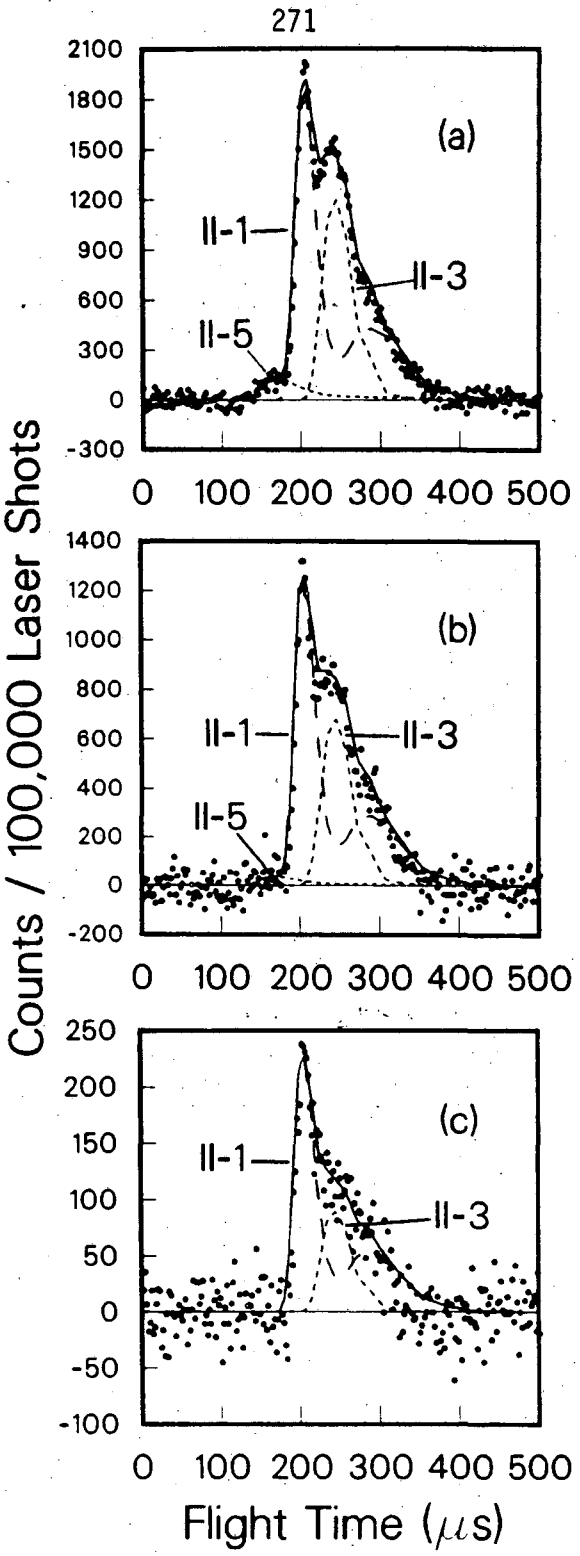
(a)
II-1
II-3
II-5
(b)
II-1
II-3
II-5
(c)
II-1
II-3
Counts / 100,000 Laser Shots
Flight Time (μs)
XBL 8910-3681

Fig. 18

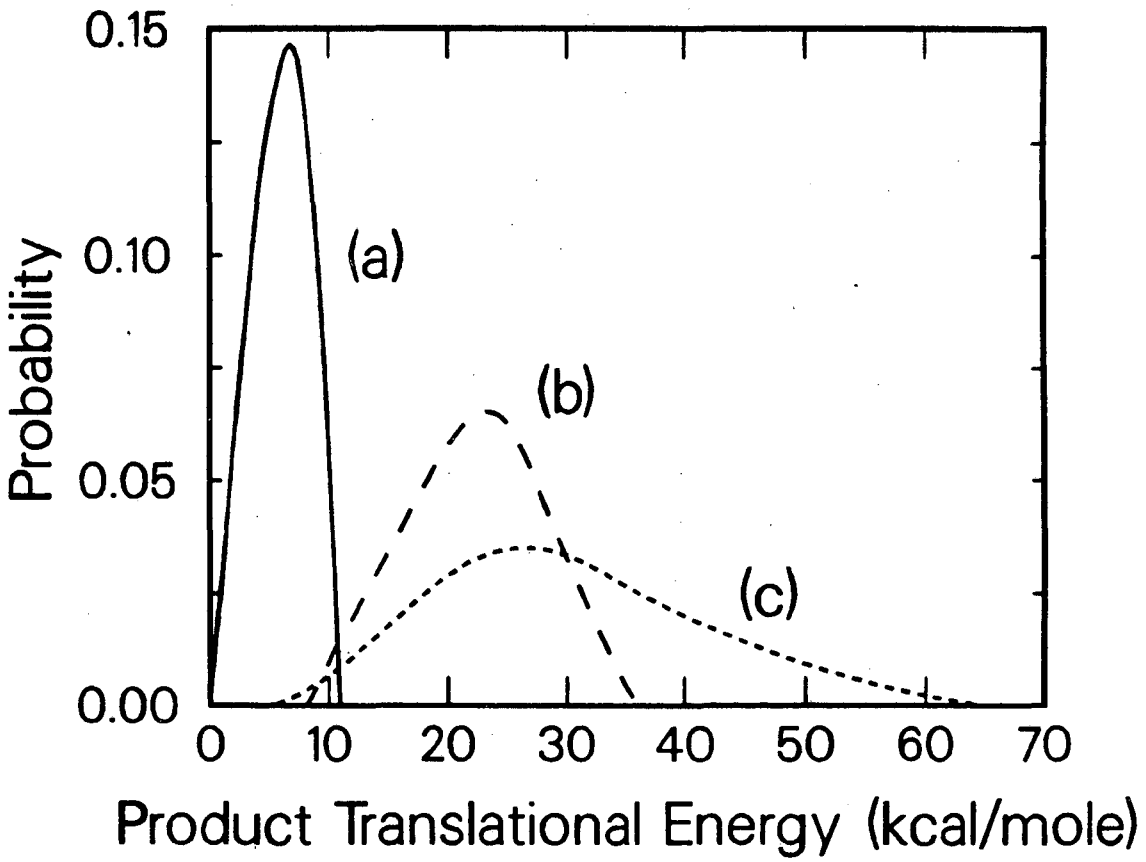

XBL 8910-3680

Fig. 19

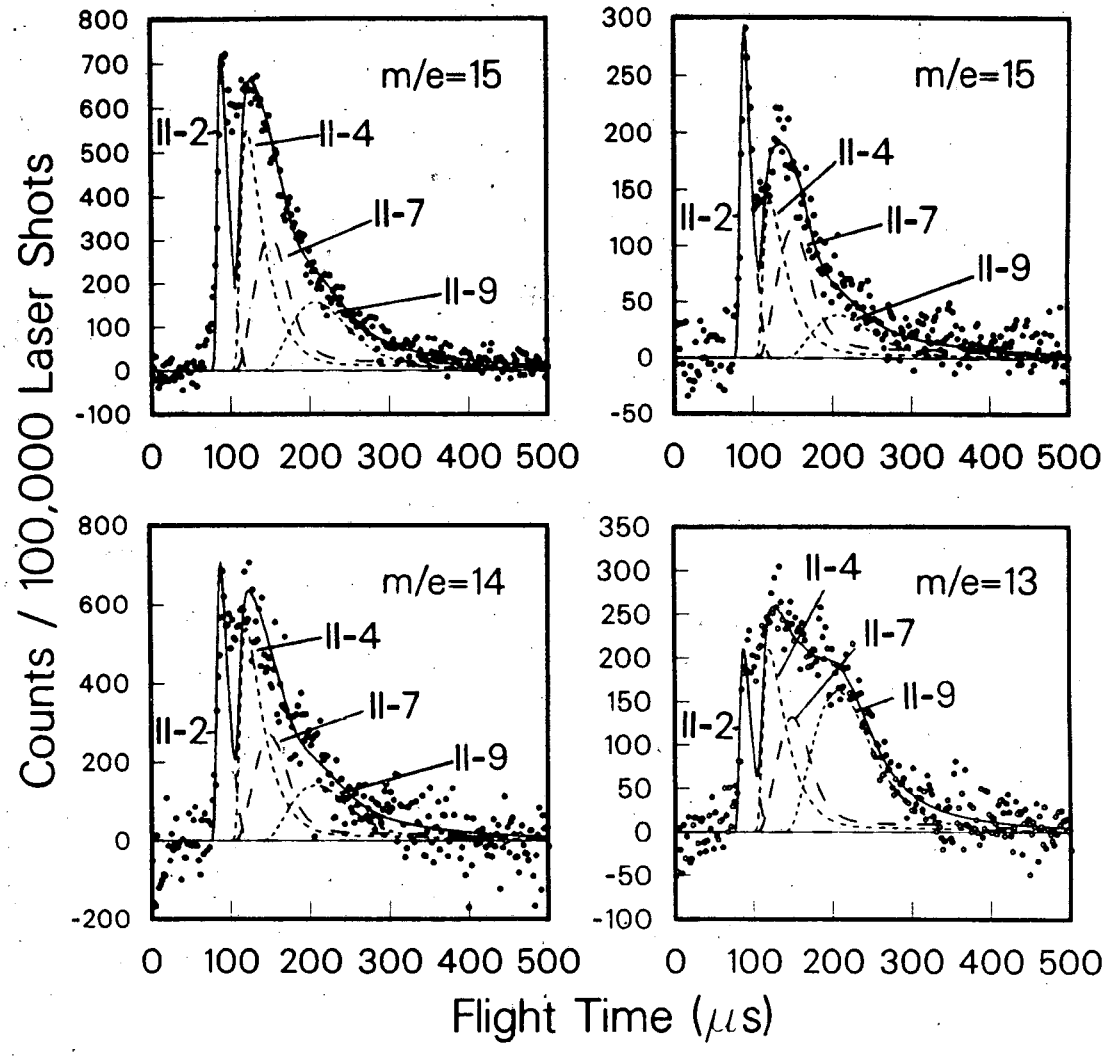
m/e=15
II-2
II-4
II-7
II-9
m/e=15
II-2
II-4
II-7
II-9
m/e=14
II-2
II-4
II-7
II-9
m/e=13
II-2
II-4
II-7
II-9
Counts / 100,000 Laser Shots
Flight Time (μs)
XBL 8910-3679

Fig. 20

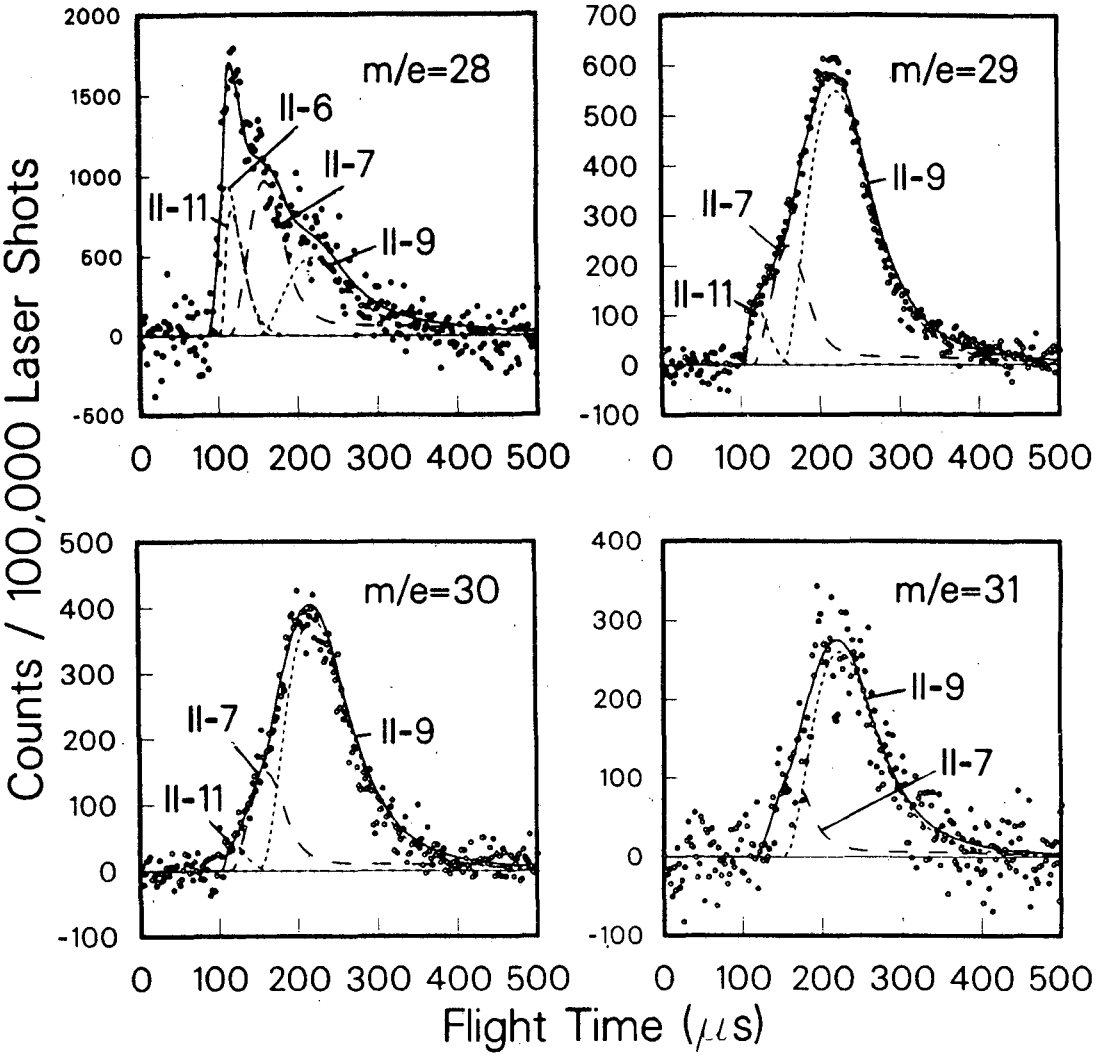

XBL 8910-3678

Fig. 21

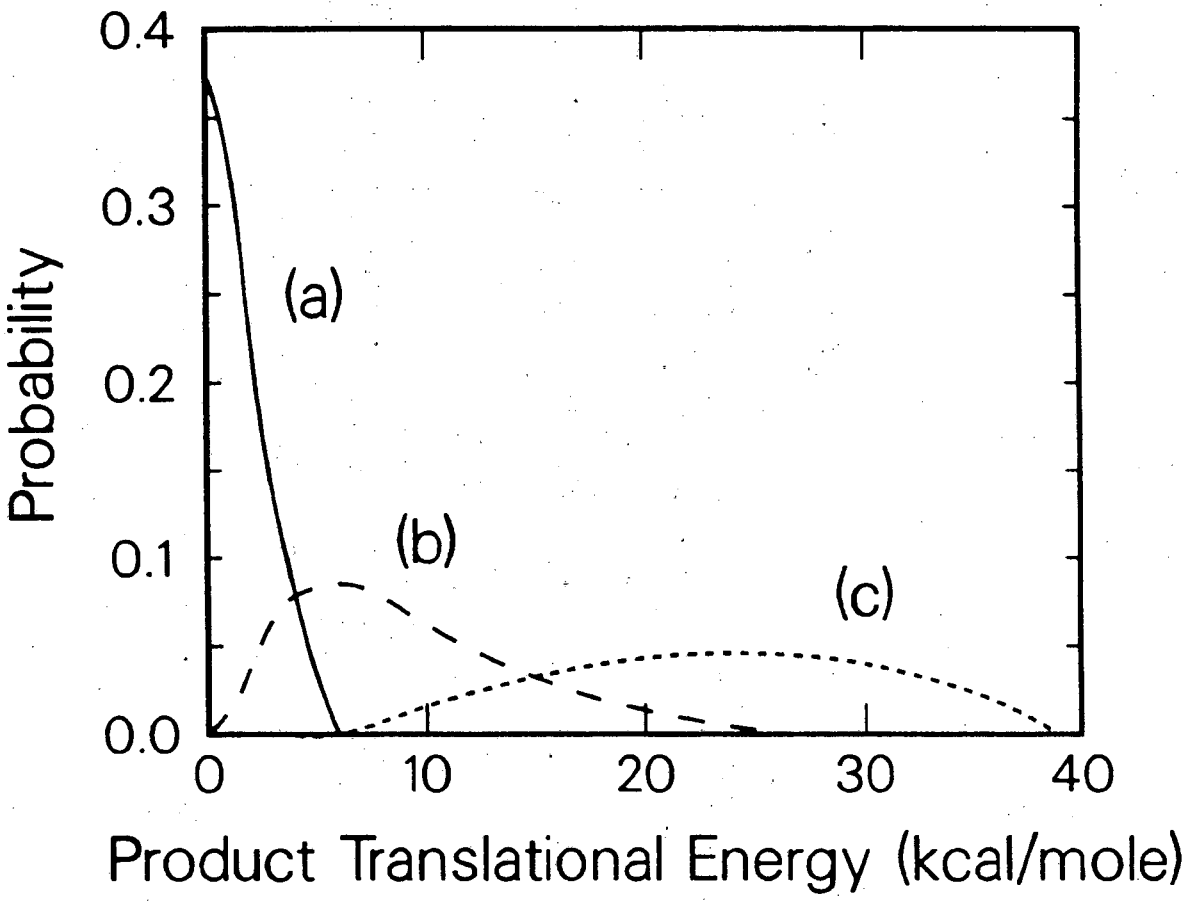

XBL 8910-3677

Fig. 22

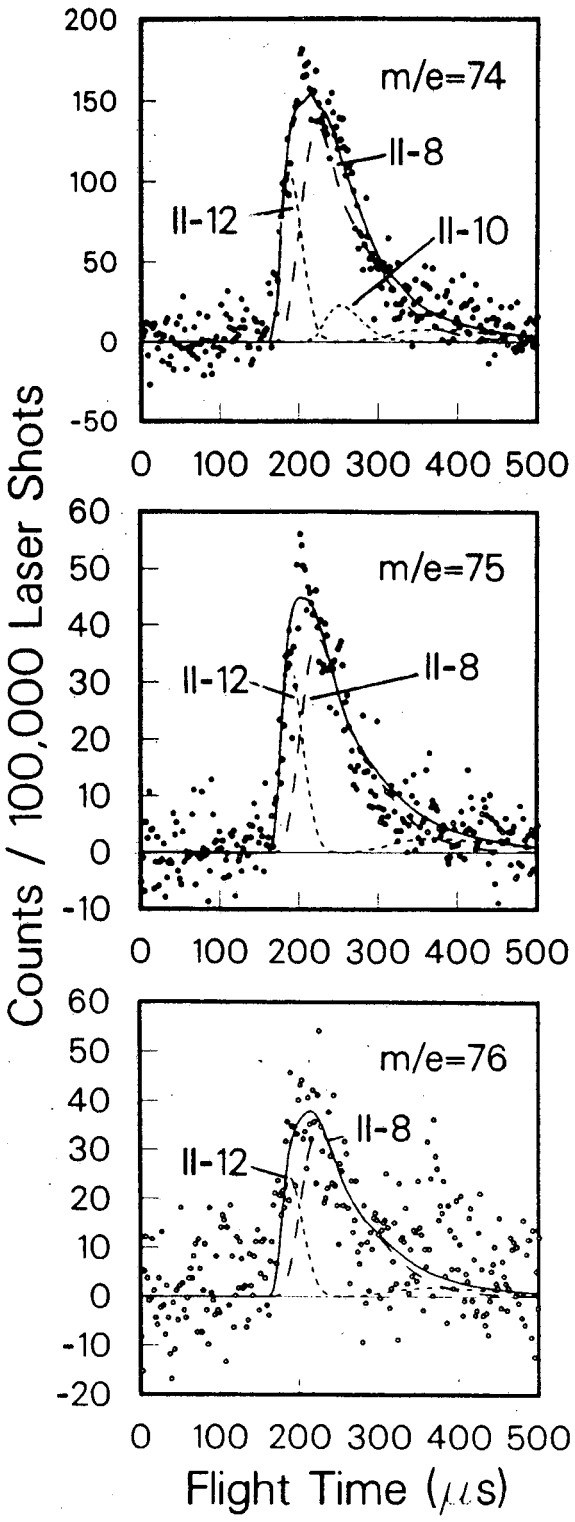
m/e=74
II-8
II-12
II-10
m/e=75
II-12
II-8
m/e=76
II-8
II-12
Counts / 100,000 Laser Shots
Flight Time (μs)
XBL 8910-3676

Fig. 23

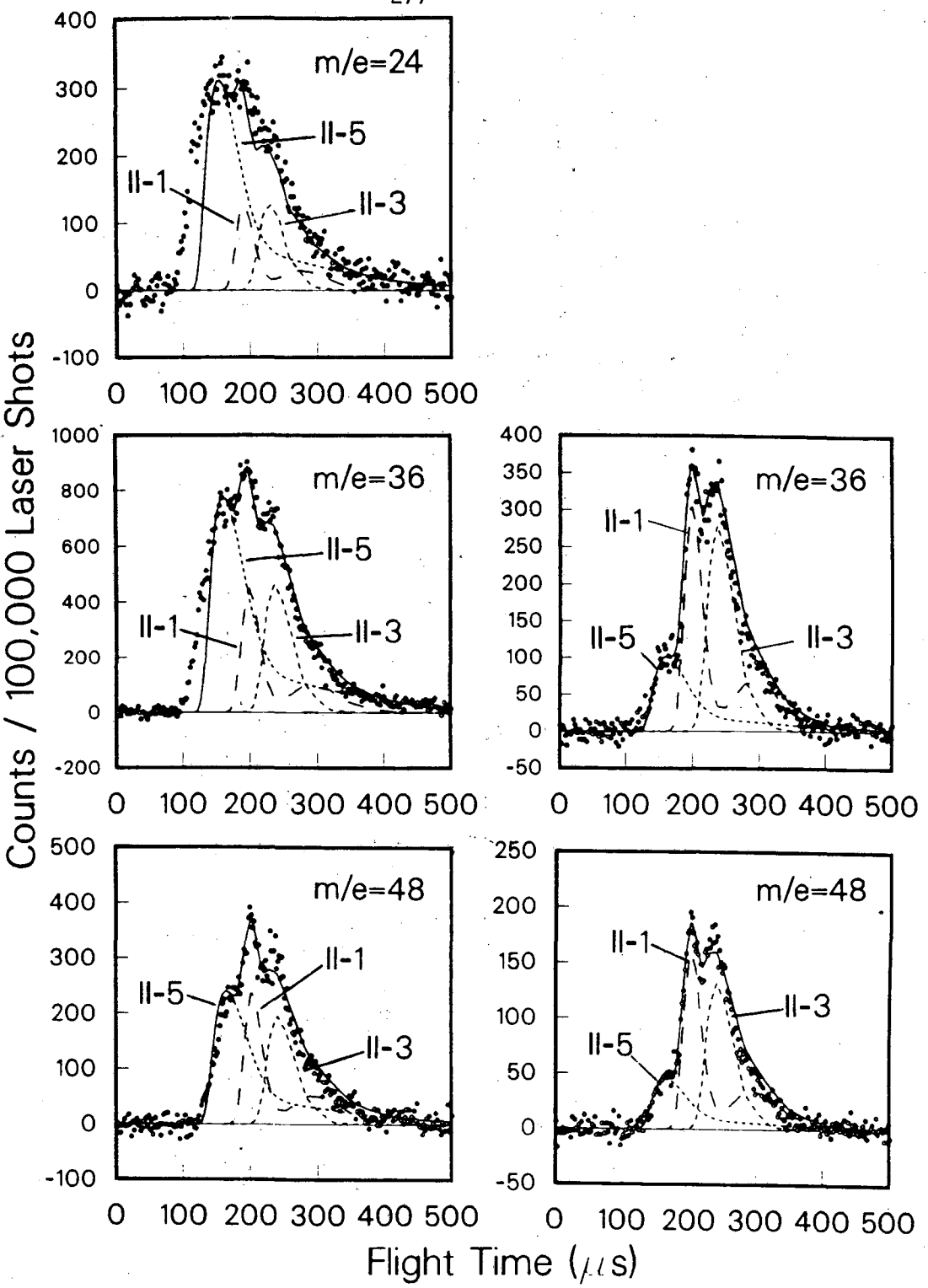

XBL 8910-3675

Fig. 24

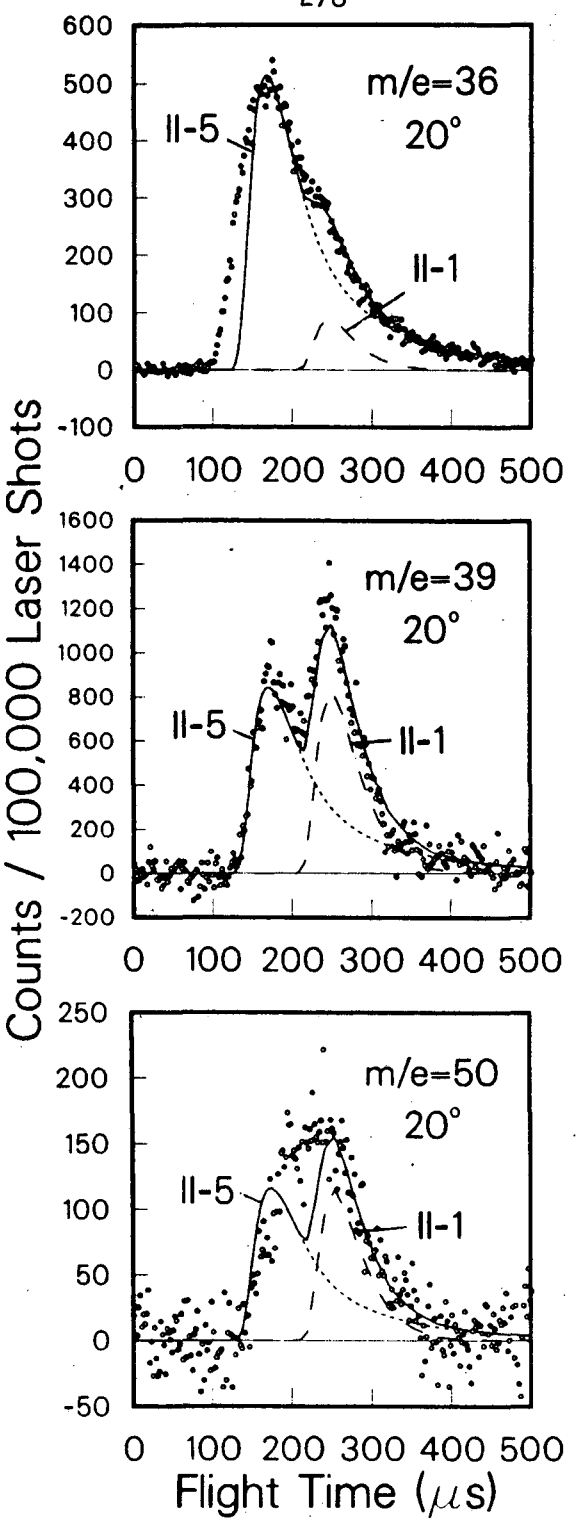

XBL 8910-3674

Fig. 25

APPENDIX 1

Approximation of Ionization Cross Sections

In order to use the awesome molecular beam method for any kind of quantitative determination, great care has to be taken to estimate all factors that enter the calculation of quantities such as relative scattering cross sections (branching ratios). If a branching ratio is to be determined from the "apparent" relative cross sections - which are obtained as output of the computer fit to angular distribution and/or time-of-flight data - correction factors need to be applied which reflect the ionization probability of the product species of interest and the probability of that species to fragment upon electron-impact ionization into the ion monitored:

$$R = \frac{\sigma_a}{\sigma_b} = \frac{\sigma_a^0}{\sigma_b^0} \times \frac{Q_B}{Q_A} \times \frac{f_B^{mB}}{f_A^{mA}} \quad .$$

In this expression R denotes the branching ratio or ratio of the relative cross sections σ for channels (a) and (b), σ_a^0 and σ_b^0 are the "apparent" relative cross sections as measured in the crossed molecular beams experiment by monitoring mass m_A and m_B, Q_A and Q_B are the ionization cross sections for product A of channel (a) and product B of channel (b), and f_A^{mA} and f_B^{mB} are the probabilities of product A (B) to give a fragment of mass m_A (m_B) in the ionization process. This equation differs from the

ones given previously[1] by omission of the "kinematic factors" which in our case are included in the "apparent" cross sections since they are the output of a computer program which performs all the center-of-mass to laboratory frame transformations properly.

It has been the tradition in the Lee group[1] to use the linear relationship between the maximum ionization cross sections and the square root of the polarizability suggested by Center and Mandl[2] and to approximate the molecular polarizability as the sum of the atomic polarizabilities as tabulated by Miller and Bederson[3]. It appeared to be worthwhile to search in the literature for more recent and hopefully more accurate methods for approximating molecular ionization cross sections.

Experimental data on absolute ionization cross sections are surprisingly sparse[4]. Märk has reviewed experimental methods employed for these measurements[5]. The general features of the ionization cross section vs. electron energy curves are very similar for most substances: a sharp initial rise to a maximum at about 70-80 eV followed by a plateau or slow decline. The alkali atoms exhibit somewhat different behavior: the cross sections peak at lower energies and fall off faster.

Very few data are available for absolute ionization cross sections of radicals[6]. We will make the assumption that approximate methods for the calculation of ionization cross sections will be applicable for radicals as well.

Numerous semi-empirical and semi-classical approximation methods have been developed[7] for calculation of electron impact ionization cross sections as a function of electron energy. However, due to the limited availability and limited accuracy of the experimental determinations (on the order of 10-20%[8]), the general validity of these relations can not be easily ascertained.

Of practical importance for mass spectrometrists are the ionization cross sections at a given electron energy, which is typically optimized for maximum ionization efficiency. In the literature ionization cross sections have been reported for 70 or 75 eV or at the maximum, and these conditions can be considered equivalent. It should be noted that the term "total ionization cross section" strictly applies to single ionization events only, including those resulting in fragmentation.

Due to the lack of reliable data, numerous efforts have been made to find empirical or semiempirical relationships between the molecular ionization cross section and some convenient quantity which would allow easy calculation of approximate values.

An early and much used relationship was suggested by Otvos and Stevenson[9]: the molecular ionization cross sections were approximated as the sum of atomic cross-sections, which in turn were calculated by the weighted sum of the outer, or valence, electrons (having ionization potentials of less than 35 eV). The weights were the mean square radii of the electrons.

Refined methods for calculating the atomic polarizabilities were developed (e.g. Ref. 10), but it was also shown that the relationships suggested by Otvos and Stevenson are not generally valid[11], but valid within a given molecular class[12,13].

Grosse and Bothe[14] suggested an additivity scheme where ionization cross sections are calculated as linear combinations of "bond cross sections". Taking the influence of the chemical bonds into account, an improved fit to experimental data was obtained.

Direct correlations between the maximum ionization cross section and other molecular properties have been suggested: Lampe et al.[11] found that the measured ionization cross sections were linearly related to polarizability; Beran and Kevan[13] tested correlations of ionization cross sections with polarizability, diamagnetic susceptibility, and additivity of ionization cross sections; Center and Mandl[2] suggested a linear correlation of the maximum cross sections and the square root of the polarizability; Oono and Nishimura[15] found a linear relation between the square root of the electron-impact ionization cross sections and the cube roots of the van der Waals volumes for molecules; and Bartmess and Georgiadis[16] tested the correlation between ion gauge sensitivities and the number of electrons, the Otvos-Stevenson function[9] and polarizability, and found a linear relationship between the sensitivity values and polarizability. However, in order to apply these relationships, approximation methods have to be used to calculate properties such as

polarizability and magnetic susceptibility which in turn typically are based on the additivity of contributions from the constituent atoms or bonds[17,18].

Taking up the idea of a simple additivity rule, Fitch and Sauter[19] have recently proposed a strikingly simple scheme in which the relative ionization cross sections (Q) are calculated from atomic ionization cross sections (a_i) according to

$$Q = b + \sum_{i=1} a_i n_i$$

where the summation is performed over all different atoms (The n_i are the number of atoms of kind i in the molecule). The values for b and a_i were obtained from a least squares fit to 179 published ionization cross sections. The a_i parameters were given for C, H, O, Cl, Br, I, F, N, D, and S (See Table I.). A second set of parameters was obtained by differentiating different hybridization states of C and O, but no significant improvement over the simpler regression was found. The average error in the prediction of relative total ionization cross section for the 179 molecules was reported as 4.69%. Deutsch and Schmidt[20] extended this method to include coefficients for P, As, B, and Si.

The method suggested by Fitch and Sauter[19] appears to be very appealing for our purposes, due to its ease of use. Even the hybridization state of the atoms can be neglected. Since our reaction products are typically radicals, none of the

refined approximations requiring parameters for homologous series can be applied anyway.

Applying different approximation methods (Ref. 9, Ref. 2 plus Ref 3, Ref. 2 plus Ref. 18, Ref. 16 plus Ref. 3, Ref. 16 plus Ref. 18, Ref. 9) to specific examples (Q_{vinoxy}/Q_{CHO}, Q_{ketyl}/Q_{CO}) results in values differing by up to about 25%. At this point not enough experimental data are available in order to evaluate critically the different schemes and their validity for our purposes. Since the values obtained from the method of Fitch and Sauter[19] are in satisfactory agreement with the values obtained from other methods and due to the ease of their calculation and the fact that no additional molecular property needs to be computed, we conclude that this simple scheme can be applied for our purposes. Hopefully future investigations will produce more and better data allowing for refined and more reliable calculation procedures. Until then we will have to live with a sizable uncertainty in our branching ratio correction factor.

References

1. D. J. Krajnovich, Ph. D. Thesis, University of California, Berkeley, 1983, Appendix B.
2. R. E. Center, and A. Mandl, J. Chem. Phys. 57, 4104 (1972).
3. T. M. Miller and B. Bederson, Adv. At. Mol. Phys., 13, 1 (1977).
4. T. D. Märk, in: Electron Impact Ionization, T. D. Märk and G. H. Dunn, editors, (Springer, Wien, 1985), Chapter 5.
5. T. D. Märk, Beitr. Plasmaphys. 22, 257 (1982); T. D. Märk, Int. J. Mass Spectrom. Ion Phys. 45, 125 (1982).
6. F. A. Baiocchi, R. C. Wetzel, and R. S. Freund, Phys. Rev. Lett 53, 771 (84); T. R. Hayes, R. C. Wetzel, F. A. Baiocchi, and R. S. Freund, J. Chem. Phys. 88, 823 (1988).
7. S. M. Younger and T. D. Märk, in: Electron Impact Ionization, T. D. Märk and G. H. Dunn, editors, (Springer, Wien, 1985), Chapter 2.
8. H. Deutsch, and M. Schmidt, Beitr. Plasmaphys. 24, 475 (1984).
9. J. W. Otvos and D. P. Stevenson, J. Am. Chem. Soc. 78, 546 (1956).
10. J. B. Mann, J. Chem. Phys. 46, 1646 (1967).
11. F. W. Lampe, J. L. Franklin, and F. H. Field, J. Am. Chem. Soc. 79, 6129 (1957).
12. A. G. Harrison, E. G. Jones, S. K. Gupta, and G. P. Nagy, Can. J. Chem. 44, 1967 (1966).

13. J. A. Beran and L. Kevan, J. Phys. Chem. 73, 3866 (1969).

14. H.-J. Grosse and H.-K. Bothe, Z. Naturforsch. 23a, 1583 (1968).

15. Y. Oono and Y. Nishimura, Bull. Chem. Soc. Jpn 50, 1379 (1977).

16. J. E. Bartmess and R. M. Georgiadis, Vacuum 33, 149 (1983).

17. J. A. Beran and L. Kevan, J. Phys. Chem. 73, 3860 (1969).

18. K. J. Miller and J. A. Savchik, J. Am. Chem. Soc. 101, 7206 (1979).

19. W. L. Fitch and A. D. Sauter, Anal. Chem. 55, 832 (1983).

20. H. Deutsch and M. Schmidt, Contrib. Plasma Phys. 25, 475 (1985).

Table I - Cross Section Coefficients (from Ref. 19)

(units: 10^{-16} cm^2)

$$Q = 0.082 + \sum_{i=1} a_i n_i$$

Atom	a_i
C	1.43
H	0.73
O	1.10
Cl	3.98
Br	5.19
I	6.62
F	0.61
N	1.20
D	0.93
S	3.80

APPENDIX 2: THE EVALUATION OF RELATIVE REACTION CROSS SECTIONS AND BRANCHING RATIOS FROM CROSSED MOLECULAR BEAM DATA

Chemical kinetics deals with the question of rates of chemical reactions. Reaction rates, however, are bulk quantities, and research efforts have been directed towards more and more detailed information, namely reaction probabilities as a function of specific conditions. The rate of the production of a product p in a simple bimolecular reaction, that is the number of product molecules (or moles) produced per unit time and unit volume, is proportional to the number density of both reactants, as well as to the relative velocity between the two reactants:

$$\frac{dn_p}{dt} = \sigma \cdot g \cdot n_1 \cdot n_2 \qquad (1)$$

where n_p, n_1, and n_2 are the number densities of product and reactants 1 and 2, respectively, and g is the relative velocity. The proportionality factor σ is identified with the total reaction cross section and has the dimensions of an area.

For the case of a molecular beam experiment where the velocity vectors of the reactant molecules are well defined and the products can be detected and measured as a function of angle, the differential cross section $\sigma(\theta_L,\varphi_L)$ can be

determined:

$$\sigma(\theta_L,\varphi_L) = \frac{d^2\sigma}{d\Omega_L} \tag{2}$$

where $$d\Omega_L = \sin\theta_L d\theta_L d\varphi_L \tag{3}$$

The information obtained in a crossed molecular beams experiment combined with time-of-flight (TOF) measurements of velocity distributions is in fact even more detailed: Distributions are measured as a function of angle and flight time. Since the flight length is easily determined and essentially constant, this information is equivalent to angularly resolved velocity distributions:

$$\sigma(v,\theta_L,\varphi_L) = \frac{\partial^3\sigma}{\partial v\partial\Omega_L} \tag{4}$$

where v represents the product velocity and Ω_L the solid angle in the laboratory frame. This information can be rewritten in many different ways corresponding to different reference frames.

The analysis procedure is greatly simplified if the angular distribution and the translational energy distributions are assumed to be independent of each other. This assumption appears reasonable for the case of a long-lived complex, and has

been applied successfully for the analysis of most molecular beam experiments performed in this group, however, exceptions are known to occur, especially when the reaction is direct[1]. Thus the goal of our analysis is to find the distribution of relative translational energies between the products, $P(E_T)$, and the angular distribution in the center-of-mass (CM) frame, $T(\theta_C)$. The angular information reduces to one angle θ_C because of the symmetry of the scattering process around the relative velocity vector.

In our analysis procedure, $P(E_T)$ and $T(\theta_C)$ are guessed initially and then varied until, after convolution over the relevant beam parameters, a satisfactory agreement of the calculated spectra with the data is obtained. This appendix describes how all the proper transformations are performed in the analysis program used in order to obtain correct relative reactive cross sections.

First, the input $P(E_T)$ and $T(\theta_C)$ distributions are normalized, such that:

$$\int P(E_T)\, dE_T = 1 \tag{5}$$

and

$$\iint T(\theta_C)\, \sin\theta_C\, d\varphi_C d\theta_C = 2\pi \int T(\theta_C)\, \sin\theta_C\, d\theta_C = 1 \tag{6}$$

The tradition of the group has been to report $P(E_T)$ for reactive scattering scaled such that the maximum equals 1, whereas for photodissociation the correct normalization, i.e. the integral equals 1 - as is appropriate for a probability distribution - has been used.

The differential cross section $\sigma(E_T,\theta_C)$, expressed in terms of translational energy and CM angle, is proportional to the product of $P(E_T)$ and $T(\theta_C)$:

$$\sigma(E_T,\theta_C) = Z \cdot P(E_T) \cdot T(\theta_C) \tag{7}$$

and the total cross section is obtained as

$$\sigma = \iint Z \cdot P(E_T) \cdot T(\theta_C)\ dE_T\ \sin\theta_C d\theta_C d\varphi_C = Z \tag{8}$$

The differential cross section as defined in (6) has to be expressed in terms of laboratory velocity v and laboratory angle θ_L in order to be compared the TOF data from molecular beam experiments. Consider first the transformation from translational energy to velocity in the CM-frame:

$$\sigma(u_p,\theta_C) = \sigma(E_T,\theta_C) \cdot \frac{dE_T}{du_p} \tag{9}$$

$$E_T = \frac{m_p}{2} u_p^{\,2} + \frac{m_{p'}}{2} u_{p'}^{\,2} \tag{10}$$

where u_p and $u_{p'}$ are the CM-velocities of the corresponding products p and p', m_p and $m_{p'}$ are their masses. Using

$$m_p u_p = m_{p'} u_{p'} \tag{11}$$

(10) rearranges to

$$E_T = \frac{1}{2} \cdot m_p \left(\frac{m_p}{m_{p'}} + 1\right) \cdot u_p^2 = \frac{\bar{\mu}}{2} \cdot u_p^2 \tag{12}$$

where $$\bar{\mu} = m_p \left(\frac{m_p}{m_{p'}} + 1\right) \tag{13}$$

thus $$\frac{dE_T}{du_p} = \bar{\mu} \cdot u_p \tag{14}$$

The mass factor $\bar{\mu}$ is extremely important if different reaction channels (with different reduced product masses $\mu_p = m_p m_{p'} / (m_p + m_{p'})$) are to be compared and the branching ratio determined. It was omitted in previous versions of the program[2]. In programs "GM*" $\bar{\mu}$ is identical with the variable "GB".

The next transformation is from the CM to the laboratory frame:

$$\sigma(v,\theta_L) = \sigma(u_p,\theta_C)\cdot J\left[\frac{(u,\theta_C)}{(v,\theta_L)}\right] \tag{15}$$

where $$J\left[\frac{(u,\theta_C)}{(v,\theta_L)}\right] = \frac{v^2}{u^2} \tag{16}$$

A derivation for the transformation Jacobian (16) was given in Ref. 3.

Finally, to account for the fact that the electron impact ionizer/Daly ion detector measures number density and not flux, an additional factor 1/v has to be included. If the TOF distributions are calculated, the transformation from velocity to time-frame has to be included as well:

$$\frac{dv}{dt} = -\frac{v^2}{s} \tag{17}$$

where s denotes the flight length, a constant in any experiment.

In the analysis program used for the reactive scattering experiments described in this thesis, angular or TOF distributions were calculated by applying the normalizations for $P(E_T)$ and $T(\theta_L)$ as described above. Then all the proper transformations as well as the averaging over as many Newton diagrams as needed is performed. The averaging procedure was described in detail in Ref. 2. Subsequently the calculated distributions are scaled to the input distributions (data) using a linear least-square procedure. The scaling factor obtained in

this manner, Z, can be identified with the (relative) total cross section σ, see eq. (8). Absolute cross sections can typically not be measured, since the densities of the beams, the exact size of the collision zone, and the detection efficiency are not known exactly. Finally these relative cross sections (denoted σ_0 in chapters 1 and 2) are corrected for ionization probabilities and ionizer cracking patterns, as described in detail in chapter 1, in order to obtain the correct branching ratios.

References

1. $F + H_2$: D. M. Neumark, Ph. D. Thesis, University of California, Berkeley, 1983; D. M. Neumark, A. M. Wodtke, G. N. Robinson, C. C. Hayden, and Y. T. Lee, J. Chem. Phys. 82, 3045 (1985);
$D + H_2$: N. C. Blais and D. G. Truhlar, J. Chem. Phys. 88, 5457 (1988); J. Z. H. Zhang and W. H. Miller, J. Chem. Phys. 91, 1528 (1989).

2. R. J. Buss, Ph. D. Thesis, University of California, Berkeley, 1979.

3. G. L. Catchen, J. Husain, and R. N. Zare, J. Chem. Phys. 69, 1737 (78).

LAWRENCE BERKELEY LABORATORY
TECHNICAL INFORMATION DEPARTMENT
1 CYCLOTRON ROAD
BERKELEY, CALIFORNIA 94720